GAS CONTAMINATION IN DISCHARGE EXCITED XEF EXCIMER LASERS

A.B. Duval

A Thesis Submitted for the Degree of PhD
at the
University of St Andrews

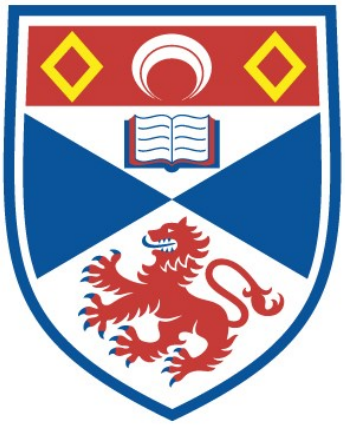

1984

GAS CONTAMINATION IN DISCHARGE EXCITED XeF EXCIMER LASERS

A thesis presented by

A B Duval, BSc

to the

University of St Andrews

in application for the degree of

Doctor of Philosophy

June 1983

Th 9950

CERTIFICATE

I certify that A B Duval BSc has spent nine terms at research work in the Physical Science Laboratory of St Salvator's College, in the University of St Andrews, under my direction, that he has fulfilled the conditions of Ordinance No16 (St Andrews) and that he is qualified to submit the following thesis in application for the Degree of Doctor of Philosophy.

A Maitland

Research Supervisor

DECLARATION

I hereby certify that this thesis has been composed by me, and is a record of work done by me, and has not previously been presented for a higher degree.

This research was carried out in the Physical Sciences Laboratory of St Salvator's College, in the University of St Andrews, under the supervision of Dr A Maitland.

A B Duval

CAREER

The author was born in Mauritius, where he completed his secondary schooling. After teaching and civil service work, he obtained a B.Sc. degree with first class honours from the University of New England, Australia, in 1978. He was awarded a research scholarship, and worked on the development of a method of measuring oscillator strengths by tunable laser interferometry. In 1979 he was awarded the Keith and Dorothy Mackay Travelling Scholarship by the University of New England, and commenced postgraduate studies at the University of St. Andrews in November of the same year. Since then, he has been involved in research on the problem of gas contamination in discharge excited XeF lasers.

ACKNOWLEDGEMENT

I wish to thank Dr A Maitland for his help, encouragement, and advice throughout this work. I gratefully acknowledge many helpful discussions with members of the laser 1 group, in particular, with T. Govindanunny. Thanks are also due to Fritz Akerboom for the glass-work, the workshop staff for their technical assistance in the construction of the laser, and Miss H. Walshaw for the use of UV and IR spectrophotometers. Finally, I wish to thank the University of New England for awarding me the Keith and Dorothy Mackay Travelling Scholarship, without wnich this work would not have been possible.

TABLE OF CONTENTS

CHAPTER 1		INTRODUCTION	1
(1.1)		Brief history of rare gas halide lasers	
(1.2)		Spectroscopy of rare gas halide molecules	
(1.3)		Kinetic processes	
(1.4)		Pumping requirements	
(1.5)		Rare gas halide laser lifetime	
	(1.5.1)	Material corrosion	
	(1.5.2)	Gas contamination	
(1.6)		Gas-life extension	
(1.7)		Thesis format	
(1.8)		Principles of mass spectrometry	
	(1.8.1)	Pressure requirements	
	(1.8.2)	The sample inlet system	
	(1.8.3)	Mass spectra of volatile halides	
(1.9)		Identification and analysis of mass spectra	
	(1.9.1)	Qualitative analysis	
	(1.9.2)	Quantitative analysis	
CHAPTER 2		THE XeF LASER SYSTEM	24
(2.1)		Introduction	
(2.2)		General design requirements	
	(2.2.1)	High-pressure gas discharges	
	(2.2.2)	Preionization techniques	
(2.3)		Laser construction	
	(2.3.1)	Mechanical	

(2.3.2) The laser body

(2.4) Electrical

(2.4.1) Electrical circuit

(2.5) Laser performance

CHAPTER 3 MASS SPECTRAL IR AND UV STUDIES 45

(3.1) Introduction

(3.2) NF_3 reaction kinetics

(3.3) IR absorption studies

(3.3.1) Experimental

(3.3.2) Results and discussion

(3.3.3) Summary of results of IR spectroscopy

(3.4) Mass spectral analysis

(3.4.1) Minimum detection levels

(3.4.2) Resolution

(3.4.3) Gas handling and sampling

(3.4.4) Data analysis

(3.5) Preliminary results

(3.6) Identification of contaminants

(3.6.1) Fresh gas mixtures

(3.6.2) Used gas mixtures

(3.7) NF_3 depletion

(3.7.1) NF_2 formation

(3.7.2) N_2F_2 formation

(3.8) Rate of contaminant formation

(3.8.1) He and He/Xe mixtures

(3.8.2) He/Xe/NF_3 mixtures

(3.9) UV absorption spectroscopy

(3.9.1) Experimental

(3.9.2) UV absorption measurements

(3.10) Summary

CHAPTER 4 CONTAMINANT EFFECTS 85

(4.1) Introduction

(4.2) Experimental

(4.3) Pulse energy variations

(4.4) Gas-life variations

(4.4.1) Effects of adding H_2

(4.5) Discussion

CHAPTER 5 COLD TRAP STUDIES 100

(5.1) Introduction

(5.2) Liquid nitrogen trap

(5.3) Gas-life extension

(5.3.1) Pulse energy variation

(5.4) UV absorption spectroscopy

(5.5) Mass spectrometric analysis

(5.5.1) Contaminant formation for -150°C trap

(5.6) Contaminant boil-off

(5.7) Summary

CHAPTER 6 CONCLUSIONS 117

(6.1) Introduction

(6.2) NF_3 depletion and contaminant formation

(6.3) Effects of contaminants on laser performance

(6.4) Use of cold traps

(6.5) Discussion

(6.6) Suggested design modifications for long gas-life

APPENDIX 1 COMPUTER PROGRAM 'BLUM' 129

APPENDIX 2 INFRARED LASER EMISSION 138

(A2.1) Introduction

(A2.2) Laser wavelength

(A2.3) Some performance characteristics

(A2.4) Gas-life

REFERENCES 142

ABSTRACT

Infrared, ultraviolet and mass spectrometric techniques have been used to investigate the short gas-life of discharge excited XeF lasers, for $He/Xe/NF_3$ mixtures. Infrared absorption studies provided initial information on the changes which occur in the laser gas composition during pulsing. The information was used to complement those of mass spectrometric studies, in which the chemical composition of laser gas mixtures were determined as a function of the number of laser pulses. Ultraviolet absorption spectroscopy was used to study optical absorption at the laser wavelength in fresh and used gas mixtures. The effects of several contaminants on laser performance were studied by adding small concentrations of these contaminants to the basic gas mixture of $He/Xe/NF_3$. The results provided information on the identity of the main contaminants. Cold traps were used to extend the gas-life, and to identify dominant contaminants.

The laser device used in this work is excited by a conventional blumlein circuit, which is triggered by a pressurised spark-gap switch. For a single gas fill of the basic mixture ($He/Xe/NF_3$), the number of laser pulses to half-energy is approximately 150/litre atm. Infrared and mass spectrometric studies show that the fast deterioration of laser performance is due to the depletion of NF_3, and to the accumulation of contaminants in the laser. The contaminants have been identified as N_2, O_2, NO, NO_2, N_2O, CO, CO_2, NF_2, N_2F_2, HF and CF_4. Of these, NO_2 absorbs at the laser wavelength (351nm), but the absorption coefficient in used gas mixtures is small compared to small signal gains of laser devices similar to the one used in this work. There is strong evidence that water vapour, which is one of the main impurities in fresh gas mixtures, may be the source of oxygen in the formation of oxides of nitrogen (NO, NO_2, N_2O) and carbon (CO, CO_2).

For fresh gas mixtures, the laser pulse energy is insensitive to the addition of small concentrations of N_2, H_2 and CF_4. In contrast, the addition of 0.05% of CO_2, CO and O_2 results in approximately 60, 40 and 20% reductions in the laser pulse energy respectively. The estimated change in laser output after 1000 shots due to the accumulation of CO_2, O_2 and CO is 20, 10 and 5% respectively. The addition of small concentrations (< 1 torr) of N_2, CO_2, CO, O_2 and H_2 results in negligible changes in the gas-life. However, when 2 torr of CF_4 is added to the basic mixture of $He/Xe/NF_3$ a threefold increase in the gas-life is observed. The improved gas-life is attributed to lower rates of formation of O_2, NO_2 and NO. After using $He/Xe/NF_3/H_2$ mixtures, the gas-life of the basic mixture increased by a factor of five to about 700 shots/litre atm. Mass spectrometric analysis of the gas mixture before and after lasing shows that the improvement in the gas-life is mainly due to lower levels of O_2, NO_2 and NO, and to a significant reduction in the rate of depletion of NF_3. The eventual deterioration of laser performance is mainly attributed to the accumulation of CO and CO_2 in the laser.

For the laser device and gas mixture used in this work, the optimum trap temperature lies in the region of -100 to -150°C. For a trap temperature of -150°C, the gas-life is 1500 shots/litre atm for a single gas fill. This is about 2.5 times the best result obtained without the use of cold traps. The eventual termination of laser action is due to NF_3 depletion and the accumulation of contaminants in the laser. By boiling-off the contaminants sequentially, CO_2 has been identified as a major contaminant.

CHAPTER ONE

INTRODUCTION

(1.1) Brief history of rare gas halide excimer lasers

Initial interest in rare gas halide excimer lasers started with the identification of an ArCl continuum band at 170 nm by Golde and Thrush (1974), during studies of argon metastable reactions with the halogens. This was followed by the observation of UV emissions from XeF, XeCl, XeBr, and XeI by Velazco and Setser (1975). The spectroscopy of these excimers was studied by Ewing and Brau (1975), who also predicted the emission wavelengths of the most intense bands of potential rare gas halide emitters (Brau and Ewing 1975). Laser action from rare gas halide molecules was first demonstrated by Searles and Hart (1975), who produced weak lasing from XeBr using an electron-beam excited mixture of xenon and bromine. Subsequently, Brau and Ewing (1975) produced stronger emission from an electron-beam excited XeF laser. Discharge excitation was first achieved by Mangano and Jacob (1975) with an electron-beam controlled electrical discharge in KrF. Laser action was later observed from XeF using self-sustained fast discharge excitation (Burnham et al 1976a), and from XeF and KrF using uv-preionized fast discharge excitation (Burnham et al 1976b, Sarjeant et al 1976). Since these early experiments, several other methods of excitation have been reported. These include the use of high-energy proton-beams (Eden et al 1979), of capacitively coupled discharges (Newman 1978) and microwave discharges (Mendelson et al 1981). Table (1.1) lists the emission wavelengths of rare gas halide

molecules which have shown laser action.

(1.2) Spectroscopy of rare gas halide molecules

The potential energy diagram of a rare gas halide molecule is shown in fig. (1.1). The ground state is covalently bound, and it is formed from the interaction of ground state ^1S rare gas and ^2P halogen atoms at close internuclear separation. Due to spin-orbit coupling, the ground state manifold consists of two states which are labelled X and A. Of these, the A state is higher in energy and is purely repulsive. In general, the X state has a relatively flat potential, except in XeF and XeCl for which the binding energies are 1200 cm^{-1} and 255 cm^{-1} respectively (Smith and Kobrinsky 1978, Tellinghuisen et al 1976a). Charge transfer interaction between excited noble gas and halogen atoms gives rise to three upper electronic states which are normally designated by B, C and D, in order of increasing energy. However, Waynant and Eden (1979) have shown that in XeF, the C state lies 610 cm^{-1} below the B state.

Radiative emissions occur on B -> X, C -> A and D -> X transitions (Hutchinson 1980). The emission spectrum consists of several bands, the strongest of which is attributed to B -> X transitions (Brau and Ewing 1975) which give rise to efficient laser emission in the UV and VUV spectral regions, as listed in table (1.1). In general, the B -> X transitions show only weak vibrational structure due to the flat potential of the lower state. However, in the case of XeF and XeCl, in which the lower state is weakly bound, B -> X transitions show normal bound-bound vibrational structure (Brau and Ewing 1975). At low pressures (less than 0.5 atm) the B -> X

spectrum is spread out towards the blue due to incomplete vibrational relaxation of the upper electronic state prior to radiative emission. At high pressures, high vibrational levels of the upper state are relaxed, and the emission bandwidths of B -> X transitions are then typically 2nm (Hutchinson 1980).

Weaker bands due to C -> A transitions are obtained at longer wavelengths. These have larger bandwidths (70nm in XeF, Bishel et al 1981) than the B -> X transitions, as they terminate on a purely repulsive A state. In XeF, the C state is lower than the B state by 610 cm^{-1}, and at high buffer gas pressures, it is populated by collisional quenching of the latter, with the result that the C to B population ratio tends to unity (Finn et al 1979). However, since the C -> A transition has a long lifetime (93 ns, Waynant and Eden 1979) and is broader than the B -> X transition, its stimulated emission cross-section is roughly fifty times smaller. To achieve laser action on C -> A transitions, B -> X emission must be supressed. Laser emission on the C -> A transition has been observed in XeF in the region of 490nm using electron-beam pumping (Ernst and Tittel 1979), fast discharge excitation (Fisher et al 1979) and photolytic pumping of XeF_2 (Bishel et al 1981). The wide bandwidth of the emission makes it attractive as a source of high-power tunable laser radiation in the visible. Liegel et al (1981) have achieved broad-band tuning from 455nm to 529nm in an electron-beam excited XeF laser.

The D -> X band is observed at shorter wavelengths in the UV (Brau 1979), and it is generally structured like the B -> X band, although its intensity is much lower. This is due to collisional quenching to lower states in the upper electronic manifold. For this

reason, the D -> X band is not likely to be a good candidate for an efficient high-power laser.

(1.3) Kinetic processes

The formation kinetics of rare gas halide molecules are complex. They involve ground state and excited atomic and molecular species, and many ionic species. Rokni et al (1978), and Brau (1979), have considered in detail the formation, quenching and transient absorption processes in discharge and electron-beam excited KrF and XeF lasers. In this section, the main features will be briefly discussed with particular reference to XeF, which is most relevant to this work.

In discharge excited rare gas halogen mixtures, the excimers are predominantly formed in 'harpooning' reactions (Rokni et al 1978) such as

$$Xe^{*} + F_2 \rightarrow XeF^{*} + F$$

These occur with large cross-sections, and in many cases have near unit efficiency for producing the excited products (Velazco et al 1976). In electron-beam excited lasers, three-body ion recombination reactions such as

$$Xe^{+} + F^{-} + M \rightarrow XeF^{*} + M$$

play a major role, where M is the third body. These reactions are fast, and the branching ratio for forming the excited molecules is

thought to be high (Brau 1979).

In addition to the halogens (F_2, Cl_2, etc.), several other molecules (NF_3, N_2F_4, SF_6, HCl, CCl_4) have been used with varying degrees of success (Andrews et al 1977, Burlamacchi and Salimbeni 1978). In XeF lasers, NF_3 is normally preferred to F_2 for three main reasons: (i) it is not as corrosive as fluorine, (ii) it does not absorb at the laser wavelength (LaPaglia and Duncan 1961), and (iii) the quenching rate of XeF^* by F_2 is seventeen times that of quenching by NF_3 (Rokni et al 1978). However in KrF lasers, F_2 is normally used because of the low branching ratio for the formation of KrF^* from NF_3 (Velazco et al 1976).

Rare gas halide lasers use either Ar, He or Ne as the dilutant buffer gas. In XeF lasers, Champagne and Harris (1977) have shown that the laser efficiency can be significantly improved by replacing Ar with Ne. The improved performance is due to three main reasons: (i) Ne quenches XeF^* less rapidly than Ar (Eden and Waynant 1978), (ii) photoabsorption by Ne_2^+ at the laser wavelength is much smaller than by Ar_2^+, and (iii) the formation of Xe_2^+, which photoabsorbs at the laser wavelength, is slower in Ne (Rokni et al 1978). In discharge excited XeF lasers, Burnham et al (1976a) obtained comparable performance with Ne and He dilutants.

At low pressures, excited rare gas halide molecules are predominantly quenched by the halogen bearing species in reactions of the form

$$XeF^* + F_2 \rightarrow Xe + 3F$$

The quenching process is fast, and proceeds with a rate constant of

the order of 10^{-9} cm^3s^{-1} (Ault et al 1975). Quenching by rare gas atoms is generally much slower (Brau 1979). However at high pressures, the excited molecules are quenched in three-body interactions of the form

$$KrF^* + Kr + Ar \rightarrow Kr_2F^* + Ar$$

which result in the formation of triatomic species (Rokni et al 1978).

The dominant absorbing species in electron-beam excited XeF^* mixtures have been identified by Rokni et al (1978) as Xe_2^+, Ne_2^+ and Ar_2^+. Of these Xe_2^+ is the dominant absorber. A decrease in XeF laser efficiency is observed for Xe concentrations exceeding 1%. For this reason the partial pressure of Xe must be kept small in XeF lasers. In KrF lasers, photoabsorption is attributed to F_2, to positive and negative ions (Ar_2^+, Kr_2^+, F^-) and to triatomic species such as Kr_2F^* (Hawryluk et al 1977).

(1.4) Pumping requirements

An indication of the problems of constructing short-wavelength lasers can be gained by considering the pumping power densities required to achieve laser gain. In this respect, a significant parameter is the stimulated emission cross-section, which is a function of the lifetime, shape and width of the emission band. Assuming that near the peak of the emission band, the band shape is approximately gaussian, the stimulated emission cross-section σ can be estimated (Brau 1979) using the expression

$$\sigma\tau = (1/4\pi)(\ln 2/\pi)^{1/2}\lambda^4/(c\,\Delta\lambda) \qquad (1.1)$$

where λ is the wavelength, c the speed of light, τ the average lifetime of the upper laser level, and $\Delta\lambda$ the optical bandwidth (FWHM). As an example, the bandwidth of the B -> X band in KrF is about 2nm (Brau and Ewing 1975), and the measured lifetime is 9ns (Burnham and Searles 1977). Using these values in equation (1.1), a stimulated emission cross-section of 2×10^{-16} cm^2 is obtained. The cross-sections of the other rare gas halide molecules are of the same order of magnitude.

The pumping power density required to produce a small signal gain g_o is given by (Brau 1979)

$$P = h\nu g_o/n_Q n_D \sigma\tau$$

$$= 4\pi(\pi/\ln 2)^{1/2} hc^2 \Delta\lambda\, g_o/n_D n_Q\, \lambda^5 \qquad (1.2)$$

where n_Q is the quantum efficiency, n_D the discharge efficiency and $\Delta\lambda$ the width (FWHM) of the emission band which is here assumed to have a gaussian shape. Equation (1.2) shows that the pumping power density is proportional to $\Delta\lambda/\lambda^5$, which explains the high power densities required to achieve laser action in rare gas halogen mixtures. Using typical values of 10^{-16} cm^2 for the stimulated cross-section, and 0.5 for the product of n_D and n_Q (Brau 1979), a power density of more than 1 MW/cm^3 is obtained.

The two most commonly used methods of exciting rare gas halide lasers is by high-energy electron-beams, and in high-voltage fast discharge devices. Electron-beam excitation of rare gas halides has

shown efficiencies of 15% (Bhaumik et al 1976), and pulse energies of 350J (Brau 1979). However the method has several limitations. Electron-beam excited lasers are bulky, complex and expensive, and they cannot be operated at high repetition rates due to limitations imposed by heating of the metallic foil which separates the laser gases from the electron-gun.

Efficiencies of 1.7% (Chen Jianwen et al 1980) and pulse energies of 3.2J (Levatter et al 1981) have been achieved from fast discharge excited rare gas halide lasers. Compared to electron-beam pumped systems, they are cheap and simple in construction, and repetition rates of 10^3 pps or more have been achieved in transverse flow systems, with average powers of 200W (Wang and Gibb 1979, Fahlen 1980). Discharge excited rare gas halide lasers are being increasingly used in small scale laboratory applications which require an intense source of radiation in the UV and VUV spectral regions (McKee and Nielson 1982). The main obstacle to their wide application is the rapid deterioration of their performance on single gas fills.

(1.5) Rare gas halide laser lifetime

The long-term stable operation of discharge excited rare gas halide lasers is limited by (i) the fundamentally unstable nature of the gas discharge, and (ii) the rapid deterioration of laser performance due to chemical processes in the discharge. The problem of discharge instability in high pressure (1 atm or more) rare gas halide mixtures has been extensively investigated (Levatter and Lin 1980, Herziger et al 1981, Hasson and Von Bergman 1980), and it is now possible to achieve stable uniform glow discharges by the use of

preionization and fast discharge excitation techniques. However, the rapid short-term degradation of laser performance is still a subject of intense investigation.

From a single gas fill, the maximum number of laser pulses is normally quoted as being typically 10^6 for XeCl lasers, and 10^3 to 10^4 for the rare gas fluoride lasers (McKee et al 1980, Tenant 1981, Christensen 1977, Gower et al 1980). These figures refer to the number of laser pulses to half-energy (when the pulse energy has decreased to half its maximum value). Since the gas volume is not normally given in the literature, the long-term performance of different rare gas halide lasers cannot be compared. A more useful definition of the gas-life would be the number of laser pulses/litre atmosphere to half-energy. Several processes are responsible for the fast deterioration of laser performance. These include optical and chemical damage of the laser windows, and contamination of the laser gas mixture by the formation of new species from the corrosion of materials within the laser body and gas handling system, and in gas-phase reactions in the laser discharge. XeCl lasers are relatively insensitive to the formation of contaminants (Gower et al 1980, Burlamacchi and Salimbeni 1978), and the problem of gas contamination is secondary to that of optical damage and material corrosion. In rare gas fluoride lasers, both material corrosion and gas contamination are severe problems.

(1.5.1) Material corrosion

Rare gas halide lasers use a mixture of three components (i) a buffer gas (He,Ne,Ar) at pressures of one atmosphere and above, (ii) a

few tens of torr of a rare gas, and (iii) a few torr of a halogen donor ($HCl, CCl_4, F_2, NF_3, SF_6$). The halogen component of the gas mixture is generally corrosive, and in the discharge it is partially converted to other reactive halogenated compounds. This results in rapid corrosion of exposed surfaces which are not halogen compatible. Material corrosion depletes the halogen donor and produces chemical species which may degrade laser performance. It can be minimized by a judicious choice of materials for the laser body and gas handling system. More will be said about this aspect of the problem in Chapter 2.

(1.5.2) Gas contamination

There are several ways in which gas chemistry can severely degrade the performance of rare gas halide lasers. Most important among these are the following:

(i) The halogen donor is depleted through material corrosion and gas-phase reactions in the discharge.

(ii) Stable species are formed and these then absorb at the laser wavelength and collisionally deactivate the excited rare gas halide molecules and their metastable precursors.

(iii) Stable species are formed which then absorb in the UV spectral region where preionization takes place. They may also form negative ions through electron dissociative-attachment reactions. Both processes result in a filamentary discharge which degrades laser

performance.

Several studies of gas contamination in discharge and electron-beam excited rare gas fluoride lasers have been reported. Using a quadrupole mass spectrometer, Chow et al (1977) studied the consumption of NF_3 and the formation of NF_2 and N_2F_2 in discharge excited KrF lasers. Other stable species formed during the discharge were not investigated. The results showed that during laser action, the rate of depletion of NF_3 was almost constant, that NF_2 was produced and used, and that N_2F_2 accumulated in the laser cavity. It was suggested that a reservoir of NF_3 could be used to maintain the optimum partial pressure of NF_3, and that contaminants formed in the discharge could be removed using a cold trap at $-110^{\circ}C$.

Christensen (1977) identified CO_2, NO_2 and SiF_4, in fast discharge excited $He/Xe/NF_3$ mixtures after lasing ceased. The materials in contact with the gases were those of the perspex envelope, brass electrode mounts, stainless steel electrodes and fibre-glass epoxy dielectric. It was suggested that the formation of the above contaminants could be due to the reaction of nitrogen-fluorine compounds with SiO_2 present in the dielectric. Analysis of the spent gas mixture showed that only 30% of the original NF_3 had been lost after laser action ceased. Degradation of laser performance was attributed to the formation of stable species which quench the XeF excimer, as well as to NF_3 depletion.

Gower et al (1980) observed the formation of NO_2, SiF_4, CO_2, ClO_2, F_2CO, FNO, FNO_2, and NF_3 in fast discharge excited rare gas fluorine mixtures. The laser envelope consisted of a glass tube, and the electrodes were made of aluminium bars. Preionization was by a sliding-spark flash board mounted along one side of the main discharge

gap. In $He/Xe/F_2$ mixtures, absorption at the XeF laser wavelength (351nm) was measured as $0.1\% cm^{-1}$, and the absorbing species were identified as NO_2 and ClO_2. Fluorine depletion was through the formation of SiF_4, by chemical reactions with the glass envelope, and also of other fluorinated compounds. The use of high purity F_2, and of more compatible building materials was suggested for extending the gas life.

Gas contamination in electron-beam excited mixtures of $Ar/Xe/NF_3$ has been studied by Brannon (1982). The stable species present in spent gas mixtures were identified as N_2F_2, CO_2, CF_4 and oxides of nitrogen. The materials exposed to the gas mixture were aluminium (with traces of Si, Ti, Cu, Mg, Cr), stainless steel, viton and fused silica. Absorption at the laser wavelength (XeF, 351nm) was attributed to NO_2. Suggested methods of minimizing contaminant formation during laser action include the use of titanium getters, cold traps and high-purity gases.

With the exception of the mass spectral studies of Chow et al (1977), in all the above investigations the contaminants were identified from their IR absorption spectra. Consequently, dimers such as F_2, H_2, N_2 and O_2 were not detected due to their inactivity in the IR spectral region. Furthermore, although several species were identified there is as yet no report of their effects on laser performance.

(1.6) Gas-life extension

Even though the chemical processes which contribute to gas contamination are not well understood, various attempts have been made

to extend the gas life of rare gas halide lasers by reclaiming expensive rare gases such as Xe and Kr, using cold traps, getters and molecular sieves. Christensen (1977) has described a method in which XeF laser gas mixtures containing $He/Xe/NF_3$ are flowed through the laser, and the used gas stored in a dump tank to be processed at a later stage using two cold traps at $-150^{\circ}C$ and $-196^{\circ}C$ respectively. The first trap removes contaminants other than Xe and NF_3, and the latter are removed in the second trap. Using this procedure, approximately 95% of the Xe and 60% of the NF_3 were recovered. Helium and additional NF_3 were then added to produce a fresh gas mixture. Although the method can be used to recycle a single Xe fill several times, it requires a large volume of gas and wastes the helium dilutant.

Johnson et al (1978) have described a closed-cycle recirculating system to clean-up and reuse rare gas fluorine mixtures continuously. After passing through the laser, the fluorine in the gas mixture is removed by titanium getters at about $300^{\circ}C$. Fluorine reacts with the titanium to form titanium tetrafluoride, which sublimes from the hot region and is trapped on glass wool and in a dry-ice-acetone trap. The gas mixture is next flowed over titanium getters at $850^{\circ}C$, which remove O_2, N_2, H_2 and other contaminants. Fluorine is then added and the gas mixture is returned to the laser. The procedure consumes 2g of fluorine and 1.2g of titanium per hour. A similar technique has been used by Mandl et al (1982) to remove fluorine from $Ne/Xe/NF_3$ mixtures.

Gas-life extension in XeCl lasers has been investigated by Burlamacchi et al (1979). Cold traps, active carbon and molecular sieves were used to selectively remove contaminants. Best results

were obtained by flowing the gas mixture over a 3Å molecular sieve which was placed in the laser envelope. Using CCl_4 as the chlorine donor, the number of laser pulses to half-energy was increased from $15x10^3$ to $18x10^4$ shots. However the molecular sieve had to be saturated with CCl_4 before achieving the optimum performance. McKee et al (1980) have extended the lifetime of XeCl and KrCl lasers by adding small amounts (1 torr or less) of hydrogen to the gas mixtures. The gas-life of XeCl lasers was increased from 10^6 to $3x10^6$ shots to half-energy, and that of KrCl lasers from 10^4 to $2x10^5$ shots. The improved performance was attributed to the inhibition of the formation of absorbing species in the region of 230nm by hydrogen. It was suggested that the stability and lifetime of XeCl lasers may be strongly influenced by preionization-related effects rather than by photoabsorption at the laser wavelength. Similar procedures have been used by Kutschke et al (1981) to recover Xe from XeCl lasers. Their system can be modified to recover Kr and Xe from KrF and XeF lasers respectively.

(1.7) Thesis format

This thesis reports on a study of gas contamination in a rare gas fluoride laser, using a combination of mass spectral analysis and IR and UV absorption spectroscopy. Mass spectral analysis involves the separation and identification of the masses of the species in the sample being analysed. Consequently all species whose mass numbers fall within the range of the mass spectrometer can be detected, and quantitative measurements can be made quite easily. These aspects of mass spectrometry will be discussed in section (1.8).

The study has involved the following:

(i) The design and construction of a fluorine-compatible uv-preionized fast discharge excited laser.

(ii) The use of IR absorption spectroscopy to obtain initial information on the identity of infrared active contaminants formed in discharge excited mixtures of $He/Xe/NF_3$.

(iii) The use of a magnetic deflection mass spectrometer to identify stable species produced in the gas discharge, and to follow their formation and the rate of NF_3 depletion as a function of the number of XeF laser pulses.

(iv) An investigation of contaminant absorption at the laser wavelength using UV absorption spectroscopy.

(v) A study of the effects of several stable species on laser performance, to identify major contaminants.

(vi) The use of cold traps at several temperatures to extend the gas life.

Discussion of the experimental work starts in Chapter 2 with a detailed analysis of the design, construction, and performance of a uv-preionized fast discharge excited XeF laser. The laser was used in an investigation of gas contamination in $He/Xe/NF_3$ mixtures. The techniques and results of the investigation are the subjects of Chapter 3. The effects of several stable species on laser performance

is treated in Chapter 4, and Chapter 5 deals with the results of cold trap studies. Finally in Chapter 6, the results of Chapters 3, 4 and 5 are summarised. The remainder of this chapter is devoted to an outline of the basic ideas and concepts required in mass spectrometry. The general principle of operation of a magnetic mass spectrometer is explained. This is followed by a discussion of the inlet system, and of pressure requirements at the inlet and in the analyser tube of the mass spectrometer. Finally, qualitative and quantitative techniques of mass spectral analysis are briefly discussed.

(1.8) Principles of mass spectroscopy

A mass spectrometer is an instrument which analyses gas samples by the separation and identification of the masses of the species in the samples. The basic principle of a 180° deflection mass spectrometer is illustrated in fig. (1.2). The sample to be analysed is introduced in an analyser tube at low pressure (10^{-4} torr or less), and the molecules are ionized by a controlled beam of electrons from a hot filament. The positive ions so formed are pushed out of the source by a 'repeller' potential, and are then accelerated through a potential of a few thousand volts. After passing through a slit, they are deflected by a transverse magnetic field whose focusing properties are such that the ion beam is refocused on a second slit after a deflection of 180°. The ions which pass through the slit impinge on a collector where they give up their charge, and the ion current so formed is detected by an electrometer, amplified and displayed on a meter.

After acceleration through a potential V, an ion of mass m and charge e acquires an energy eV given by

$$eV = mv^2/2 \tag{1.3}$$

where v is the ionic velocity. In the magnetic field, the ion experiences a force evB which is given by

$$evB = mv^2/R \tag{1.4}$$

where R is the radius of the ionic path, and B the magnetic flux in the analyser. Eliminating v from equations (1.3) and (1.4) leads to

$$m/e = R^2B^2/2V \tag{1.5}$$

Some important conclusions can be drawn from equation (1.5). Firstly for given radius R and field B, the mass-to-charge ratio (m/e) of the particles which reach the collector, can be selected by varying the accelerating voltage. Since the radius of each ionic path depends on the value of m/e, the ion beam is separated into individual beams containing ions belonging to one particular value of m/e. These beams are successively brought in focus on the collector by scanning the accelerating voltage. The ion current so formed is recorded as a function of m/e to form a mass spectrum which is characteristic of the gas being analysed. In a multi-component system, each component is characterised by its own spectrum, and the overall result is the sum of the individual spectra.

Secondly, for given values of the field B and voltage V,

particles with mass nm and charge ne (n is an integer) arrive at the collector. This implies that the ion current at a mass peak may be due to the collection of singly or multiply ionised species, a fact which is important in the interpretation of mass spectra. Under normal operating conditions, most of the species are singly ionised. Doubly ionised particles are less frequent, and higher levels of ionisation are not normally encountered.

(1.8.1) Pressure requirements

The highest pressures at which analyser tubes operate is typically 10^{-4} torr. This upper limit is imposed by filament life, by non-linearity effects due to space charges in the source, and gas scattering in the analyser. In practice, the pressure of the analyser tube is kept well below 10^{-4} torr before the admission of a gas sample. This ensures that the mass spectrum of the sample is not masked by that of residual gases. Residual pressures of 10^{-8} torr or less are normally achieved with the combined use of a two-stage rotary pump, an oil diffusion pump and a liquid nitrogen cold trap.

For most applications, the inlet system to the mass analyser tube is pumped by a single or two-stage rotary pump so that the ultimate pressure under these conditions is typically 0.05 torr or less. However, for the determination of species which are present in low ppm, it is necessary to use a diffusion pump to further reduce the zero-flow pressure at the inlet.

(1.8.2) The sample inlet system

The low pressures at which analyser tubes operate makes it necessary to use some form of constriction between the sample and the mass spectrometer, so that high sample pressures can be used. The constriction must be such that it causes a negligible or predictable change in the composition of the sample to be analysed.

Gas flow through the constriction can be either viscous or molecular in nature. In the case of viscous flow, the pressure at the inlet of the constriction is so high that the mean free paths of the molecules in the sample are small compared to the dimensions of the constriction. Gas flow is then determined by the viscosity of the sample as a whole, and all the molecules travel with the bulk gas.

When the pressure is so low that the mean free paths of the molecules are large compared to the size of the constriction, the gas flow is molecular in nature. The flow of each component in the sample is then determined by its mass. For two components 1 and 2, the ratio of the number of molecules which pass through the constriction is given by (Tasman et al 1963)

$$N_1/N_2 = (M_2/M_1)^{1/2}(P_1/P_2) \qquad (1.6)$$

where N is the number of molecules passing through the constriction, M the molar mass and P the partial pressure. Equation (1.6) shows that under molecular flow conditions, lighter components are removed from the sample at a faster rate. As a result of this, the composition of the sample changes, and the latter becomes enriched with the heavier

components. The results of quantitative analysis must then be corrected by a factor equal to the inverse ratio of the square root of the molecular weights of the constituent gases.

The most generally used inlet system is the batch-handling system which is schematically shown in fig. (1.3). An inlet manifold is used to introduce a sample from a high-pressure source to a large reservoir. A tap is then used to admit the sample into the analyser tube using a porous plug leak. Since gas flow from the reservoir through the analyser tube and to the vacuum system is molecular in nature, continued sampling from the reservoir enriches the sample with species of high molecular weights. Errors due to this fractionation can be minimized by closing the inlet tap after a mass spectrum has been taken, and by using a large reservoir.

(1.8.3) Mass spectra of volatile halides

The volatile halides are generally very corrosive, and in addition to the usual problems of obtaining the spectra of molecular species, special care must be taken in the handling and sampling techniques to obtain reproducible results. The gas handling system must be made of halogen compatible materials, and it should be kept as simple and compact as possible to minimise the surface-to-volume ratio. In addition the mass spectrometer must be given time to passivate before a mass spectrum is taken. This is essential if the sample contains fluorine. In the case of fluorides such as CF_4, SF_6, SiF_4 and NF_3, extensive conditioning is not necessary.

(1.9) Identification and analysis of mass spectra

The mass spectrum of a gas mixture is interpreted with the use of 'fingerprint' spectra which are known as cracking patterns. These uniquely identify the molecules they represent. As an example, when CO_2 is introduced in the analyser tube of a mass spectrometer, the ions C^+, CO^{++}, O^+, and CO^+ are formed. These produce a characteristic mass spectrum with peaks at mass numbers 12, 14, 16 and 28 respectively. The relative intensities of these peaks is always the same, provided the conditions under which the spectrum is taken do not change. The cracking pattern then consists of a tabulation of the spectral peaks, with the most intense peak scaled as 100. The mass spectra and cracking patterns of some common gases (CO, CO_2, O_2, N_2) are given in fig. (1.4).

(1.9.1) Qualitative analysis

In a multi-component sample, the overall spectrum is the sum of the individual spectra of the components. If these do not overlap, the composition of the sample can be determined by comparing its mass spectrum with published tables of cracking patterns. This procedure makes use of the fact that a molecule is uniquely identified by its cracking pattern. In practice, overlapping of the individual mass spectra occurs, and the mass spectrum of the sample becomes very complex. Qualitative analysis is then difficult, and it is only possible to identify those components which have a unique peak in the overall mass spectrum. To determine the composition of the sample,

computational analysis of the mass spectral data is required.

(1.9.2) Quantitative analysis

Quantitative analysis of the mass spectrum of a gas mixture requires the knowledge of (i) the cracking patterns of the suspected components of the mixture and (ii) the sensitivity of the instrument at a mass peak in the spectrum of each possible component.

Under low pressure conditions (10^{-4} torr or less), the ion current I^+ at a given mass peak is linearly related to the parent gas pressure P in the analyser tube by

$$I^+ = SP \qquad (1.7)$$

where S is the sensivity in amps $torr^{-1}$. The sensitivity is a function of the mass number at which the ion current is measured. At higher pressures, non-linearity effects due to space charges and to gas scattering becomes important, and the sensitivity then becomes pressure dependent.

The partial pressure of a component of a gas mixture can be determined from equation (1.7), provided the mass spectrum of the mixture contains a peak which uniquely identifies that component, and the sensitivity and ion current at that peak are known. In practice, overlapping of the mass spectra of the components occur, and it is not possible to determine the partial pressure of every component separately. In such a case, a list of possible components is compiled by comparing the mass spectrum of the mixture with published tables of cracking patterns. The partial pressures of the components are then

determined by solving a set of simultaneous equations of the form:

$$\begin{aligned} i_1 &= S_{11}P_1 + \ldots\ldots\ldots\ldots + S_{1n}P_n \\ i_2 &= S_{21}P_1 + \ldots\ldots\ldots\ldots + S_{2n}P_n \end{aligned} \qquad (1.8)$$

$$i_m = S_{m1}P_1 + \ldots\ldots\ldots\ldots + S_{mn}P_n$$

where i_m is the measured ion current at mass m in the mass spectrum of the mixture, P_n the partial pressure of component n, and S_{mn} the sensitivity due to component n at mass m. In general, there are more unknowns than equations (n>m) and the problem must be solved using a least-squares method to find the partial pressures P_n.

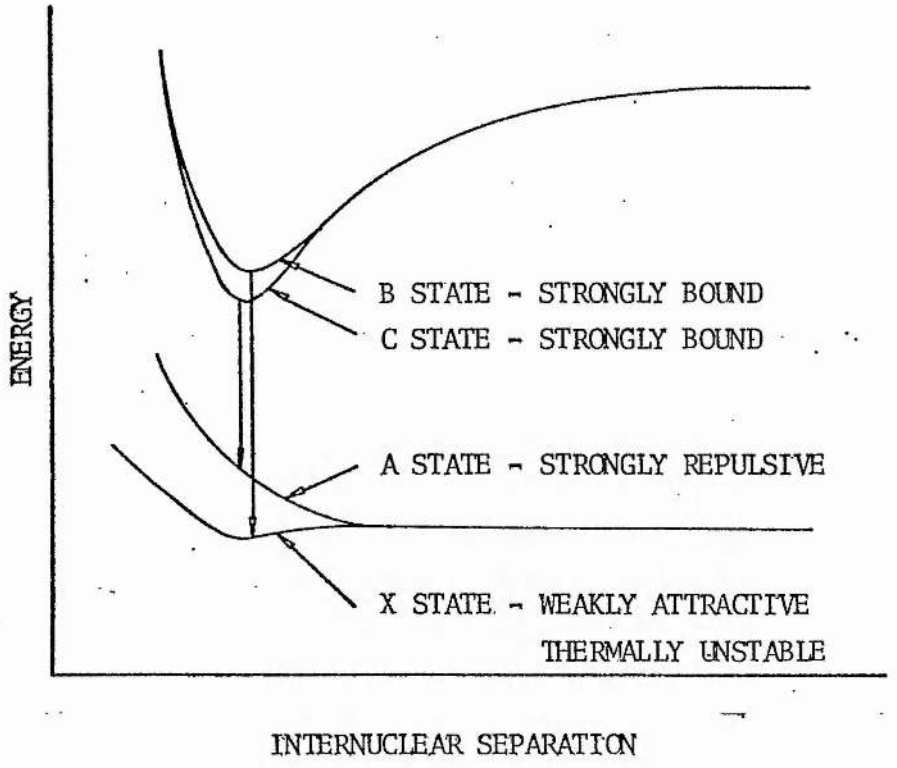

Fig.(1.1) Schematic potential energy diagram of rare gas halide molecule showing B→X and C→A transitions.

TABLE (1.1)

B→X and C→A laser emissions of rare gas halide molecules

Excimer	Transition	Wavelength nm	Reference
ArF	B→X	193	Hoffman et al 1976
KrF	B→X	249	Tellinghuisen et al 1976b
KrCl	B→X	222	Murray and Powell 1976
XeF	B→X	351	Tellinghuisen et al 1976c
XeF	C→A	481	Bischel et al 1981
XeCl	B→X	308	Tellinghuisen et al 1976a
XeBr	B→X	282	Tellinghuisen et al 1976b

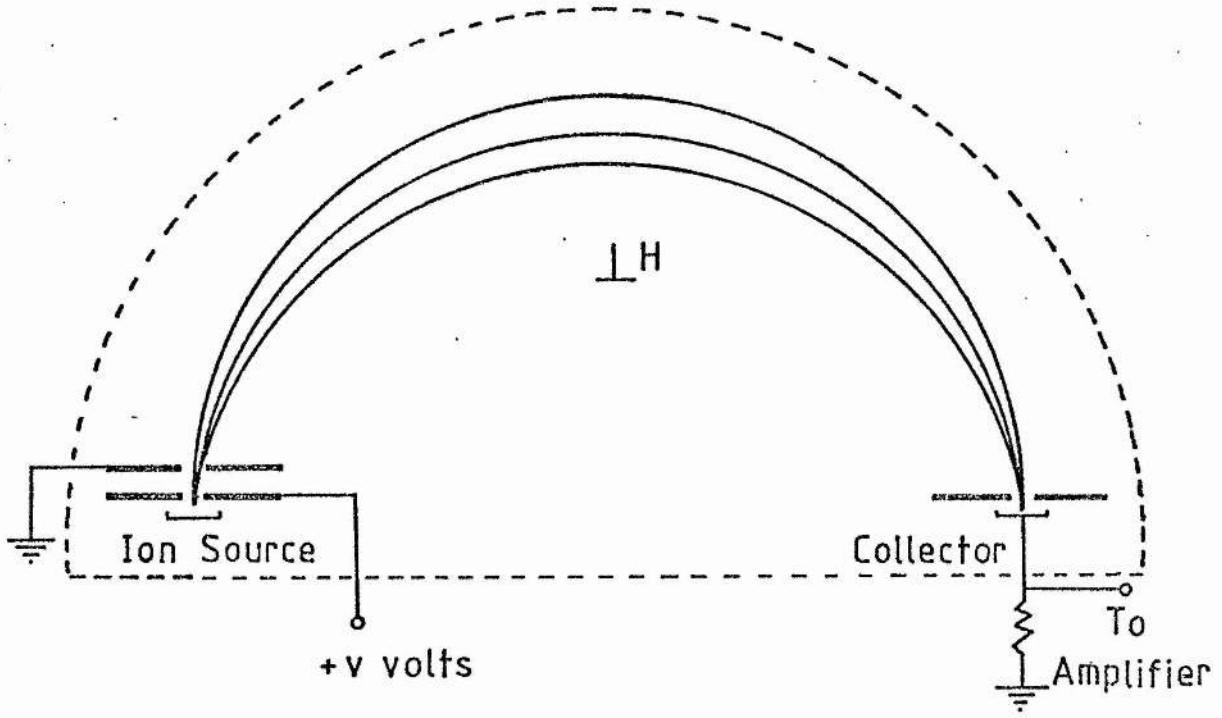

Fig. (1.2) Basic principle of a 180° deflection mass spectrometer.

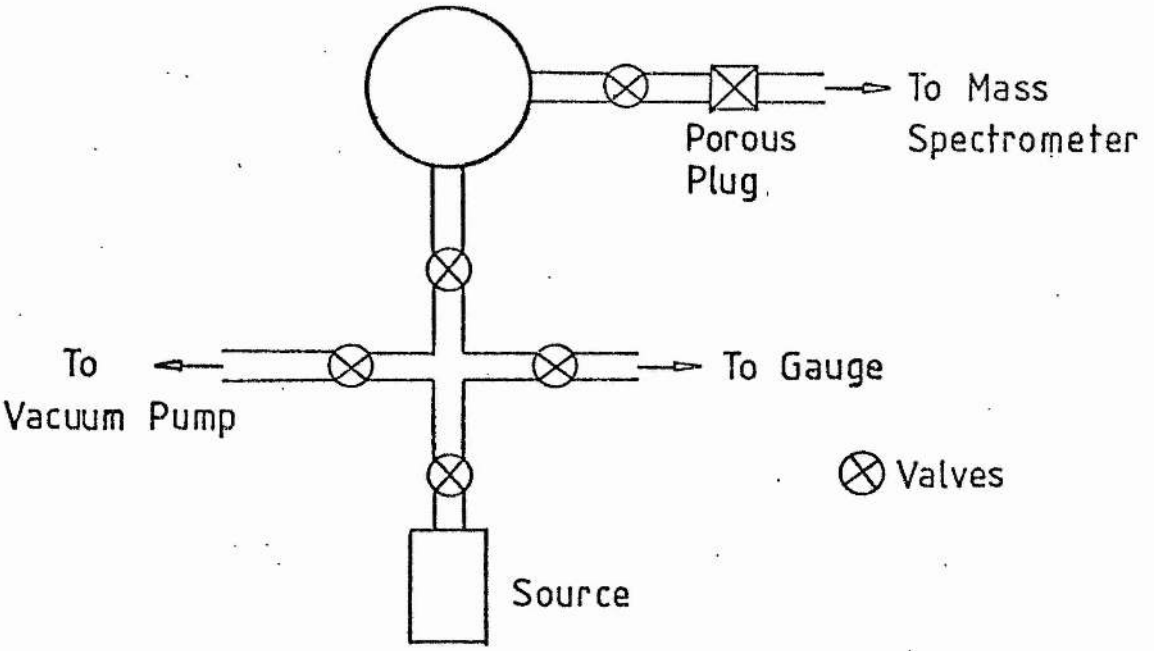

Fig. (1.3) Schematic diagram of batch-sampling inlet system.

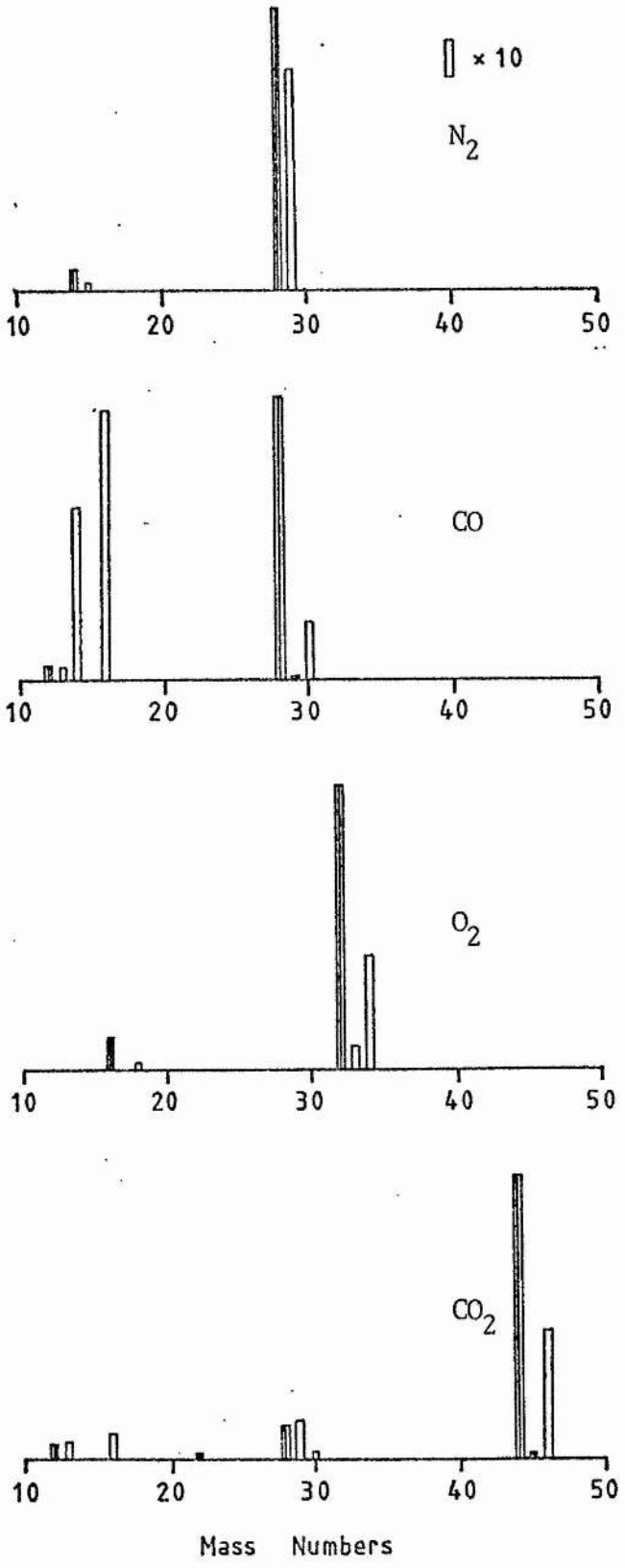

m/e	Relative Intensity
14	7.18
15	0.021
28	100.0
29	0.77
30	0.002

m/e	Relative Intensity
12	4.49
13	0.048
14	0.61
14.5	0.007
15	0.001
16	0.95
28	100.0
29	1.13
30	0.21

m/e	Relative Intensity
16	11.4
17	0.004
18	0.023
32	100.0
33	0.08
34	0.40

m/e	Relative Intensity
12	6.0
13	0.065
16	8.51
22	1.16
28	11.4
29	0.13
30	0.024
44	100.0
45	1.27
46	0.45

Fig. (1.4) Mass spectra and cracking patterns of N_2, CO, O_2 and CO_2.

CHAPTER TWO

THE XeF LASER SYSTEM

(2.1) Introduction

For the work reported in this thesis, a fast discharge excited XeF laser was built. In this chapter, the mechanical and electrical design, and the performance characteristics of the laser are presented. Section (2.2) deals with the general design requirements of high-pressure discharge excited rare gas halide excimer lasers. This is followed in section (2.3) by a description of the laser body and gas handling system. Section (2.4) is devoted to a discussion of the electrical circuitry, and finally in section (2.5), the performance of the laser is discussed.

(2.2) General design requirements

In discharge excited rare gas halide lasers, the surfaces of several materials are in contact with high-pressure gas mixtures (1 atm or more), containing several torr of a halogen donor (F_2, NF_3, HCl, CCl_4, etc.). The exposed surfaces include those of the laser envelope, gas-handling system, preionizer (corona wires, flashboard, etc.), laser windows and laser discharge electrodes. In the presence of highly reactive halogenated compounds, forming part of fresh gas mixtures or produced in the discharge, these surfaces can be rapidly corroded. This depletes the halogen donor, and produces stable species which may degrade laser performance. To achieve long-term

laser operation on single gas fills, it is at least necessary to build the laser system from halogen compatible materials.

The high pressures at which rare gas halide lasers operate presents other problems. The laser envelope and gas handling system must be built to sustain pressures of both vacuum and several atmospheres. Other problems derive from the instability of gas discharges at high pressures.

(2.2.1) High-pressure gas discharges

Transverse discharges in high-pressure gas mixtures are fundamentally unstable. At the onset of electrical breakdown, free electrons in the gas multiply rapidly through avalanche processes. Spatial non-uniformities in the electron distribution along the discharge then grow with time, and develop into constricted arcs. This has several adverse effects on laser performance.

(i) Laser pumping becomes inefficient due to the small excitation rates in the regions of low current density.

(ii) The distribution of refractive index in the gas becomes non-uniform, resulting in a laser beam of poor optical quality.

(iii) The discharge impedance collapses to a value which is well below that of the driving circuit. When this occurs, the discharge becomes impedance limited and it either self-terminates, or it reverts to an oscillatory mode with a resulting drop in the laser pulse energy.

(iv) The surfaces of metallic electrodes are changed in the regions of arc formation. This destroys the passivation of these surfaces to halogen attack, and so at least depletes the halogen donor.

To achieve long-term stable operation, it is therefore essential to inhibit the formation of discharge instabilities. Arc formation in high-pressure gas discharges is mainly due to the absence of strong diffusion of electronic and ionic species within the discharge volume (Levatter and Lin 1980). In low pressure transverse discharges, secondary electrons and ions produced during the avalanche process spread rapidly by diffusion to homogenize the ionization in the gas. Under these conditions, a glow discharge is normally obtained. In high pressure gas discharges similar to those used in rare gas halide lasers, the ability of ions and electrons to diffuse throughout the discharge volume is limited. In rare gas halide lasers, the high electronegativity of the halogen component of the gas mixture makes the discharge even more sensitive to changes in the electron distribution. To achieve a uniform glow discharge, some form of preionization must be used to distribute primary electrons uniformly along the length of the high pressure discharge. In addition, the laser electrodes must have smooth contours so that there are no strong localised electric field gradients. These enhance the electron formation process, and thus destroy homogeneous electron distributions achieved through preionization. Specially contoured electrodes that produce a uniform electric field distribution on the electrode surfaces have been studied by Rogowski (1923), Bruce (1947), Chang (1973), and Stappaerts (1982).

Levatter and Lin (1980) have investigated the necessary preionization levels for the formation of a uniform pulsed discharge at high gas pressures in $He/Xe/F_2$ mixtures. The minimum initial number density of free electrons needed to maintain a homogeneous discharge was found to be in the range of 10^4 to 10^6 electrons/cm^3 at one atmosphere, and 10^5 to 10^7 electrons/cm^3 at 6 atmospheres. The results also showed that the minimum preionization level required for homogeneous discharge initiation decreases with increasing voltage risetime, due to an increase in diffusive spreading of the electron avalanche head. Shin Sumida et al (1981) have shown that the laser pulse energy and pulse width (FWHM) are logarithmic functions of the initial electron density. The laser discharge parameters were only slightly dependent on preionization electron densities in the device used.

Arc formation in high-pressure gas discharges is also inhibited by the use of fast-rising voltage pulses of short duration. This ensures that laser action occurs before discharge instabilities have time to develop. To obtain fast discharge excitation, it is necessary to minimize the inductance of the electrical circuit used to excite the gas mixture. This is normally achieved by using (i) Blumlein circuits with low-inductance storage capacitors, (ii) low-inductance high-voltage switches to initiate the laser discharge, and (iii) compact arrangements of all electrical components to minimize the size and hence the inductance of discharge loops. In practice, the minimum size of the laser system is determined by high-voltage breakdown considerations, and the need to mount a preionizer inside the laser envelope.

Another method of inhibiting arc formation involves the use of ballast resistors (Sze and Scot 1976) to limit the discharge current density in the regions of arc formation. This technique makes use of the large increase in the current density in an arc to reduce the electric field by a 'negative feed-back' effect, thus terminating the arc formation process. Using resistive stabilisation of a discharge excited XeCl laser, Hogan et al (1980) have obtained pulse energies up to 15mJ, and laser pulse-widths of 80nS (FWHM).

(2.2.2) Preionization techniques

Several preionization techniques have been successfully used to obtain glow discharge operation in high-pressure rare gas halogen mixtures. These include the use of UV radiation from spark-arrays (Sze and Loree 1978, Watanabe et al 1981), and corona discharges (Burnham et al 1976a, Hasson and Von Bergman 1979, Fahlen 1979), and the use of x-rays (Shin Sumida et al 1978, Shields and Alcock 1982). In the spark-array technique, UV radiation is generated by a series of sparks distributed along the length of the laser. The sparks are formed in devices similar to the one shown in fig. (2.1). To achieve optimum laser performance, the voltage pulse applied to the laser electrodes must be delayed by as much as ten microseconds (Akins et al 1978) with respect to that applied to the spark array. The finite delay is attributed to the time required for attachment and recombination processes to homogenize the ionization in the gas, prior to initiating the main discharge (Hsia 1977). Separate pulse forming networks are normally used to drive the preionizer and the laser, so

that the delay between the two discharges can be optimized.

In the corona preionization technique, fine wires lying parallel to the laser axis are connected to one of the laser electrodes by small coupling capacitors C_p, as shown in fig. (2.2). When the main discharge is initiated, a sheet discharge is produced between the wires and one of the laser electrodes. This discharge, which is limited in energy by the coupling capacitors (5 -> 10% of the stored energy), generates UV radiation for preionization. Corona surface discharges have also been used as sources of UV radiation (Hasson et al 1977). In both the corona and spark array techniques, the preionizer is either mounted in a plane normal to that of the main discharge (Chen Jianwen et al 1980, Burnham et al 1976), or behind a perforated electrode (Fahlen 1979, Watanabe et al 1981). The latter confines the discharge to a region near the centre of the electrodes, and thus relaxes the need for specially contoured electrode surfaces. The corona technique has several advantages over the spark-array preionization method. It is simple in construction, and does not require a separate pulse forming network, since it has been found that the main discharge need not be delayed with respect to that applied to the corona wire (Fahlen 1979). Another advantage is that low energy corona discharges are less likely to contribute to gas contamination than high-energy spark-arrays, in which sputtered materials may react with halogenated species in the discharge.

X-ray preionization of rare gas halide lasers was first demonstrated by Shin Sumida et al (1978) in a fast discharge excited KrF laser. The laser pulse energy was four times that obtained using corona preionization, and a broad maximum in output energy was observed at pressures up to 5 atmospheres. Using similar

preionization techniques in a discharge excited XeCl laser at pressures of 1 -> 4 atmospheres, Levatter et al (1981) obtained pulse energies of 3.2J/litre with an intrinsic efficiency of 4%. The laser pulse-width was 200nS. Compared to the spark-array and corona preionization techniques, x-ray preionization is complex and expensive. However it has two advantages: (i) it can be used to homogeneously preionize large volumes of high-pressure gas mixtures, and (ii) the preionization source does not contribute to gas contamination, because it is mounted outside the laser envelope.

(2.3) Laser construction

The laser used in this work was built with the aim of achieving halogen compatibility and arc-free operation at pressures of one atmosphere or more. To obtain fast voltage risetimes, the laser discharge was excited using a Blumlein circuit, with striplines as storage capacitors. Since high pulse energies were not considered to be important for this work, low capacitance striplines which were available at the time were used. The laser discharge was initiated by a low inductance spark gap. Corona preionization was chosen because of its simplicity, in comparison with other methods. In the remainder of this chapter, the mechanical and electrical configurations, and the laser output characteristics are considered in detail.

(2.3.1) Mechanical

The choice of materials for the laser envelope of discharge excited rare gas halide lasers is governed by the following

requirements: (i) the materials should be good insulators, to reduce the possibility of electrical breakdown at high voltages, (ii) they should be rigid and of high tensile strength, to sustain the high pressures at which rare gas halide lasers operate, and (iii) they should be compatible with the halogens, to minimize gas contamination and depletion of the halogen donor. The first two requirements are satisfied to varying degrees by several common materials such as unplasticised polyvinyl chloride (UPVC), polyvinylidene fluoride (PVDF), polytetrafluoroethylene (PTFE), perspex and nylon. Of these, only PVDF and PTFE are compatible with the halogens. PTFE is by far the best material in terms of its resistance to chemical attack. However, it tends to flow under stress, and it is porous (Foon and Kaufman 1975, Bailey 1964). Table(2.1) shows that the permeabilities of PTFE to common gases is significantly higher than those of perspex, nylon and viton. Similar data was not available for PVDF and UPVC. PVDF is structurally more rigid than PTFE, does not suffer from cold-flow problems, and is compatible with the halogens at room temperature. At higher temperatures (60^{o}C and above) it is attacked by fluorine, but it then forms a protective layer of PTFE (Laser Focus, staff report, September 1980, p. 22). Water absorption by PVDF and PTFE is typically 0.03% and <0.01% respectively.

From the information available, it is difficult to decide which of the two materials is more suitable. PVDF is structurally better than PTFE, but the latter appears to be more resistant to halogen attack. A PVDF pipe was used as the basis for the laser envelope. However, the choice of PVDF over PTFE was mainly determined by its availability at the time of construction.

Metallic components which are exposed to the gas mixture must

also be chosen for their halogen compatibility. Several materials are available, and in order of suitability they are nickel, monel, stainless steel and aluminium. Both stainless steel and aluminium form passive layers when exposed to the halogens.

(2.3.2) The laser body

Schematic drawings of the laser system are shown in figs. (2.3) and (2.4). The laser envelope consists of a PVDF pipe which is 62 cm long, with inner and outer diameters of 7 cm and 9 cm respectively. The inner diameter of 7 cm was chosen to minimize the size of the main discharge loop, and at the same time to accommodate corona wires at distances of about 2.5 cm from the surfaces of the laser discharge electrodes. Smaller separations lead to arcing between the wires and electrodes. The ends of the laser are sealed to one inch thick circular teflon flanges. Quartz windows were initially used, but due to corrosion problems, they were later replaced by one inch diameter and 1/4 inch thick calcium fluoride windows. The latter are mounted on centrally placed openings in the teflon flanges. The whole assembly is held together by four stainless steel rods which are bolted to nylon flanges as illustrated in fig. (2.4). All components are sealed with viton 'O' rings.

The laser electrodes are made from 2cm thick aluminium bars (containing 0.1% Cu, 0.5% Mg, 0.7% Si, 0.5% Fe, 0.4% Mn, 0.2% Zn, 0.25% Cr and 0.2% Ti). They are 53cm long and are separated by 2cm. The electrode surfaces facing the discharge have simple rounded edges and tapered ends, to reduce field enhancement. The opposite surfaces are machined to the radius of the inner surface of the PVDF pipe. To

minimize the inductance of the laser discharge loop, the electrodes are connected to external storage capacitors at 25 equally spaced points along their lengths. Sealing to the PVDF pipe is achieved using strips of viton sheets 2cm in width. The laser envelope has been successfully tested to 5 atmospheres, which is well above the operating pressure range of 1 to 2 atmospheres.

The optical cavity consists of a calcium fluoride flat (one of the laser windows) at one end, and an externally mounted 2m total reflector at the other. The latter is multi-coated for maximum reflectivity at the XeF laser wavelength (351nm). The distance between the mirror and the calcium fluoride output coupler is roughly one metre.

(2.3.3) The "gas-handling" system

A schematic drawing of the "gas-handling" system is shown in fig. (2.5). All gas connections are made from 1/4 inch O.D. monel, teflon and stainless steel pipes, using Swagelock couplings. The gas taps are in monel (Nupro M-4BK) and stainless steel (Nupro SS-4BK). The use of stainless steel was kept to a minimum. Three gauges are used to monitor gas pressure in the laser. In the low pressure region, an Edwards gauge with a range of 0 -> 40 torr is used. The gauge has brass wetted parts, and it is isolated during laser operation to prevent corrosion by halogenated compounds. The two other gauges cover the pressure range of 0 -> 4atm. The first is an Edwards Capsulon gauge (inconel wetted parts, 0 -> 760 torr absolute), and the second is a Matheson gauge (monel wetted parts, 0 -> 4atm gauge).

The whole system can be evacuated to 60um, using a single-stage rotary pump, and the leak rate is less than 0.1 torr/hour. The gas mixture is circulated using a Vanton pump (Vanton CC-B series) which has a viton body and flexible lining. The maximum flow-rate on line is 3 litres/min. This is roughly equivalent to a single gas change in the laser every minute.

(2.4) Electrical

Several electrical configurations have been used to excite rare gas halide lasers. These include L-C inversion circuits (Burnham and Djeu 1976); Blumlein circuits with charged coaxial cables (Fahlen 1979), lumped element transmission lines (Sarjeant et al 1977), and striplines (Burnham et al 1976b); and charge-transfer (C-C) circuits (Burnham et al 1976a). Of these methods, Blumlein excitation has produced the highest efficiencies and pulse energies (Chen Jianwen et al 1980, Levatter et al 1981). This is mainly due to the fast voltage and current risetimes which can be achieved in Blumlein devices.

The lumped element equivalent circuit of a conventional spark gap switched flat-plate blumlein configuration (Schawb and Hollinger 1976) is shown in fig. (2.6). In the equivalent circuit, C_1 and C_2 represent parallel plate storage capacitors with inductances L_1 and L_2 respectively, R_g is the spark gap impedance, R_{L1}, R_{L2} the laser discharge impedance before and after discharge initiation respectively, L_g the spark gap inductance, and L_L the inductance of the laser discharge loop.

The values of C_1, C_2, L_1, and L_2 can be estimated from the physical dimensions of the storage capacitors. The capacitance C is

given by

$$C = kE_oA/d \tag{2.1}$$

and the inductance L/unit length by

$$L = ud/w \tag{2.2}$$

In these expressions, k is the dielectric constant, E_o the permittivity, u the permeability, A and w the surface area and width of the capacitor plates, and d the thickness of the dielectric.

The parameters L_g, R_g and R_{L2} can be estimated from the ringing frequencies and attenuations of voltage oscillograms. Prior to gas breakdown in the laser, the secondary loop containing L_g, R_g and C_1 is equivalent to a simple LCR circuit, provided that L_1 is small compared to the total loop inductance. This condition is normally satisfied, since in practice the inductance of the storage capacitors is of the order of 1nH. The voltage V across C_1 is then given by

$$V = (V_o/w)e^{-at}(w\cos(wt) + a\sin(wt)) \tag{2.3}$$

where

$$a = R_g/2L_g \tag{2.4}$$

and

$$w^2 = 1/L_gC_1 - (R_g/2L_g)^2 \tag{2.5}$$

If $(R_g/2L_g)^2 < 1/L_gC_1$, the ringing frequency (f) can be approximated by

$$f = 1/2\pi(L_gC_1)^{1/2} \tag{2.6}$$

from which L_g can be determined if f and C_1 are known. The attenuation constant $R_g/2L_g$ can then be used to determine the impedance R_g. The laser discharge loop inductance L_L can be estimated using the single-turn solenoid formula (Ramo et al 1965)

$$L_L = \pi u R^2/(X + 0.9R) \qquad (2.7)$$

where X is the length and R the radius of the solenoid. The laser discharge impedance RL_2 can then be obtained from the exponential decay of the voltage across capacitor C_2.

The electrical characteristics of the Blumlein discharge circuit have been studied using a simple computer model based on the lumped element equivalent circuit of fig. (2.6). The aim of the study was to investigate the effects of the electrical parameters on voltage and current risetimes, which determine the stability of the discharge and the useful energy deposited in the gas, respectively. The equivalent circuit of fig. (2.6) can be described by a set of first-order differential equations of the form:

$$\dot{Y}_1 = Y_2 \qquad (2.8)$$

$$\dot{Y}_2 = (2(Y_3 - Y_1)/C_1 - R_g Y_2 - \dot{R}_g Y_1)/L_g \qquad (2.9)$$

$$\dot{Y}_3 = Y_4 \qquad (2.10)$$

$$\dot{Y}_4 = 2(Y_5 - 2Y_3 + Y_1)/C_1 L_1 \qquad (2.11)$$

$$\dot{Y}_5 = Y_6 \qquad (2.12)$$

$$\dot{Y}_6 = (2(Y_3 - Y_5)/C_1 - 2(Y_5 - Y_7)/C_2 - R_L Y_6 - \dot{R}_L Y_5)/L_L \qquad (2.13)$$

$$\dot{Y}_7 = Y_8 \qquad (2.14)$$

$$\dot{Y}_8 = 2(Y_5 - 2Y_7)/C_2 L_2 \qquad (2.15)$$

where $Y_1 = I_1$, $Y_2 = \dot{I}_1$, $Y_3 = I_2$, $Y_4 = \dot{I}_2$, $Y_5 = I_3$, $Y_6 = \dot{I}_3$, $Y_7 = I_4$, $Y_8 = \dot{I}_4$, with I_1, I_2, I_3 and I_4 as shown as fig. (2.6). Equations 8 -> 15 were solved using a variable-order variable-step Gear method (NAG routine D02QBF, St Andrews University VAX computer), subject to the following initial conditions:

$$Y_i = 0.0 \quad i = 1, 3 \rightarrow 8 \tag{2.16}$$

$$Y_2 = V_o/L_g \tag{2.17}$$

where V_o is the supply voltage. The Fortran computer program is listed in Appendix 1.

The impedance of pressurized spark gaps collapses in a time which is short (typically 1nS) compared to the ringing time of the secondary loop containing the spark gap (Cary and Mazzie 1979). Consequently, in the present model the spark gap impedance is assumed to be constant and equal to R_g which is the value after spark gap closure. The laser discharge impedance R_{L1} before gas breakdown is taken as 10^6 ohms. The other parameters are assigned values which are typical of small spark gap switched Blumlein devices. Gas breakdown in the laser is assumed to occur at the peak of the voltage pulse V_L across the laser electrodes. The results of the analysis can be summarised as follows:

(i) The temporal variation of voltage V_L across the laser electrodes is determined by the rate of change of voltage V_1 across capacitor C_1. The latter is in turn determined by the inductance of the secondary loop containing the spark gap. Figure (2.7) shows that

to achieve fast voltage risetimes, for a given value of the stripline capacitance, it is essential to minimize the inductance of the spark gap. This result is consistent with that of equation (2.6), which shows that the rate of rise of voltage V_1 is inversely proportional to the square root of the spark gap inductance.

(ii) The rate of current rise in the laser gas is determined by the inductance of the main discharge loop. To obtain large power deposition, the discharge current should peak soon after gas breakdown. Figure (2.8) shows that this can be achieved by minimizing the inductance of the laser discharge loop.

(iii) Due to voltage ringing in the arm containing the spark gap, the voltage V_L across the laser electrodes is higher than the supply voltage V_o. Just before the spark gap breaks down, the voltage across the laser electrodes is zero. At the instant of spark gap closure, the secondary circuit oscillates with a frequency given by equation (2.5). This causes V_L to rise towards $2V_o$. In practice, voltage doubling is not normally observed due to gas breakdown in the laser at a lower voltage.

(iv) Figure (2.9) shows the current variation in the laser gas as a function of the stripline capacitance. This result was obtained with the assumption that gas breakdown in the laser occurs when the voltage across the laser electrodes reaches its optimum value. Figure (2.9) shows that the smaller the capacitance of the stripline, the larger the rate of current rise in the laser gas.

(2.4.1) Electrical circuit

The results of section (2.4) were used as general guidelines for building the electrical circuit of the laser. The latter is excited using a conventional low impedance flat-plate Blumlein circuit, similar to that shown in fig. (2.3). The electrical circuit is shown in fig. (2.10), using lumped parameters. Capacitors C_1 and C_2 are made of double-sided copper clad fibre-epoxy sheets. High voltage breakdown along the edges of the capacitors is inhibited by etching the copper surfaces to form insulating strips 3cm wide on one surface, and 2cm wide on the other surface. The strips are staggered on opposite sides to reduce the possibility of dielectric breakdown at the edges of the copper surfaces due to the high electric fields in these regions. Failure to stagger results in a significant reduction in the life of the capacitors. After etching, C_1 and C_2 have a capacitance of 6nF each. Capacitor charging is from a high-voltage supply (0->30 KV dc), which is connected to the plate common to C_1 and C_2 as shown in fig. (2.10). The plate of C_1 which is adjacent to the high-voltage switch is earthed.

Preionization is achieved by mounting a fine corona wire on each side of the electrodes. Each wire is connected to earth through a 350pF capacitor which limits the energy deposited in the corona discharge to about 6% of the total stored energy. Wires of various diameters were used, and the thinnest wire available at the time (high corrosion resistance stainless steel, 0.15mm diameter, containing 0.12% C, 17% Cr and 8% Ni) worked best when mounted at a distance of 2.5cm from the electrodes. At smaller distances, arcing occurred

between the wires and the high-voltage electrode. This arcing resulted in a deterioration of the main discharge, due to inadequate preionization.

The gas discharge is initiated by a low-inductance spark-gap switch (6.5nH), built as shown in fig. (2.11). The high voltage electrode is made of a brass disc with rounded edges, and the trigger electrode consists of an outboard motor spark plug (Champion Spark Plug Co., type L-76V). The gap separation is 3 mm. The spark gap is pressurized with nitrogen at one to three atmospheres, depending on the supply voltage, and it is triggered by 1us pulses from a high-voltage pulse generator.

To reduce electrical noise in the vicinity of the laser, the latter is enclosed in a shielded cage which is earthed to the mains earth through the high-voltage supply. All other earth connections are made at the same point on the cage. This prevents multiple grounding of the circuitry, which would otherwise generate excessive amounts of electrical noise.

To check the validity of the computer model discussed in section (2.4), comparisons of calculated and experimentally measured voltage waveforms have been made. The electrical parameters used in the analysis were determined using the methods discussed in section (2.4). The voltage waveforms were measured using a Tektronix high voltage probe (type P6015, with an attenuation ratio of 1000:1 and a risetime of 4.6nS), and a fast Tektronix storage oscilloscope (Tektronix 7854). Figure (2.12) shows measured and theoretically determined temporal variations of voltage V_1 across capacitor C_1, in the absence of gas breakdown in the laser. This was achieved by filling the latter with one atmosphere of nitrogen. The agreement

between the two waveforms is good.

Computed and experimentally obtained voltage waveforms V_L across the main electrodes are shown in fig. (2.13). The initial voltage rise is well predicted. However after gas breakdown occurs, agreement between the computed and experimental curves is poor. This is attributed to the slow response of the high-voltage probe, and to the effects of stray inductances in the probe connections (Schawb and Hollinger 1976). These effects are enhanced by the fast current rise in the laser after gas breakdown. The voltage risetime of 20 nS across the laser electrodes justifies the use of a lumped parameter equivalent circuit in the analysis, as opposed to a transmission line approach. The condition for travelling wave excitation is that the voltage risetime across the laser electrodes is less than the two-way transit time on the transmission line. In the present case, the two-way transit time is roughly 2nS, which is an order of magnitude smaller than the voltage risetime. Consequently, this makes the transmission line approach inapplicable.

(2.5) Laser performance

Prior to operating the laser on rare gas halide mixtures, the laser body and gas manifold were treated with fluorine. This was done to determine the degree to which the whole system could be passivated. The laser was filled with 50 torr of fluorine, and after several hours, it was evacuated and refilled. The procedure was repeated several times. Figure (2.14) shows temporal variations of the partial pressure of fluorine for the first three fills. The rate of fluorine consumption decreased significantly with successive

fills. The amount of fluorine consumed for the first and third fills were 44% and 9% respectively. This indicates significant passivation of the laser envelope and gas manifold.

After passivation by fluorine, the laser envelope was not opened to the atmosphere unless it was essential to do so. When the need did arise, the laser was pressurised with nitrogen or helium to above one atmosphere, before the laser windows were removed. This was done to prevent moisture from entering the laser, since this invariably leads to corrosion of metal surfaces and of the laser windows, if the latter are of quartz (within minutes, a white sludge is formed on quartz windows which must then be repolished).

The laser gas mixture consists of grade A helium, research grade xenon (both from BOC Special Gases), and technical grade NF_3 (from Air Products), with typical analysis (supplied by the manufacturers) as shown in table (2.2). The gases were used without further purification. Gas mixing was done in the laser using the following procedure: NF_3 and Xe were first introduced, and He was then added in bursts of a few hundred torr at alternate ends of the laser. The gas mixture was then circulated for approximately five minutes, after which the laser was operated. Using this procedure, the initial pulse energy was reproducible to within 2% for successive fills.

Optical spectra of the laser pulses were recorded using an optical spectrum analyser, whose wavelength scale was calibrated using a mercury lamp. A typical spectrum is shown in fig. (2.15). Laser action is achieved on two lines at 351nm and 353nm, corresponding to the 0 -> 2; 1 -> 4, and 0 -> 3 transitions of the XeF molecule respectively (Tellinghuisen et al 1978). Figure (2.16) shows the temporal characteristics of a laser pulse, which was obtained using a

fast photodiode (ITT TF1850-M20 with S20 response, and sub-nanosecond risetime), and a fast Tektronix storage oscilloscope (Tektronix 7834). Two optical pulses are observed separated by 20nS. The width of the main pulse is 7nS (FWHM). Weak laser action in the red is also observed in the vicinity of the high-voltage electrode. This is attributed to emission from neutral atomic fluorine formed in the discharge (Lawler et al 1979, Bigio and Begley 1976).

The laser pulse energy was measured using a Laser Precision Corp. energy meter (model Rj 7200). Figures (2.17) and (2.18) show the variation of the pulse energy with the partial pressure of NF_3 and Xe respectively. At a total pressure of one atmosphere, the optimum pulse energy is achieved with a mixture of $He/Xe/NF_3$ in the ratio of 350:6:1. The optimum partial pressure of NF_3 is 1.5 to 2 torr at total pressures up to 2 atmospheres. The decrease in pulse energy at higher pressures of NF_3 is partly due to collisional quenching of XeF^* by NF_3 (Burnham et al 1976a), and to a deterioration of the discharge homogeneity. In fact, if the partial pressure of NF_3 is above 4 torr, severe arcing occurs and laser emission is not observed . The decrease in the pulse energy at high Xe concentrations is mainly due to quenching of XeF^* by Xe (Rokni et al 1977), and to photoabsorption at the laser wavelength by Xe_2^+ (Champagne and Harris 1977). The laser has been operated at pressures up to 2 atmospheres on very lean gas mixtures. Figure (2.19) shows the variation of the pulse energy with total gas pressure for a mixture containing 0.3% NF_3 and 1.6% Xe. The optimum laser pulse energy is achieved at a pressure of about one atmosphere. The sharp drop in the pulse energy above one atmosphere is mainly due to insufficient preionization of the main discharge. Above 2 atmospheres, arcing occurs and laser action is severely

degraded. Figure (2.20) shows the variation of the pulse energy as a function of the supply voltage. At 25 KV, the optimum pulse energy is about 4mJ, corresponding to an overall efficiency of 0.1%.

The variation of the pulse energy with the number of laser pulses is shown in fig. (2.21). The maximum number of laser pulses to half-energy is typically 250 shots. This corresponds to about 100 pulses/litre atm. The fast decay of the laser energy has been investigated with the aim of determining the processes responsible for the short gas-life. In the chapters that follow, the results of the study are presented.

TABLE (2.1)

Permeability constants at ambient temperatures

	Permeability (cm^3 cm^{-2} cm (thickness) s^{-1} (cm Hg)$^{-1}$(pressure difference))			
Material	Nitrogen	Oxygen	Hydrogen	Helium
PTFE	3.1×10^{-10}	1.0×10^{-9}	2.4×10^{-9}	7.0×10^{-8}
Perspex	$< 10^{-11}$	$< 10^{-11}$	3.3×10^{-10}	7.0×10^{-10}
Nylon 31	$< 10^{-11}$	$< 10^{-11}$	1.6×10^{-11}	3.7×10^{-11}
Nylon 51	$< 10^{-11}$	$< 10^{-11}$	6.3×10^{-11}	1.1×10^{-10}
Viton A	$< 10^{-11}$	$< 10^{-11}$	2.7×10^{-10}	1.0×10^{-9}

TABLE (2.2)

Typical analysis of the components of the laser gas mixture

Helium (grade A)

He	99.998%
Ne	5vpm
N_2	2vpm
O_2	2vpm
Ar	< 1vpm
H_2	< 1vpm
CO_2	< 1vpm
H_2O	3vpm
Hydrocarbons	< 1vpm

Xenon (research grade)

Xe	99.995%
Kr	40vpm
Ar	< 1vpm
N_2	5vpm
O_2	< 1vpm
CO_2	< 1vpm
H_2	< 1vpm
H_2O	< 1vpm
Hydrocarbons	< 1vpm

Nitrogen Trifluoride

(technical grade)

NF_3	98.6 %
O_2	0.6 %
N_2	0.1 %
CF_4	0.15%
N_2O	0.2 %
SF_6	0.05%
Reactive Fluorides	0.3 %

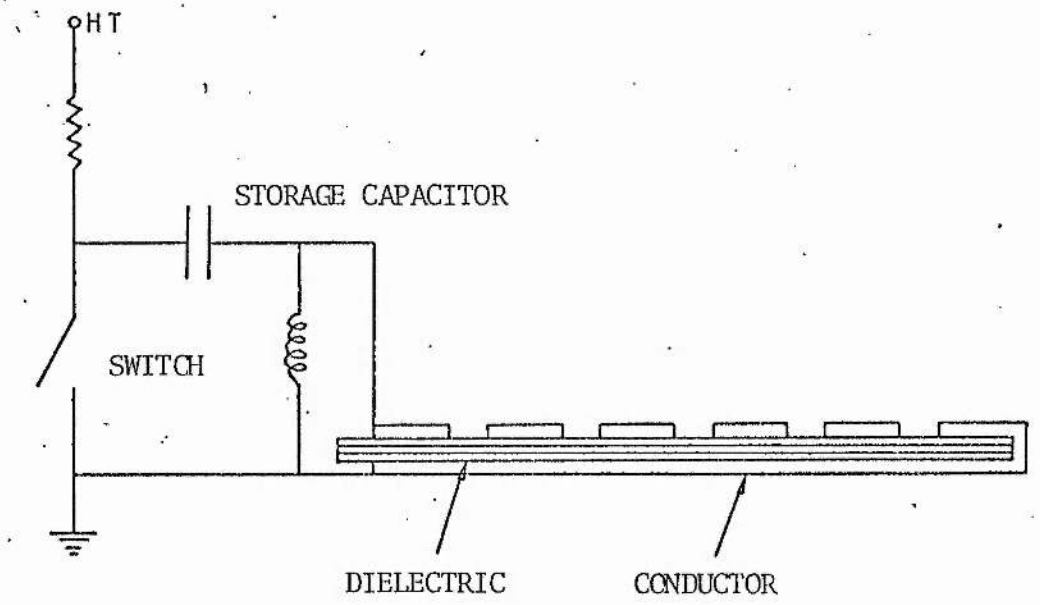

Fig.(2.1) Schematic diagram of spark-board preionizer.

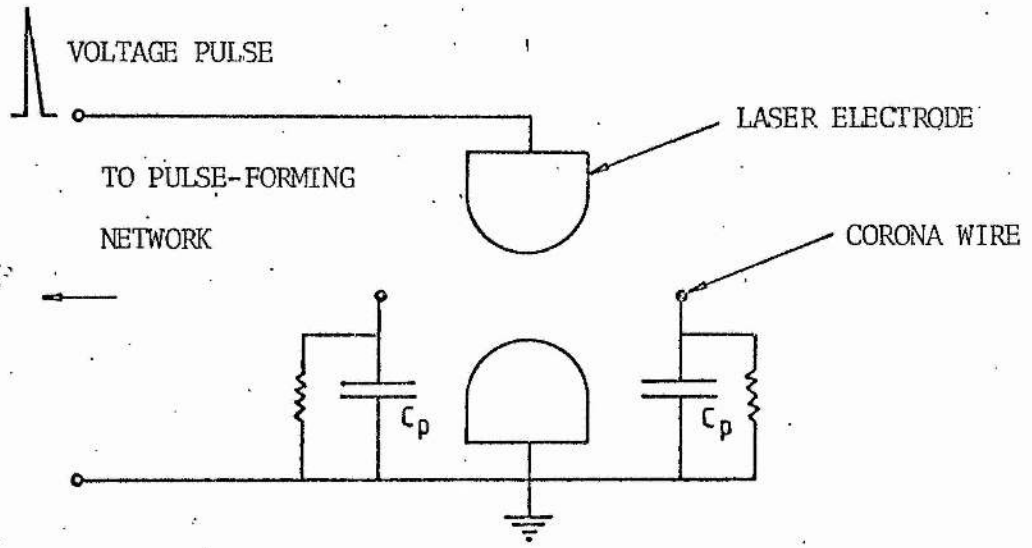

Fig.(2.2) Schematic representation of corona preionization technique.

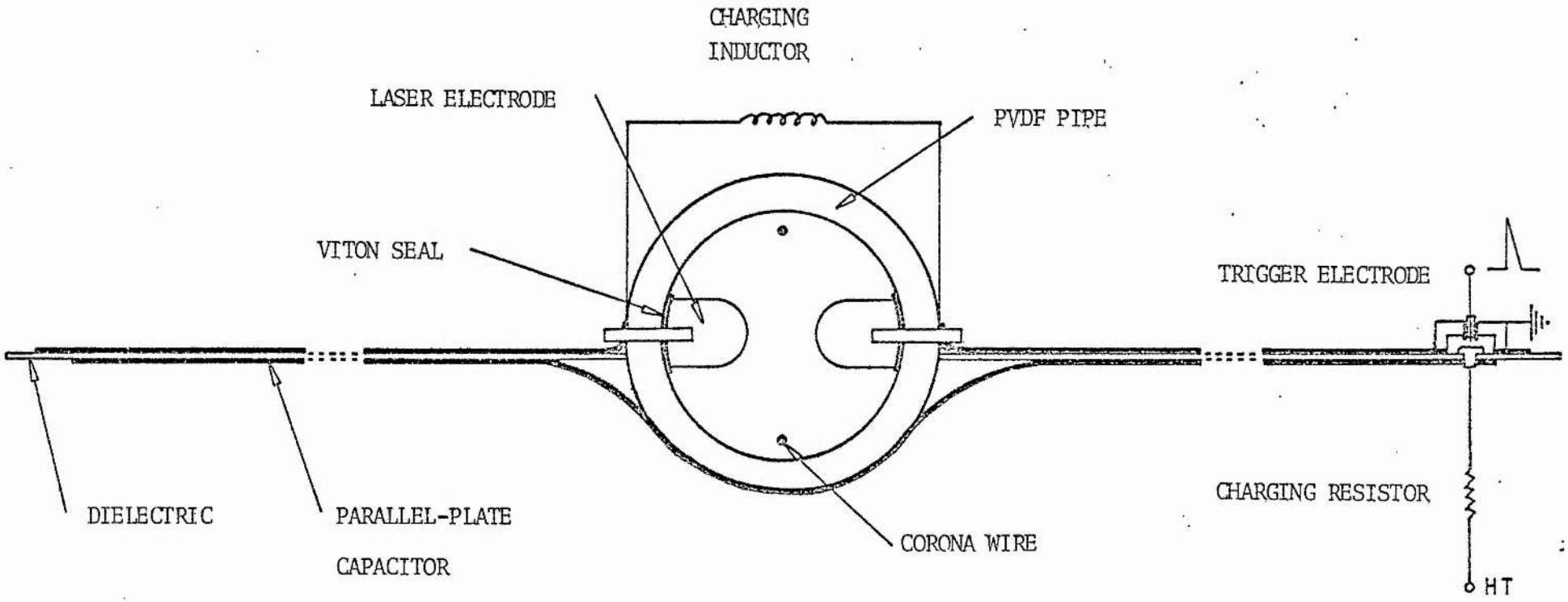

Fig.(2.3) Schematic drawing of laser system.

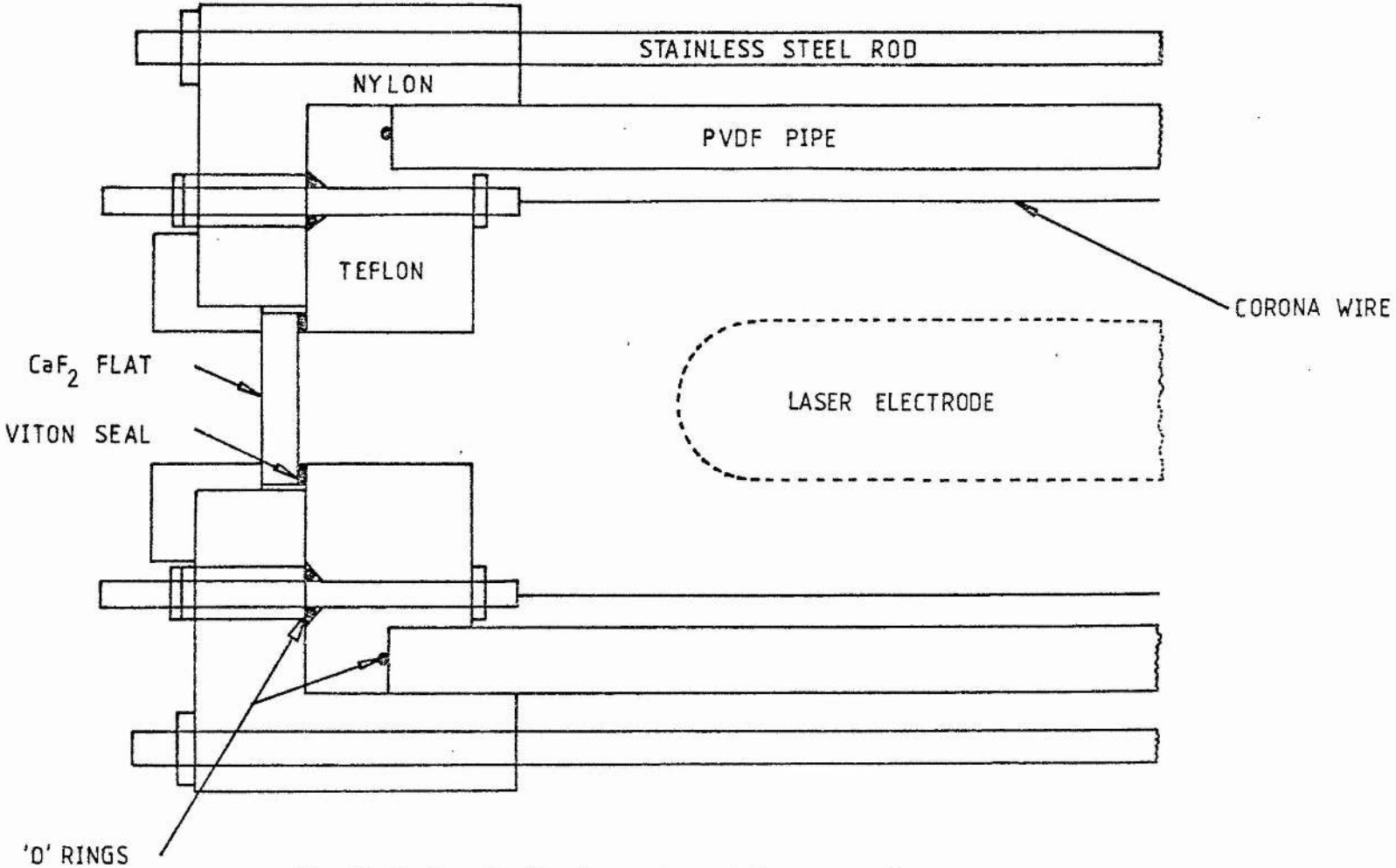

Fig.(2.4) Longitudinal section of laser envelope.

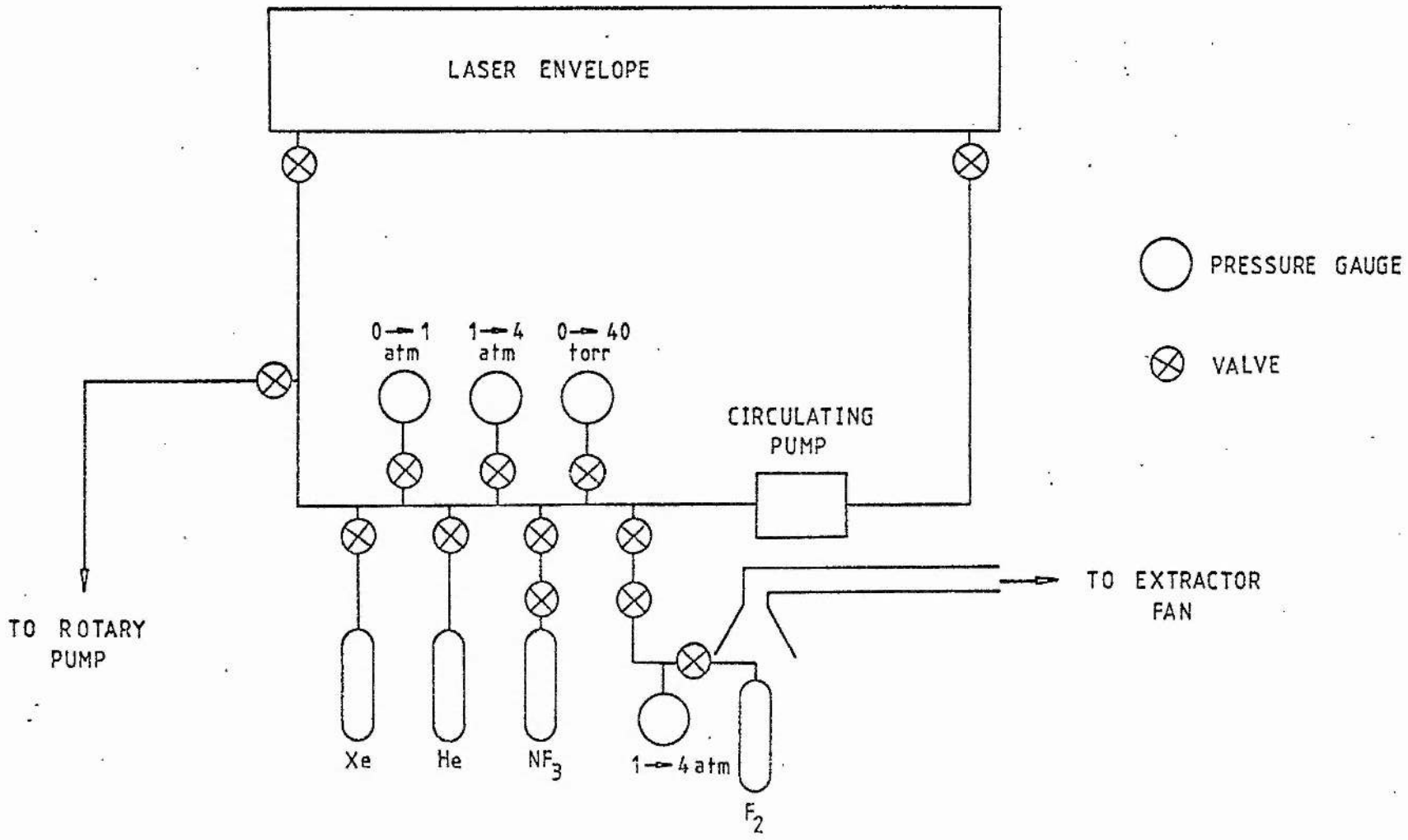

Fig. (2.5) Schematic drawing of the gas-handling system.

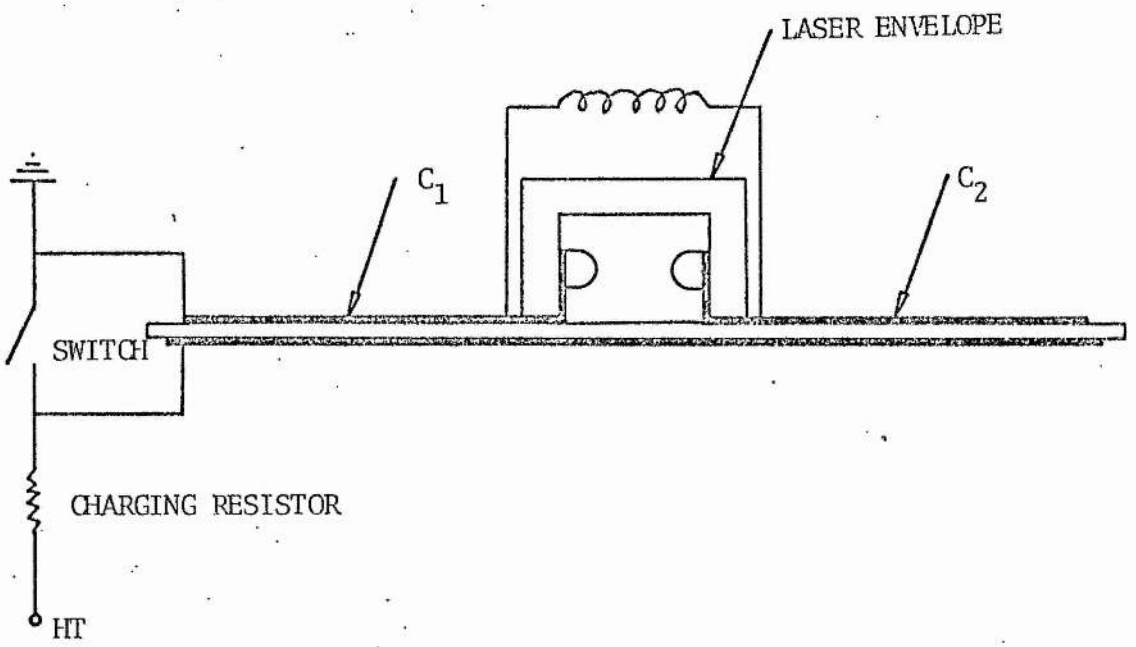

Fig.(2.6a) Parallel-plate Blumlein configuration.

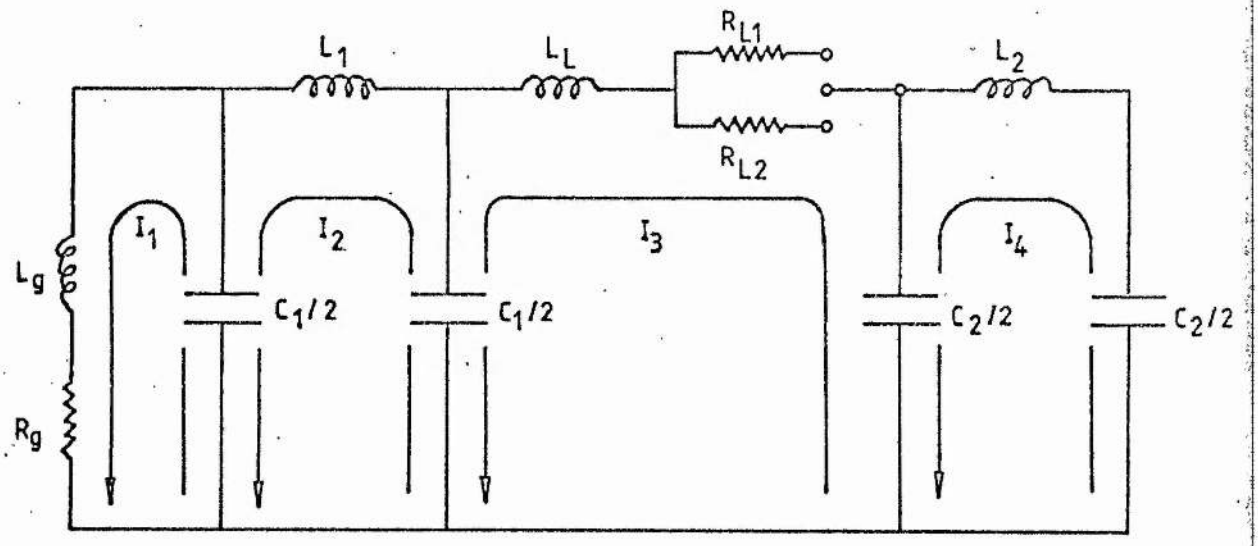

Fig.(2.6b) Lumped-element equivalent circuit.

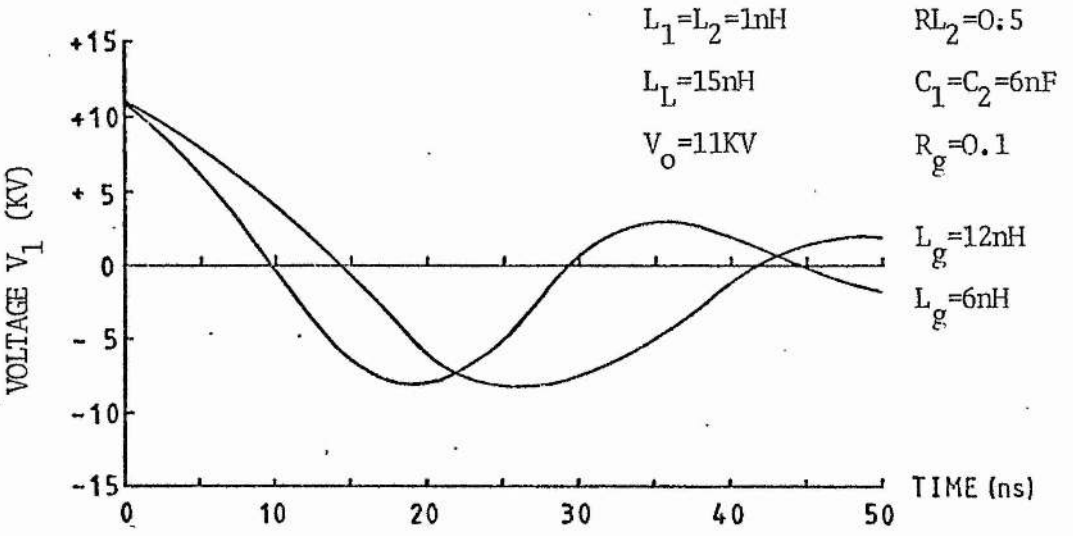

Fig.(2.7) Temporal variation of voltage V_1 as a function of inductance L_g in the absence of gas breakdown in the laser.

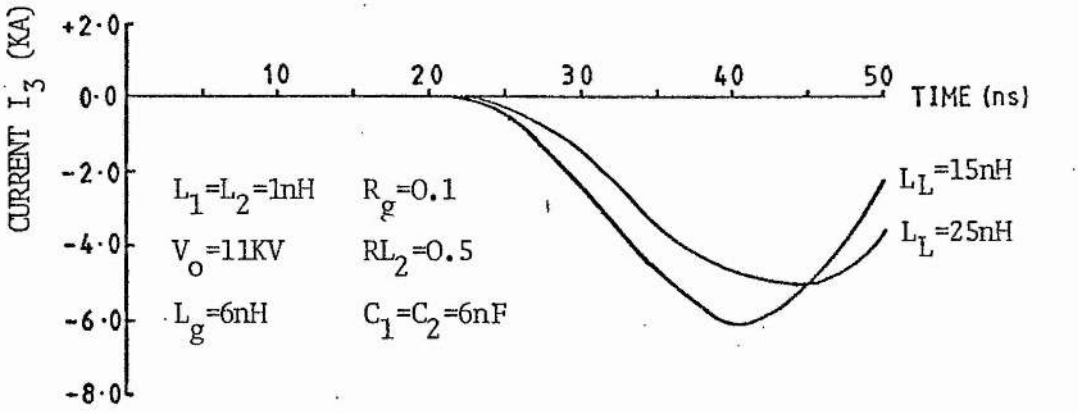

Fig.(2.8) Temporal variation of current I_3 as a function of the inductance L_L.

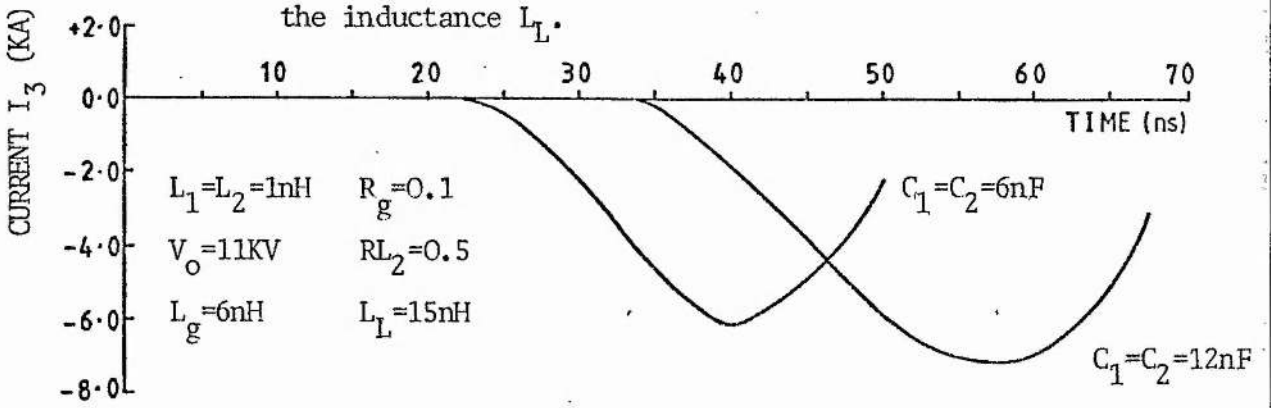

Fig.(2.9) Temporal variation of current I_3 as a function of C_1 and C_2:

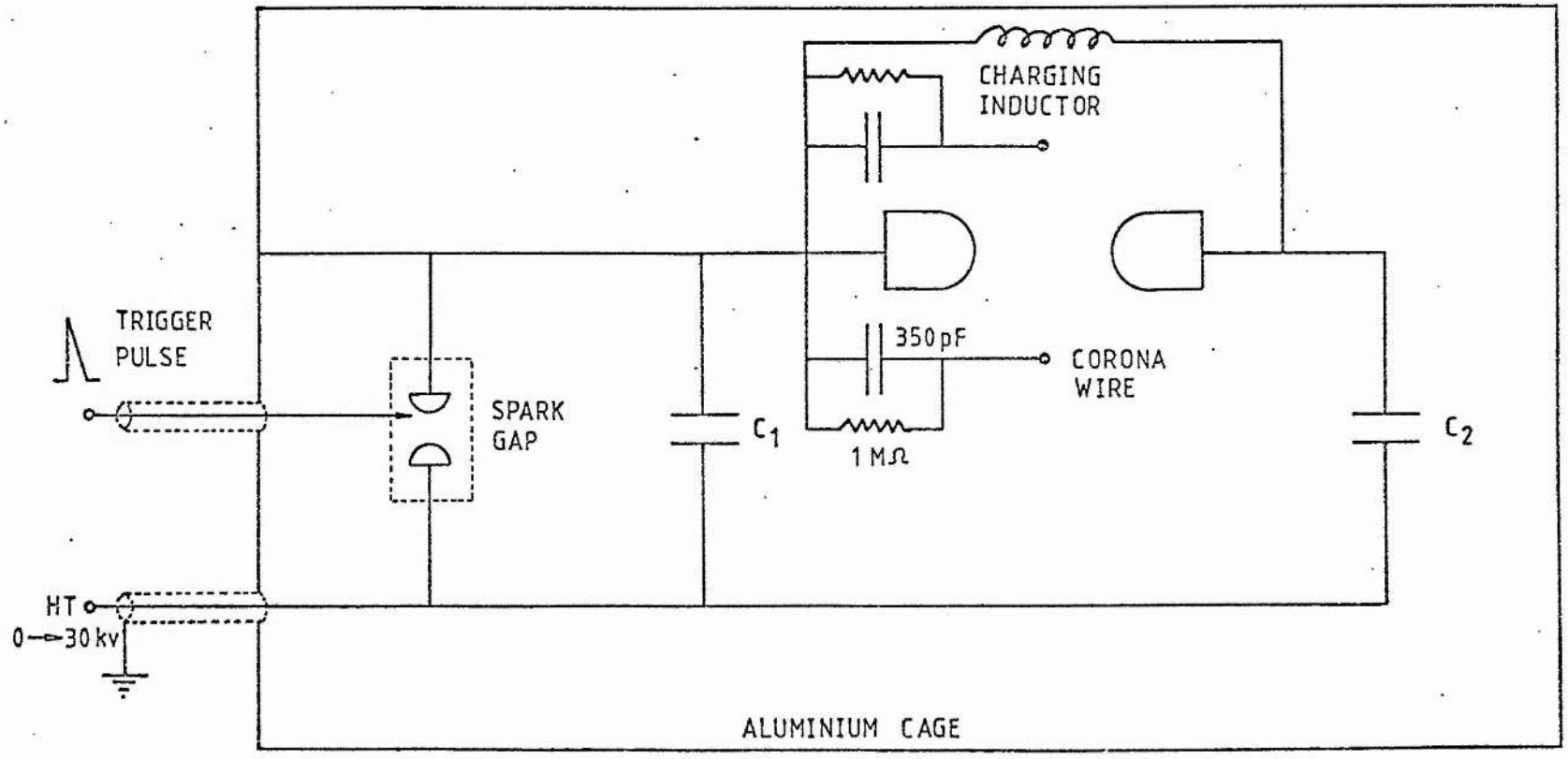

Fig.(2.10) Schematic drawing of electrical circuit.

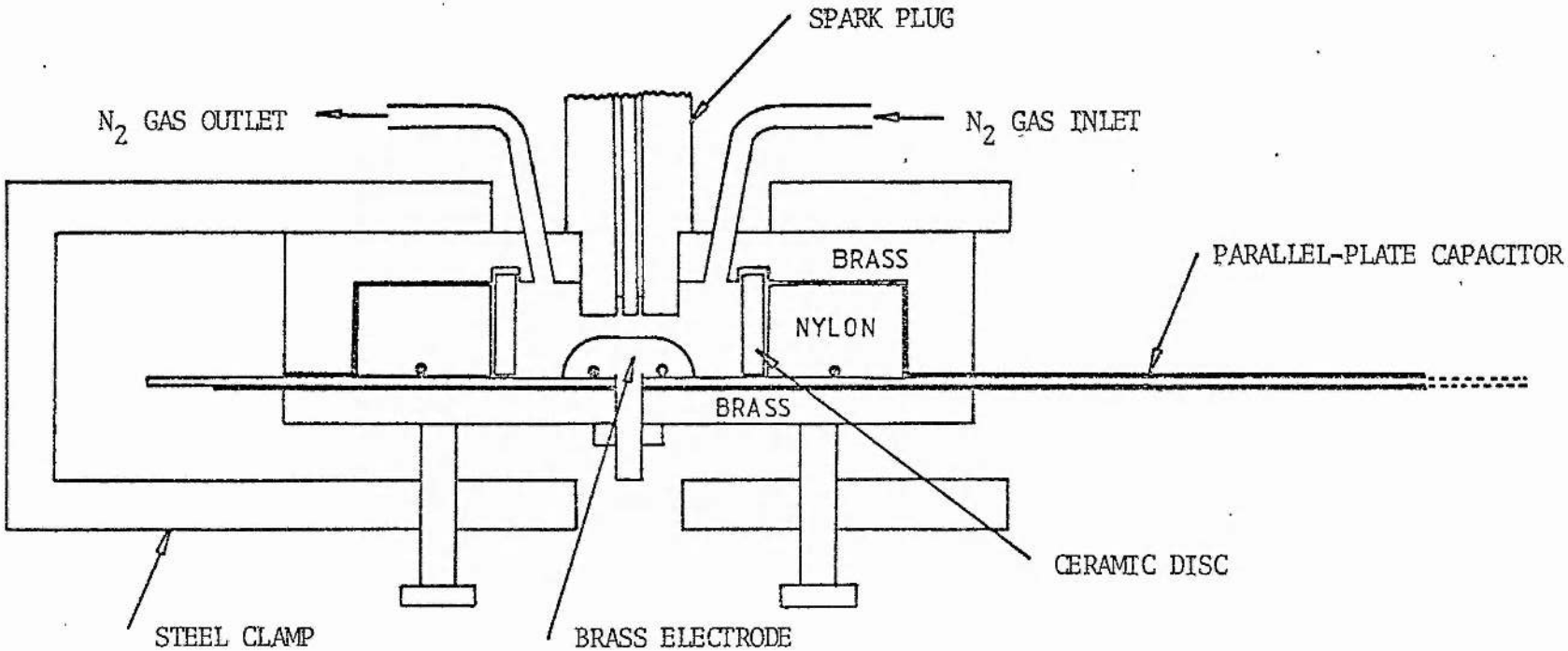

Fig.(2.11) Schematic drawing of the spark-gap switch.

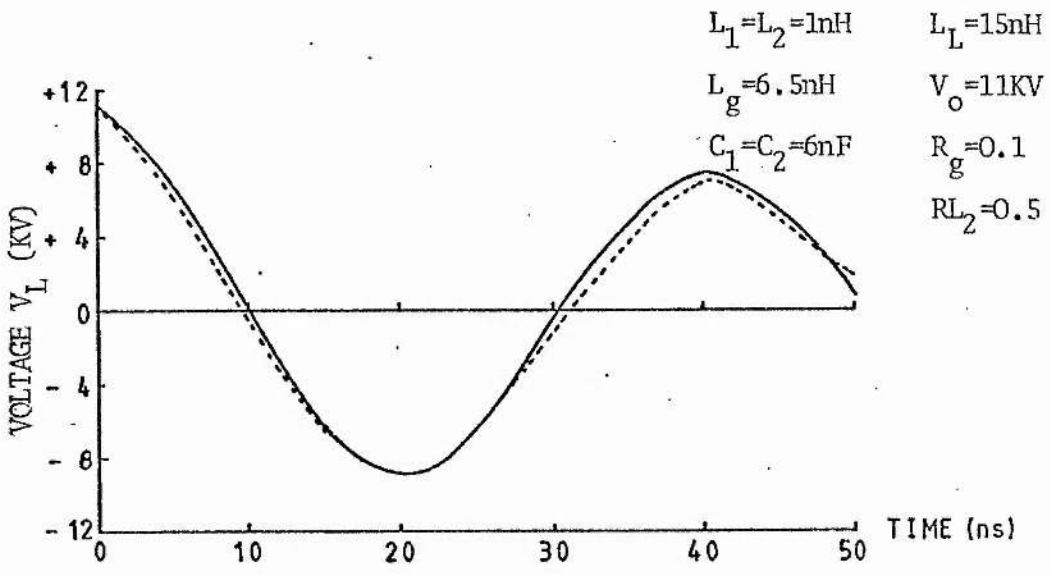

Fig.(2.12) Computed (-----) and experimental (——) voltage V_1 in the absence of gas breakdown in the laser.

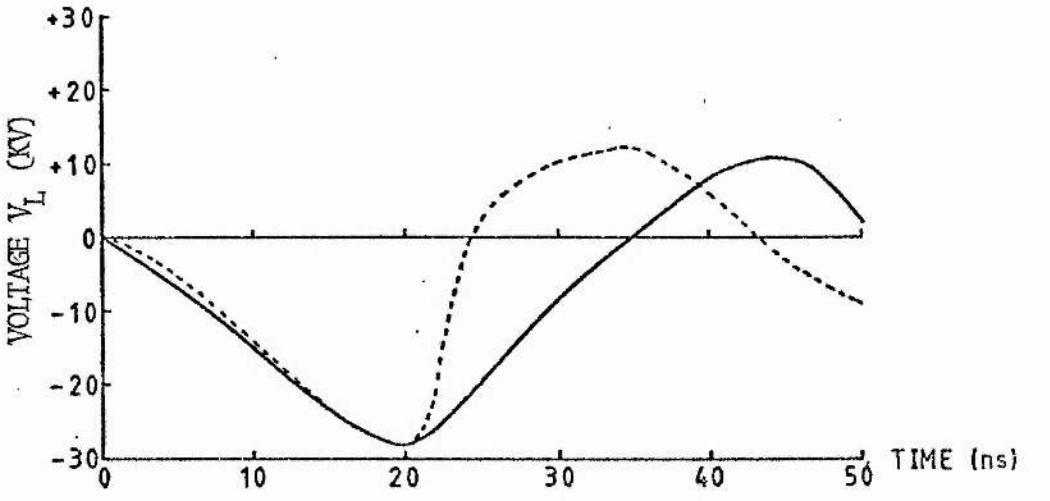

Fig.(2.13) Computed (-----) and experimental (——) voltage V_L across the laser electrodes.

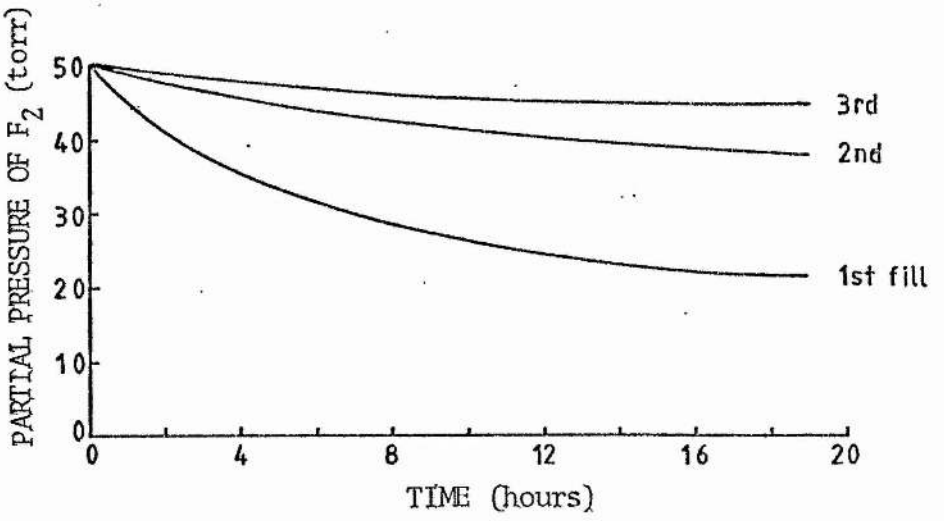

Fig.(2.14) Temporal variation of partial pressure of F_2 during passivation.

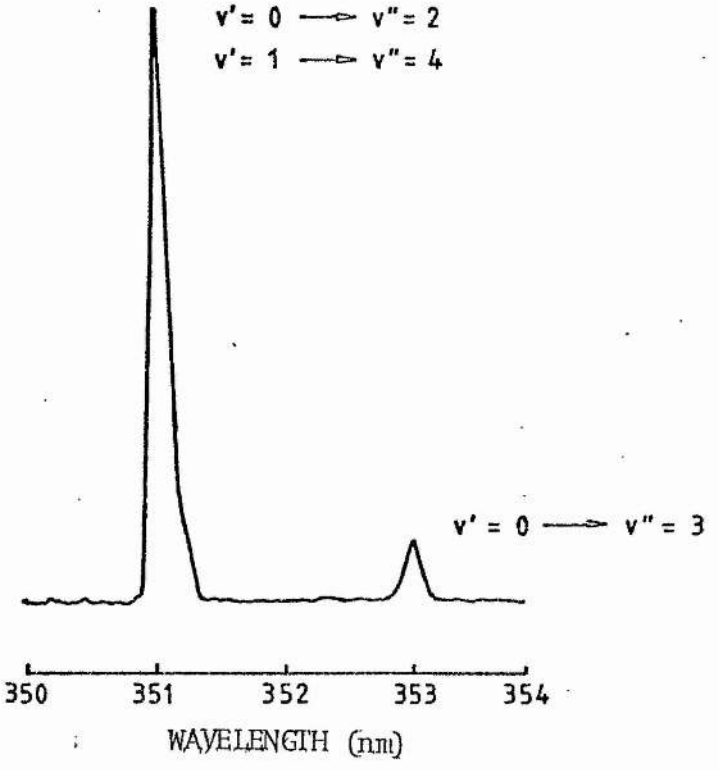

Fig.(2.15) Optical spectrum of laser pulse.

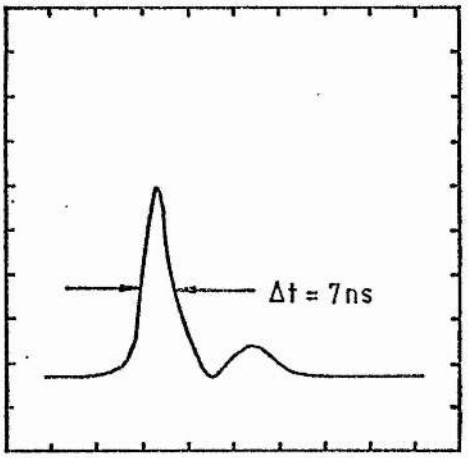

Fig.(2.16) Temporal variation of laser pulse.

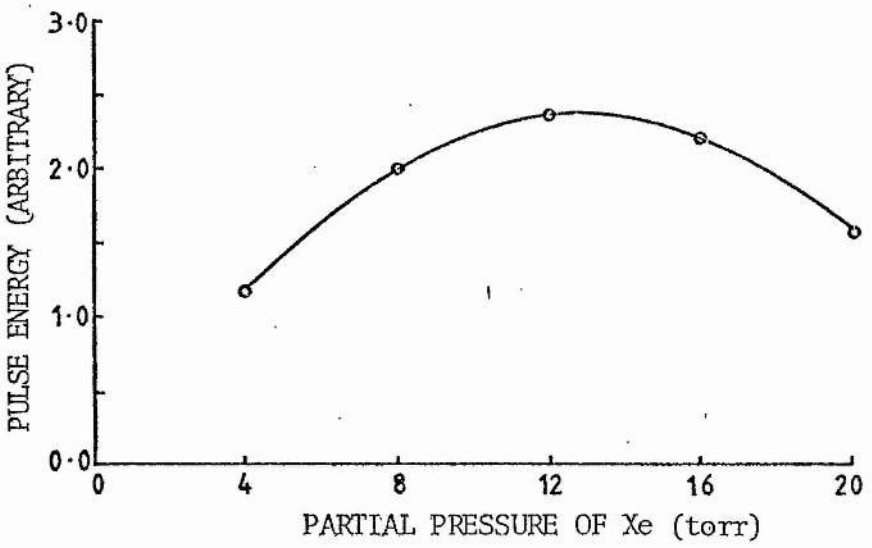

Fig.(2.17) Variation of pulse energy with partial pressure of Xe.

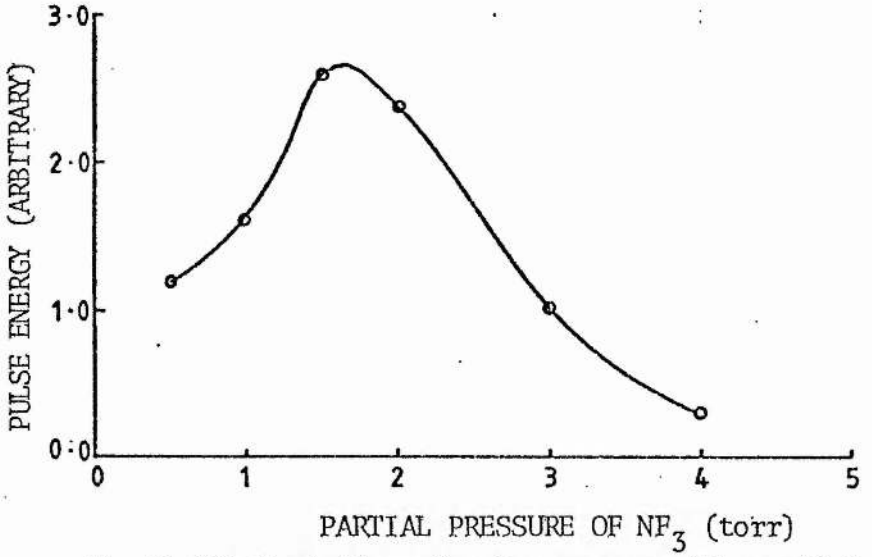

Fig.(2.18) Variation of pulse energy with partial pressure of NF_3.

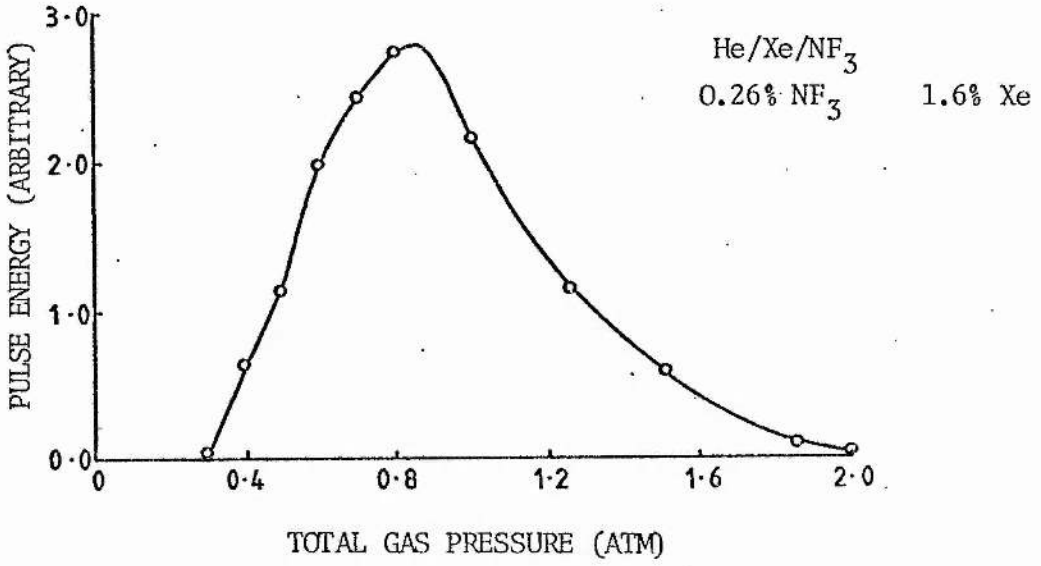

Fig.(2.19) Variation of pulse energy with total gas pressure.

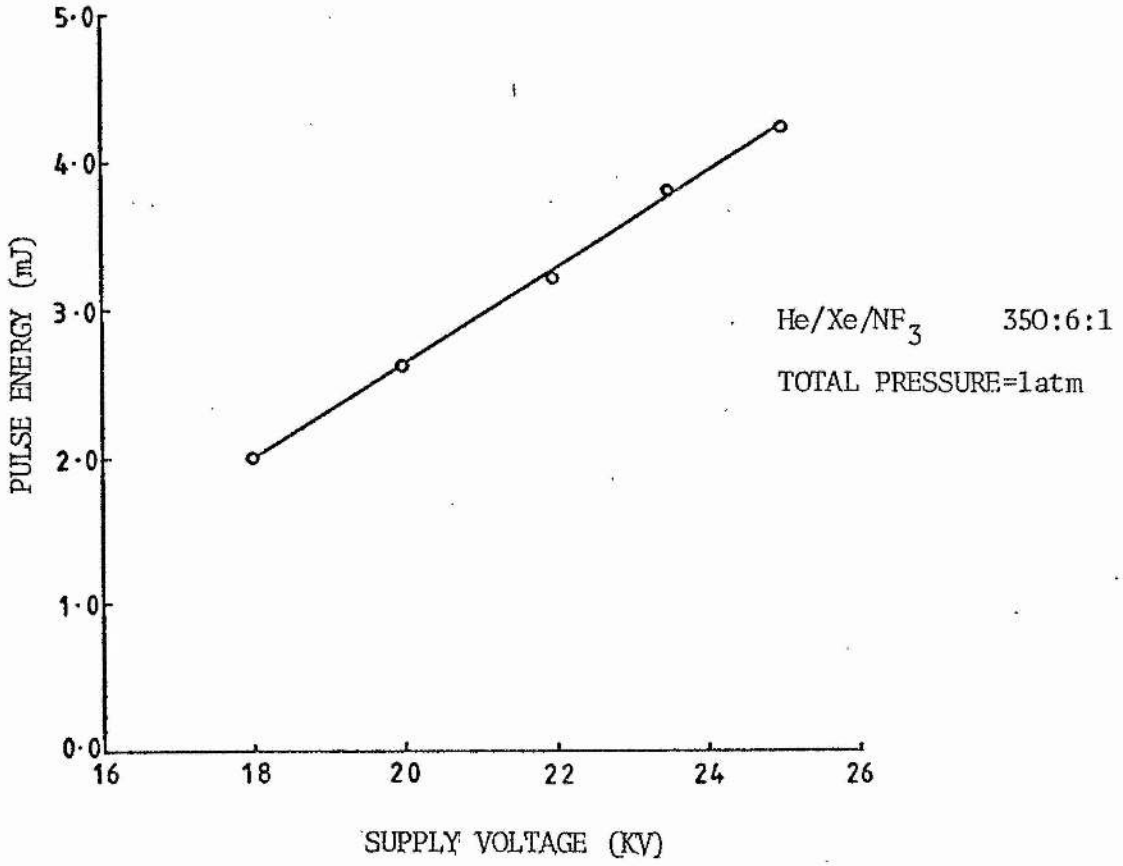

Fig.(2.20) Variation of pulse energy with supply voltage.

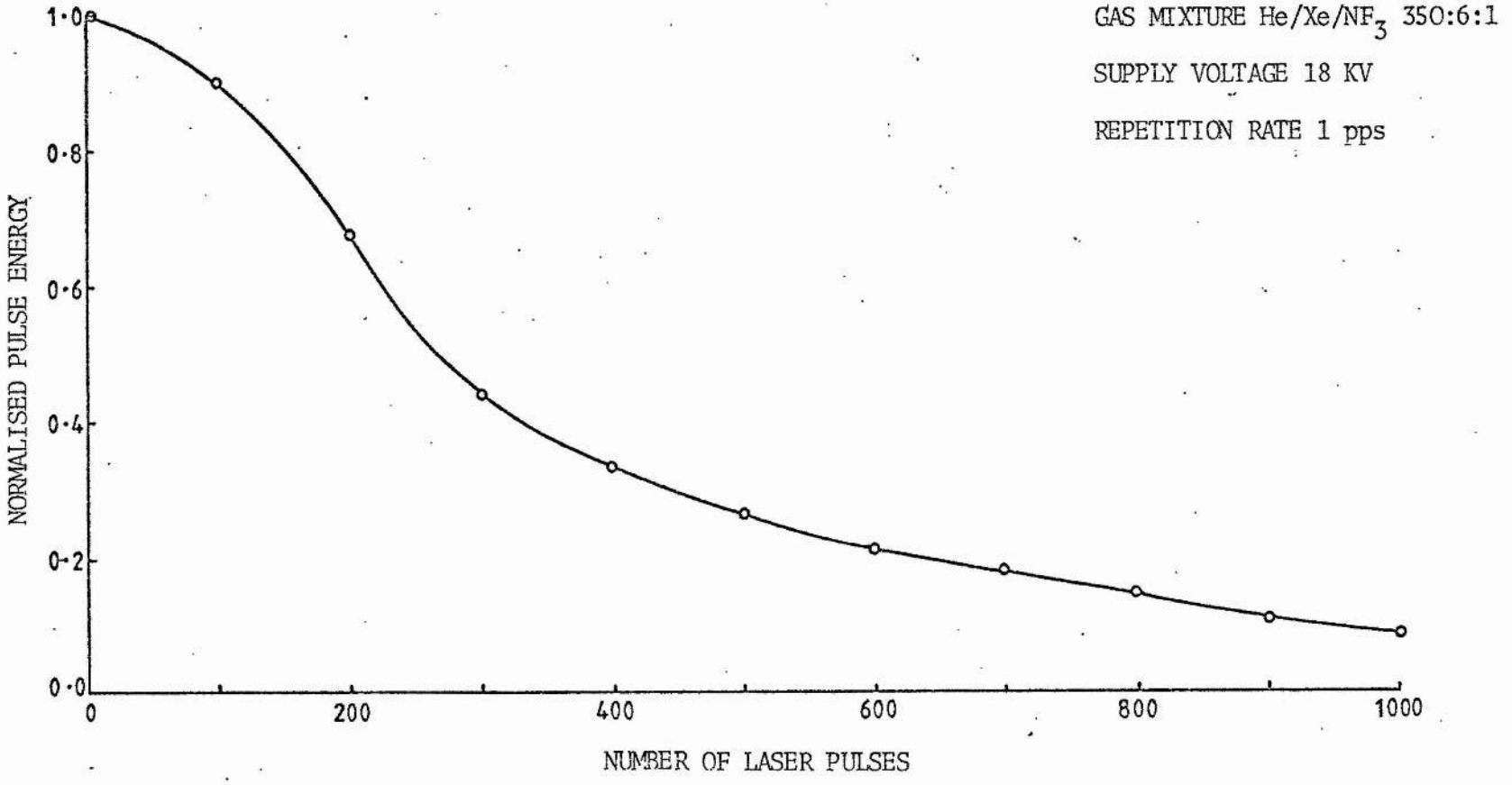

Fig.(2.21) Normalised pulse energy as a function of the number of laser pulses.

CHAPTER THREE

MASS SPECTRAL IR AND UV STUDIES

(3.1) Introduction

The fast deterioration of the performance of discharge excited XeF excimer lasers is due to several processes, of which the following may be significant: (i) depletion of the fluorine donor (NF_3) through the formation of fluorine compounds which are either not volatile, or have low branching ratios for the formation of the excited rare gas halide molecules (XeF^*); (ii) depletion of Xe by the formation of xenon fluorides such as XeF_2, XeF_4, and XeF_6; (iii) the formation of stable species which absorb at the laser wavelength (351nm), quench the excited rare gas halide molecules and their xenon metastable precursors (Xe^*), or cause a deterioration of the laser discharge; (iv) optical and chemical damage of the laser windows.

To extend the gas life of discharge excited XeF lasers, a knowledge of the relative importance of the above processes is required. In this chapter, the results of UV and IR spectroscopy, and mass spectrometric studies of discharge excited XeF laser gas mixtures are presented. The aims of the study were (i) to determine the significance of NF_3 and Xe depletion in the degradation of laser performance, (ii) to identify stable species formed in the discharge, and to follow changes in their partial pressures as a function of the number of laser pulses, and (iii) to investigate optical absorption at the laser wavelength. In the laser device used here, damage of the laser windows is not an important consideration. The pulse energy is

too low to cause optical damage, and for a single fill, the gas life is too short to cause a significant reduction of the window transmission by the formation of deposits. This is confirmed by the reproducibility of the pulse energies obtained from successive fresh gas fills.

In section (3.2) of this chapter, we consider the basic processes by which NF_3 may be consumed and generated in the laser discharge. Possible products of the fragmentation of NF_3 are also considered. This provides a background for the study of gas contamination. The results of infrared absorption studies of the laser gas mixture before and after pulsing are discussed in section (3.3). Several contaminants are identified, and the absence of several other possible contaminants is noted. In sections (3.3) to (3.8), the results of mass spectrometric studies of gas contamination are considered. Section (3.9) is devoted to a study of UV absorption by stable species at the laser wavelength, and finally the main results of the studies reported in this chapter are summarised in section (3.10).

(3.2) NF_3 reaction kinetics

The kinetic processes by which excited rare gas halide molecules are formed, normally start from molecular donors such as F_2, NF_3 and SF_6, rather than from atomic halogens (Brau 1979). The choice of a halogen donor is determined by several factors, which include large branching ratios for the formation of the excited rare gas halide molecules, negligible or no absorption at the laser wavelength, and non-toxic, non-corrosive properties. In the laser gas discharge, the chosen fluorine donor, (NF_3 in the case of XeF), is converted to other

fluorine compounds some of which may be non-volatile. In addition, some of the volatile products may have poor donor properties, causing a reduction of the laser extraction efficiency. Velazco et al (1976) have shown that efficient formation of XeF^* and KrF^* only occurs for a limited number of fluorine donors such as F_2, molecules with O-F and N-F bonds (NF_3, F_2O, FNO), and some simple interhalogens (ClF_3, ClF). This is illustrated in table (3.1), which lists formation rates of XeF^* and KrF^*, quenching cross-sections, and branching ratios for several fluorine donors. We note that CF_4 is not a suitable donor. Rothe and Gibson (1977) have observed optical gain in discharge excited mixtures of $He/Kr/CF_4$ and $He/Xe/CF_4$, but laser action was not achieved. The fact that CF_4 is a poor donor is significant, since it is normally the end product in the fluorination of carbon containing compounds (Cotton and Wilkinson 1972). Any CF_4 which is formed in the laser results in a permanent loss of fluorine.

In discharge excited rare gas halide lasers, the excited rare gas halide molecules are predominantly formed via metastable channels in which the rare gas metastables are formed by electron impact excitation. Rokni et al (1978) have shown that in discharge excited mixtures of $Ne/Xe/NF_3$, in which Ne is the buffer gas, most of the discharge energy results in the formation of xenon metastables (Xe^*). The Xe^* then produce XeF^* in harpoon reactions with NF_3 (Velazco et al 1976). These proceed with a rate constant of $9\times10^{-11} cm^3 s^{-1}$, and have unit branching ratio.

$$e + Xe \rightarrow e + Xe^* \qquad (3.1)$$

$$Xe^* + NF_3 \rightarrow XeF^* + NF_2 \qquad (3.2)$$

Reaction (3.2) results in the formation of difluoroamino radicals (NF_2), which are known to be stable (Chow et al 1977, Cotton and Wilkinson 1972). The free radicals may also be formed in electron dissociative-attachment, and electron impact dissociative reactions.

$$e + NF_3 \rightarrow NF_2 + F^- \qquad (3.3)$$

$$e + NF_3 \rightarrow e + NF_2 + F \qquad (3.4)$$

The rate of reaction (3.3) has been measured by Shaw and Jones (1977) to be $(16 \pm 6)\times10^{-10} cm^3 s^{-1}$. Reaction (3.4) proceeds with a rate constant of $2\times10^{-11} cm^3 s^{-1}$ (Mkrtchyan and Platonenko 1979). Molecules of NF_2 are very reactive and may take part in homogeneous gas phase reactions such as:

$$NF_2 + NF_2 \rightleftharpoons N_2F_4 \qquad (3.5)$$

$$Xe^* + NF_2 \rightarrow XeF^* + NF \qquad (3.6)$$

$$NF + NF \rightarrow N_2F_2 \qquad (3.7)$$

$$NF_2 + F + M \rightarrow NF_3 + M \qquad (3.8)$$

Reactions (3.5) and (3.7) have been investigated by Colburn (1963). The rate of reaction (3.6) has not been reported. In discharge excited mixtures of $He/Kr/NF_3$, Chow et al (1977) measured a rate constant of $1.8\times10^{-10} cm^3 s^{-1}$ for the formation of KrF^* by the reaction of Kr^* with NF_2. Chow et al also observed the formation of N_2F_2 in the discharge. Reaction (3.8) provides a path for the formation of NF_3 from NF_2, and is therefore an important process. In helium as the third body (written as M in 3.8), it proceeds with a three-body rate constant of $8.9\times10^{-31} cm^6 s^{-1}$ (Smith and Huestis 1981). In this work,

the laser gas mixture consisted of $He/Xe/NF_3$ in the typical ratio of 350:6:1 at a total pressure of one atmosphere. Using the rate constant of Smith and Huestis, and the above gas composition, a recombination time of about 1us is calculated. This is long compared with the optical pulse length of 10ns reported in Chapter 2, but short in comparison with the inter-pulse time of about one second. Reaction (3.8) is therefore considered to be unimportant during a laser pulse, but it may be an important process for the formation of NF_3 in between pulses. Other compounds may be formed by NF_2 in homogeneous reactions with gaseous impurities, and in reactions with exposed materials in the laser.

Another product of the gas discharge is atomic fluorine (F), which can recombine to form molecular fluorine (F_2). Both F and F_2 can take part in numerous reactions in the gas phase, and with exposed materials in the laser (the laser envelope, preionizer, electrodes, etc.), to form a large number of compounds (Foon and Kaufman 1975, Colburn 1963, Kemmitt and Sharp 1965, Cotton and Wilkinson 1972). Molecular fluorine can also form XeF^* in harpoon reactions with Xe^*, but it absorbs at the XeF laser wavelength (Steunenberg and Vogel 1956).

$$Xe^* + F_2 \rightarrow XeF^* + F \qquad (3.9)$$

Reaction (3.9) proceeds with a rate constant of $7.5 \times 10^{-10} cm^3 s^{-1}$, and has unit branching ratio (Velazco et al 1976).

In the discharge, xenon fluorides may also be formed by the direct fluorination of Xe in reactions such as:

$$Xe + F_2 \rightarrow XeF_2 \quad (3.10)$$

$$XeF_2 + F_2 \rightarrow XeF_4 \quad (3.11)$$

$$XeF_4 + F_2 \rightarrow XeF_6 \quad (3.12)$$

and under various conditions (Selig 1967, Moody and Thomas 1964, Lagowski 1973). XeF_2 has been prepared (i) by circulating F_2 and Xe at respective partial pressures of 240 torr and 60 torr, through a nickel tube at 400°C, (ii) by ultraviolet photolysis of Xe and F_2 in nickel vessels, and (iii) in electrical discharges in 1:2 mixtures of Xe and F_2. High-voltage (6KV) discharges in mixtures of Xe and CF_4 have been found to form XeF_2. After 2 hours, 50mg of XeF_2 was obtained. Three methods for preparing XeF_4 are: (i) by heating 1:5 mixtures of Xe and F_2 in nickel tubes for one hour; (ii) by flowing 1:5 mixtures of Xe and F_2 in nickel tubes at 300°C; (iii) by running electrical discharges (1100 -> 2800v) in 1:2 mixtures of Xe and F_2 over a period of 3.5 hours. Production of XeF_6 may be by heating 6:40 mixtures of Xe and F_2 from 350°C to 450°C in stainless steel vessels at pressures of 70 atm, or by heating Xe in an excess of F_2 for 16 hours in nickel vessels. The melting points of XeF_2, XeF_4 and XeF_6 are 140, 114 and 46°C, respectively. At room temperature, the partial pressure of XeF_2 and XeF_4 is 3 torr, and that of XeF_6 is 30 torr.

The stable fluorides which are formed in the laser gas discharge may either act as fluorine donors in the formation of XeF^*, or they may accumulate in the laser, resulting in a loss of fluorine and a deterioration of laser performance.

(3.3) IR absorption studies

In this work, the results of infrared absorption studies of the laser gas mixture were used to complement those of mass spectrometry, which was the main investigative technique. When applied to a mixture of gases, mass spectral analysis requires a knowledge of the cracking pattern of each possible component of the gas mixture. It is therefore necessary to compile a list of components by comparing the mass spectrum of the mixture with tables of cracking patterns. Only those compounds whose cracking patterns are in general agreement with the mass spectrum are included in the list. Due to the reactive nature of fluorine compounds, the number of contaminants which can be formed in discharge excited XeF laser gas mixtures is large. Consequently, if all possible contaminants are included in the analysis, the latter becomes time consuming and the accuracy of the results is reduced. By combining the results of mass spectrometry with those of infrared absorption spectroscopy, the number of possible contaminants can be reduced, and the contribution of each contaminant can therefore be determined with greater accuracy.

(3.3.1) Experimental

The analysis of gas mixtures by infrared absorption spectroscopy is an established technique (Potts 1963, Houghton and Smith 1966). For analytical purposes, only the positions of the vibrational frequencies in the infrared spectrum of a sample are required, and a spectrometer of low resolution can therefore be used. The technique

involves (i) collecting a gas sample in a cell fitted with infrared transmitting windows, (ii) recording the infrared spectrum of the sample over a suitable wavelength range, and (iii) comparing the recorded spectrum with published tables of absorption spectra to identify the absorbing species.

The laser used in this work has been described in Chapter 2. The infrared absorption cell is shown in fig. (3.1). It consists of a quartz tube fitted with a cold finger, and with inlet and outlet ports which can be closed using greaseless teflon stopcocks. The cell windows consist of sodium chloride flats which are sealed to the quartz tube using viton 'O' rings. Sodium chloride windows were used because they are relatively cheap and easily polished, and they have useful transmission from 0.25μm to 16μm. Gas samples are obtained by circulating the laser gas mixture through the absorption cell, in which condensable components are trapped in the cold finger which is cooled with liquid nitrogen. Table (3.2) shows that the boiling point of most volatile compounds which are likely to be formed in the laser, lie above that of liquid nitrogen. Consequently the cold trap is effective in condensing most of the contaminants formed in the laser discharge. After circulating the gas for about fifteen minutes, the cell is isolated using the stopcocks. The cold finger is then allowed to warm up to room temperature, and the contents of the cell are analysed using a Perkin-Elmer infrared spectrophotometer (model 257), which has a wavelength range of 2.5μm to 16μm. The wavelength scale of the spectrophotometer is calibrated using the infrared spectrum of polystyrene, whose vibrational frequencies are known.

(3.3.2) Results and discussion

Typical infrared spectra of a fresh gas mixture, and a used mixture after 2.10^3 shots are shown in figs. (3.2) and (3.3) respectively. The laser was pulsed at a repetition rate of 1 pps, and the capacitor charging voltage was 18 KV. Absorption spectra of spent gas mixtures are obtained by first running the laser on a fresh mixture for the required number of shots. The absorption cell is then connected to the gas manifold, and a sample is taken for subsequent analysis. The fresh gas mixtures consist of He, Xe, and NF_3 in the ratio of 350:6:1 at total pressures of one atmosphere. These gases are used as supplied by the manufacturers, without any further purification. The trapped components are identified by comparing the observed absorption spectra with published infrared spectra of possible contaminants (Nakamoto 1963, and references therein). In figs. (3.2) and (3.3), only those peaks which have been identified with some degree of confidence are labelled. Figure (3.2) shows that for fresh mixtures, the trapped contents of the cell include H_2O, NF_3, and CF_4. The upward peak in the region of 4.3μm is due to absorption by atmospheric CO_2 in the reference arm of the spectrometer, which did not contain a reference cell at the time the spectrum was taken. The broad absorption bands in the region of 9.2μm and 14μm are attributed to sodium silico fluoride (Na_2SiF_6), which is thought to be formed as a thin film on the sodium chloride windows. These bands grow with successive use of the absorption cell, and they are also observed unchanged, after the cell is evacuated. After repolishing the cell windows, the height of the bands are significantly reduced. Chlorine

dioxide (ClO_2) may also contribute to the absorption band in the region of 9.2μm. The structure in the region of 5μm is due to an automatic change of the dispersive element in the spectrophotometer.

A comparison of the absorption spectra taken before lasing and after $2x10^3$ laser pulses shows several changes in the gas composition. The partial pressure of NF_3 has decreased considerably, and those of CO_2 and CF_4 have increased. The increase in the intensity of the band at 9.2μm is attributed to an increase in the amount of Na_2SiF_6 formed on the cell windows, with a possible minor contribution from ClO_2. This conclusion is based on the observation that there is a negligible change in the intensity of the peak when the cell is evacuated. Several new peaks are also evident. They have been identified as the absorption peaks of NO_2, NO, N_2O, CO, and SiF_4. These compounds are similar to the ones observed in electron-beam excited mixtures of $He/Xe/NF_3$ by Brannon (1982). The broad absorption band below 3.2μm is attributed to HF polymers which are known to be formed at low temperatures. At high temperatures, HF is monomeric (Smith 1958). Formation of SiF_4 is mainly by reactions of HF with the quartz body of the absorption cell. Another possible source of SiF_4 is from corrosion of the aluminium electrodes, which contain 0.7% silicon, by fluorine compounds. The absorption band in the region of 7.1μm is tentatively assigned to the cis-isomer of difluorodiazine (N_2F_2), which is thought to be a product of the fragmentation of NF_3 in the gas discharge. The infrared spectrum of tetrafluorohydrazine (N_2F_4) also shows an absorption band in the region of 7.1μm (Colburn 1963). However, N_2F_4 dissociates readily into two difluoroamino free radicals (NF_2), and it is therefore not likely to accumulate during laser action. The free radicals NF_2 were

not detected in the used mixture. There is no evidence of the formation of species such as FNO, FNO_2, and F_2CO, which were observed by Gower et al (1980) in discharge excited mixtures of helium, xenon and fluorine. Since FNO, FNO_2, and F_2CO are formed when molecular fluorine reacts with NO, NO_2, and CO respectively, we have

$$F_2 + NO \rightarrow FNO + F$$
$$F_2 + NO_2 \rightarrow FNO_2 + F$$
$$F_2 + CO \rightarrow F_2CO$$

The absence of these species in the used gas may indicate that F_2 is not produced in significant amounts in the gas discharge.

The xenon fluorides show strong absorption in the infrared spectral region at 549 cm^{-1} (XeF_2), 590 cm^{-1} (XeF_4), and 610 cm^{-1} (XeF_6), (Moody and Thomas 1964). Since these absorption bands lie outside the range of the model 257 Perkin Elmer IR spectrophotometer, the formation of xenon fluorides could not be investigated.

(3.3.3) Summary of results of IR spectroscopy

The results of the infrared absorption study of the laser gas mixture before and after lasing, can be summarised as follows :

(i) In the gas discharge, NF_3 is consumed and CF_4 and HF are formed. Other fluorine compounds such as SiF_4 and N_2F_2 may also be formed, the former by the reaction of volatile fluorides with silicon in the aluminium electrodes, and the latter as a result of the fragmentation of NF_3. Molecules of NF_2 were not present in the used

mixture after $2x10^3$ laser pulses.

(ii) Other stable compounds formed in the discharge are : NO, NO_2, N_2O, CO, CO_2, and possibly ClO_2. Of these, only NO_2 and ClO_2 absorb at the laser wavelength (Hall and Blacet 1952, Goodeve and Wallace 1930).

(iii) Homonuclear diatomic molecules such as N_2, O_2, and F_2 could not be detected, due to their inactivity in the infrared spectral region. The absence of compounds such as FNO, FNO_2, and F_2CO, (which have been observed in discharge excited $He/Xe/F_2$ mixtures by Gower et al 1980), in the used gas mixture may indicate that F_2 is not a major product of the discharge.

(3.4) Mass spectral analysis

With the above information available, the problem of gas contamination was investigated further using mass spectrometric techniques. The aims were (i) to confirm the results of the infrared absorption study of section (3.3), (ii) to investigate the formation of homonuclear diatomic molecules such as O_2, N_2, and F_2, and (iii) to follow the rate of contaminant formation as a function of the number of laser pulses. Mass spectral data was obtained using a Kratos MS10S 180° deflection mass spectrometer, which is schematically shown in fig. (3.4). The analyser tube of the spectrometer is made of stainless steel. It is pumped by the combined use of a two-stage rotary pump, an oil diffusion pump, and a liquid nitrogen cold trap. The corrosive nature of the laser gas mixture makes it necessary to

use chemically inert oils in both pumps. Fomblin Vac (a fluorinated chemically inert oil, supplied by Edwards High Vacuum) is used in the rotary pump, and Santavac 5 (a chemically inert oil, with high flash-point, supplied by Edwards High Vacuum) is used in the diffusion pump. Gold 'O' rings are used to seal to the analyser tube. Gas pressure in the tube is measured using a Kratos VC-95 ion gauge. After baking to 250 -> 300^{o}C, the lowest pressure obtained is better than 10^{-8} torr. This is four orders of magnitude smaller than the maximum operating pressure of the analyser tube.

In the MS10S ion source, ions which are representative of the components of a gas sample, are produced by bombardment in an electron beam. The energy of the ionizing electrons can be varied from 5 to 105 eV, at trap currents of 50, 100, and 150uA. The positive ions produced are pushed out of the source by a repeller voltage variable from 0 to +10V, and they are then accelerated by an applied voltage which can be continuously varied from 20V to 2KV. The accelerated ions describe circular orbits due to the influence of the uniform magnetic field of 0.184 tesla of a permanent magnet. By continuously varying the accelerating voltage, ions of different masses are brought to the collector. The distance between the source and collector slits is 10cm, so that only ions which describe a circular path of 5cm can reach the collector. Since the magnetic field is 0.184 tesla, the product of the ionic mass and the accelerating voltage must be about 4000. Hence by changing the accelerating voltage from 20V to 2000V, a mass range of 2 to 200amu is obtained. The ions which reach the collector give up their electrical charge, and the current produced is detected by an electrometer, amplified and displayed either on a meter, or on a chart recorder to form a mass spectrum of the gas

sample. In this work, all mass spectra were taken using a standard electron energy of 70eV, a trap current of 50uA, and a repeller voltage of +1V.

A Kratos MS10S control unit is used to scan over two separate mass ranges, which extend from 2 to 50amu, and 2 to 200amu respectively. Six scanning speeds ranging from 0.1 to 3amu/s are available. Mass numbers and ion currents are read off a meter attached to the control unit. On the low range (2 -> 50 amu), each division on the scale corresponds to one mass unit, and mass numbers are assigned from the scale reading. When necessary, these are checked using the easily identifiable peaks at masses 18, 28, 32, 40 and 44, which are due to residual air and moisture in the system. Starting from a known peak, and counting either downwards, or upwards, the mass numbers can be easily verified. On the high mass range (2 -> 200amu), each division on the scale corresponds to four mass units, and the meter reading can only be used as a rough guide. Mass numbers are then assigned by calibrating the spectra using known peaks such as the ones mentioned above, as well as those of NF_3 and Xe.

(3.4.1) Minimum detection levels

The sensitivity of the amplifier in the control unit can be varied from 0.1 to 100pA fsd in six steps. The smallest ion current which can be measured is 2fA, corresponding to one division on the most sensitive range of the amplifier. If S (A $torr^{-1}$) is the sensitivity of the MS10S to some component of a gas sample, the minimum detectable partial pressure P_m of that component is given by

$$P_m = 2\times10^{-15}/S \quad \text{torr} \tag{3.13}$$

For a sample pressure of 2×10^{-5} torr, the minimum detection level in parts per million (ppm) is given by

$$P_m(\text{ppm}) = 10^{-4}/S \tag{3.14}$$

Table (3.3) lists estimated minimum detection levels for several commom gases. Typical sensitivities of the MS10S to these gases were used, corresponding to a standard collector slit of 0.25mm (AEI technical information sheet A506, Craig and Harden 1965). It must be emphasized that in practice, the minimum detection levels are slightly higher than the tabulated values, due to amplifier noise on the most sensitive range.

(3.4.2) Resolution

Two mass peaks are said to be resolved when the valley between them is 10% of the peak height. With the MS10S mass spectrometer, 10% valley resolution can be obtained up to mass 100 (manufacturer's specification), for a standard collector slit of 0.25μm. Adjacent mass peaks can be distinguished up to mass 150.

(3.4.3) Gas handling and sampling

The gas handling system is schematically shown in fig. (3.5). It is similar to that described in section (2.3) of Chapter 2, except for the addition of an inlet to the mass spectrometer analyser tube. The

latter is connected to the laser gas manifold by one metre of teflon tube (4mm I.D.). The laser envelope is used as the gas reservoir. Since gas pressure in the inlet tube is typically several hundred torr, the mean free path of the gas molecules is much less than the internal dimensions of the tube. Consequently, gas flow in the tube is viscous in nature. In the analyser tube the pressure is normally 10^{-4} or less, and molecular flow prevails. Since gas pressure in the reservoir feeding the mass spectrometer is orders of magnitude higher than that in the analyser tube, the ion beam intensity is proportional to the reservoir pressure (Honig 1945). However, due to the molecular nature of gas flow in the analyser tube, fractionation of the gas sample occurs. In this work, the volume of the gas reservoir is large, and changes in the gas composition is negligible. Gas flow in the inlet pipe is controlled by three taps, labelled T1, T2, and T3 in fig. (3.5). Taps T1 and T2 are used to admit gas samples in the analyser tube, through a sintered disc leak. Tap T1 is mounted as close to the main gas line as possible, to reduce the volume of dead space. The inlet volume between T1 and the disc leak can be pumped down to 60μm, using a single-stage rotary pump.

The general procedure for taking a mass spectrum is as follows: The MS10S control unit is switched on and the filament is energised. The recommended warm-up time is 10 minutes (Kratos instruction manual), but in the present case, stabilisation was only achieved after one to two hours. The ion current meter on the control unit is then "zeroed", and the mass scale reading checked against the nitrogen peak at mass 28. With T1 and the disc leak closed, and T2 and T3 open, the inlet volume is evacuated. Taps T2, T3 are then closed, the leak fully opened, and T1 is used to admit the laser gas mixture in

the inlet pipe. The pressure in the analyser tube is then set by using T2. The disc leak was not used for that purpose, because of difficulties in adjusting the gas flow. In this work, the sample pressure was typically 2×10^{-5} torr. After pressure and ion current stabilisation in the analyser tube, a mass spectrum is taken. Tap T1 and the leak are then closed, T2, T3 opened and the inlet volume evacuated before the next sample is admitted. On the low mass range (2 to 50amu), a scanning speed of 0.3amu/s is used. On the high mass range (2 to 200amu), the scanning speed is 1amu/s.

(3.4.4) Data analysis

In a mixture of gases, some components may be uniquely identified by one or more peaks in their cracking patterns. This is illustrated in table (3.4), which lists the cracking patterns of several compounds. A survey of the list also shows that at some mass numbers (12, 14, 16, 28, 30, etc.), the cracking pattern of some compounds overlap. The composition of a gas sample whose mass spectrum consists of overlapping spectra, must be determined by solving a set of simultaneous equations, as discussed in section (1.9.2) of Chapter 1. We recall that the equations are of the form:

$$\begin{aligned} I_1 &= S_{11}P_1 + S_{12}P_2 + \ldots\ldots\ldots + S_{1n}P_n \\ I_2 &= S_{21}P_1 + S_{22}P_2 + \ldots\ldots\ldots + S_{2n}P_n \end{aligned} \qquad (3.15)$$

$$I_m = S_{m1}P_1 + S_{m2}P_2 + \ldots\ldots\ldots + S_{mn}P_n$$

where I_m is the total ion current at mass m, S_{mn} the sensitivity of the mass spectrometer to component n at mass m, and P_n the partial pressure of component n. Assuming that the cracking pattern of each component is known, P_n can only be determined if the sensitivity S_{mn} of the mass spectrometer is known for at least one peak in the cracking pattern of each component n. Since in this work, the cracking patterns of all the compounds listed in table (3.4) were known, but the sensitivities of several compounds were not available, equation (3.15) was modified as follows:

The ion currents $I_j (j=1 \rightarrow m)$ can be expressed as

$$\begin{aligned} I_1 &= I_{11} + I_{12} + \ldots\ldots\ldots + I_{1n} \\ I_2 &= I_{21} + I_{22} + \ldots\ldots\ldots + I_{2n} \end{aligned} \qquad (3.16)$$

$$I_m = I_{m1} + I_{m2} + \ldots\ldots\ldots + I_{mn}$$

where I_{mn} is the ion current due to component n at mass m. The ratios $I_{1n} : I_{2n} : \ldots : I_{mn}$ are equivalent to the cracking pattern $C_{1n} : C_{2n} : \ldots : C_{mn}$ of component n. If I_{mn} is given by

$$I_{mn} = C_{mn} i_n \qquad (3.17)$$

equation (3.16) can be written as

$$I_1 = C_{11}i_1 + C_{12}i_2 + \ldots\ldots\ldots C_{1n}i_n$$
$$I_2 = C_{21}i_1 + C_{22}i_2 + \ldots\ldots\ldots C_{2n}i_n \qquad (3.18)$$

$$I_m = C_{m1}i_1 + C_{m2}i_2 + \ldots\ldots\ldots C_{mn}i_n$$

Since $I_j (j = 1 \rightarrow m)$ are measured ion currents, and C_{jk} $(j = 1 \rightarrow m, k = 1 \rightarrow n)$ are known cracking patterns, equation (3.18) can be solved for $i_k (k = 1 \rightarrow n)$. The contribution I_{mn} to the ion current at mass m due to component n is then given by equation (3.17). The temporal variation of the partial pressure of any component n included in equation (3.18) can be followed by plotting the ion current I_{mn} for some mass m, as a function of time. If the sensitivity S_{mn} of the mass spectrometer to that component is known at mass m, its absolute partial pressure P_n can be determined using the expression

$$P_n = C_{mn}i_n/S_{mn} \qquad (3.19)$$

Ideally, the mass spectrometer must be calibrated for the cracking patterns and sensitivities of each gas or vapour which may form part of a gas sample. This is normally done by introducing calibration gases at the time of analysis. However, to a first approximation, published data can also be used, provided that the mass spectra are taken under the same conditions with regard to parameters such as the electron energy, trap current, and ion repeller voltage.

To illustrate this point, table (3.5) compares the cracking pattern of N_2 obtained here using the MS10S mass spectrometer, with the corresponding cracking pattern from published tables (Cornu and Massot 1966). We note that good agreement exists between the two sets of data. Due to the relatively large number of possible contaminants in the laser gas mixture after pulsing, calibration of the MS10S mass spectrometer for each contaminant was not attempted in this work. Published cracking patterns corresponding to standard electron energies of 70 eV, trap currents of 50uA, and repeller voltages of +1V, were used (Cornu and Massot 1966, Eight peak index of mass spectra 1970). Typical sensitivities of the MS10S mass spectrometer were used to determine the partial pressures of contaminants from equation (3.18). Craig and Harden (1965) have shown that without specific calibration of an MS10S mass spectrometer, published sensitivities can be relied on to within ±10%. When a particular instrument is calibrated, the accuracy is within ±2%. For several contaminants, the sensitivity of the MS10S was not known, and approximate values were used. These were estimated from the data of Cornu and Massot (1966), and at worse can be relied on to within ±25%.

After taking a mass spectrum, the total ion current I_m at some mass m is determined by first manually scanning to mass m using a coarse control. A fine adjustment is then made to maximize the ion current which is recorded. On the higher ion current ranges (0.3pA fsd and above), the accuracy of the measurements is within ±3%. On the lowest range of 0.1pA fsd, the accuracy is within ±1% for full-scale deflection, and ±25% near the detection limit of the instrument.

After measuring the ion currents I_j(j=1 -> m) at relevant peaks in the mass spectrum of a sample, the ion currents i_k(k=1 -> n) are determined by solving a set of linear simultaneous equations similar to equation (3.19), using NAG (Numerical Algorithms Group) fortran library routine F04JGF. The routine finds a solution from a least squares fit to the experimental data.

(3.5) Preliminary investigations

The compositions of residual gases in the analyser tube, and the laser and gas handling system, were determined by taking 'blank' mass spectra after both systems had been evacuated. A typical 'blank' spectrum (2 -> 50 amu) of the analyser tube is shown in fig. (3.6) for a tube pressure of $< 10^{-8}$ torr. The mass spectrum was taken using the most sensitive range (0.1pA fsd) of the amplifier. Only three peaks are discernable at masses 18, 20, and 28. Mass 18 signifies the presence of water vapour. The peak at mass 20 is attributed to desorbed HF from the stainless steel body of the analyser tube (Bentley et al 1959). The presence of HF is undoubtedly due to the admission of fluorine compounds in the analyser tube in previous uses of the mass spectrometer. The peak at mass 28 is due to traces of N_2 from residual air, and possibly to CO from the ion gauge filament. A mass scan from 2 to 200 amu showed no other peaks.

Figure (3.7) shows a typical 'blank' mass spectrum (2 -> 50 amu) of the laser envelope and gas handling system after pumping to about 60μm. The spectrum consists of prominant peaks at masses 14, 16, 17, 18, 20, 28, 32, 40, and 44. Analysis of the ion currents at these peaks shows the presence of H_2O(16,17,18,20), N_2(14,28), CO(14,16,28),

CO_2(16,28,44), O_2(16,32), Ar(40), and HF(20). The numbers within brackets are the mass numbers corresponding to ion peaks in the cracking pattern of each compound. Mass scans over the range 2 -> 200 amu showed no other peaks. The contribution to the ion current at mass 28 due to CO formation by chemical reactions at the ion gauge filament, was investigated by measuring the ion current at mass 28 with the ion gauge working, and the ion gauge switched off. The results showed a 10% increase in the CO content when the gauge was switched on. Blears (1951) has suggested that CO may be produced from tungsten carbide formed in previous contamination of ion gauge filaments. The filament in the ion source of the MS10S analyser tube is made of rhenium wire, to minimize the evolution of CO (Sharkey et al 1959).

(3.6) Identification of contaminants

The stable contaminants which are formed in the laser discharge are identified by investigating the changes which occur in the gas composition during laser action. This is done by comparing the mass spectra of fresh mixtures with those of used mixtures after 10^3 laser pulses. The fresh mixtures consist of He, Xe, and NF_3 in the ratio of 350:6:1 at a total pressure of one atmosphere. These gases are used as supplied by the manufacturers (see table 2.2 for typical analysis), without further purification. Gas mixing is done in the laser, using the procedure described in section (2.5) of Chapter 2. The laser is pulsed at a repetition frequency of 1pps, and the capacitor charging voltage is 18KV. The latter is limited by the breakdown voltage of the parallel-plate storage capacitors. The experimental procedure is

as follows. The laser is evacuated to about 60μm, and it is then filled with a fresh gas mixture which is circulated for five minutes to mix the three components, (without adequate mixing, the discharge may develop into constricted arcs, which can result in rapid depletion of the fluorine donor due to hot spots formed on the electrode surfaces). After gas mixing, a sample is taken and its mass spectrum is recorded over the range of 2 to 200amu. The laser is then pulsed, and after 10^3 pulses, a mass spectrum of the used mixture is taken. The recorded mass spectra are then analysed, and the results are compared to identify the stable contaminants formed in the discharge.

(3.6.1) Fresh gas mixtures

Typical mass spectra (2 -> 50amu and 2 -> 200amu) of a fresh gas mixture are shown in figs. (3.8a,b). A comparison with the 'blank' spectrum of the laser reveals the presence of several new peaks. Table (3.6) lists the peaks in the mass spectra of the fresh mixture. Against each mass number is a list of selected compounds, whose cracking patterns contain a peak at the mass number of interest, and are also in broad agreement with the mass spectrum of the gas mixture. The selection process is also based on the results of the infrared absorption studies of section (3.3). In compiling the table, ion current contributions of <1% have been neglected. A survey of table (3.6) shows that several compounds are uniquely identified. These include He at mass 4, H_2O at masses 17 and 18, HF at mass 20 (the contributions from H_2O and Ar are negligible), O_2 at mass 32, Ar at mass 40, Xe at masses 64.5, 65.5, 68, 129, 132, 134, and 136, and NF_3 at mass 71. It must be emphasised that these conclusions apply to

the gas mixtures used in this work, and may not be generally true. The remaining peaks in the spectra of figs. (3.8a,b) are due to contributions from several compounds.

The sets of peaks in the region of masses 65 and 130 in fig. (3.8b) belong to Xe^{2+} and Xe^{+} respectively. The peaks at masses 33 and 52 are mainly due to NF^{+} and NF_2^{+} from NF_3. Table (3.6) shows that the minor peaks at masses 26, 27, 41, 42, and 43 belong to hydrocarbon impurities. The identity of the broad peak at mass 104, which is also observed in Xe alone, is not known. The cracking pattern of SiF_4 contains a peak at mass 104, but the absence of a higher peak at mass 85 ($I^{+}_{85}/I^{+}_{104}=6.7$) in the recorded spectrum excludes SiF_4 as the impurity. The diffuse nature of the peak at mass 104 suggests that it may be due to metastables formed in the ion source (Hipple and Condon 1945).

The composition of the fresh gas mixture was determined using the method of section (3.4.4). Apart from He, Xe, and NF_3, which are the main components, the analysis showed the presence of H_2O, N_2, O_2, CO, CO_2, HF, NO, NO_2, N_2O and hydrocarbon impurities. The amount of CF_4 present was negligibly small. The molecules ClO_2 and F_2 were not detected. The relatively large ion current at mass 20 is partly due to the conversion of NF_3 to HF in the analyser tube of the mass spectrometer. When the ion gauge filament is switched off, there is a significant drop in the peak height at mass 20, and the ion current at mass 71, which is proportional to the NF_3 content of the gas mixture, increases by about 10%.

The concentrations in parts per million (ppm) of H_2O, N_2, O_2, CO, CO_2, NO, NO_2, and N_2O were estimated using equation (3.19), which is reproduced here as equation (3.20), for the sake of convenience.

$$P_n = C_{mn} i_n / S_{mn} \qquad (3.20)$$

The ion current i_n is as defined in section (3.4.4). Typical values of the sensitivity S_{mn} of the Kratos MS10S mass spectrometer were used for H_2O, N_2, O_2, CO, and CO_2 (AEI technical information sheets A506 and A512). In the case of NO, N_2O, NO_2 and CF_4, estimated values were used. The concentration of HF could not be estimated because the corresponding sensitivity was not known. In addition, the ion currrent at mass 20 is not a reliable measure of the amount of HF present in the gas mixture, because HF undergoes strong surface adsorption in the analyser tube (Bentley et al 1959), where it is also formed in reactions of fluorine compounds with water vapour (Blears 1951). The results of the analysis are shown in table (3.7). The main impurities in fresh gas mixtures are H_2O, CO, N_2, and O_2. These are either from residual water vapour and air in the laser, or they are impurities in He, Xe, and NF_3. The other compounds (NO, NO_2, N_2O) are mainly impurities in NF_3.

(3.6.2) Used gas mixtures

Typical mass spectra of the laser gas mixture after 10^3 shots are shown in figs. (3.9a,b). A comparison with the spectra of figs. (3.8a,b) reveals several changes in the mass spectral pattern. In particular, we note that the peaks at mass numbers 26, 27, 29, 33, 52, and 71 have decreased, while those at mass numbers 28, 30, 32, and 44 have increased. There is also a small increase at mass 69, which identifies CF_4. Apart from He and Xe, analysis of the mass spectrum

reveals the presence of H_2O, N_2, O_2, CO_2, CO, NO, NO_2, N_2O, NF_3, NF_2, N_2F_2, HF, CF_4 and hydrocarbon impurities. The molecules F_2, ClO_2 and SiF_4 were not detected, and the intensity of the broad peak at mass 104 did not change. The concentrations in ppm of H_2O, N_2, O_2, CO_2, CO, NO, NO_2, N_2O and CF_4 in the used mixture are listed in table (3.8). In fig. (3.10) the composition of the used mixture is compared with that of the corresponding fresh mixture. Several changes are evident. We note that after 10^3 shots, the partial pressure of NF_3 has decreased by about 50%, and there is an increase in the partial pressures of N_2, O_2, CO, CO_2, NO, NO_2, N_2O, N_2F_2, NF_2 and CF_4. The behaviour of water vapour was not reproducible, but in general its partial pressure decreased during pulsing. There is no significant change in the partial pressure of Xe even though Xe is known to form xenon fluorides by direct fluorination. In the ion source of a mass spectrometer, XeF_2, XeF_4, and XeF_6 form fragment ions such as XeF_2^+, XeF_2^{++}, XeF_3^+, XeF_4^+, XeF_5^+, and XeF_6^+. The mass numbers corresponding to $XeF_4^+(208)$, $XeF_5^+(227)$, and $XeF_6^+(246)$ lie outside the mass range (2 to 200 amu) of the Kratos MS10S mass spectrometer. A search for the peaks corresponding to XeF_2^+, XeF_2^{++}, and XeF_3^+ proved negative. We therefore conclude that xenon fluorides do not accumulate in the laser.

The large change in the partial pressure of NF_3 observed after 10^3 laser pulses, may in itself be responsible for the rapid deterioration of laser performance. The consumption of NF_3 was therefore studied in more detail to determine its significance in the overall degradation process. The formation of fragment products such as NF_2 and N_2F_2 was also investigated.

(3.7) NF_3 depletion

Nitrogen trifluoride (NF_3) is uniquely identified by a peak at mass number 71. The variation in its partial pressure during laser action was therefore determined by measuring the ion current at mass 71 as a function of the number of laser pulses. The gas mixture was similar to those used previously. Mass spectra were taken at intervals of 10 minutes, for 40 minutes before lasing, and subsequently after every 100 laser pulses. The laser was operated at a pulse repetition frequency of 1pps, and the capacitor charging voltage was 18KV. The results are shown in fig. (3.11). In the absence af a gas discharge, the partial pressure of NF_3 (which is proportional to the ion current at mass 71) appears to decrease in time, reaching a steady value after about 20 minutes. Since NF_3 is very stable at room temperature, the decrease in its partial pressure is most probably due to gas mixing, rather than to NF_3 consumption by chemical reactions in the laser. During laser action, the partial pressure of NF_3 decreases rapidly to about 70% of its original value after the first 500 shots. Subsequently the rate of NF_3 loss is more gradual, and it is almost a linear function of the number of laser pulses.

To convert the measured ion currents at mass 71 to partial pressures of NF_3, the sensitivity $S(NF_3^+)$ of the mass spectrometer to NF_3^+ ions must be known. The sensitivity was determined from measurements of the ion current I_{71}^+ at mass 71 for gas mixtures containing known partial pressures $P(NF_3)$ of NF_3. In fig. (3.12), the measured ion currents are plotted as a function of the partial pressure of NF_3 in the mass spectrometer analyser tube. The

sensitivity $S(NF_3^+)$, determined from the slope of the graph is $2x10^{-6}$ $Atorr^{-1}$. Using this value, the estimated partial pressure of NF_3 at the half energy point is 1 torr, and the rate at which NF_3 is consumed is roughly $5x10^{-2}$ torr/100 shots over the linear region of fig. (3.11). After 10^3 shots, the partial pressure of NF_3 is down to about 50% of its value in the fresh gas mixture.

To determine whether NF_3 consumption is in itself responsible for the termination of laser action, the laser pulse energy was measured for two separate gas mixtures containing the same amount of He and Xe, but with 1 torr and 0.5 torr of NF_3 respectively. Fig. (3.13) shows the maximum pulse energy for the two mixtures, together with the pulse energies corresponding to 1 torr and 0.5 torr of NF_3 when the laser is run on a single gas fill containing 2 torr of NF_3 before pulsing. The results show that the consumption of NF_3 does not in itself account for the rapid degradation of laser performance. The latter must be due to NF_3 consumption as well as to other processes involving contaminants formed in the discharge. This result is significant, since it implies that the gas life of the laser cannot be extended indefinitly by replenishing the NF_3 consumed. Due to contaminant build-up in the laser gas mixture, laser action will eventually terminate. To achieve long gas life on single fills, the major contaminants must be identified, so that they can either be removed as they are formed, or their formation inhibited.

(3.7.1) NF_2 formation

The mass spectrum of NF_2 consists of peaks at mass numbers $52(NF_2^+)$, $33(NF^+)$, $19(F^+)$ and $14(N^+)$. Of these, the peak at mass 52

was chosen to study the formation of NF_2 in the laser gas discharge. Table (3.4) shows that NF_3 also contributes to the ion current at mass 52. Since the partial pressure of NF_3 is known to change during laser action, a correction must be made to the measured ion current I^+_{52} at mass 52, to obtain the ion current due to NF_2. The latter is given by

$$I^+_N(52NF_2) = I^+_N(52t) - I^+_N(71NF_3).I^+_0(52NF_3)/I^+_0(71NF_3) \qquad (3.21)$$

where $I^+_N(52NF_2)$ is the ion current at mass 52 after N shots due to NF_2, $I^+_N(52t)$ the total ion current at mass 52, $I^+_N(71NF_3)$ the ion current at mass 71 after N shots due to NF_3, and $I^+_0(52NF_3)/I^+_0(71NF_3)$ the ratio of ion currents at masses 52 and 71 due to NF_3 before lasing.

The results are shown in fig. (3.14), in which $I^+_N(52NF_2)$ is plotted as a function of the number of laser pulses. Molecules of NF_2 first accumulate in the laser during the first 300 (or so) laser pulses, after which they are rapidly used up. The depletion of NF_2 may be due to inhomogeneous reactions with exposed materials in the laser, and to homogeneous gas phase reactions resulting in the formation of XeF^*, and other fluorine compounds.

(3.7.2) N_2F_2 formation

The N_2F_2 content of the gas mixture was determined from the analysis described in the next section. However for the sake of completeness, the results are presented here. Figure (3.14) shows that the partial pressure of N_2F_2 increases for the first 500 shots

(or so), after which N_2F_2 is consumed. We note that the initial rise in the partial pressure of NF_2 and N_2F_2 corresponds to the region where the partial pressure of NF_3 decreases rapidly.

(3.8) Rate of contaminant formation

In sections (3.3) and (3.6), the major contaminants formed in discharge excited mixtures of He, Xe, and NF_3 were identified. In this section, we discuss the results of a study in which the rate of formation of the contaminants was determined as a function of the number of laser pulses.

The increase in the partial pressures of the contaminants may be due to several causes of which the following may be important: (i) a small air leak in the laser envelope or gas handling system, in which case the amount of N_2, O_2, CO_2 and Ar would increase with time even in the absence of a gas discharge; (ii) evolution of surface adsorbed gases, and diffusion of gases trapped in the plastic body of the laser; (iii) inhomogeneous chemical reactions involving exposed materials in the laser; (iv) homogeneous gas phase reactions in the laser discharge. To differentiate between contaminant formation by processes (iii) and (iv), and a possible increase in contaminant levels due to (i) and (ii) above, the experiment was performed in two steps. Firstly, the laser gas mixture was circulated and its composition was determined at intervals of 10 minutes over a period of 40 minutes, without a gas discharge. The laser was then pulsed at a repetition rate of 1 pps, and mass spectra were taken at intervals of 500 laser pulses for a total of 2000 pulses. The experiment was performed in He, He/Xe and $He/Xe/NF_3$ mixtures. The rate of

contaminant formation in He and He/Xe mixtures was compared with that of $He/Xe/NF_3$ mixtures, with the hope that this would provide information on the possible sources of the contaminants.

(3.8.1) He and He/Xe mixtures

Figures (3.15a,b,c) and (3.16a,b,c) show partial pressure variations of several contaminants in He and He/Xe mixtures. The ion current at the major peak of each contaminant is plotted as a function of time before lasing, and the number of laser pulses. In both He and He/Xe mixtures, there are negligible changes in the gas composition before lasing. When the laser is pulsed, there are small increases in the partial pressures of CO, N_2, O_2, NO_2 and NO, and comparatively large increases in those of N_2O and CO_2. In He/Xe mixtures, the rate of increase of N_2O and CO_2 are notably higher than in He. The partial pressure of water vapour did not change in a reproducible manner. The source of N_2 and O_2 is not precisely known. Possible sources are (i) the plastic body of the laser from which N_2 and O_2 may desorb or diffuse in the laser gas mixture, and (ii) water vapour which may act as a source of oxygen atoms. The second possibility is discussed further in a later section.

(3.8.2) $He/Xe/NF_3$ mixtures

Figures (3.17) to (3.20) show variations in the partial pressures of contaminants in $He/Xe/NF_3$ mixtures. The behaviour of Xe is also included for completeness. In the absence of a gas discharge, there are small changes in the partial pressure of the various gases. This

may be due to gas mixing, and to desorption and diffusion of gases from the walls of the laser. In comparison with the small changes before lasing, there are large increases in the partial pressures of N_2, O_2, CO, CO_2, NO_2, N_2O, NO and CF_4 during laser action. The behaviour of NF_3, N_2F_2 and NF_2 were discussed in section (3.7), and will not be considered here. There is no significant change in the partial pressure of Xe. As in the case of He, and He/Xe mixtures, the behaviour of water vapour was not reproducible. In general however, its partial pressure decreased during laser action. Unlike NF_2 and N_2F_2, CF_4 accumulates in the laser, resulting in a permanent loss of fluorine.

A comparison of the results obtained in He/Xe/NF_3 mixtures with those of He and He/Xe mixtures, shows that the rate of contaminant formation in the former is significantly higher. The relatively large amounts of NO, NO_2 and N_2O which are formed in He/Xe/NF_3 are undoubtedly due to the presence of higher concentrations of N_2. The latter is presumably a product of the fragmentation of NF_3. We note that after about 1500 shots, when approximately 70% of the original NF_3 has been consumed, there is a drop in the amount of CO_2 and N_2O, and a reduction in the rate of formation of NO and NO_2.

With the exception of water vapour, the partial pressure of all the contaminants which contain oxygen increases during lasing. A question therefore arises regarding the source of oxygen. It cannot be wholly attributed to desorption and diffusion from the walls of the laser, since before pulsing there are only small changes in the partial pressures of all the contaminants. Water vapour, which is one of the main impurities in fresh and used gas mixtures, may be a possible source. It is known that hydroxyl radicals (OH) are formed

in electrical discharges in water vapour. Oxygen atoms are thought to be formed by the continued excitation and dissociation of the hydroxyl radicals so formed (Shahin 1971). Molecular oxygen may then be formed in very fast reactions between atomic oxygen and OH.

$$O + OH \rightarrow O_2 + H \qquad (3.22)$$

When extensive dissociation of OH does not occur in the discharge, O_2 and H can be formed in the following reactions:

$$2OH \rightarrow H_2O + O \qquad (3.23)$$

$$OH + O \rightarrow O_2 + H \qquad (3.24)$$

Molecular oxygen can also be formed in the reaction of molecular fluorine with water.

$$2F_2 + 2H_2O \rightarrow 4HF + O_2 \qquad (3.25)$$

The decrease in the partial pressure of water vapour which is generally observed after pulsing, may support the above hypothesis.

There is also some uncertainty regarding the fate of fluorine atoms from NF_3. Of the fluorine compounds which are formed in the gas discharge, CF_4 is known to accumulate in the laser, but the amount of CF_4 produced does not account for the loss of NF_3. It is difficult to determine whether HF accumulates in the laser from mass spectral data. As previously mentioned, this is mainly due to the formation of HF in the analyser tube of the mass spectrometer, and to strong surface adsorption. However, the results of the infrared study of

section (3.3) show that HF is present in used gas mixtures after 2.10^3 laser pulses. Formation of HF may therefore account for some of the lost fluorine. Other processes by which fluorine atoms may be lost include the formation of solid fluorides such as AlF_3, and possibly the conversion of the exposed surface of the PVDF body of the laser to teflon. The last process involves the replacement of hydrogen atoms in PVDF by fluorine atoms, and has been previously observed (Laser Focus, Sept. 1980, p.22).

$$-(CH_2-CF_2)_n- + \text{Fluorine} \rightarrow -(CF_2-CF_2)_n- \qquad (3.26)$$

(3.9) UV absorption spectroscopy

Optical absorption at the laser wavelength is an important loss process in rare gas halide excimer lasers. The absorbing molecules are of two types: (i)transient species formed in the laser discharge, and (ii) stable species which are also formed in the discharge, and which accumulate in the laser. Since both types of absorber can lower the laser extraction efficiency, an understanding of the absorption phenomena is desireable. Transient absorption in XeF excimer lasers has been studied by Champagne and Harris (1977), who have shown that Xe_2^+ is a dominant absorber. In this section, we present the results of a study of optical absorption at the XeF laser wavelength by stable species formed in the discharge. The aim was to identify the absorbing molecules, and to determine the importance of the absorption process.

(3.9.1) Experimental

The experimental procedure involves the analysis of gas samples taken before lasing, and after 10^3 laser pulses. The samples are collected in an absorption cell which is similar in construction to the infrared cell of fig. (3.1), with the exception that the optical windows are made of quartz flats which are fused to the quartz body of the cell. Gas samples are collected by circulating the gas mixture through the absorption cell, in which condensable components are trapped in a cold finger which is cooled with liquid nitrogen. After 15 minutes circulation, the cell is isolated, and the cold trap is warmed up to room temperature. The contents of the cell are then analysed using a Pye Unicam SP.800 UV spectrophotometer.

Figure (3.21) shows UV absorption spectra of (a) the residual gas in the absorption cell evacuated to about 50μm, (b) a fresh laser gas mixture consisting of He, Xe and NF_3 in the ratio of 350:6:1 at a total pressure of one atmosphere, and (c) a spent mixture after 10^3 shots. The laser was operated under conditions similar to those used previously. We note that there is negligible absorption at the XeF laser wavelength (351nm) in the fresh mixture. After 10^3 laser pulses, there is significant absorption at the laser wavelength. The absorption spectrum from 240 to 450nm has been identified as that of NO_2. A published absorption spectrum of NO_2 (Hall and Blacet 1952) is shown in fig. (3.22) for easy reference. The broad absorption band below 240nm is thought to be mainly due to HNO_2 (Cox and Derwent 1976), with minor contributions from NO_2, N_2O and O_2 (Johnston and Selwyn 1975, Ogawa 1971). The reaction of NO_2 with H_2O in the

absorption cell is presumed to form HNO_2. The prominant absorption peaks in the region of 250, 215 and 226nm are attributed to NO (Marmo 1953).

The above results show that NO_2 is the dominant absorber at the laser wavelength. To determine the importance of NO_2 absorption, the absorption coefficient must be determined at the laser wavelength. This was done using the experimental set-up of fig. (3.23). The UV source consists of a tungsten halogen lamp. After collimation by the UV achromat L1, the light beam is divided by a semi-coated aluminium flat B1. One of the resulting beams is transmitted through the laser, and the other is transmitted through an evacuated cell whose optical path length is equal to that of the laser. The transmitted beams are then recombined at beam splitter B2, and the resulting beam is focused onto the entrance slit of an optical spectrum analyser (B & M OSA 500). The latter consists of a monochromator (Ebert mount), a vidicon tube, and a control and display unit. A spectrum at the exit of the monochromator is detected by the vidicon as a function of its intensity and position, where it falls on a small target. The latter consists of a silicon multi-diode array. The information acquired by the vidicon is processed by the control unit, and subsequently stored in 500 memory channels which span the recorded spectrum. The latter can be displayed on a video screen, and the content of each channel can be read by moving a cursor to the corresponding position on the screen. The vidicon tube of the B & M OSA 500 has a spectral range of 300 to 950nm. The vidicon signal increases linearly (within 1%) with the intensity of the incident light. When a high-dispersion grating (2400 lines/mm) is used in the monochromator, the wavelength separation of adjacent channels is 0.3 Å.

(3.9.2) UV absorption measurements

When light of low intensity passes through an absorbing medium, its intensity changes and over a distance dx, the change $dI_u(x)$ is given by

$$dI_u(x) = -k_u I_u(x)dx \tag{3.27}$$

where $I_u(x)$ is the intensity of the incident light, and k_u is the absorption coefficient, usually expressed in cm^{-1}. In general k_u is a function of the frequency u. Integrating equation (3.27) over an absorption path of length z, we obtain

$$I_u(z) = I_u(0)\exp(-\int_0^z k_u dx) \tag{3.28}$$

where $\int_0^z k_u dx$ is the optical depth of the medium. If the absorbing medium is homogeneous, k_u is independent of x and equation (3.28) reduces to

$$I_u(z) = I_u(0)\exp(-k_u z) \tag{3.29}$$

from which we obtain

$$k_u = (1/z)\ln I_u(0)/I_u(z) \tag{3.30}$$

Equation (3.30) was used to determine the absorption coefficient at the laser wavelength in fresh gas mixtures, and in spent mixtures

after 500 and 10^3 laser pulses. An optical spectrum of the laser output was first recorded, and the cursor was set at the memory channel corresponding to the peak at 351nm. Channel counts were then recorded (i) when the laser was evacuated, (ii) for a fresh gas mixture, and (iii) for the same gas fill after 500 and 10^3 laser pulses. For a given number of laser pulses, $I_u(0)$ was determined by blocking off the transmitted beam from the laser, and recording the channel count corresponding to the transmitted beam from the evacuated cell. The reverse procedure was then used to determine $I_u(z)$. Since the time interval between the two measurements was only a few seconds, errors due to long-term fluctuations in the intensity of the source, and drift in the control unit of the OSA were negligible. A small correction was made to the the channel count corresponding to $I_u(0)$, to account for the fact that B1 and B2 are not exactly 50% transmitting. Several measurements of k_u were made and the results were then averaged. The calculated values of k_u are listed in table (3.9), as a function of the number of laser pulses. As a check, the magnitude of k_u after 10^3 laser pulses was determined from the calculated ion current and the estimated sensitivity corresponding to NO_2 at mass 30, and the absorption cross section of NO_2 at 351nm (5.7×10^{-19} cm^2, Hall and Blacet 1952). A value of $11 \times 10^{-2}\%$ cm^{-1} was obtained, which is of the same order of magnitude as the measured value of $8 \times 10^{-2}\% cm^{-1}$.

For small Blumlein laser devices similar to the one used in this work, the small signal gain is typically 0.1 to 1 cm^{-1} (Hasson et al 1977). This takes into account absorption losses due to species such as Xe_2^+. Absorption by NO_2 is therefore smaller than the small signal gain by about two orders of magnitude. Consequently, NO_2 absorption

is not considered to be a major factor in the overall degradation of laser performance.

(3.10) Summary

The main results of the studies reported in this chapter can be summarised as follows:

(i) In discharge excited lasers which use He/Xe/NF_3 mixtures, the fluorine donor (NF_3) is depleted in the discharge. Although NF_3 depletion results in a reduction of the laser pulse energy, it does not in itself explain the observed fast deterioration of laser performance. The latter is attributed to NF_3 depletion, and to other processes involving contaminants which are formed in the discharge. These processes may include (a) absorption at the laser wavelength, (b) quenching of the excited rare gas halide molecules (XeF^*), and their xenon metastable precursors (Xe^*), and (c) deterioration of the laser discharge due to negative-ion formation (Nighan 1976), and optical absorption in the spectral region where preionization occurs.

(ii) Infrared spectral and mass spectrometric analysis of the laser gas mixture shows that N_2, O_2, CO, CO_2, NO, NO_2, N_2O, NF_2, N_2F_2, HF and CF_4 are formed in the discharge. Fragment products of NF_3 which first accumulate in the laser are NF_2 and N_2F_2, but these are rapidly depleted after about 300 laser pulses (or so). Accumulation of CF_4 in the laser constitutes a permanent loss of fluorine atoms. It is known that HF is present in used gas mixtures, but its behaviour could not be determined from mass spectral data. The other

contaminants build up in the laser. After about 1500 laser pulses, when the NF_3 content is down by 70%, there is a drop in the amount of CO_2 and N_2O, and a reduction in the rate of formation of NO and NO_2.

(iii) Of the identified contaminants, only NO_2 absorbs at the laser wavelength. This is confirmed by UV absorption studies of the laser gas mixture. However, NO_2 absorption is negligibly small compared to the small signal gain of Blumlein devices similar to the one used in this work. Absorption at the laser wavelength is therefore not considered to be a major factor in the short term degradation process.

(v) The source of oxygen atoms for the formation of O_2, NO, etc., is not known. Water vapour, which is a major impurity in fresh gas mixtures, is a possible source. If this is so, it may be possible to extend the gas life by using a bakable laser system. In this respect, PVDF may not be a suitable building material. It has a high water absorption coefficient (0.03% compared to <0.01% for PTFE), and its maximum operating temperature is 150 -> 170^{o}C (compared to 250 -> 260 ^{o}C for PTFE). PVDF may also contribute to fluorine depletion by reacting with fluorine compounds to form teflon.

Table(3.1)

Formation and quenching rates, and branching ratios for XeF^* and KrF^*

Compound	Formation rate 10^{-11} cm^{3}S^{-1} (1)		Branching ratio (1)		Quenching rate 10^{-19} cm^{3}S^{-1}	
	XeF^*	KrF^*	XeF^*	KrF^*	XeF^*	KrF^*
F_2	75	72	1.0	1.0	53(2)	50(3)
F_2O	57	53	0.92	1.0		
SF_6	~0	~0				
NF_3	9	8.9	1.16	0.57	2.4(2)	
N_2F_4		33	0.63	0.5		
FNO	39	47	0.77	<0.09		
XeF_2	*	*	*	*		
CF_4	0	0				

(1)Velazco et al (1976)

(2)Brashears et al (1977)

(3)Eden et al (1978)

(*)Thought to be large.

Table (3.2)

Table of boiling points

Name	Formula	M.W.	B.P.(°C)
Acetylene	CH:CH	26	-84
Argon	Ar	39	-186
Carbon Dioxide	CO_2	44	-75 (sublimes)
Carbon Monoxide	CO	28	-192
Carbon Tetrafluoride	CF_4	88	-128
Carbonyl Fluoride	COF_2	66	-81
Difluorohydrazine	N_2F_2	66	-106
1,1-Difluoroethane	$CHF_2.CH_3$	66	-25
1,1-Difluoroethylene	$CF_2:CH_2$	64	-84
Ethane	$CH_3:CH_3$	30	-89
Ethylene	$CH_2:CH_2$	28	-104
Fluorine	F_2	38	-188
Fluorine Oxide	F_2O	54	-145
Fluoroethane	$CH_3.CH_2F$	48	-38
Fluoromethane	CH_3F	34	-78
Helium	He	4	-269
Hexafluoroacetone	$CH_3.CO.CF_3$	166	-28
Hexafluoromethane	$CF_3.CF_3$	138	-78
Hexafluoropropane	$CF_3.CF_3:CF_3$	150	-30
Hydrogen	H_2	2	-253
Hydrogen Fluoride	HF	20	19.5
Krypton	Kr	83	-153
Methane	CH_4	16	-162

Table (3.2) contd.

Nitric Oxide	NO	30	-152
Nitrogen	N_2	28	-196
Nitrogen Dioxide	NO_2	46	21
Nitrogen Trifluoride	NF_3	71	-129
Nitrogen Trioxide	N_2O_3	76	-30
Nitrosyl Fluoride	FNO	49	-60
Nitrous Oxide	N_2O	44	-88
Nitryl Fluoride	FNO_2	65	-72
Oxygen	O_2	32	-183
Silicon Tetrafluoride	SiF_4	104	-95 (sublimes)
Tetrafluorohydrazine	$NF_2.NF_2$	104	-74
Trifluoromethane	CHF_3	70	-84
Vinyl Fluoride	$CH_2.CHF$	46	-72
Xenon	Xe	131	-108

TABLE (3.3)

Minimum detection level of several gases by the MS10S mass spectrometer (sample pressure = 2.10^{-5} torr)

Compounds	Mass amu	Sensitivity, $x10^{-6}$ Atorr^{-1}	P_m(ppm)
H_2	2	63	2
He	4	15	7
H_2O	18	46	2
N_2	28	42	2
CO	28	46	2
O_2	32	22	5
Ar	40	43	2
CO_2	44	37	3
Xe	132	14	7

TABLE (3.4)

CRACKING PATTERNS

m/e	2	4	12	14	16	17	18	19	20	22	26	27	28	29	30	32	33	40	44	46	47	52	64.5	65.5	66	71
H_2	100																									
He		100																								
H_2O	0.7				1.1	23	100	0.1	0.3																	
N_2				7.2									100	0.8												
CO			4.5	0.6	0.9								100	1.1	0.2											
NO				7.5	1.5										100	0.2										
O_2					11.4											100	0.1									
NO_2				9.6	22.3										100					37	0.1					
N_2O				12.9	5								10.8	0.1	31.1				100	0.2						
CO_2			6		8.5					1.2			11.4	0.1					100	0.4						
N_2F_2				25				5					100	1			11				97				26	
COF_2			3		1								14								100				55	
NF_3				9				6									38					100				33
Ar									10.7									100								
Xe																							17.3	13.9	17.8	

TABLE (3.4) CONTD.

m/e	2	4	12	14	16	17	18	19	20	22	26	27	28	29	30	32	33	40	44	46	47	52	64.5	65.5	66	71
F_2O					44			10																		
ClO_2					22																	1				
CF_4								7																		
SiF_4								19					40				37				32					

m/e	25	31	35	37	50	51	53	54	67	69	85	86	87	104	128	129	130	131	132	134	136					
Xe												-			7.1	98.4	15.2	79.5	100	37.9	32					
F_2O			100					62																		
ClO_2			10	3		40	13		100	32																
CF_4	4	5			12					100																
SiF_4											100	52	34	15												

TABLE (3.5)

Comparison of the published cracking pattern of N_2 (Cornu and Massot 1966) with that obtained using the Kratos MS10S mass spectrometer.

m/e	14	28	29
Cornu and Massot	7.2	100	0.8
MS10S	7.3	100	0.9

TABLE (3.6)

Mass numbers and selected compounds corresponding to the mass spectra of figs.(3.8a,b)

Mass Number	Selected Compounds
3	He
4	He
12	CO, CO_2
14	CO, N_2, NO, CO_2, NO_2, N_2F_2, NF_3
16	H_2O, CO, NO, O_2, CO_2, NO_2, N_2O, ClO_2
17	H_2O
18	H_2O
19	HF, NF_3, N_2F_2, CF_4
20	H_2O, HF, Ar
26	C_2H_2, C_2H_4, C_2H_6, C_3H_6, C_3H_8, C_4H_{10}
27	C_2H_2, C_2H_4, C_2H_6, C_3H_6, C_3H_8, C_4H_{10}, C_7H_8, C_8H_{10}
28	CO, N_2, CO_2, N_2O, N_2F_2
29	CO, N_2
30	CO, NO_2, N_2O, NO
32	O_2
33	NF_3, N_2F_2
40	Ar
41	C_3H_6, C_3H_8, C_4H_{10}
42	C_3H_6, C_3H_8, C_4H_{10}
43	C_3H_8, C_4H_{10}
44	CO_2, N_2O
47	N_2F_2

Table(3.6) contd.

52	NF_3, NF_2
64.5	Xe
65.5	Xe
66	Xe, N_2F_2
67	Xe, ClO_2
68	Xe
69	CF_4, ClO_2
71	NF_3
129	Xe
132	Xe
134	Xe
136	Xe

TABLE (3.7)

Concentration (ppm) of impurities in fresh gas mixtures

Compound	Sensitivity $x10^{-6}$ Atorr^{-1}	Concentration (ppm)
H_2O	46	340
N_2	42	190
CO	46	190
NO	51	2
O_2	22	90
CO_2	37	17
N_2O	39	19
NO_2	11	18
CF_4	27	<4

TABLE (3.8)

Concentration of impurities in used gas mixtures after 10^3 shots.

Compound	Sensitivity $X10^{-6}$ Atorr^{-1}	Concentration (ppm)
H_2O	46	320
N_2	42	600
CO	46	250
NO	51	17
O_2	22	340
CO_2	37	62
N_2O	39	50
NO_2	11	100
CF_4	27	9

TABLE (3.9)

Absorption coefficients in fresh and used gas mixtures

Number of laser pulses	k_u $x10^{-2}$ %cm^{-1}
0	small
500	5
1000	8

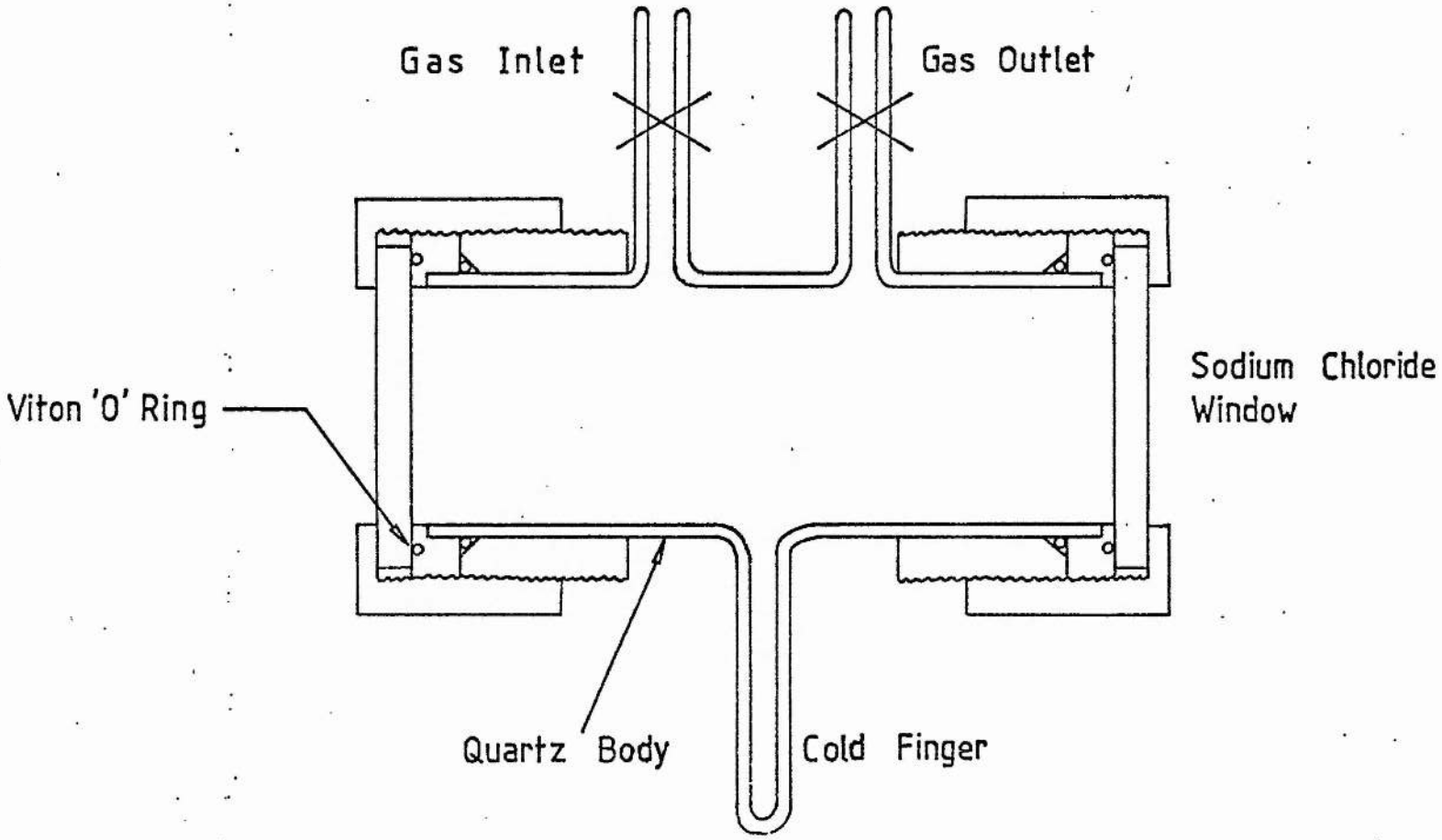

Fig.(3.1) The infrared absorption cell.

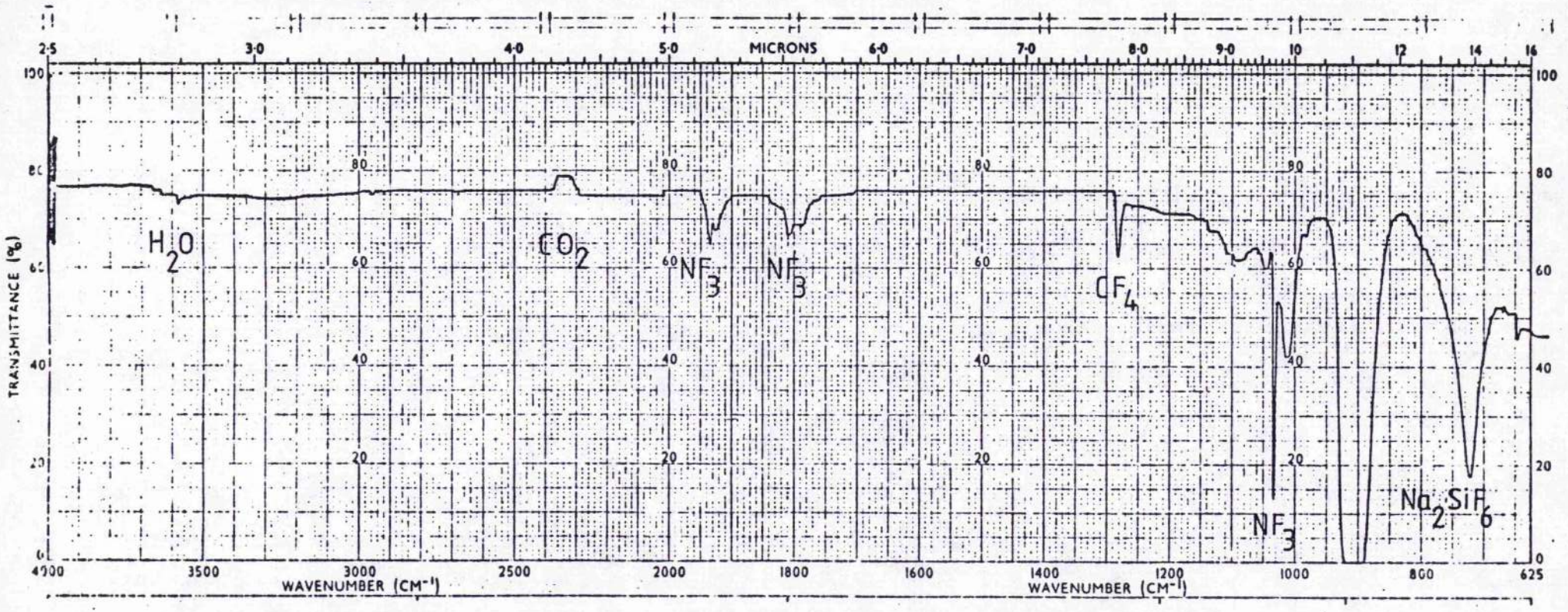

Fig.(3.2) Infrared absorption spectrum of a fresh gas mixture.

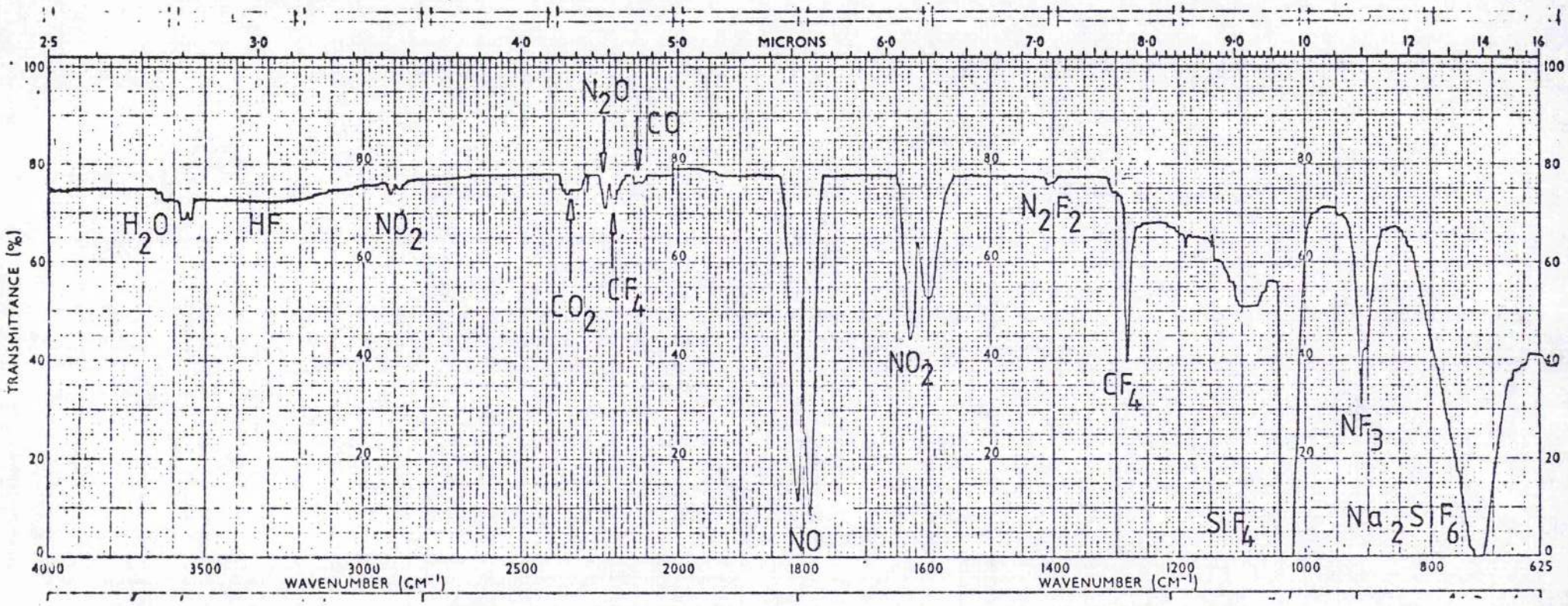

Fig.(3.3) Infrared absorption spectrum of a used gas mixture after 2000 laser pulses.

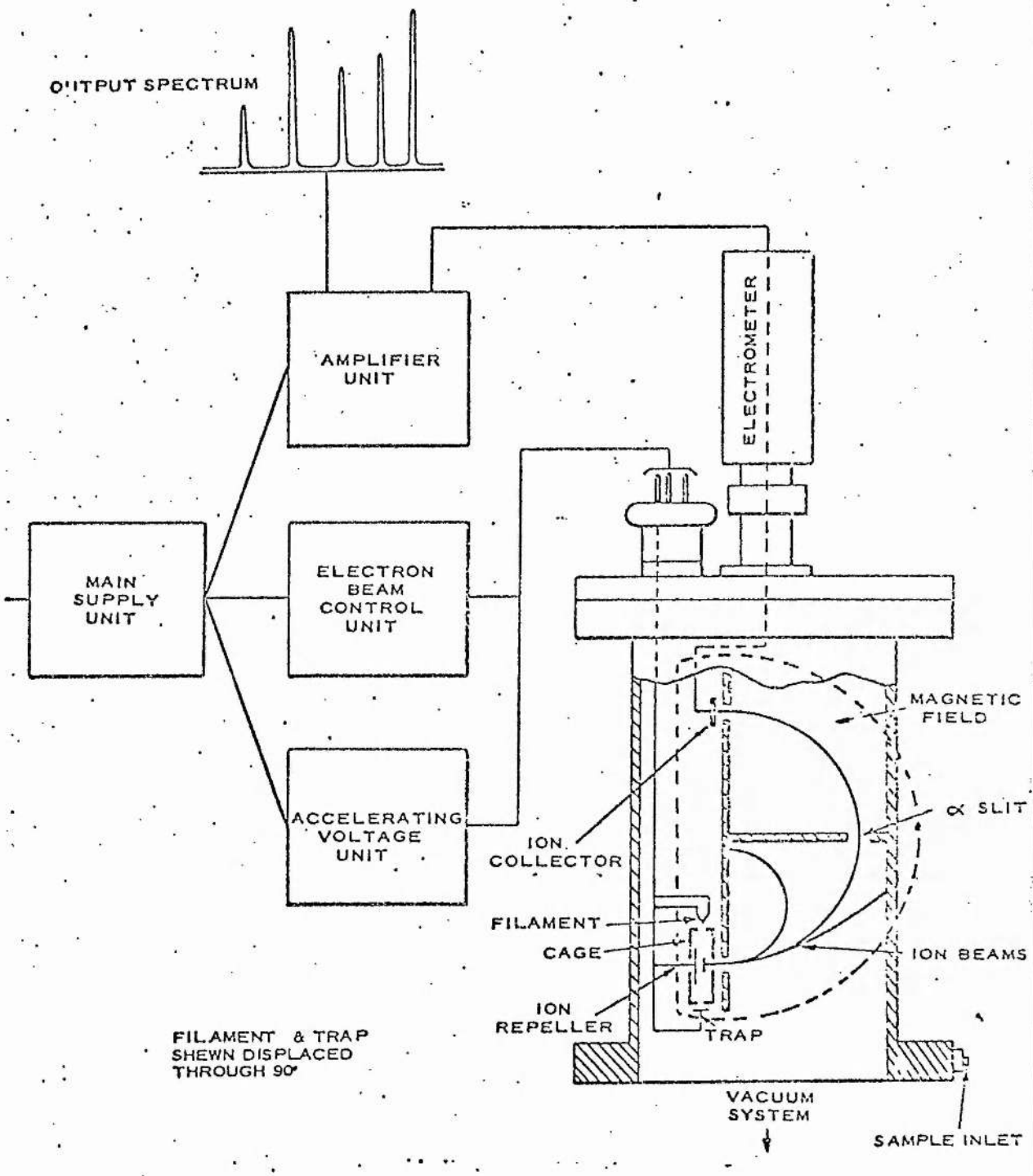

FIG. (3.4) SCHEMATIC ARRANGEMENT OF THE MS10 MASS SPECTROMETER

(Reproduced from the Kratos MS10S instruction manual)

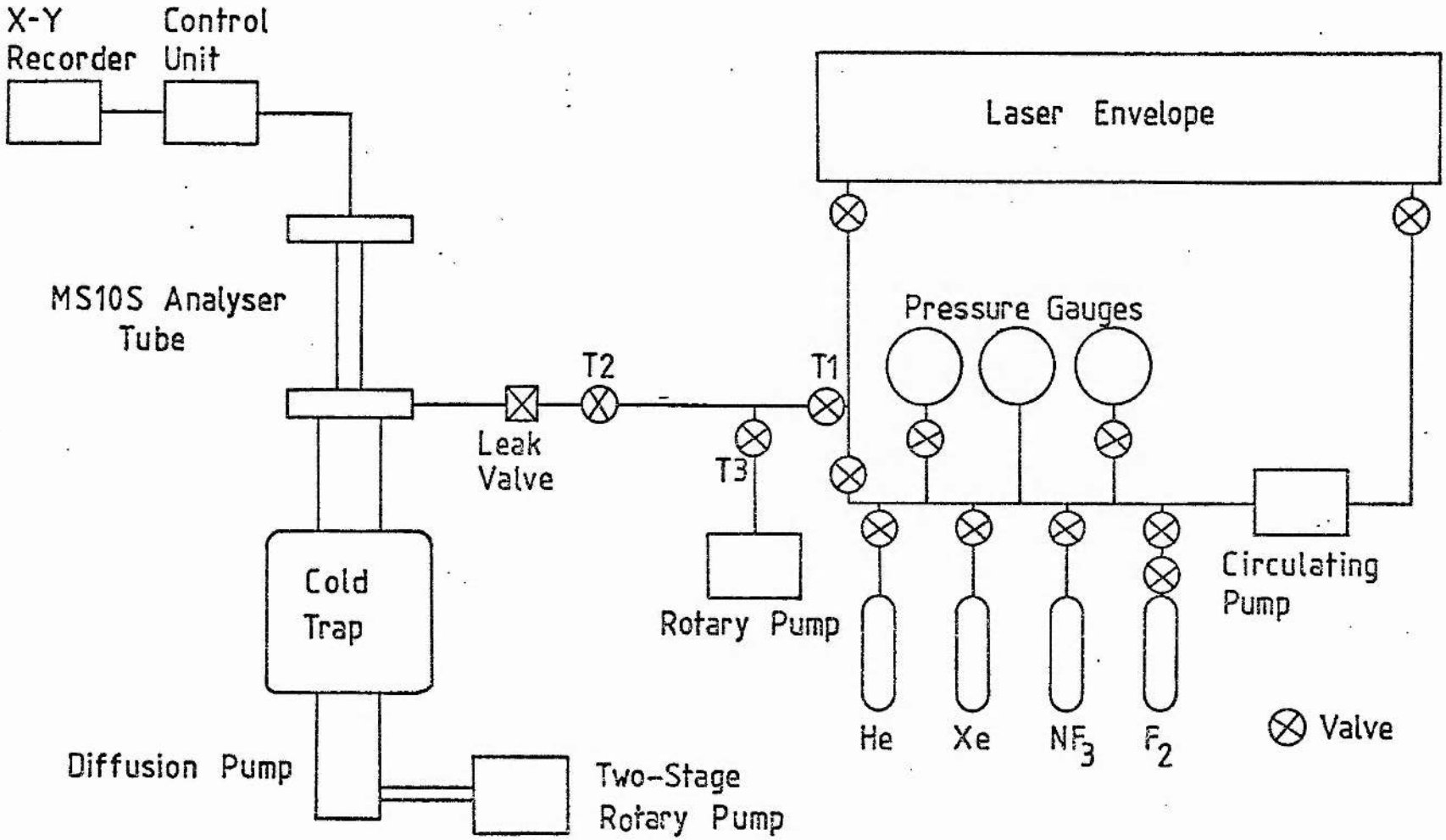

Fig. (3.5) Mass spectrometer and "gas-handling" system.

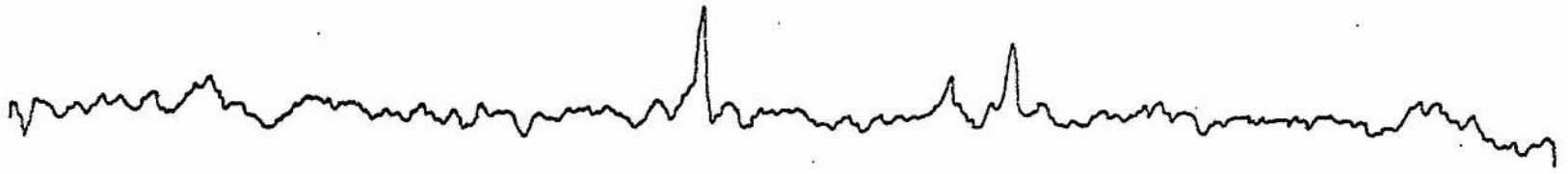

Fig.(3.6) 'Blank' mass spectrum of the analyser tube.

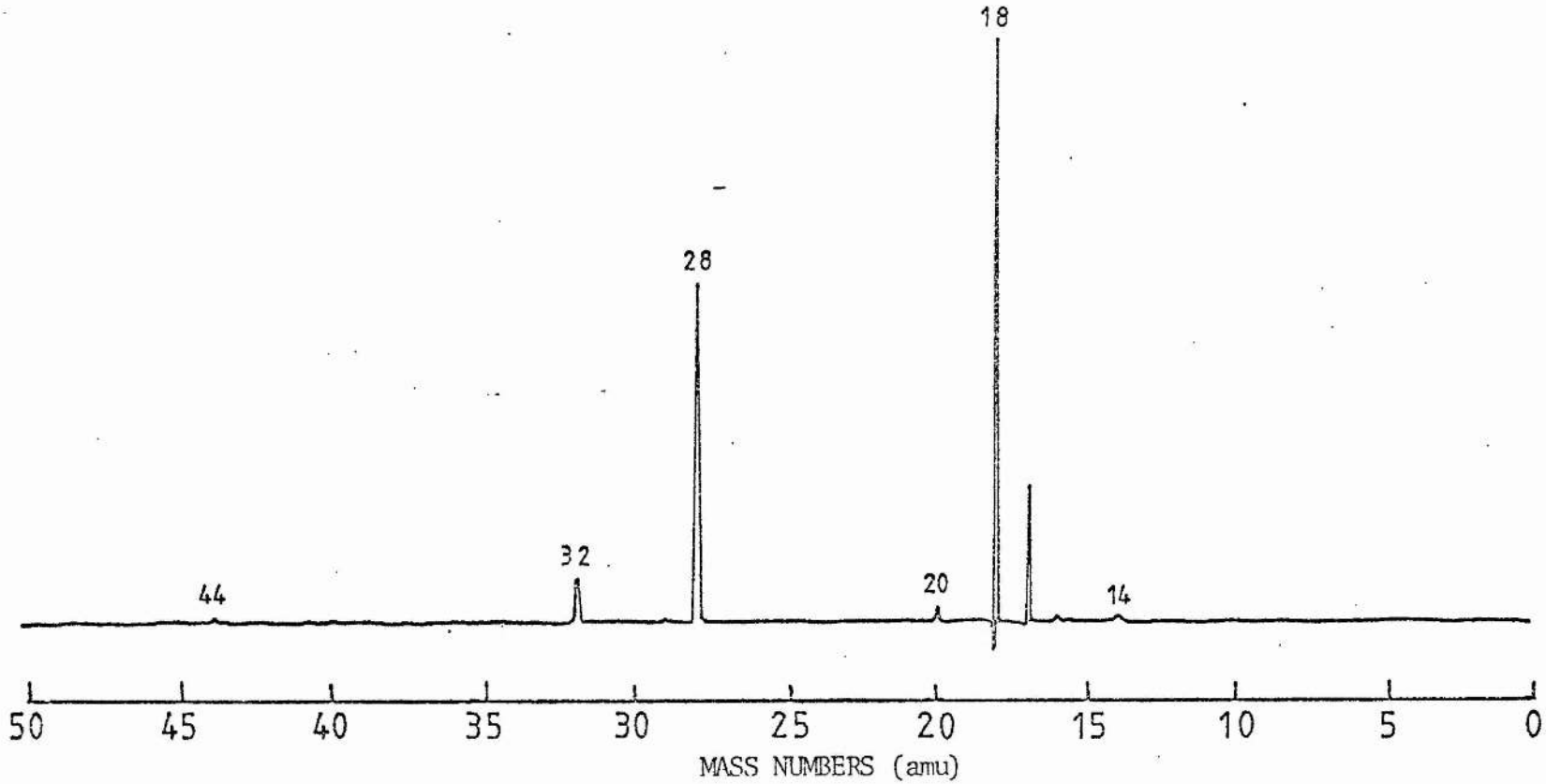

Fig.(3.7) 'Blank' mass spectrum of the laser envelope and "gas-handling" system.

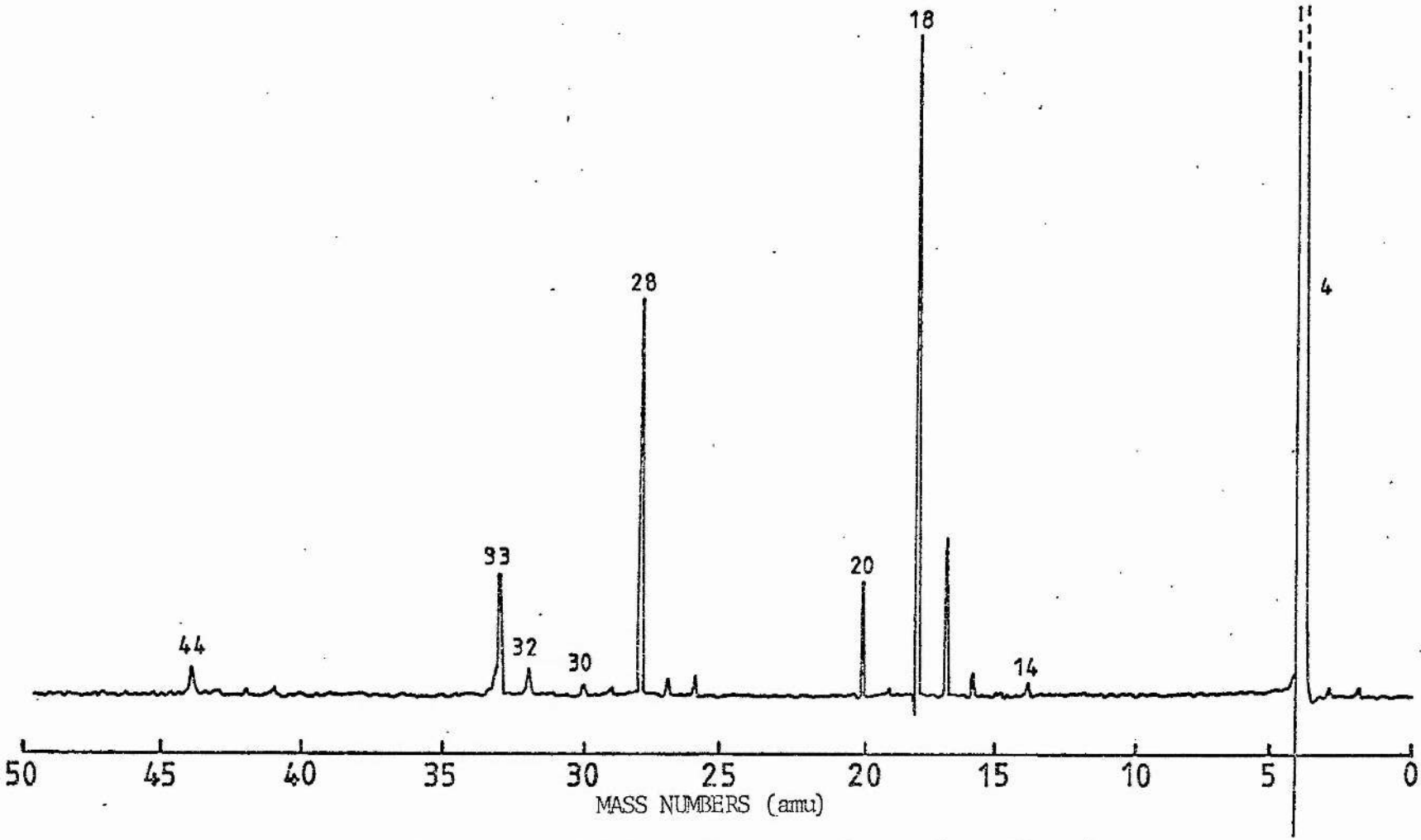

Fig.(3.8a) Mass spectrum of a fresh gas mixture (2 to 50 amu).

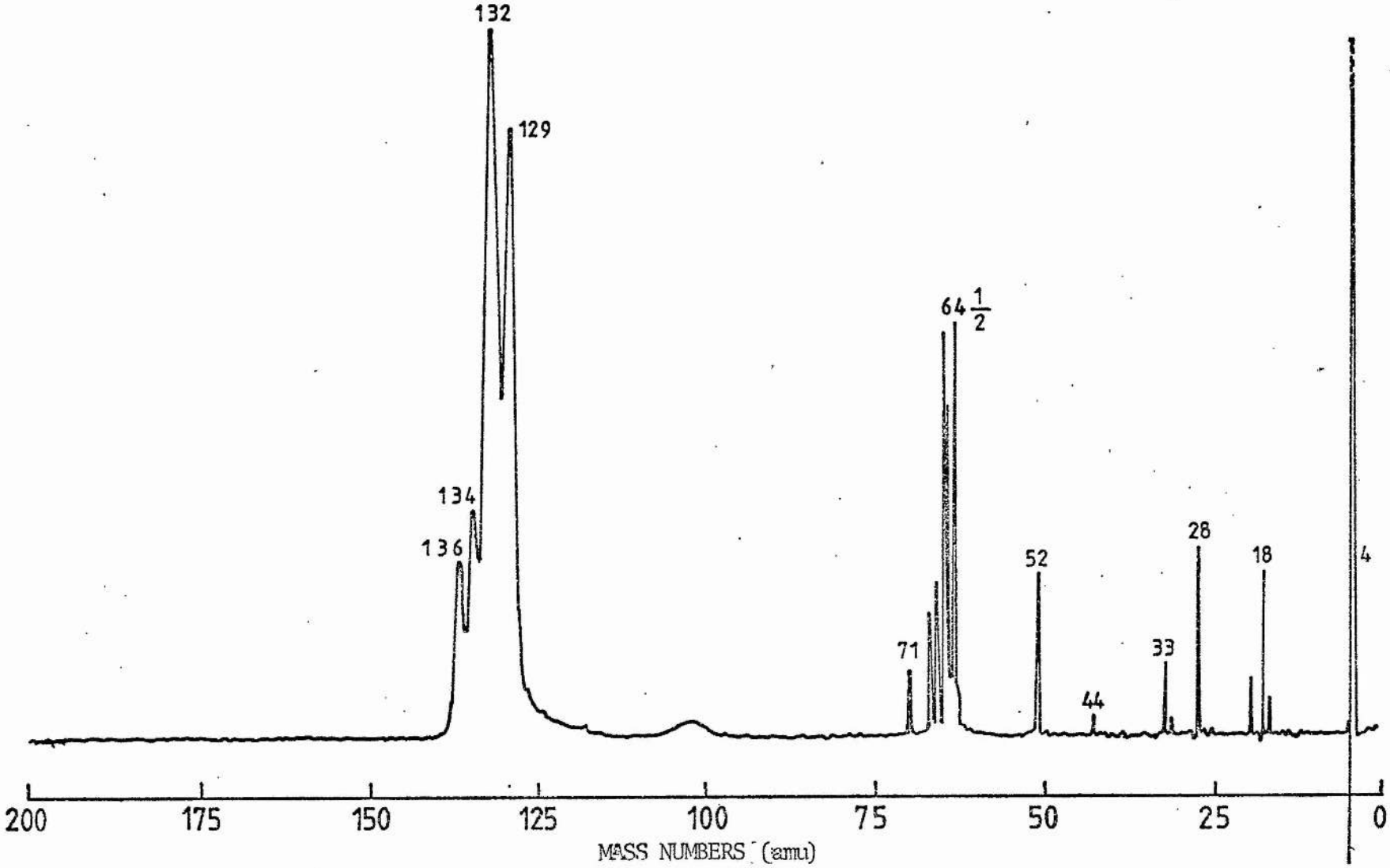

Fig.(3.8b) Mass spectrum of a fresh gas mixture (2 to 200 amu).

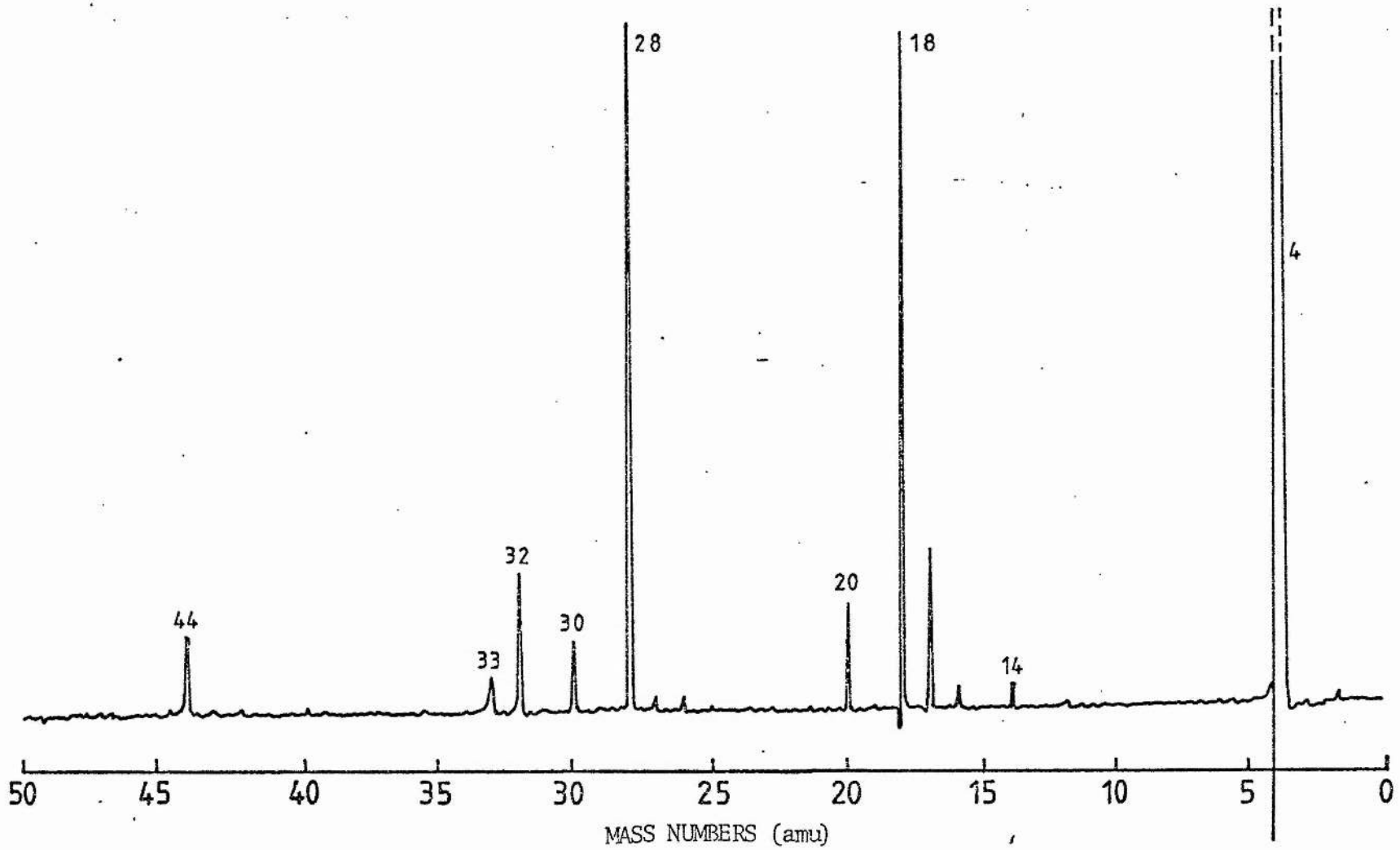

Fig.(3.9a) Mass spectrum of a used gas mixture after 1000 laser pulses (2 to 50 amu).

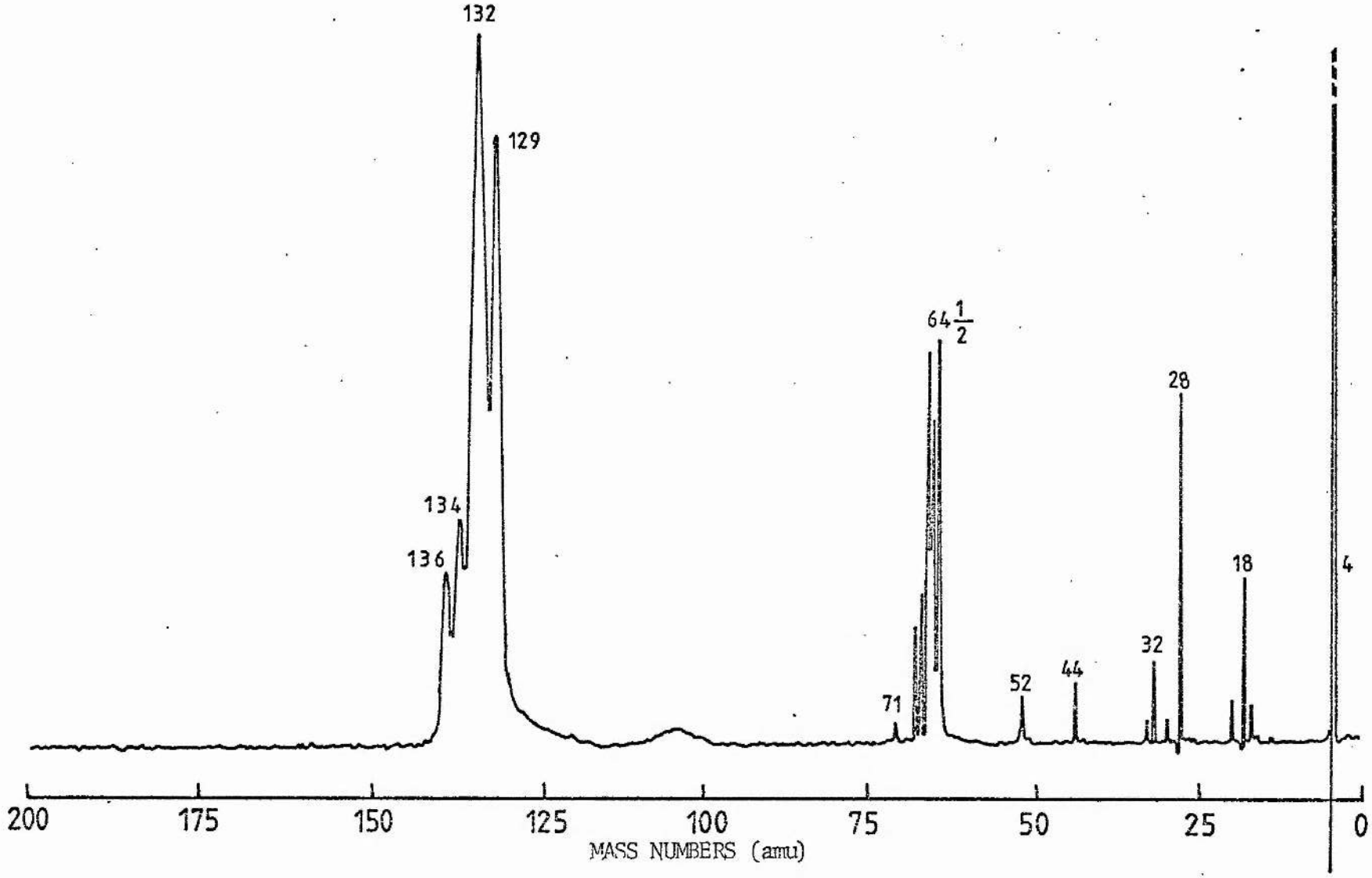

Fig.(3.9b) Mass spectrum of a used gas mixture after 1000 laser pulses (2 to 200 amu)

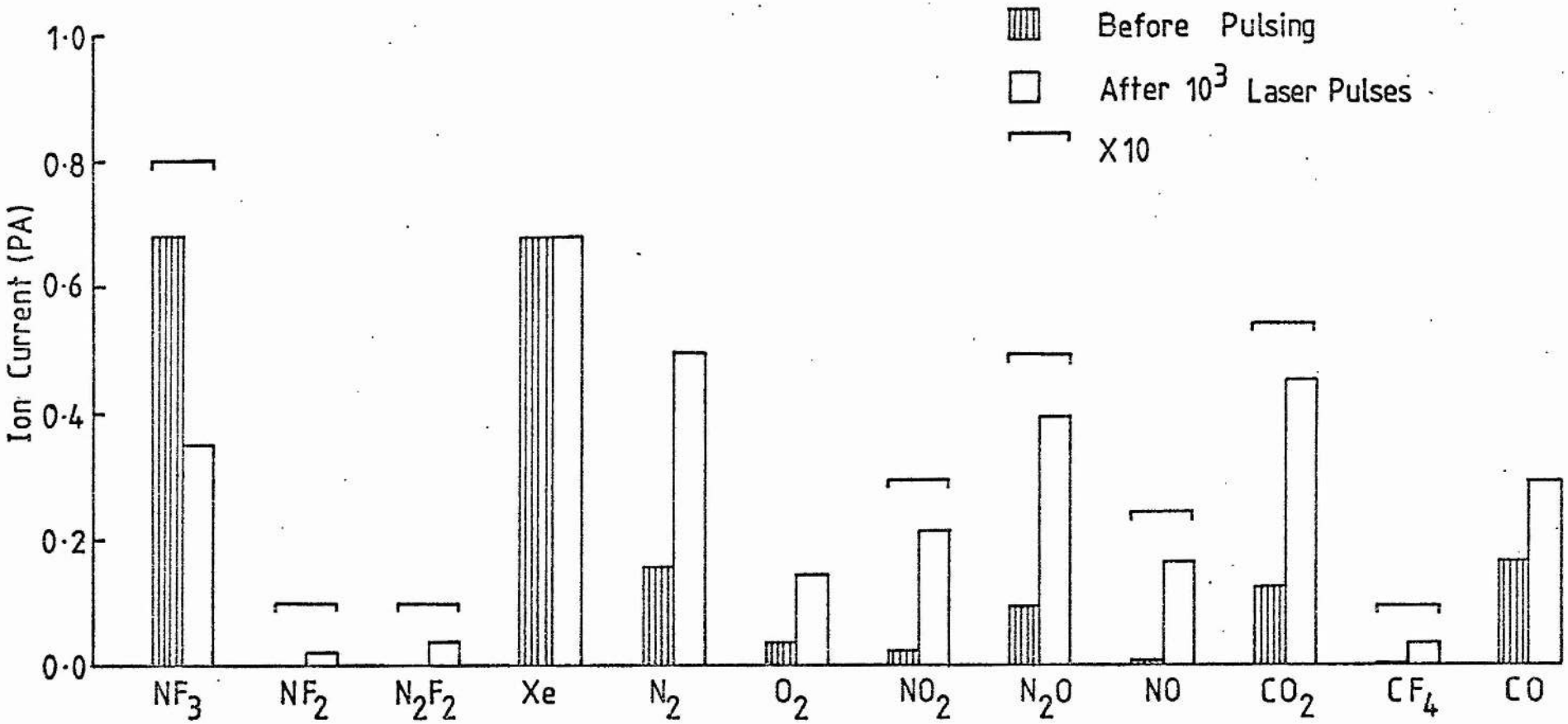

Fig.(3.10) Measured ion currents before lasing and after 1000 laser pulses.

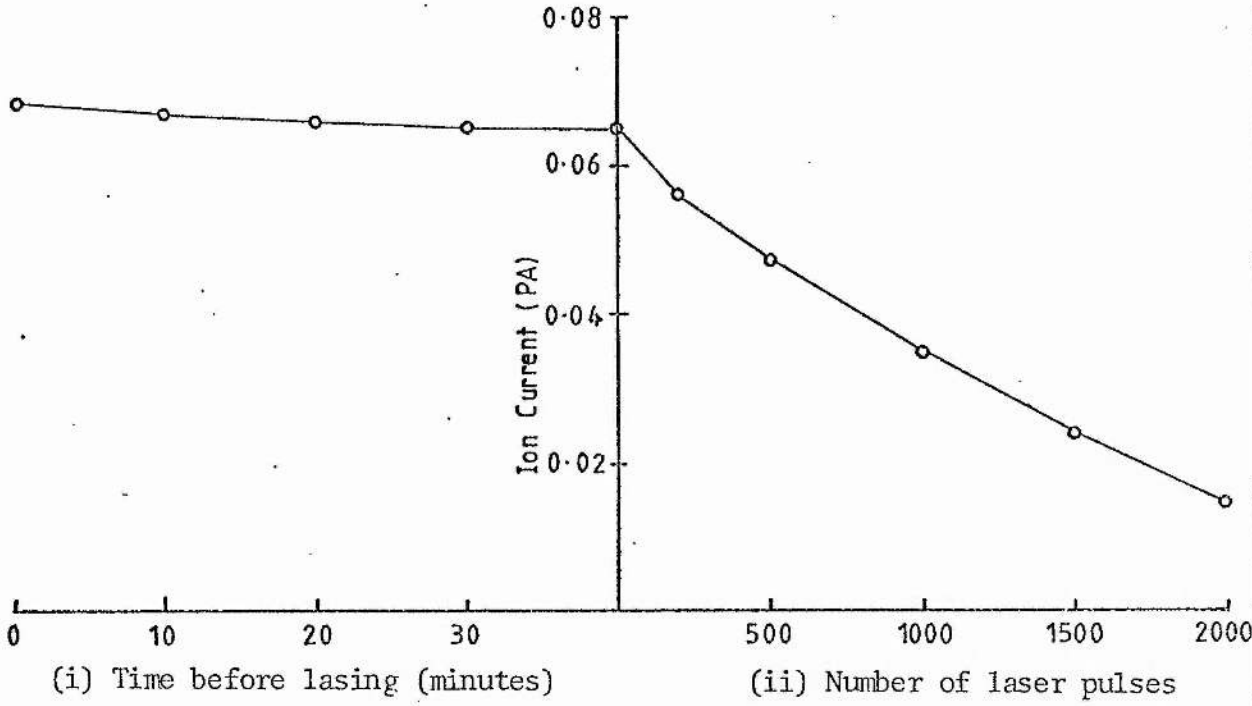

Fig.(3.11) Ion current variation at mass 71(NF_3) in He/Xe/NF_3 mixtures.

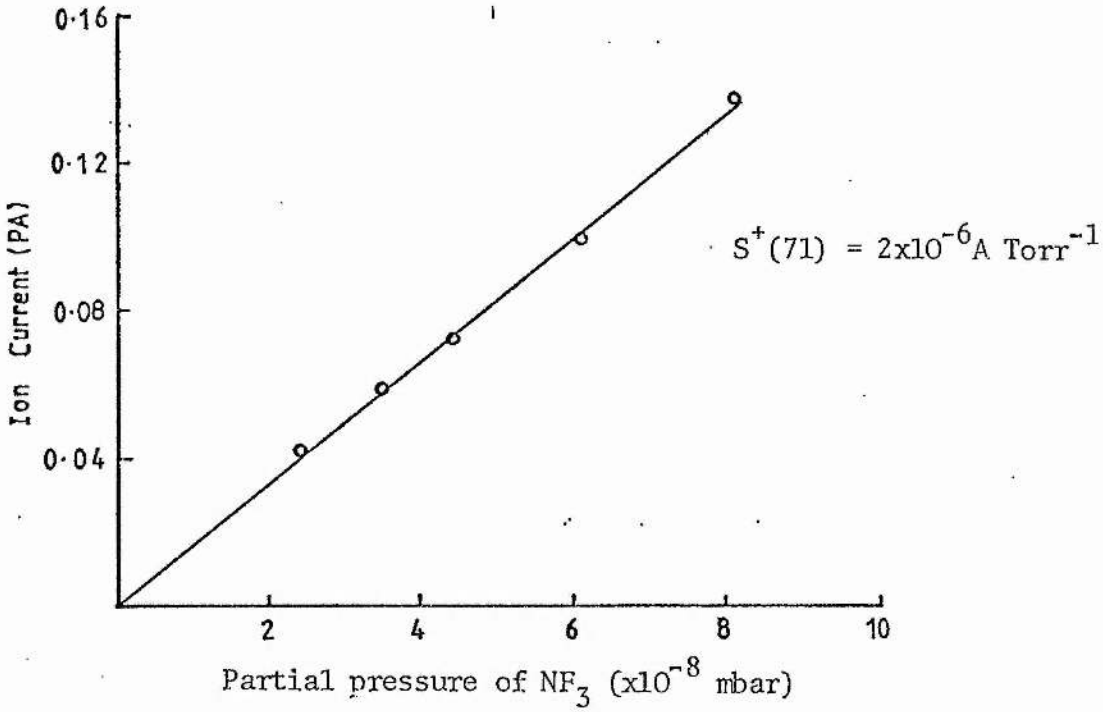

Fig.(3.12) Variation of $I^+(71)$ as a function of the partial pressure of NF_3.

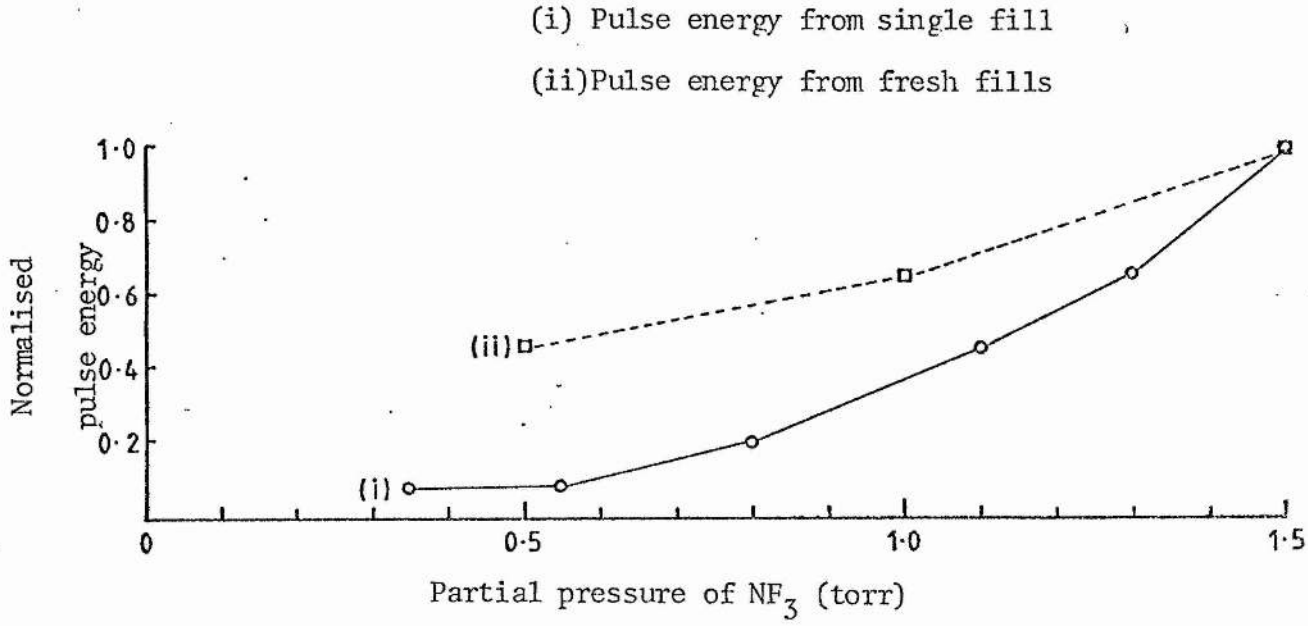

Fig. (3.13) Normalised pulse energy corresponding to (i) a single gas fill and (ii) fresh gas fills.

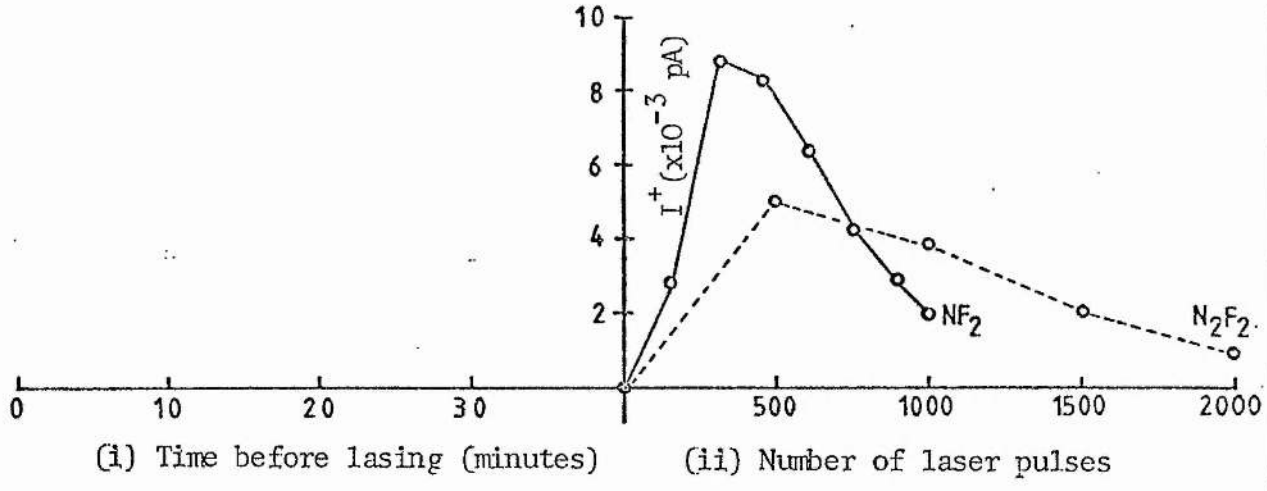

Fig. (3.14) Ion current variation for NF_2 and N_2F_2 in $He/Xe/NF_3$ mixtures.

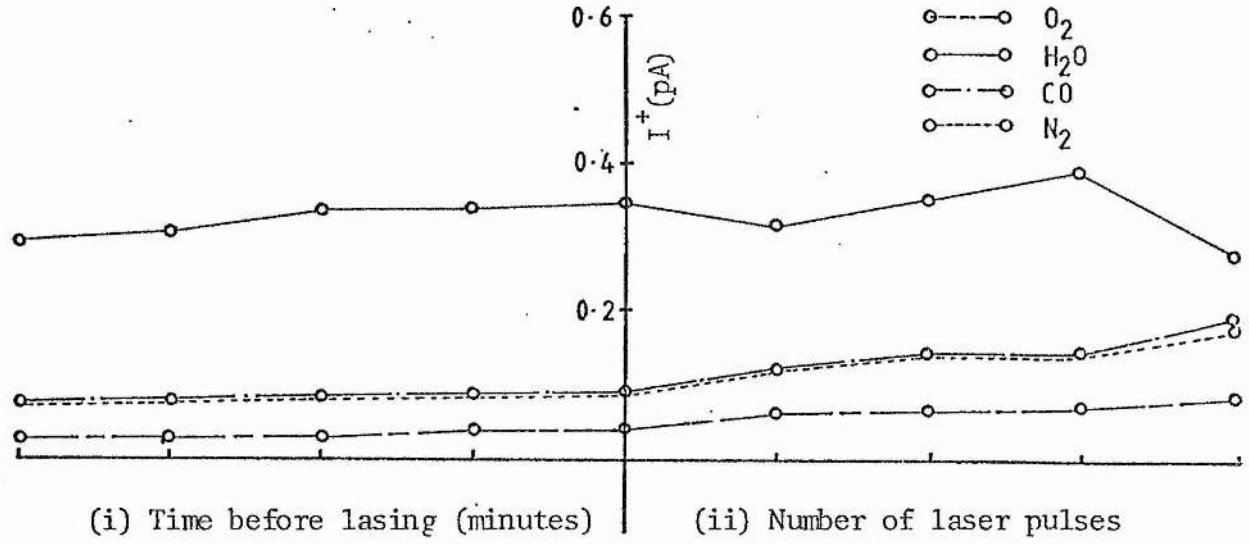

Fig.(3.15a) Ion current variation for H_2O, CO, N_2 and O_2 in helium.

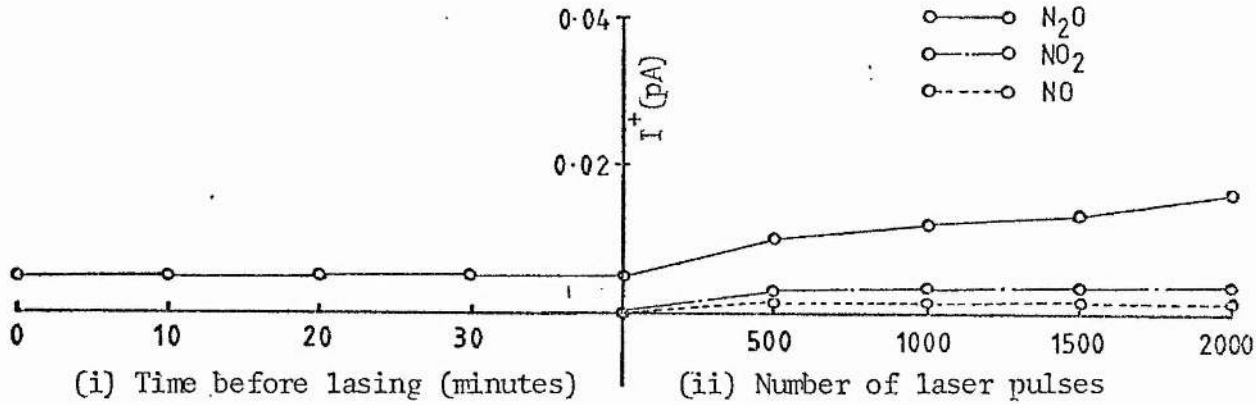

Fig.(3.15b) Ion current variation for NO, NO_2 and N_2O in helium.

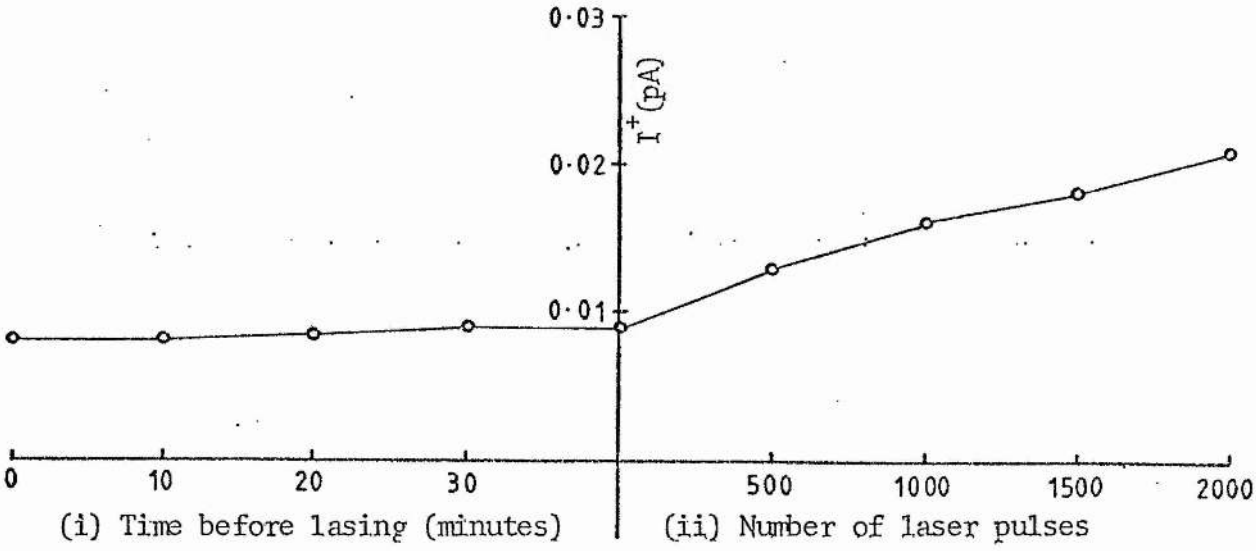

Fig.(3.15c) Ion current variation for CO_2 in helium.

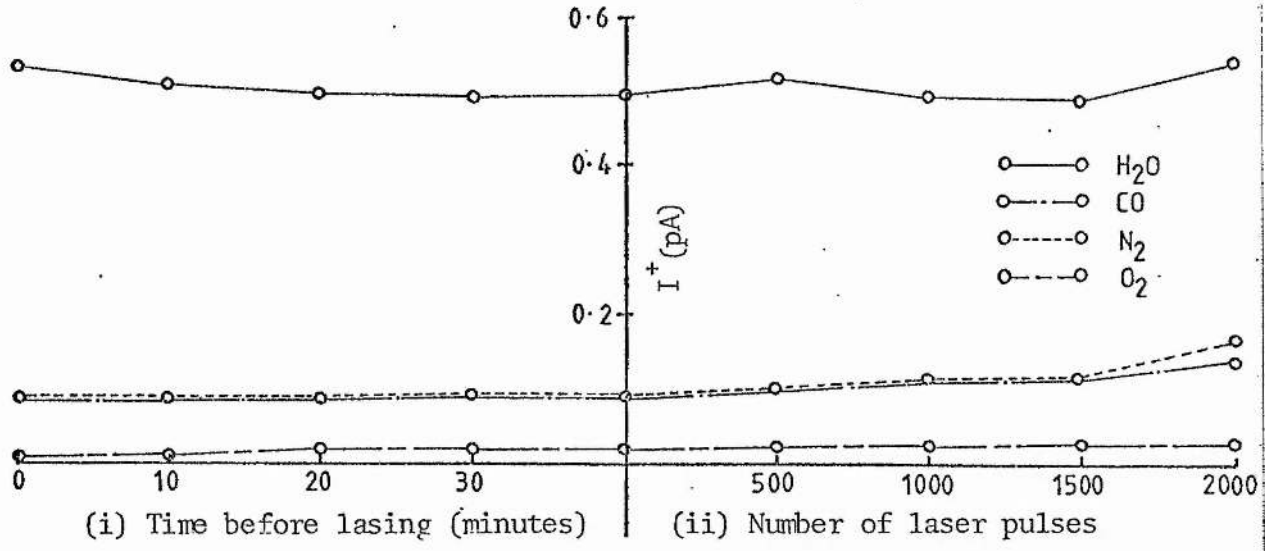

Fig.(3.16a) Ion current variation for H_2O, CO, N_2 and O_2 in He/Xe mixtures.

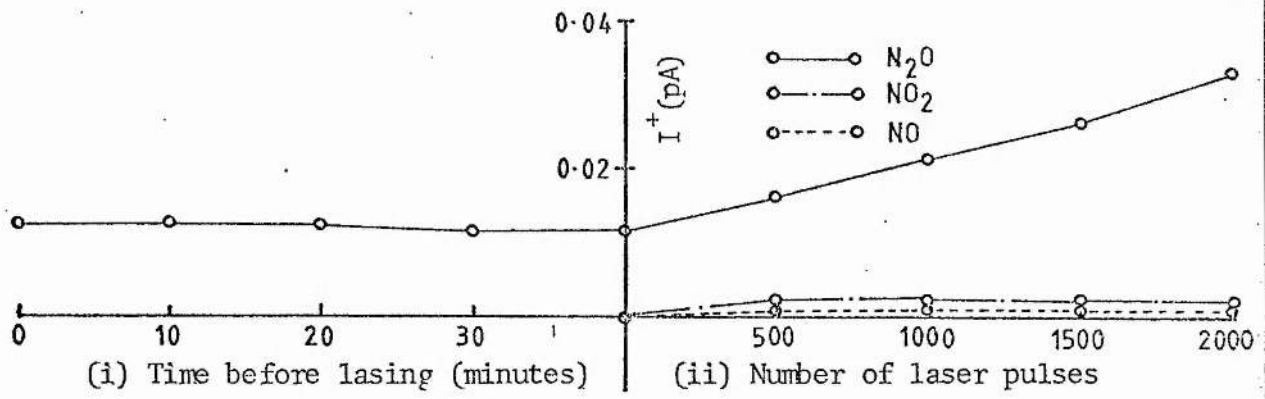

Fig.(3.16b) Ion current variation for NO, NO_2 and N_2O in He/Xe mixtures.

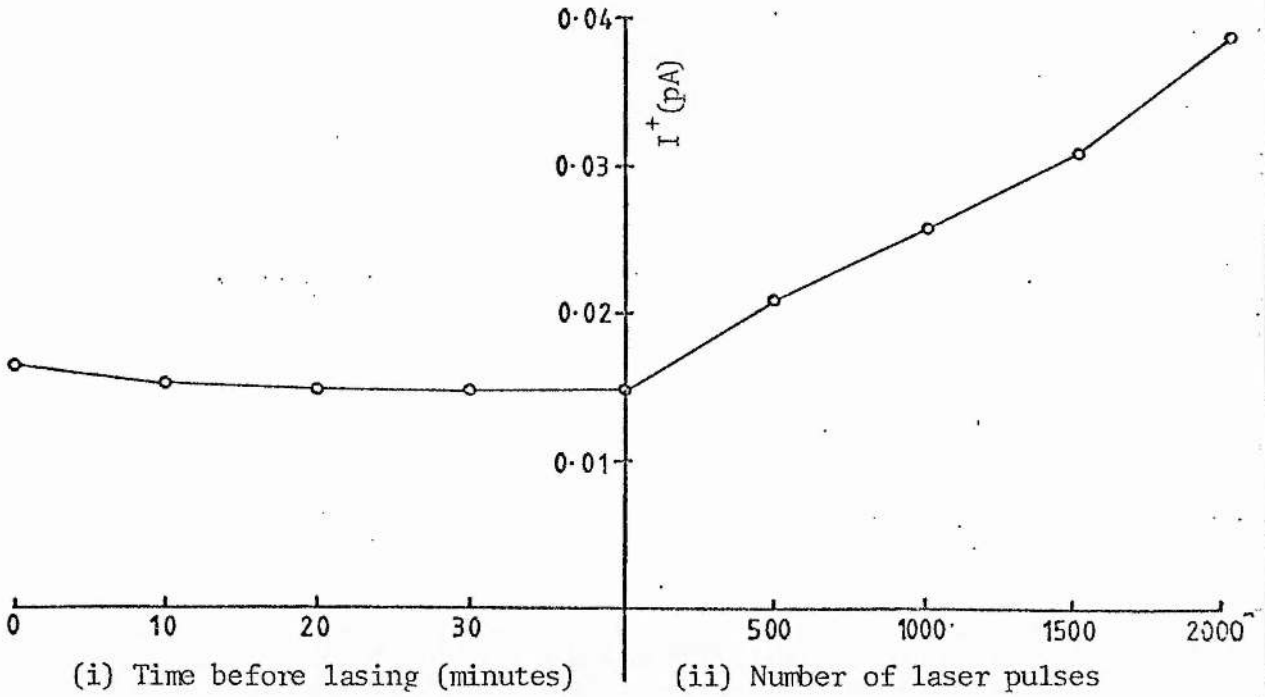

Fig(3.16c) Ion current variation for CO_2 in He/Xe mixtures.

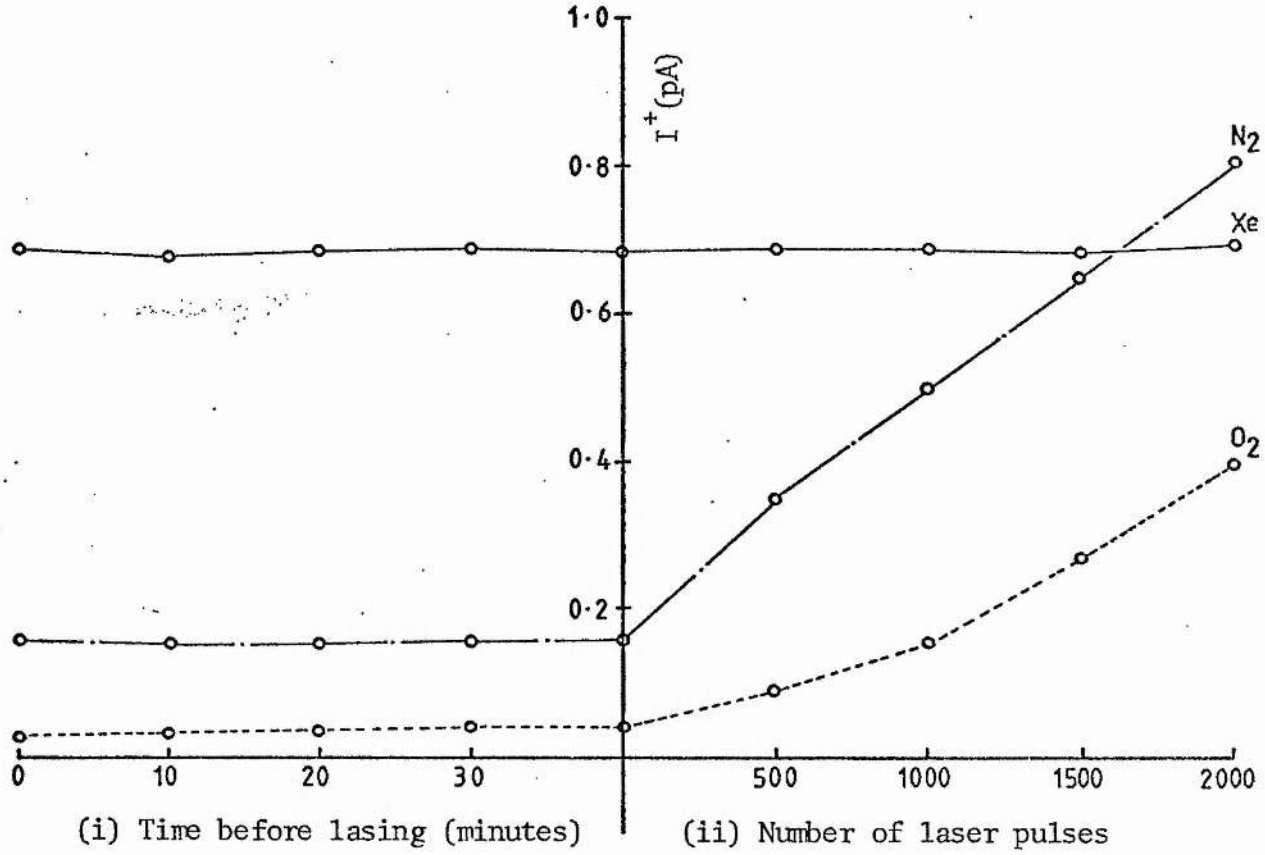

Fig.(3.17) Ion current variation for N_2, O_2 and Xe in $He/Xe/NF_3$ mixtures.

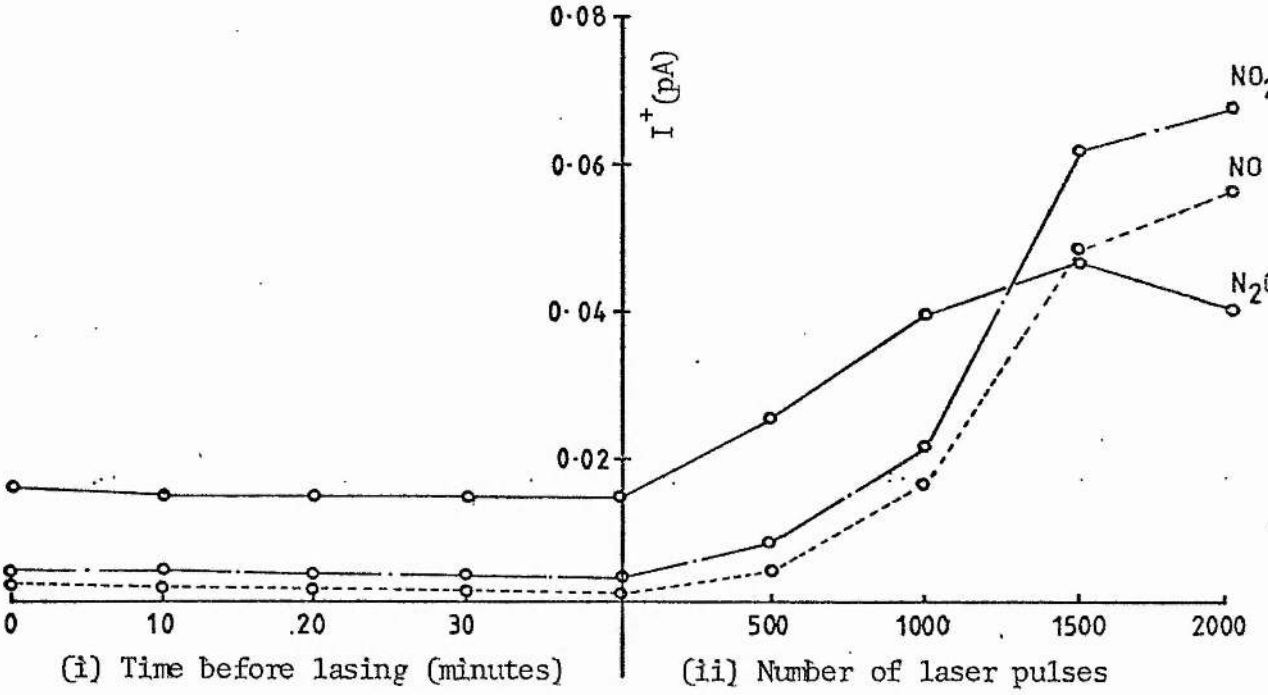

Fig.(3.18) Ion current variation for NO, NO_2 and N_2O in $He/Xe/NF_3$ mixtures.

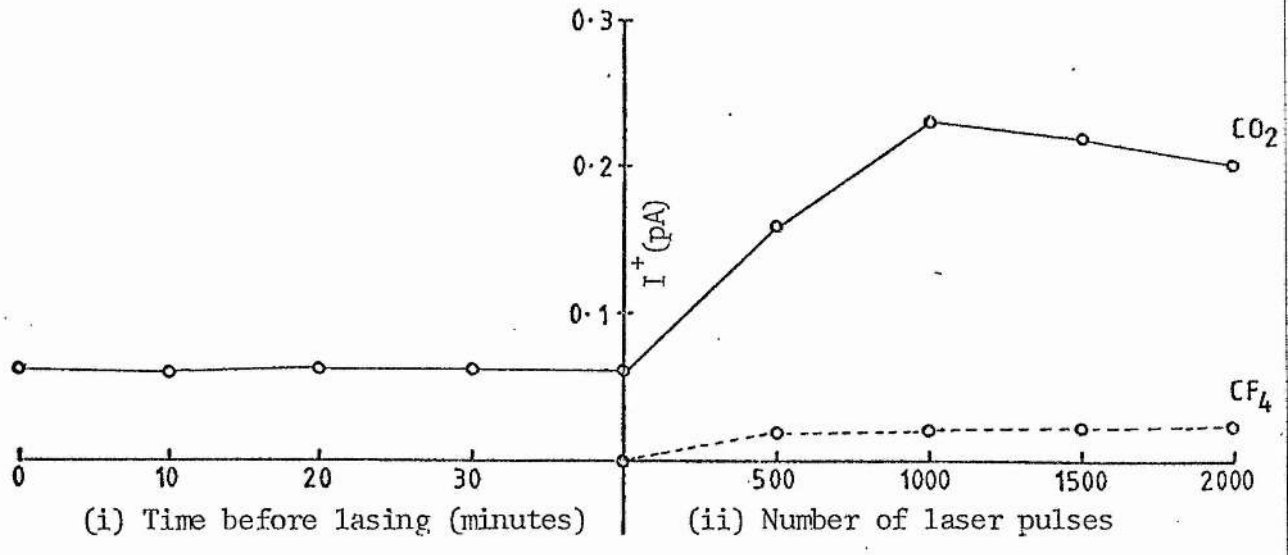

Fig. (3.19) Ion current variation for CO_2 and CF_4 in $He/Xe/NF_3$ mixtures.

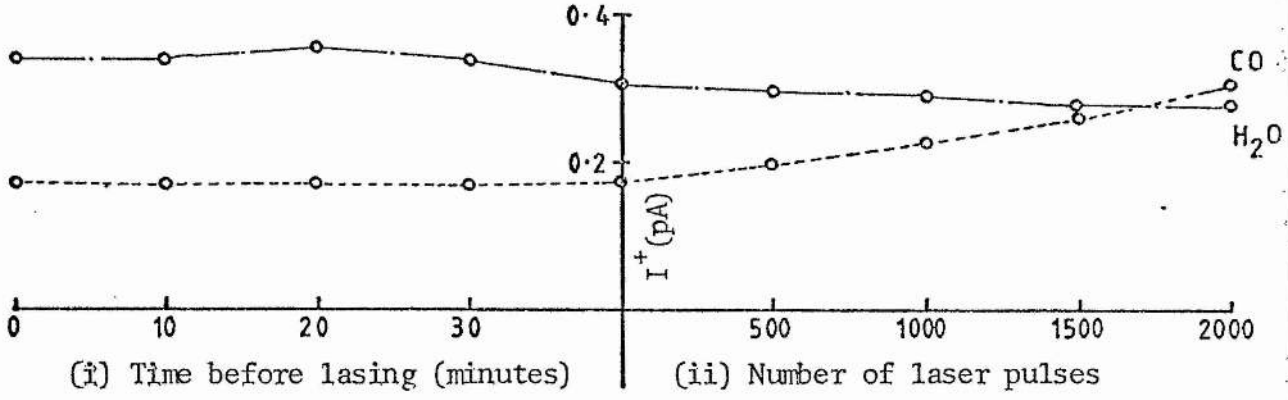

Fig. (3.20) Ion current variation for H_2O and CO in $He/Xe/NF_3$ mixtures.

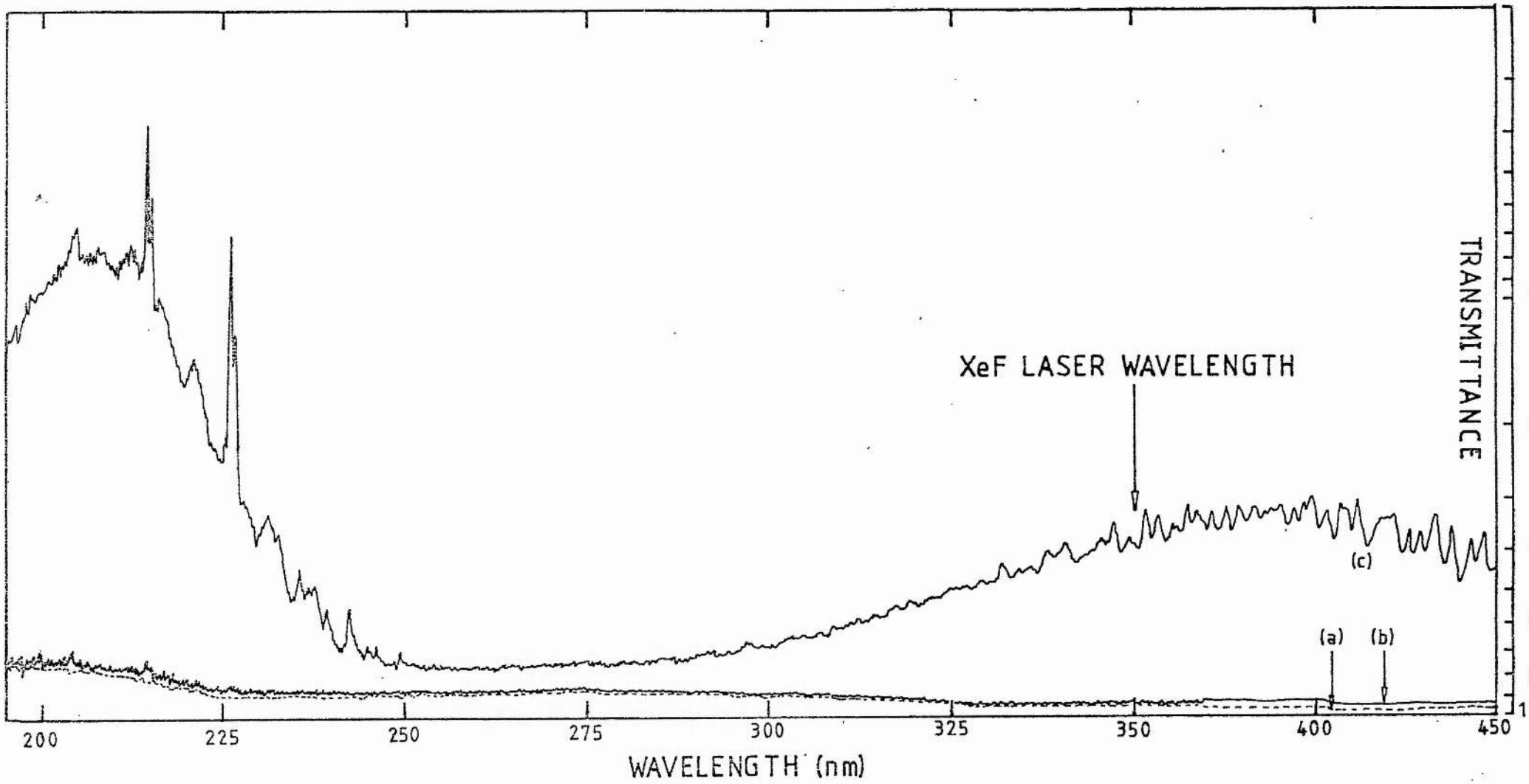

Fig.(3.21) UV absorption spectrum of (a) the evacuated absorption cell (b) a fresh gas mixture and (c) a used gas mixture after 1000 laser pulses.

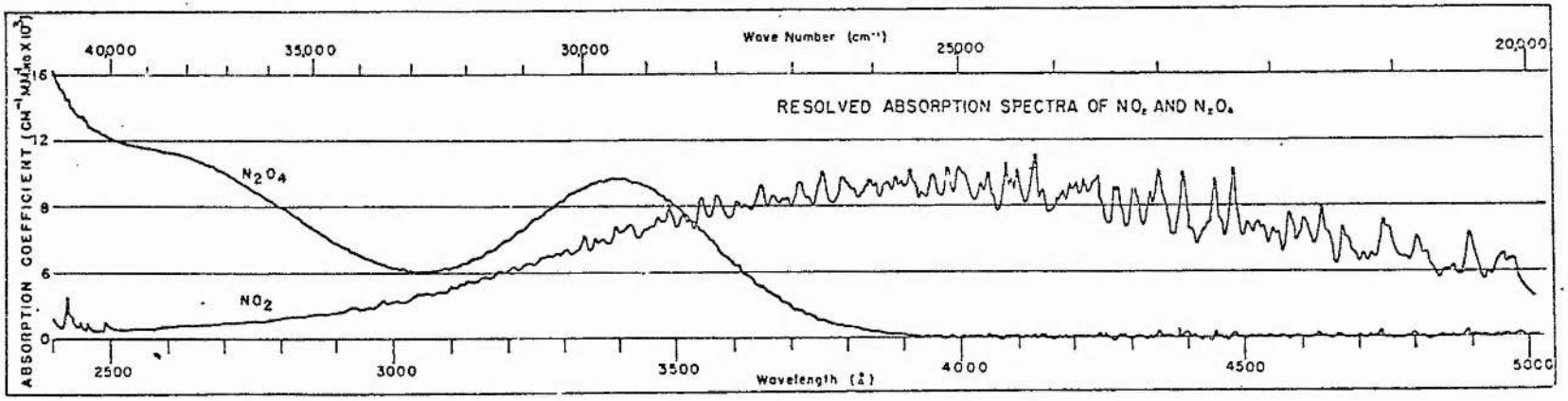

Fig. (3.22) Absorption spectrum of NO_2 (and N_2O_4), (Hall and Blacet 1952)

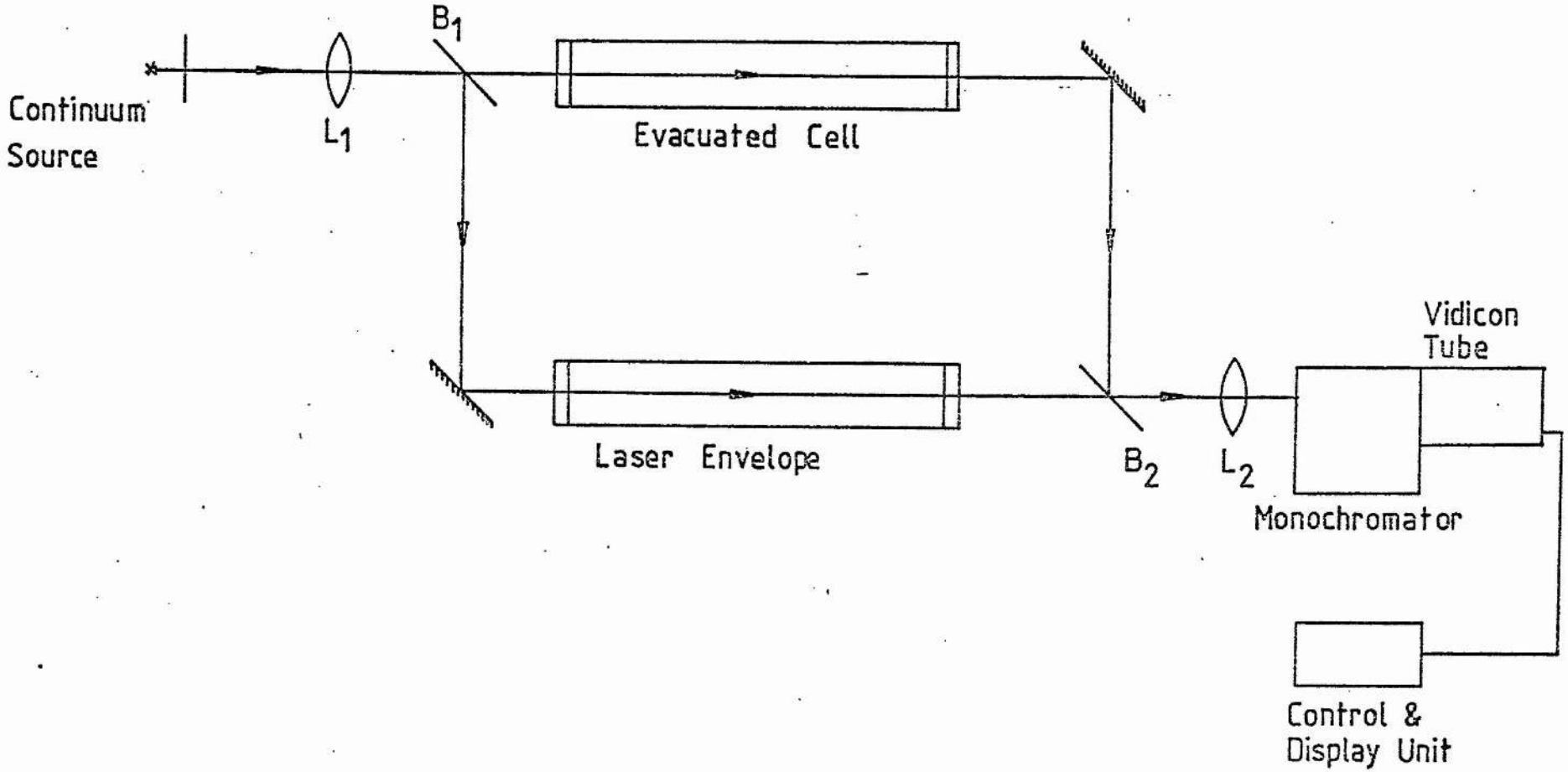

Fig. (3.23) Experimental set-up for measuring optical absorption at the laser wavelength.

CHAPTER FOUR

CONTAMINANT EFFECTS

(4.1) Introduction

In Chapter 3, the stable compounds which are formed in discharge excited mixtures of $He/Xe/NF_3$ were identified. It was shown that during laser pulsing, NF_3 is depleted and several impurities (N_2, O_2, CO, CO_2, NO, NO_2, N_2O, HF, CF_4, NF_2, N_2F_2) accumulate in the gas mixture. Even though NF_3 depletion causes a reduction of the laser extraction efficiency, it does not completely explain the observed fast deterioration of laser performance. Absorption measurements at the laser wavelength show that of the contaminants which accumulate in the laser, NO_2 is the dominant absorber at the XeF laser wavelength. However, absorption by NO_2 is small compared to typical small signal gains of laser devices similar to the one used in this work. Damage of the laser windows is not considered to be an important process here, since reproducible pulse energies were obtained with successive fresh gas fills. These results point to the significance of other processes involving contaminants which accumulate in the laser.

In all previous investigations of gas contamination in XeF lasers, the emphasis has been on the identification of stable species which are formed in the discharge. Except for studies of optical absorption at the laser wavelength (Gower et al 1980, Brannon 1982), the effects of these species on laser performance have not been investigated. For economical and efficient gas life extension, it is necessary to know the identity of the contaminants which are most

detrimental to the long-term performance of rare gas halide lasers. It may then be possible to selectively remove these contaminants, or inhibit their formation by a suitable choice of the components of the laser gas mixture, and of exposed materials in the laser (laser envelope, electrodes, preionizer, gas handling system, etc.). The second method has been successfully used by McKee et al (1980) to extend the gas life of a XeCl laser from 10^6 to $3x10^6$ laser pulses by the addition of 0.05% of H_2 to the laser gas mixture, which normally consists of helium, xenon and hydrogen chloride.

In this chapter, we report on a study of the effects of adding low concentrations of several contaminants (N_2, O_2, CO, CO_2, CF_4) on the performance of discharge excited XeF lasers. The aim of the study was to determine the relative importance of these contaminants in the degradation of laser performance. The effects of adding small concentrations of H_2 to the laser gas mixture were also investigated. This was prompted by the results of the study conducted by McKee et al (1980).

In section (4.2) of this chapter, the experimental set-up and procedure are considered. Section (4.3) deals with the dependence of the laser output on the partial pressures of several contaminants. This is followed in section (4.4) by a discussion of the effects of these contaminants on the laser gas-life. Finally, section (4.5) is devoted to a consideration of some of the processes by which the contaminants can cause a reduction of the laser extraction efficiency.

(4.2) Experimental

The effects of small concentrations of contaminants on the laser output were determined by measuring the laser pulse energy as a function of the partial pressure of each contaminant. The laser device used in this study has been described earlier. The contaminant gases were obtained from BDH chemicals and from BOC Special Gases. A typical analysis of each gas (as supplied by the manufacturers) is listed in table (4.1). The laser gas mixture consisted of the basic mixture of $He/Xe/NF_3$ in the ratio of 350:6:1, to which a small amount of one of the contaminants was added. A calibrated volume was used to measure partial pressures below 0.5 torr. It consisted of a stainless steel pipe 20 cm long and 4 mm inner diameter. To introduce a given contaminant in the laser, the pipe was first filled to a predetermined pressure, and the gas was then expanded into the laser. Gas mixing was done in the laser envelope using the procedure described in section (2.5) of Chapter 2. To ensure that the gases were adequately mixed, the contaminant gas was first introduced followed by NF_3 and Xe. Helium was then added in bursts of about 100 torr at alternate ends of the laser envelope, until the total gas pressure in the laser was one atmosphere. The gases were then circulated for about 5 minutes, after which the laser was pulsed at a repetition rate of 1 pps. The capacitor charging voltage was 18 KV. The laser pulse energy was measured using a Laser Precision Coorporation energy meter (model Rj-7200).

(4.3) Pulse energy variations

Figure (4.1) shows the normalised laser pulse energy as a function of the partial pressures of N_2, O_2, CO, CO_2, CF_4 and H_2. The effects of adding NO_2, N_2O, NO and N_2F_2 were not investigated. The pulse energies are average values of the first ten laser pulses for fresh gas mixtures. During the course of this work, laser emission in the infrared at about 2μm was observed when CF_4 was substituted for NF_3 as the fluorine donor. This unexpected result is discussed further in Appendix 2. It is sufficient to point out here that when CF_4 was added to the gas mixture as a dopant, laser emission was only observed on the B -> X transition of XeF.

The results shown in fig. (4.1) indicate that for fresh gas mixtures, the laser pulse energy is relatively insensitive to the addition of small concentrations of N_2, H_2 and CF_4. For partial pressures of N_2 exceeding 1 torr, the laser pulse energy drops sharply. In the case of CF_4, a decrease in energy is only observed at partial pressures exceeding 3 torr. In contrast with the results obtained for CF_4, N_2 and H_2, the presence of small concentrations of CO_2, CO and O_2 in the laser gas mixture causes a significant reduction of the laser pulse energy. The addition of 0.05% of CO_2, CO, and O_2 results in approximately 60%, 40% and 20% reductions in the laser pulse energy respectively. Table (4.2) lists estimated increases in the partial pressures of CO_2, CO, and O_2 in the laser gas mixture after 10^3 laser pulses, and expected percentage reductions in the laser pulse energy based on the results of fig. (4.1). The partial pressures were estimated from the results of Chapter 3. The third

column of table (4.2) shows that CO_2 causes the largest drop (20%) in the laser pulse energy, followed by O_2(10%) and CO(5%).

(4.4) Gas-life variations

The effects of a given contaminant on the gas-life were determined by measuring the number of laser pulses to half-energy for single gas fills doped with various partial pressures of the contaminant. The addition of small amounts (< 1 torr) of N_2, CO_2, CO, O_2 and H_2 resulted in only small changes in the gas-life. In contrast with these results, an unexpected increase in the number of laser pulses to half-energy was observed when CF_4 was added to the gas mixture. Figure (4.2) shows the gas-life for single gas fills of $He/Xe/NF_3$ containing various partial pressures of CF_4. We note that the number of laser pulses to half-energy increases by roughly a factor of three when the laser gas mixture contains 2 torr (0.3%) of CF_4. Figure (4.3b) shows the dependence of the laser output energy on the number of laser pulses for such a mixture. Figure (4.3a) shows a similar plot for $He/Xe/NF_3$ mixtures for comparison. To ensure that the observed gas-life extension was not due to laser emission in the infrared, which is observed when NF_3 is replaced by CF_4 as the fluorine donor, at regular intervals of 100 shots an infrared transmitting filter was used to exclude XeF emission at 351nm, and the energy of the transmitted beam was measured. It was found to be less than 5% of the total energy. Similar values were obtained for $He/Xe/NF_3$ mixtures . After using $He/Xe/NF_3/CF_4$ mixtures, the number of laser pulses to half-energy obtained from $He/Xe/NF_3$ mixtures increased by roughly a factor of two (250 to 450 shots). This

improvement in the gas-life shows that exposed surfaces in the laser were conditioned to some extent when $He/Xe/NF_3/CF_4$ mixtures were used. The longer gas-life obtained from $He/Xe/NF_3/CF_4$ mixtures (800 shots) indicate that in addition to the conditioning of exposed surfaces, the addition of CF_4 to the laser gas mixture results in more favourable gas kinetics in the discharge.

A mass spectrometric investigation of discharge excited $He/Xe/NF_3/CF_4$ mixtures was conducted to determine the reasons for the longer gas-life resulting from the addition of CF_4 to mixtures of $He/Xe/NF_3$. The procedure was similar to that used in the study reported in Chapter 3. The laser gas mixture consisted of $He/Xe/NF_3$ in the ratio of 350:6:1, to which 2 torr (0.3%) of CF_4 was added. The total gas pressure in the laser was one atmosphere. After gas mixing, mass spectra of the fresh mixture were recorded. The laser was then pulsed at a repetition rate of 1 pps, and mass spectra were taken at intervals of 500 shots for a total of 2000 shots. The capacitor charging voltage was 18 KV. The results are shown in figs. (4.4) to (4.8). For easy comparison, the vertical scales are identical to those used for corresponding results in figs. (3.17) to (3.20) of Chapter 3 for $He/Xe/NF_3$ mixtures. Results for $He/Xe/NF_3/CF_4$ and $He/Xe/NF_3$ mixtures were compared and show the following for $He/Xe/NF_3/CF_4$ mixtures:

(i) There are only small changes in the partial pressure of CF_4. The rate of NF_3 depletion is similar to that of $He/Xe/NF_3$ mixtures.

(ii) There are negligible changes in the partial pressure of O_2, NO_2 and NO. However, the rate of formation of N_2O is relatively high,

and the amount of N_2O produced in $He/Xe/NF_3$ and $He/Xe/NF_3/CF_4$ mixtures are roughly similar. In contrast with the decrease in N_2O content observed in $He/Xe/NF_3$ mixtures after about 1500 shots, in $He/Xe/NF_3/CF_4$ mixtures the amount of N_2O increases continuously with the number of laser shots.

(iii) Compared to the results for $He/Xe/NF_3$ mixtures, the partial pressure of N_2 is lower by about 50%, and that of CO is higher by about 20%.

(iv) The partial pressure of CO_2 is roughly similar to that of $He/Xe/NF_3$ mixtures up to about 1000 pulses, after which it increases continuously with the number of laser pulses. In $He/Xe/NF_3$ mixtures, the partial pressure of CO_2 decreases after about 1000 laser pulses.

The above observations indicate that the longer gas life of $He/Xe/NF_3/CF_4$ mixtures is mainly due to a reduction in the rate of formation of O_2, NO and NO_2. The lower partial pressure of N_2 is not expected to have a significant effect on the gas life, since from the results of section (4.3), it is known that laser performance is relatively insensitive to the presence of small amounts of N_2 in the laser gas mixture. Other processes which may be responsible for the extended gas-life include, (i) a reduction of the number density of transient species which absorb at the laser wavelength, and (ii) more favourable kinetics for the formation of excited rare gas halide molecules. These processes are subtle and difficult to investigate experimentally.

(4.4.1) Effects of adding H_2

The addition of small amounts of H_2 to the laser gas mixture does not have a significant effect on the gas life. However, after running the laser on $He/Xe/NF_3/H_2$ mixtures, a significant improvement in the gas-life was observed when $He/Xe/NF_3$ mixtures were used. A typical result is shown in fig. (4.3c), in which normalised laser pulse energies are plotted as a function of the number of laser pulses. The results show that the number of laser pulses to half-energy is about five times that of previous $He/Xe/NF_3$ mixtures, and 1.5 times that of $He/Xe/NF_3/CF_4$ mixtures.

To determine the reasons for the extended gas life, a mass spectrometric investigation of the laser gas mixture was conducted. Mass spectra were taken before lasing and after every 500 shots for a total of 2000 shots. The gas mixture consisted of $He/Xe/NF_3$ in the ratio of 350:6:1 at a total pressure of one atmosphere. The laser was operated under conditions similar to those used in the study reported in section (4.4). The results are shown in figs. (4.9) to (4.13). A comparison with the results of figs. (3.17) to (3.20) for $He/Xe/NF_3$ mixtures used earlier, and figs. (4.4) to (4.8) for $He/Xe/NF_3/CF_4$ mixtures reveals several differences.

(i) The rate of NF_3 depletion is significantly lower, as shown in fig. (4.13). After 1000 shots, approximately 75% of the initial amount of NF_3 is left, compared to about 50% for similar gas mixtures prior to the addition of H_2, and for $He/Xe/NF_3/CF_4$ mixtures.

(ii) The rate of O_2 formation is small compared to that previously observed in $He/Xe/NF_3$ mixtures, but slightly higher than the corresponding rate in $He/Xe/NF_3/CF_4$ mixtures.

(iii) The rate of formation of NO and NO_2 is negligibly small, and comparable to those of $He/Xe/NF_3/CF_4$ mixtures. The rate of N_2O formation is roughly 30% lower than for previous $He/Xe/NF_3$ mixtures and for $He/Xe/NF_3/CF_4$ mixtures.

(iv) The partial pressure of N_2 is 50% lower and that of CO is 20% higher than for previous $He/Xe/NF_3$ mixtures. These results are similar to those of $He/Xe/NF_3/CF_4$ mixtures.

(v) For the first 1500 shots, the partial pressure of CO_2 is smaller than for previous $He/Xe/NF_3$ mixtures. Subsequently it increases with the number of laser pulses in contrast with earlier results obtained from similar gas mixtures. We note however that the rate of increase is about 20% smaller than for $He/Xe/NF_3/CF_4$ mixtures.

Based on the above results, the extended gas-life of $He/Xe/NF_3$ mixtures, subsequent to the use of $He/Xe/NF_3/H_2$ mixtures, is attributed in part to, (i) the smaller rate of formation of NO_2 , O_2 and possibly NO and N_2O, and (ii) a lower rate of NF_3 depletion. The latter may also explain the longer gas-life compared to that of $He/Xe/NF_3/CF_4$ mixtures. We note that even though 75% of the initial NF_3 remains after 2000 shots, the corresponding energy is only about 15% of that obtained from fresh mixtures. Figure (3.13) of Chapter 3

shows that for a fresh gas mixture containing an equivalent amount of NF_3, the laser pulse energy should be more than four times the measured energy after 2000 shots. This indicates that the deterioration of laser performance is due to the accumulation of contaminants other than O_2, NO and NO_2, which are only present in small amounts after 2000 shots. The smaller rate of depletion of NF_3 is attributed to passivation of exposed surfaces in the laser when $He/Xe/NF_3/H_2$ mixtures are used. This conclusion is supported by the results of mass spectrometric analysis of $He/Xe/NF_3/H_2$ mixtures before pulsing and after 1000 shots. These show that after 1000 shots, approximately 25% of the initial NF_3 is left, compared to about 50% for $He/Xe/NF_3$ mixtures prior to the addition of H_2 to the laser gas mixture. The conditioning is presumably the result of inhomogeneous reactions of exposed surfaces in the laser with HF formed in reactions of H_2 with NF_3 in the gas discharge.

Information on the identity of the main contaminants can be obtained from a consideration of the results obtained so far in this study. During pulsing, there are negligible changes in the partial pressures of O_2, NO_2 and NO, and relatively large increases in the partial pressures of N_2O, CO_2, N_2 and CO. The partial pressure of Xe does not change significantly. Since it is known that the laser gas mixture is insensitive to the presence of small amounts of N_2 (less than about 1 torr), the above results indicate that N_2O, CO_2 and CO are possibly major contaminants. This is consistent with the results of section (4.2.1) in which it was shown that the addition of even small amounts of CO and CO_2 (0.05%) result in a significant reduction of the laser pulse energy. The effects of adding N_2O to the laser gas mixture was not investigated, and hence no conclusion can be drawn at

this stage on its importance as a contaminant.

(4.5) Discussion

The results obtained so far show that the short gas-life of discharge excited XeF lasers is partly due to the accumulation of contaminants in the laser gas mixture during pulsing. The contaminants can reduce the laser extraction efficiency through several processes. These include the following:

(i) Quenching of the XeF(B) state from which laser action occurs, and of xenon metastables (Xe^*), which are the dominant precursors of XeF^* in discharge excited XeF lasers.

(ii) Contaminant absorption at the laser wavelength, and in the spectral region below about 240nm where preionization is thought to occur (McKee et al 1980, Taylor et al 1983).

(iii) The formation of transient species which absorb at the laser wavelength.

(iv) The formation of negative ions by dissociative-attachment reactions, resulting in discharge instabilities.

In the XeF molecule, the B state lies above the C state. Consequently, the XeF(B) state can be deactivated by collisional transfer to the C state. It can also be quenched to the X and A states. Due to a lack of quenching data, the importance of

collisional deactivation of the upper laser level by stable contaminants cannot be estimated. Brashears and Setser (1978) have measured rate constants for the transfer and quenching of the XeF(B) state by N_2 and CF_4. Other compounds of interest here, such as O_2, CO, CO_2 and N_2O were not studied. For both N_2 and CF_4, transfer to the C state dominates over quenching, and the respective rate constants are $(2.3\pm0.1).10^{-11}$ cm^3 s^{-1} and $(2.5\pm0.1).10^{-11}$ cm^3 s^{-1}. For CO_2, Brashears and Setser point out that quenching appears to be dominant, but the quenching rate constant is not given. The quenching rates of $Xe(^3P_2)$ metastables by several small molecules (N_2, O_2, CO, CO_2, NO, N_2O, NO_2, etc.) have been determined by Velazco and Setser (1974). Rate constants k_Q for some molecules of interest in this work are listed below. We note that N_2O and CO_2, which accumulate in the laser during pulsing, have the highest quenching rates.

Rate constants for the quenching of $Xe(^3P_2)$ metastables

Compound	N_2	CO	CO_2	O_2	NO	N_2O
$k_Q(cm^3mol^{-1}s^{-1})$ $(x10^{-11})$	1.9	3.6	45	22	30	44

In fast discharge excited XeF lasers, XeF^* is predominantly formed in harpoon reactions of xenon metastables (Xe^*) with the fluorine donor (NF_3). Direct electron impact excitation of Xe forms Xe^*. The population of Xe^* is depleted in the formation of XeF^*, in direct electron ionization reactions resulting in the formation of Xe^+ and Xe_2^+, and in reactions in which it is quenched by impurities

generated in the discharge. The evolution of the Xe^* number density $[Xe^*]$ can be represented by:

$$d[Xe^*]/dt = k_1[e][Xe]-k_2[NF_3][Xe^*]-k_3[e][Xe^*]-\sum_i R_i[Q_i][Xe^*] \qquad (4.1)$$

where [ ] represent number densities. Rate constant k_1 is the direct electron excitation rate of Xe, k_2 the XeF^* formation rate in harpoon reactions of Xe^* with NF_3, k_3 the rate of direct electron ionization of Xe^*, and R_i the quenching rate of Xe^* by molecule Q_i with number density $[Q_i]$. Assuming steady state conditions, $[Xe^*]$ can be written as

$$[Xe^*] = k_1[e][Xe]/(k_2[NF_3] + k_3[e] + \sum_i R_i[Q_i]) \qquad (4.2)$$

A rough estimate of the importance of contaminant quenching of Xe^* can be obtained by comparing the magnitude of $\sum_i R_i[Q_i]$ with those of $k_2[NF_3]$ and $k_3[e]$ in equation (4.2). For a molecular gas discharge similar to that used in this work, the electron number density is typically 10^{15} cm^{-3} (Mkrtchyan and Platonenko 1979, Greene and Brau 1978). At $E/N \simeq 5.6\times10^{-16}$ V cm^2, $k_3 \simeq 9.5\times10^{-8}$ cm^3 s^{-1} (Mkrtchyan and Platonenko 1979) and $k_2 = 9.0\times10^{-11}$ cm^3 s^{-1} (Velazco et al 1976). After 1000 laser shots, we have $[NF_3] = 3.4\times10^{16}$ cm^{-3}. The value of $\sum_i R_i[Q_i]$ was determined for N_2, CO, CO_2, N_2O, and O_2 using the rate constants of Velazco and Setser (1974). The number densities $[Q_i]$ were estimated from the results of section (3.6.2) of Chapter 3. Using the above values, we have $k_2[NF_3] = 3.1\times10^6$ s^{-1}, $k_3[e] = 10^8$ s^{-1} and $\sum_i R_i[Q_i] = 2.0\times10^6$ s^{-1}. These results show that the quenching term is small compared to the sum of $k_3[e]$ and $k_2[NF_3]$. Consequently,

quenching of Xe^* by impurities in the discharge is not considered to be significant.

Of the contaminants identified in Chapter 3, only NO_2 absorbs at the laser wavelength. This was confirmed by UV absorption spectroscopy of laser gas mixtures before and after pulsing, as described in section (3.9.2) of Chapter 3. Although the other contaminants do not absorb at the laser wavelength, they show strong absorption in the region below 250nm (Okabe 1978). This is evident from the absorption spectrum of used gas mixtures shown in fig. (3.21) of Chapter 3. Since ultraviolet preionization is thought to occur in the region below 240nm (McKee et al 1980, Taylor et al 1983), the accumulation of contaminants which absorb in that region, may result in a deterioration of the laser gas discharge due to inadequate preionization. As the preionization electron density decreases, the discharge may become filamentary. The laser extraction efficiency is then reduced as a result of inefficient excitation of XeF molecules, and an apparent increase of optical absorption due to refractive index gradients. In XeCl lasers, McKee et al (1980) have proposed that the extended gas-life which is achieved by the addition of H_2 to the gas mixture of He/Xe/HCl, may be due to preionization related effects rather than a reduction of optical absorption at the laser wavelength.

Contaminant accumulation in the laser may also cause a reduction of the gas-life either by enhancing the formation of species, such as Xe_2^+, which absorb at the XeF laser wavelength, or by forming new transient absorbing species. Transient absorption causes a reduction of the overall laser gain, and hence a reduction of the laser output energy.

The degradation of laser performance may also be due to dissociative-attachment instabilities, which have been observed in both self-sustained (Nighan and Wiegand 1974), and externally sustained discharges (Douglas-Hamilton and Mani 1973). These instabilities are due to an imbalance between the rate of electron production and that of electron loss by dissociative-attachment reactions. They can be significantly influenced by the presence of small amounts of impurities which are formed in the discharge. The instabilities manifest themselves in the form of striations or constrictions of the gas discharge. Both of these result in a deterioration of the discharge homogeneity, and consequently results in a degradation of laser extraction efficiency.

TABLE (4.1)

Typical analysis of contaminant gases

Hydrogen		Oxygen	
H_2	99.99%	O_2	99.7%
O_2	< 1 ppm	CO_2	< 3 ppm
H_2O	< 1 ppm	CO	< 2 ppm
CO_2	< 0.5 ppm	N_2O	< 0.1 ppm
N_2O	< 0.1 ppm	C_2H_2	< 0.05ppm
CH_4	< 0.5 ppm	N_2	50 ppm
CO	< 1 ppm	CH_4	6 - 20 ppm
C_2H_2	< 0.05ppm	Ar	0.3 %
Hydrocarbons	< 1 ppm	Hydrocarbons	8 - 23 ppm
N_2	40 - 60 ppm	H_2O	3 - 20 ppm

Carbon Monoxide		Carbon Dioxide	
CO	99.5 %	CO_2	99.9996%
N_2	0.32 %	N_2	2 vpm
O_2	800 ppm	O_2	< 1 vpm
CO_2	550 ppm	H_2	< 1 vpm
H_2O	5 ppm	CO	< 1 vpm
Hydrocarbons	50 ppm	H_2O	1 vpm
		Hydrocarbons	< 1 vpm

Carbon Tetrafluoride		Nitrogen	
CF_4	99.9%	N_2	99.948%
H_2O	15 ppm	O_2	< 0.02 %
		H_2O	< 0.001%
		CO_2	< 0.002%
		Ar	< 0.080%

TABLE (4.2)

Estimated partial pressure of CO_2, CO, and O_2, and corresponding % reductions in the laser pulse energy.

Compound	Estimated pressure (torr)	Estimated reduction (%) in energy
CO_2	0.06	20%
O_2	0.2	10%
CO	0.04	5%

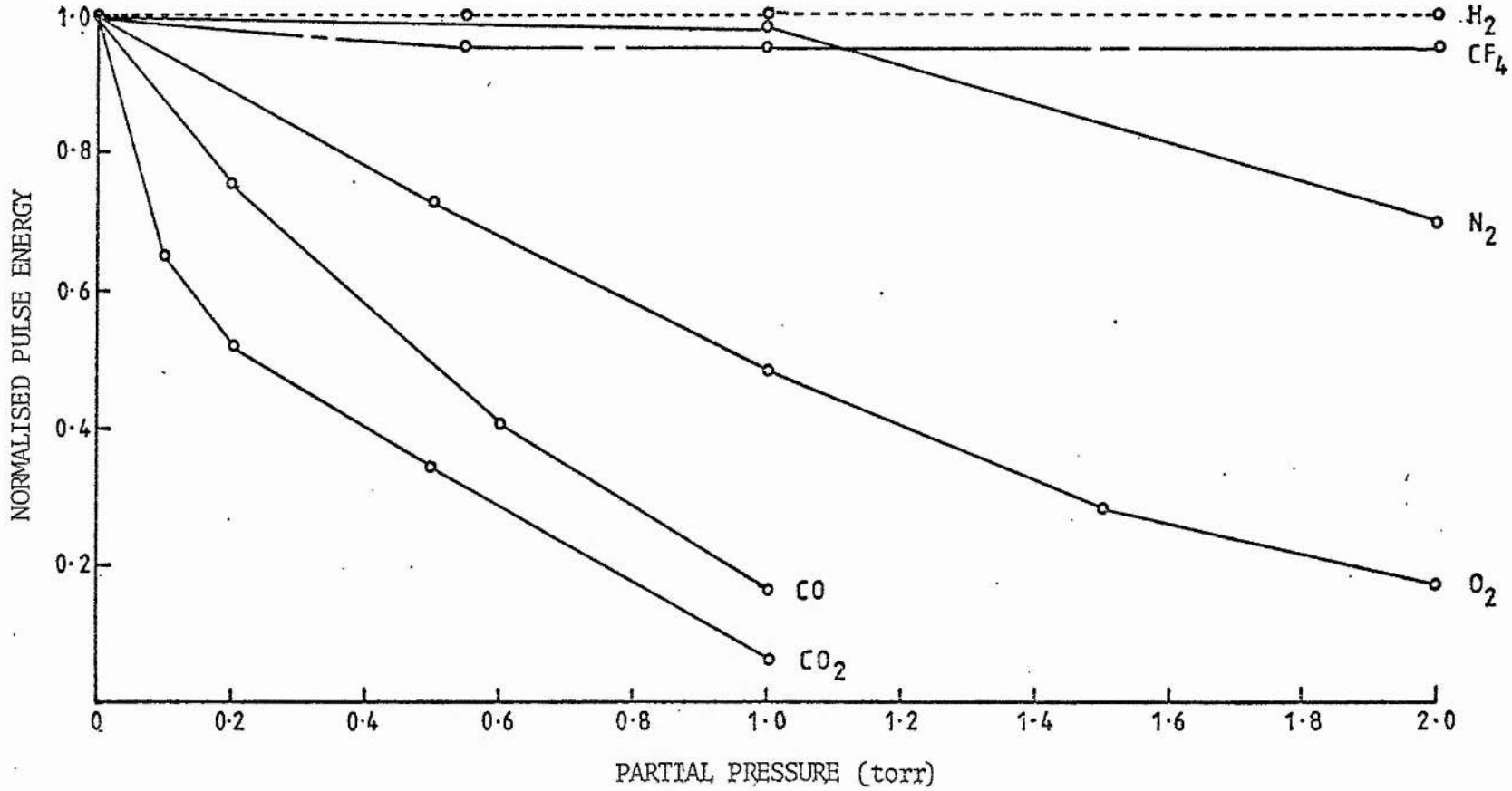

Fig. (4.1) Normalised pulse energy as a function of the partial pressure of added contaminants.

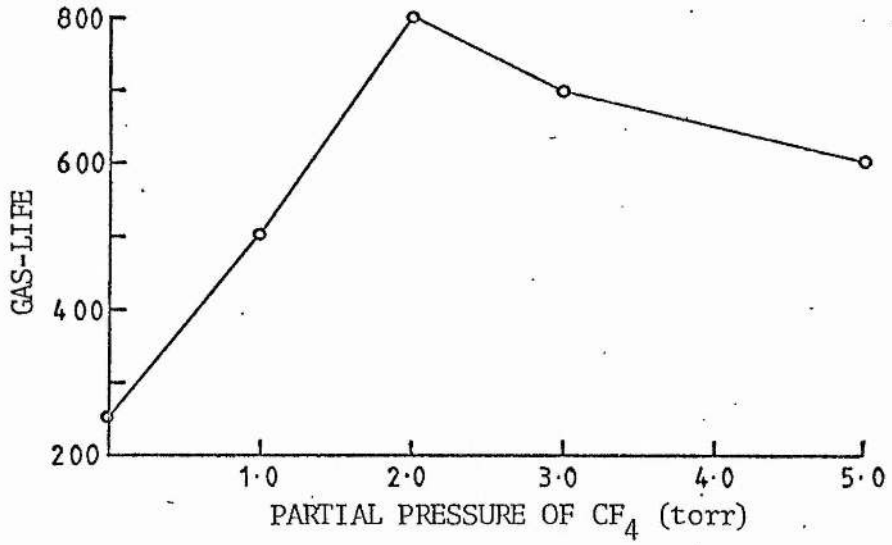

Fig.(4.2) Gas-life of $He/Xe/NF_3/CF_4$ mixtures as a function of the partial pressure of CF_4.

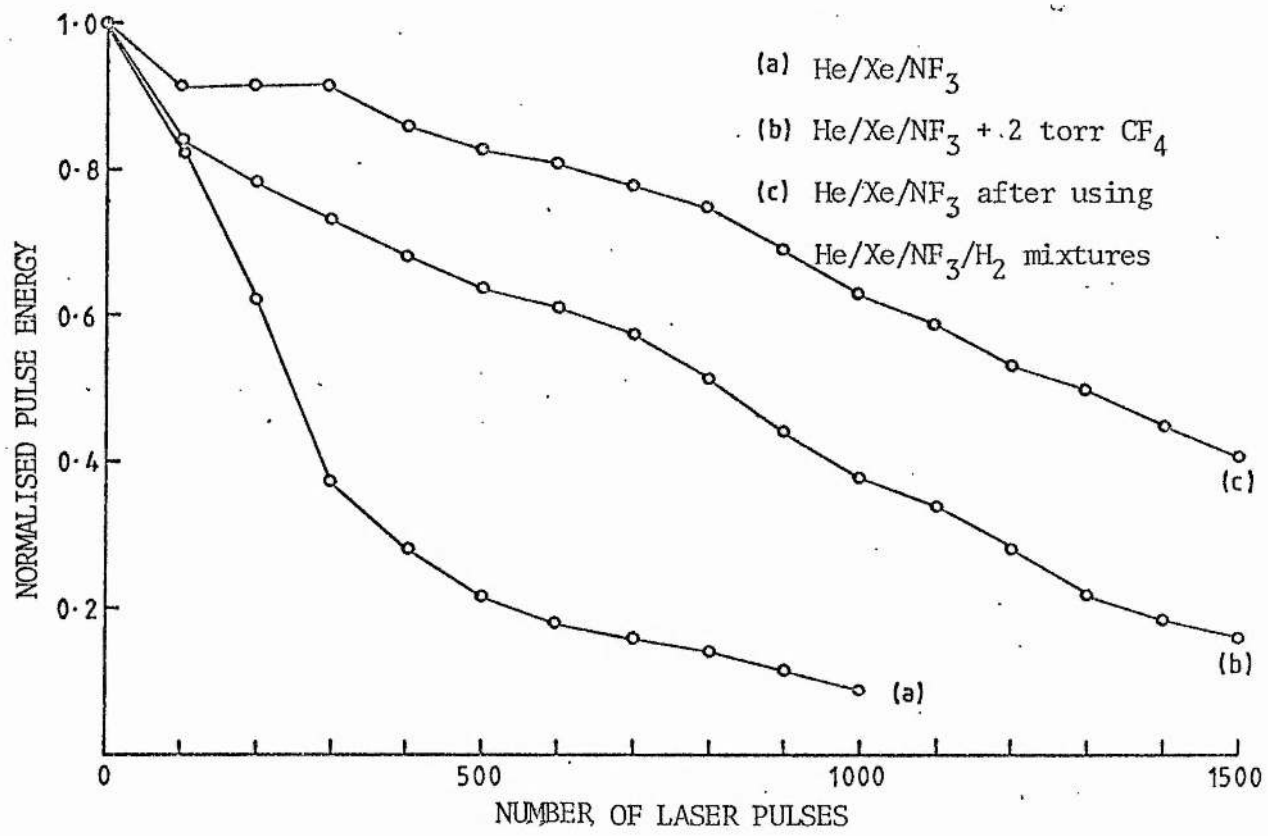

Fig.(4.3) Normalised pulse energy as a function of the number of laser pulses for (a) $He/Xe/NF_3$ (b) $He/Xe/NF_3/CF_4$ and (c) $He/Xe/NF_3$ after using $He/Xe/NF_3/H_2$ mixtures.

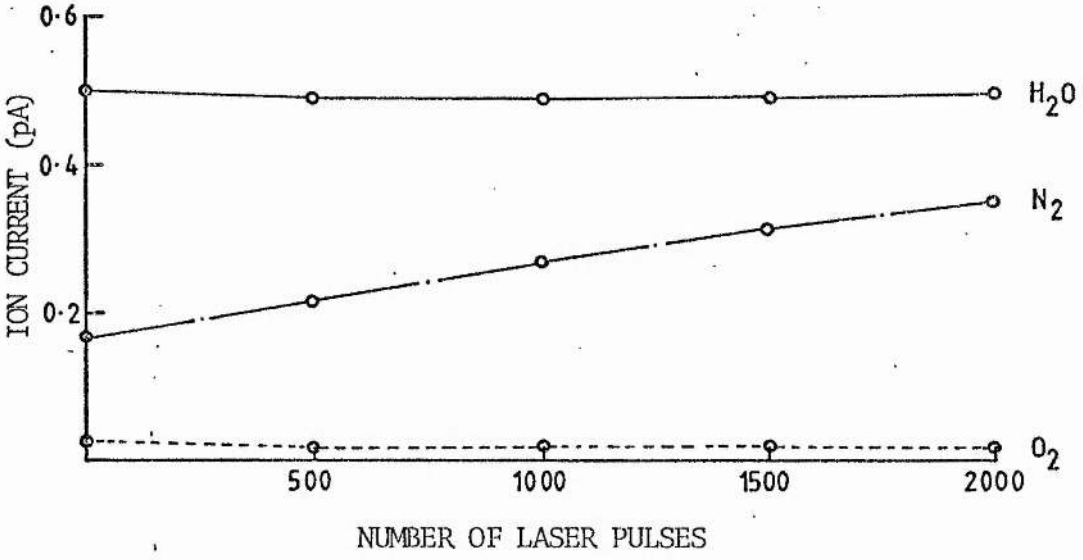

Fig. (4.4) Ion current variation for H_2O, N_2 and O_2 in $He/Xe/NF_3/CF_4$ mixtures.

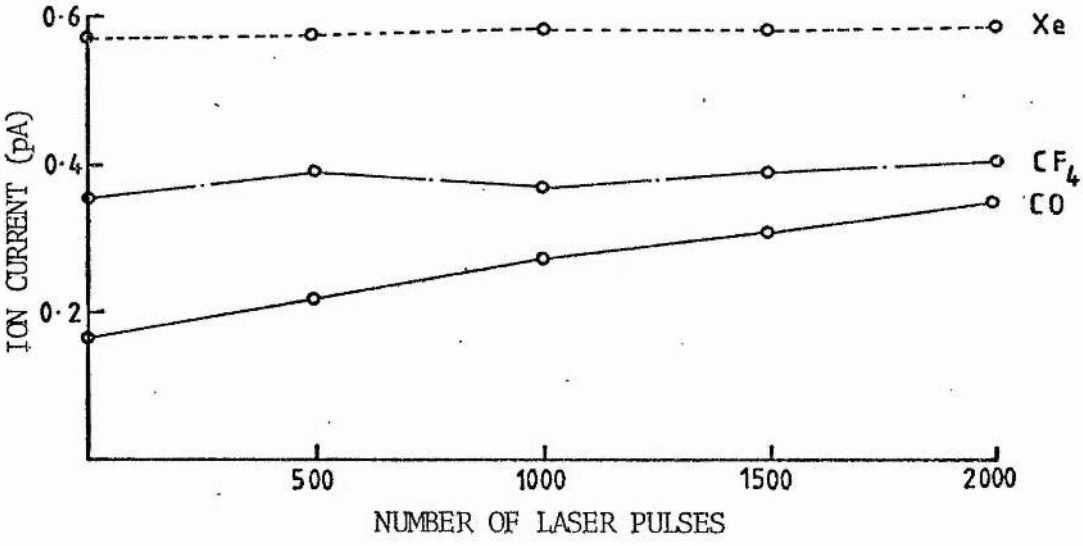

Fig. (4.5) Ion current variation for CO, CF_4 and Xe in $He/Xe/NF_3/CF_4$ mixtures.

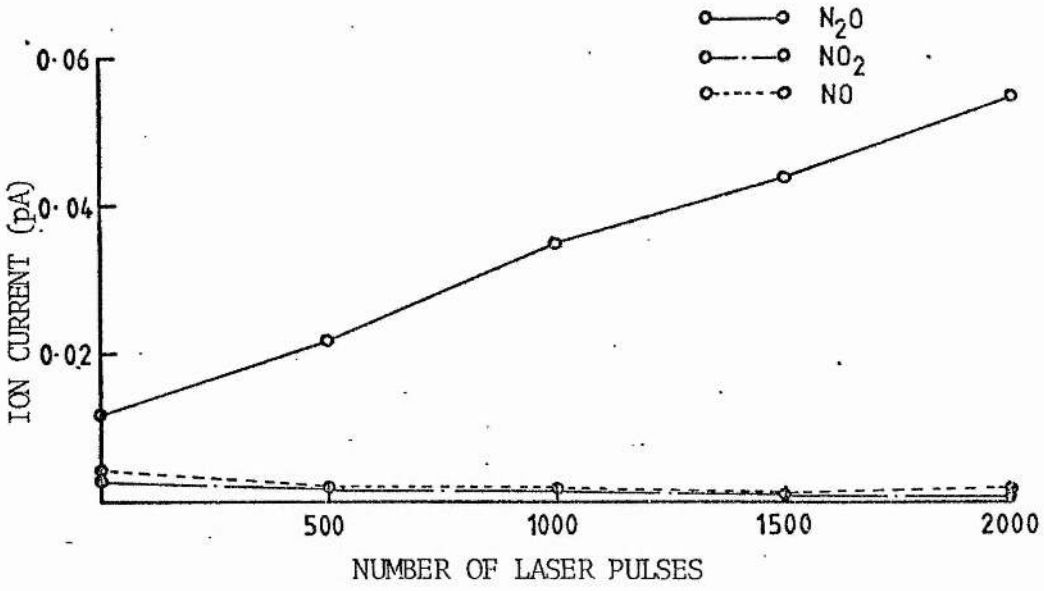

Fig. (4.6) Ion current variation for NO, NO_2 and N_2O in $He/Xe/NF_3/CF_4$ mixtures.

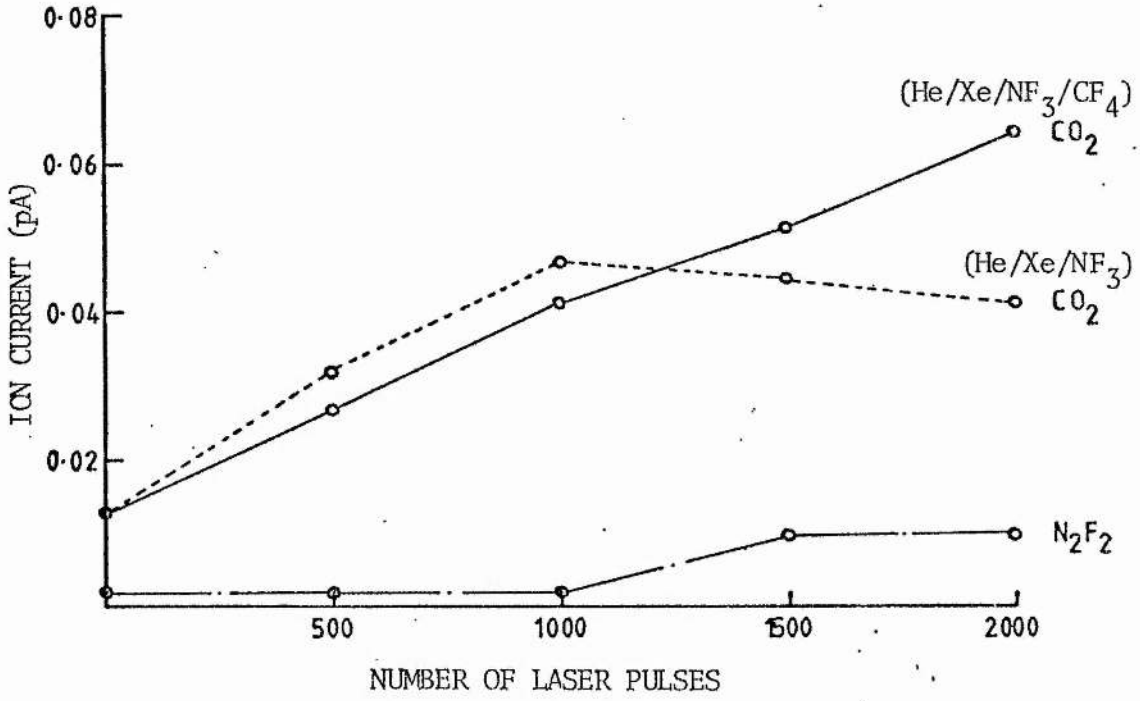

Fig. (4.7) Ion current variation for CO_2 and N_2F_2 in $He/Xe/NF_3/CF_4$ mixtures.

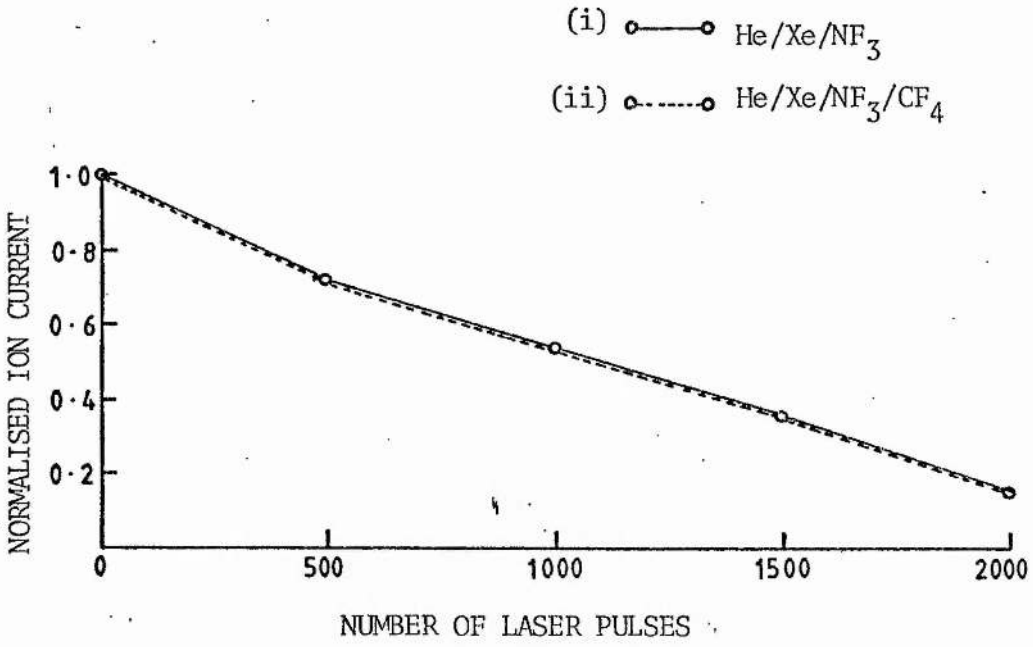

Fig.(4.8) Normalised ion current variation for NF_3 in (i) $He/Xe/NF_3$ and (ii) $He/Xe/NF_3/CF_4$ mixtures.

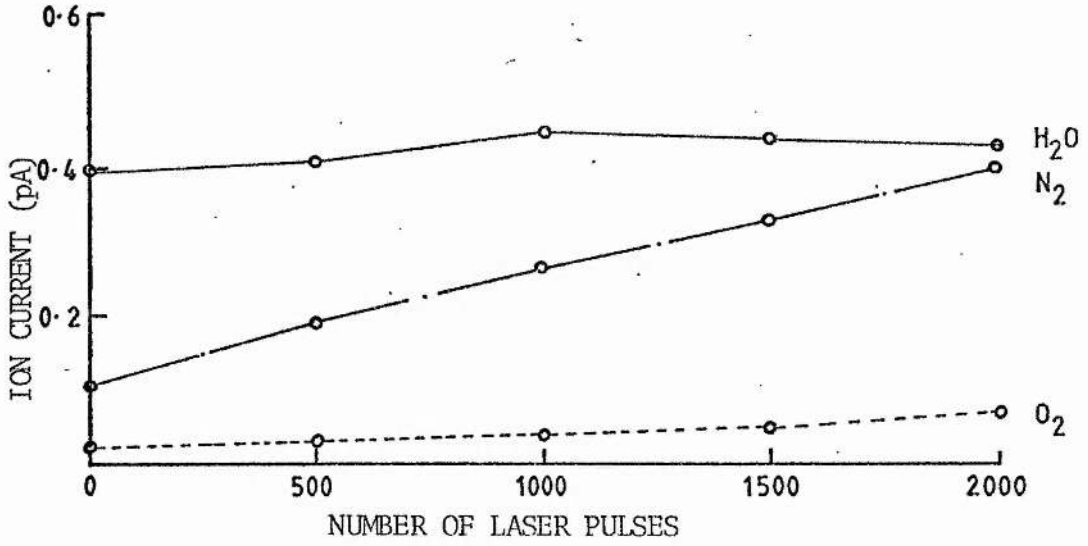

Fig.(4.9) Ion current variation for H_2O, N_2 and O_2 in $He/Xe/NF_3$ after using $He/Xe/NF_3/H_2$ mixtures.

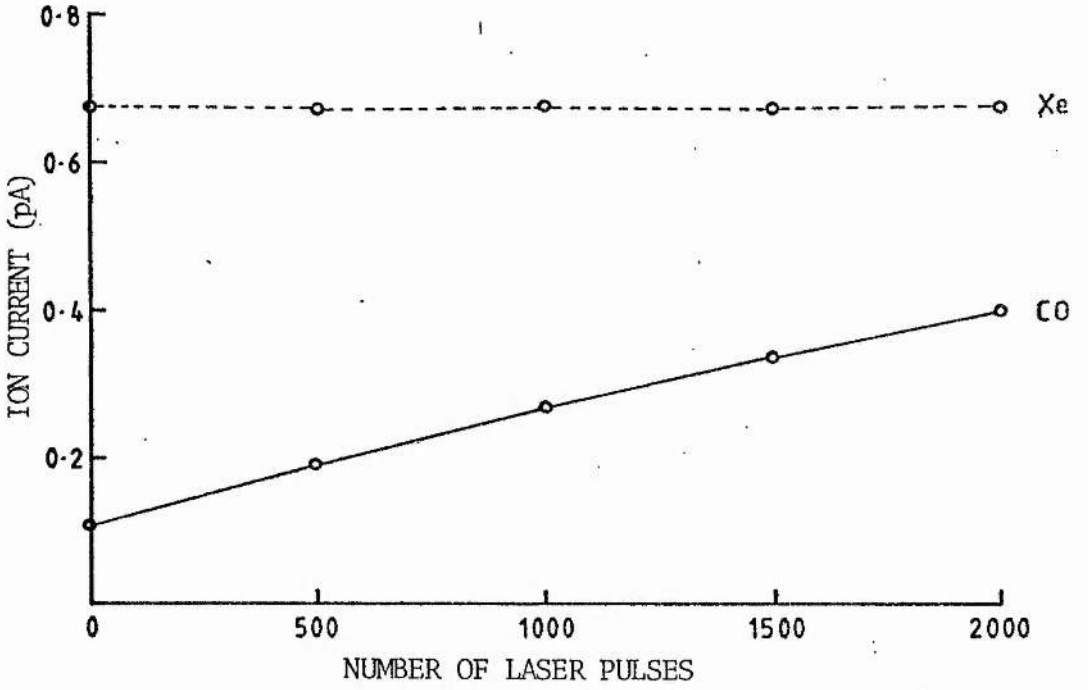

Fig.(4.10) Ion current variation for CO and Xe in $He/Xe/NF_3$ after using $He/Xe/NF_3/Xe$ mixtures.

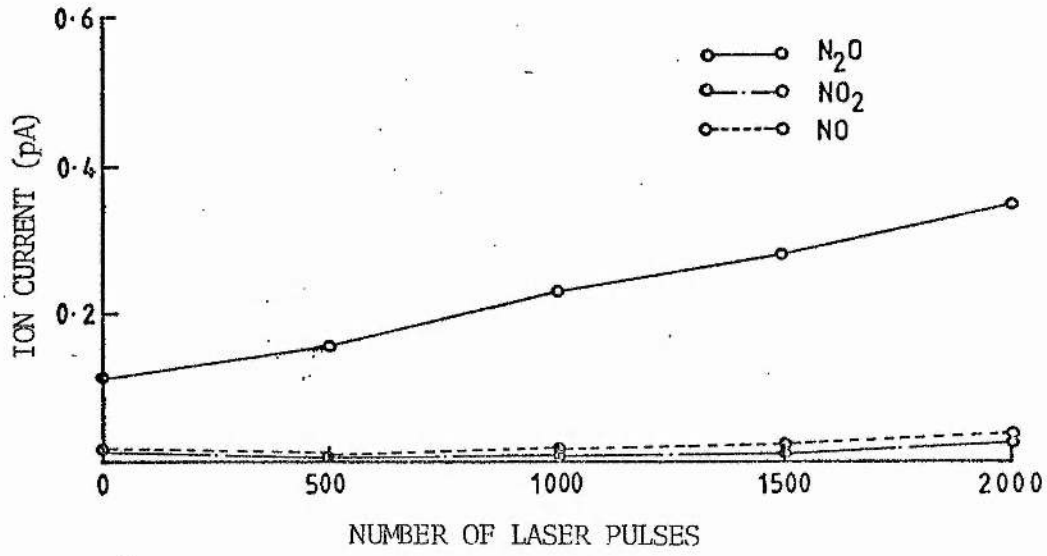

Fig.(4.11) Ion current variation for NO, NO_2 and N_2O in $He/Xe/NF_3$ after using $He/Xe/NF_3/CF_4$ mixtures.

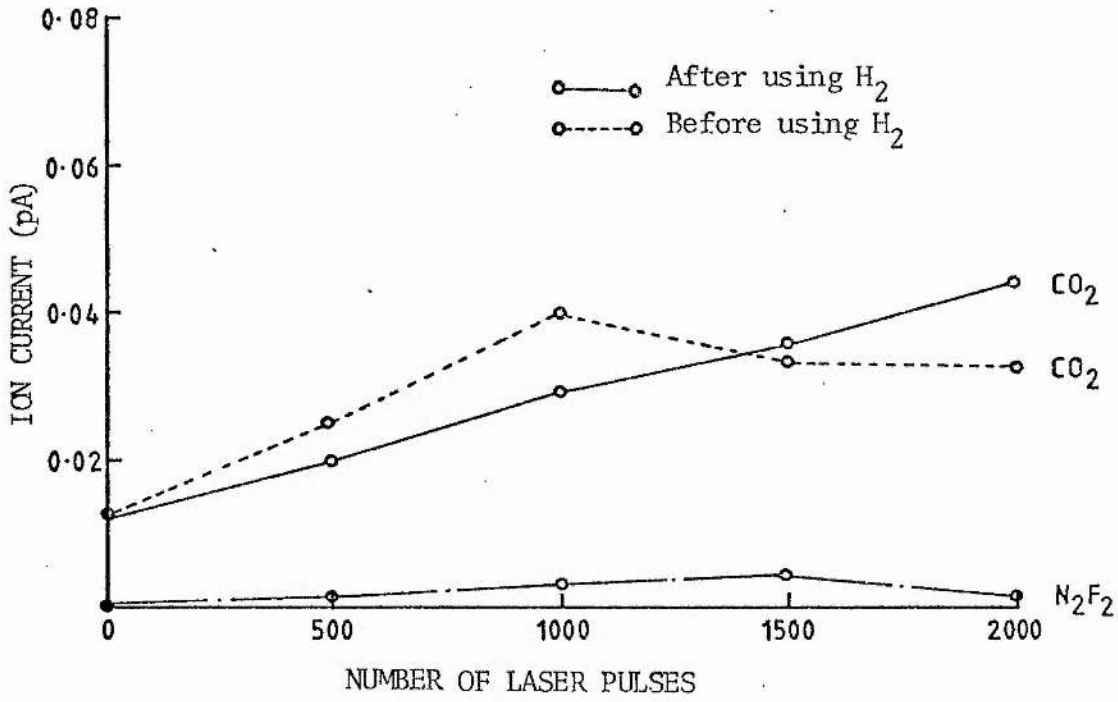

Fig.(4.12) Ion current variation for CO_2 and N_2F_2 in $He/Xe/NF_3$ after using $He/Xe/NF_3/H_2$ mixtures.

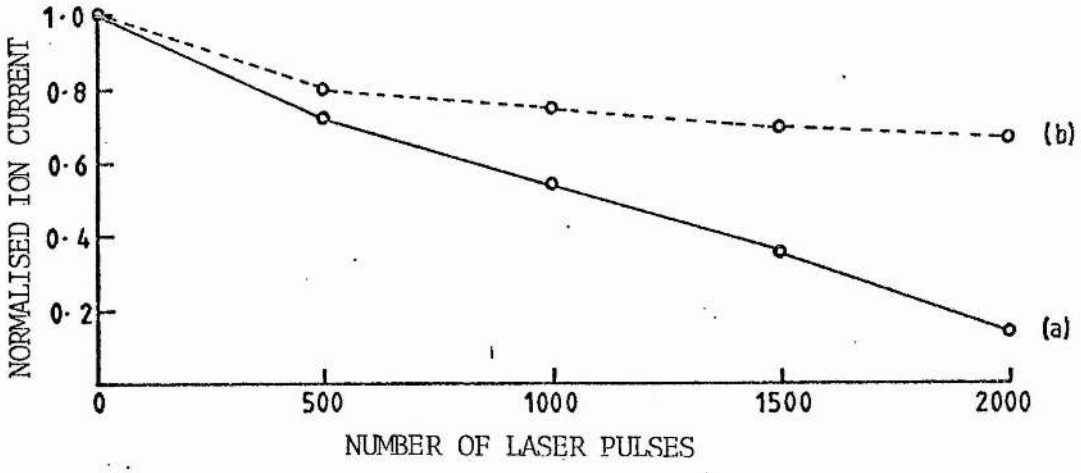

Fig. (4.13) Ion current variation for NF_3 in (a) $He/Xe/NF_3$ and (b) $He/Xe/NF_3$ after using $He/Xe/NF_3/H_2$ mixtures.

CHAPTER FIVE

COLD TRAP STUDIES

(5.1) Introduction

Cold traps are commonly used to extend the gas-life of rare gas halide lasers. Some of the schemes which have been reported in the literature were considered in section (1.6) of Chapter 1. They generally involve circulating the laser gas mixture through a combination of cold traps, getters, molecular sieves, active carbon and Ascarite absorbers, to remove contaminants which are formed in the gas discharge during pulsing (Christensen 1977, Johnson et al 1978, Kutschke et al 1981, Mandl et al 1982). Since the identities of the dominant contaminants are not known, these methods are normally designed to remove most of the contaminants using procedures which are very involved. In some schemes (Johnson et al 1978), the fluorine donor is removed after passing through the laser. It is then replenished and the "fresh" gas mixture is returned to the laser. In this chapter, we report on a study of gas contamination in XeF lasers using low temperature traps. The emphasis was on (i) gas-life extension, and a determination of the optimum trap temperature, and (ii) the identification of contaminants which are most detrimental to the long-term performance of XeF lasers for single gas fills.

In section (5.2), we consider the use of an on-line liquid nitrogen trap for contaminant removal. This is followed, in section (5.3), by a discussion of the effects of cold traps of various temperatures on the gas-life. The optimum trap temperature is

determined. The effects of replenishing the NF_3 consumed during pulsing is also considered. Section (5.4) is devoted to the results of UV absorption studies at the XeF laser wavelength. Section (5.5) deals with the results of mass spectrometric studies of the laser gas mixture. Section (5.6) reports on an experiment in which trapped contaminants are boiled off, to determine their importance in the degradation of laser performance. Finally in section (5.7), the results of this chapter are summarised.

(5.2) Liquid Nitrogen Trap

The boiling points of Xe and NF_3 are -108 and -129°C respectively, and these lie well below the boiling point of liquid nitrogen (-196°C). Consequently, liquid nitrogen traps cannot be used to extend the gas-life of XeF lasers, due to the rapid removal of Xe and NF_3 from the laser gas mixture ($He/Xe/NF_3$). In the early stages of this study, a liquid nitrogen trap was nevertheless used, and although the gas-life was significantly reduced, valuable information was obtained on the identity of the dominant contaminants.

The cold trap consisted of a spiral of stainless steel tube (1/4" O.D. and 4mm I.D.) immersed in liquid nitrogen contained in a dewar. The laser gas mixture consisted of $He/Xe/NF_3$ in the ratio of 360:6:1 at a total pressure of 1 atmosphere. Gas mixing was done in the laser using procedures similar to those described in Chapter 2. A fluorine compatible pump was used to circulate the laser gas mixture through the trap at a flow rate of about 2 litres/minute. The laser was pulsed at a repetition rate of 1 pps, and the supply voltage was 18 KV.

Starting from a fresh gas mixture, only 30 shots were obtained before laser action stopped. As mentioned earlier, this is due to the rapid removal of Xe and NF_3 by the trap. Laser action was again observed when the cold trap was warmed up. Figure (5.1) shows the results of an experiment which was conducted as follows: (i) the laser was filled with a fresh gas mixture, and it was pulsed to half-energy in the absence of a cold trap; (ii) it was then switched off, and the gas mixture was circulated through a liquid nitrogen trap for one minute, after which the trap was warmed up and the laser was again pulsed to half energy; (iii) step (ii) was repeated several times using a single gas fill. In fig. (5.1), the normalised laser pulse energy is plotted as a function of the number of laser pulses. We note that in each cycle, removal of the cold trap results in a rapid increase of the laser pulse energy, but more importantly, the maximum pulse energy in any cycle is always higher than the energy at the end of the previous cycle. In the first cycle, the energy obtained on removal of the cold trap is 90% that of fresh gas fills. This indicates that the dominant contaminants have boiling points which are above those of Xe and NF_3. The evolution of these contaminants cause the laser pulse energy to drop rapidly. The lower optimum energy reached in each cycle is mainly attributed to NF_3 depletion.

An insight into the identity of the dominant contaminants can be obtained from a consideration of fig. (5.2), which shows the boiling points of the contaminants identified in Chapter 3. We note that only N_2O, CO_2, HF and NO_2 have boiling points which lie above those of Xe and NF_3. One or more of these gases must therefore be responsible for the rapid drop in laser energy when the cold trap is warmed up. In a later section, we present the results of a similar but refined

experiment, in which the effects of the above contaminants were studied by boiling off the latter sequentially, using a cold trap whose temperature was continuously variable down to -196°C. In the section that follows, we consider the effects of cold traps on the gas-life for several trap temperatures.

(5.3) Gas-life extension

The results described in section (5.2) show that it may be possible to extend the gas-life of XeF lasers ($He/Xe/NF_3$ mixtures) by circulating the laser gas mixture through a cold trap whose temperature is low enough to remove contaminants such as N_2O, CO_2, HF and NO_2, but not NF_3 and Xe. To determine the optimum trap temperature for the laser device used in this work, a cold trap whose temperature was continuously variable down to -196°C was used. Figure (5.3) shows a schematic diagram of the trap. Oxygen-free nitrogen (supplied by BOC Special Gases) is first flowed through a melting-ice trap to remove water vapour which may otherwise solidify and obstruct the gas pipe. The dry gas is then bubbled through liquid nitrogen contained in a sealed dewar. The emergent cold gas is used to cool a coil, which is made from a length of stainless steel tube through which the laser gas mixture is circulated. The coil is situated in a well insulated dewar, and its temperature is measured using a chromel-alumel thermocouple. The trap temperature can be continuously varied from room temperature down to -196°C by changing the rate of flow of the nitrogen coolant gas. By making fine adjustments using a needle valve, the trap temperature can be kept constant to within ± 1°C.

The cold trap has been used to study the dependence of the gas-life of XeF lasers on the trap temperature for $He/Xe/NF_3$ mixtures. The results are shown in fig. (5.4), in which the number of laser pulses to half-energy is plotted as a function of the trap temperature. These results were obtained prior to those from the experiments reported in Chapter 4, in which contaminants such as CF_4 and H_2 were added to the laser gas mixture. Figure (5.4) shows that the use of an ice trap does not have a noticeable effect on the gas-life. For a trap temperature of $-50^{\circ}C$, the gas-life increases roughly by a factor of two. The best improvement occurs at $-100^{\circ}C$, when almost a sevenfold increase is obtained. At lower temperatures, there is only a small additional improvement. For the laser device and operating conditions used in this work, the optimum trap temperature is in the region of -100 to $-150^{\circ}C$. Figure (5.2) lists the boiling points of contaminants which are known to accumulate in the laser during pulsing. Only NO_2 and HF have boiling points which lie above $-50^{\circ}C$, and we therefore attribute the observed gas-life extension at $-50^{\circ}C$ to the removal of NO_2 and possibly HF. The large improvement at $-100^{\circ}C$ is attributed to the removal of CO_2 which sublimes at $-75^{\circ}C$ and possibly N_2O which boils at $-88^{\circ}C$. The additional small improvement at $-150^{\circ}C$ may be due to more efficient removal of these contaminants.

(5.3.1) Pulse energy variation

Figure (5.5a) shows the normalised pulse energy as a function of the number of laser pulses for a trap temperature of $-150^{\circ}C$. There is an initial fast drop in the laser pulse energy for about 200 shots,

followed by a plateau. After about 2000 shots, the laser output decreases gradually to half-energy near 2200 shots. Similar behaviour, characterised by the plateau effect, has been observed by McKee et al (1980) and Burlamacchi et al (1979) in their studies of gas-life extension in XeCl lasers. The above results were obtained prior to the addition of CF_4 and H_2 to the laser gas mixture. After running the laser on gas mixtures containing these additives, significantly longer gas-lifes were obtained from $He/Xe/NF_3$ mixtures, as shown in fig. (5.5b). The number of laser pulses to half-energy increased by about 35% to 3000, which corresponds to approximately 1500 pulses/litre atmosphere.

The gradual drop in laser output observed after the energy plateau may be due to (i) NF_3 depletion, and (ii) the accumulation of contaminants which are not removed by the cold trap. To determine the importance of the first process, the level of NF_3 in the used gas mixture was measured after the pulse energy had dropped to about 0.1 mJ. This was done by measuring the ion current $I^+(71)$ at mass $71(NF_3^+)$, which was then converted to a partial pressure using the previously determined sensitivity $S(NF_3^+)$ of the mass spectrometer at mass 71, and the expression

$$P(NF_3) = I^+(71)/S(NF_3^+) \qquad (5.1)$$

where $P(NF_3)$ is the partial pressure of NF_3. After about 3500 shots, the partial pressure of NF_3 was about 0.2 torr, which is too small to sustain efficient laser action.

The importance of contaminant accumulation was determined by measuring the laser pulse energy after replenishing the NF_3 lost

during laser pulsing. For adequate gas mixing, the used gas mixture was circulated and NF_3 was slowly leaked in from a calibrated volume. Figure (5.6) shows the laser output as a function of the number of laser pulses for two successive additions of NF_3 to used gas mixtures, for a single gas fill. In each case, the pulse energy does not recover completely. After the first addition, the energy increases to about 60% of the maximum for fresh gas mixtures. After the second addition, it is only about 40% of the maximum. This indicates that in addition to NF_3 depletion, the accumulation of contaminants is also responsible for the observed decline in laser output at the end of the energy plateau. In similar experiments conducted after the use of CF_4 and H_2 additives, the addition of NF_3 to used gas mixtures caused the laser output to increase to about 75% of the maximum energy. The revitalised gas mixture produced more than 4000 shots to half-energy. An attempt was made to extend laser operation on a single gas fill, by continuously bleeding NF_3 into the laser gas mixture. Although more than 5000 shots were obtained to half-energy, the experiment had only limited success, probably due to difficulties in maintaining the proper partial pressure of NF_3 in the gas mixture.

(5.4) UV-absorption spectroscopy

In Chapter 3 it was shown that NO_2 is the dominant absorber at the XeF wavelength. Since NO_2 boils at 21°C, it should be removed efficiently by a -150°C trap. This has been confirmed by UV absorption studies of used gas mixtures after circulation through a -150°C trap. The procedure was similar to that described in

section (3.9.1) of Chapter 3. Figure (5.7) shows UV absorption spectra of (a) residual gases in the absorption cell after pumping to about 50 μm and (b) a used gas mixture after 1000 shots for a trap temperature of -150°C. Comparison with the results obtained in section (3.9.1) of Chapter 3, shows that there is negligible absorption at the laser wavelength. The apparent higher absorption by residual gases in the evacuated cell is attributed to a reduction of the transmission of the quartz windows due to fluorine attack. We note that the contaminants which absorb in the region below 250nm are not completely removed by the trap.

(5.5) Mass spectrometric analysis

In section (5.3), it was shown that the gas-life of XeF lasers can be increased by circulating the laser gas mixture ($He/Xe/NF_3$) through a cold trap whose temperature is in the region of -100 to -150°C. The extended gas-life was attributed to the removal of contaminants which accumulate in the laser during pulsing. In section (5.3.1), it was shown that the gradual drop in laser output at the end of the energy plateau is due to the depletion of NF_3 as well as the accumulation of contaminants which are not efficiently removed by the cold trap. An attempt was therefore made to identify these contaminants from the results of mass spectrometric studies of fresh and used gas mixtures.

In the first part of this study, the levels of contaminants in used gas mixtures were determined in the absence of a cold trap, and also for trap temperatures of -50, -100 and -150°C. In each case, the measurements were made after the laser pulse energy had dropped to

0.1 mJ. The results are shown in figs. (5.8) and (5.9) for H_2O, CO, N_2, O_2, CO_2, NO, NO_2 and N_2O. We note the following:

(i) The partial pressure of NO_2 and N_2O are small and comparable to the corresponding background pressures in fresh gas mixtures.

(ii) Even though the boiling points of NO and O_2 are -152 and $-183^{o}C$ respectively, the partial pressures of these contaminants decrease with the trap temperature. This shows that O_2 and NO are to some extent formed from other molecules which are removed by the trap. The main photochemical reactions of NO_2 from 243.9nm to 397.8nm are the production of oxygen atoms and their fast reactions with NO_2 to form NO and O_2 (Okabe 1978).

$$NO_2 + h\upsilon \rightarrow NO + O(^3P) \qquad (5.2)$$

$$O(^3P) + NO_2 \rightarrow NO + O_2 \qquad (5.3)$$

Reaction (5.3) proceeds with a rate constant of $9.1 \times 10^{-12} cm^3\ mol^{-1}\ s^{-1}$. Since the wavelength region over which reaction (5.2) occurs includes the XeF laser wavelength (351nm), the efficient removal of NO_2 by the cold trap may be responsible for the low levels of NO and O_2 in the laser. This is supported by the results of mass spectrometric studies of $He/Xe/NF_3/CF_4$ and $He/Xe/NF_3/H_2$ mixtures, which show that during pulsing, a reduction in the rate of formation of NO_2 is accompanied by corresponding reductions in the rate of formation of NO and O_2 (figures (4.4), (4.6), (4.9) and (4.11) of Chapter 4).

Reactions (5.2) and (5.3) may explain the twofold increase in the gas-life for trap temperatures of -50°C. In section (5.3), the extended gas-life was attributed to the removal of NO_2 (and possibly HF) whose boiling point lies above -50°C. Nitrogen dioxide (NO_2) is the dominant absorber at the laser wavelength (351nm) in used gas mixtures, but the large improvement in the gas-life cannot be attributed to reduced absorption alone, since it has been shown that absorption by NO_2 at 351nm is negligibly small. However, if the removal of NO_2 results in a reduction of the levels of O_2 and NO in the laser, the laser pulse energy may improve significantly.

(iii) Carbon monoxide (B.P. -192°C) and N_2 (B.P. -196°C) are not removed by the trap. The increase in the level of CO and N_2 at lower trap temperatures is a result of the accumulation of these contaminants due to longer running times to half-energy.

(iv) The use of cold traps does not result in a reduction of the partial pressure of water vapour in the laser. This surprising result indicates the presence of a source of water, which is most likely to be the PVDF body of the laser. Water absorption by PVDF is 0.03%, compared to <0.01% for PTFE.

(v) Carbon dioxide accumulates in the laser even when the gas mixture is circulated through a cold trap at -150°C during pulsing. This result is unexpected, since CO_2 sublimes at -75°C. Analysis of the trap contents after the termination of laser action shows the presence of large amounts of CO_2.

The above results show that when a -150°C trap is used, there is a significant amount of CO, N_2, CO_2 and H_2O in the laser gas mixture after the laser pulse energy has dropped to about 0.1mJ. The presence of CO and CO_2 may explain the observed drop in laser output when the NF_3 consumed during pulsing is replenished. In Chapter 4, it was shown that the laser is insensitive to N_2 partial pressures of up to 1 torr. The presence of N_2 in the used gas mixture is therefore not likely to cause a significant reduction in laser output. However it must be emphasised that in the present case this may not be strictly true since the discharge properties may be different due to lower partial pressures of several species such as NO, N_2O, NO_2 and O_2. As mentioned earlier in Chapter 3, water vapour may indirectly cause a reduction of the laser extraction efficiency by acting as a source of oxygen in the formation of oxygen bearing species such as CO and CO_2.

(5.5.1) Contaminant formation for -150°C trap

A mass spectrometric study was conducted to investigate changes in the composition of the laser gas mixture during pulsing, for a -150°C trap. The initial composition of the gas mixture and the laser operating conditions were similar to those used previously. After gas mixing, mass spectra of the fresh gas mixture were taken. The temperature of the cold trap was then set at -150°C. The gas mixture was circulated and the laser was pulsed at a repetition rate of 1 pps. Mass spectra of the used mixture were taken at intervals of 500 shots for a total of 2000 shots. The results ,which are shown in

figs. (5.10) to (5.15), can be summarised as follows.

(i) Gas circulation through the cold trap does not result in a significant removal of Xe, which boils at -108°C. The partial pressure of water vapour changes in an unpredictable manner, but on the whole it is almost constant. This confirms earlier results (section (5.5iv) which showed that gas circulation through traps at temperatures down to -150°C does not result in a lower partial pressure of water vapour in the laser.

(ii) Gases which accumulate in the laser are N_2 and CO. This is due to their low boiling points compared to the trap temperature. The contaminants N_2F_2 and CF_4 which boil at -106 and -128°C respectively also accumulate in the laser.

(iii) The partial pressure of NO_2 (B.P. 21°C) is negligibly small even after 2000 shots. It is worth noting that the partial pressures of NO and O_2 are also small, and almost equal to their respective background levels in fresh gas mixtures. This is consistent with earlier observations that low levels of NO_2 are accompanied by low levels of NO and O_2. There is only a small change in the partial pressure of N_2O. This is unexpected since N_2O boils at -88°C.

(iv) Another unexpected result is the accumulation of CO_2, which sublimes at -75°C. This is attributed to inefficient removal by the cold trap. This conclusion is supported by the fact that N_2O, which boils at -88°C, is also not efficiently removed.

(v) The rate of depletion of NF_3 is similar to that obtained for $He/Xe/NF_3$ mixtures when a cold trap is not used. We note that in this experiment, the laser pulse energy started to drop after 1000 shots, and only about 1500 shots were obtained to half-energy. Figure (5.14) shows the rate of NF_3 depletion for $He/Xe/NF_3$ mixtures after the use of H_2 and CF_4 additives; NF_3 is consumed at a much reduced rate, in agreement with the results obtained earlier in section (4.4.1) of Chapter 4. The corresponding number of laser pulses to half-energy is 3000.

In section (5.3.1) it was shown that when a $-150^{\circ}C$ trap is used, the deterioration of laser performance after the plateau effect is due to the combined effects of (i) NF_3 depletion, and (ii) the accumulation of contaminants in the laser. The results of section (5.5) and (5.5.1) show that the two most likely contaminants are CO and CO_2, which both accumulate in the laser. Even though N_2 also accumulates, it is not expected to have a significant effect on laser performance.

(5.6) Contaminant boil-off

In Section (5.3), the optimum temperature range for gas-life extention was obtained from a determination of the number of laser pulses to half-energy for several trap temperatures. It was shown that the gas-life can be extended by a factor of seven, when the trap temperature is reduced from $-50^{\circ}C$ to $-100^{\circ}C$. In this section, we present the results of an experiment in which contaminants were boiled off a cold trap to determine their effects on laser performance.

The laser was filled with the basic mixture of $He/Xe/NF_3$ which was circulated through a cold trap at $-150^{o}C$. It was then pulsed at a repetition of 1 pps, and the output energy was recorded. After about 300 shots, the cold trap temperature was increased slowly, and the output energy was recorded as a function of the trap temperature. The latter was determined using a chromel-alumel thermocouple. The results are as shown in fig. (5.16), in which the laser output energy is plotted as a function of the number of laser pulses, for the sake of convenience. Trap temperatures for several regions of interest are also shown. The shape of the curve is explained as follows.

(i) From A to B the trap temperature is $-150^{o}C$, and the laser output is almost constant. This corresponds to to the "plateau effect" observed previously. At B the trap temperature begins to increase.

(ii) At C the trap temperature is about $-130^{o}C$, and the laser output begins to drop. Table (3.2) of Chapter 3 shows that the temperature is close to the boiling point of CF_4 (B.P. $-128^{o}C$) and NF_3 (B.P. $-129^{o}C$). From the results of Chapter 4, it is known that the laser output is insensitive to the presence of up to 3 torr of CF_4. Since the amount of CF_4 formed during pulsing is small, the behaviour of the laser output at C is not considered to be due to the evolution of CF_4 from the cold trap. One possible explanation is that the partial pressure of NF_3 increases above the optimum value of about 1.5 torr, thus causing the laser output to drop. The fresh gas mixture contained 2 torr of NF_3.

(iii) At D, the trap temperature is $-110^{o}C$ and the laser output

begins to recover. Table (3.2) shows that the trap temperature is close to the boiling point of Xe (B.P. $-108^{\circ}C$), and hence the improvement in laser output may be due to the evolution of Xe. The increase in the laser pulse energy may also be due to the depletion of NF_3. In (ii) above, it was suggested that the deterioration of laser performance at $-130^{\circ}C$ may be due to an increase in the partial pressure of NF_3 to a value which is above the optimum pressure of about 1.5 torr. If this is so, the rise in laser output observed at D may be due to the subsequent depletion of NF_3, since this would cause the partial pressure of NF_3 to decrease towards its optimum value.

(iv) At E the trap temperature is about $-75^{\circ}C$, and the laser output begins to drop sharply. The temperature corresponds to the sublimation point of CO_2. The rapid deterioration of laser performance in the region between E and F is attributed to the evolution of CO_2 from the cold trap. At F, the temperature is $-40^{\circ}C$ and the laser pulse energy is only 15% of the optimum value.

(v) At F, the trap temperature was decreased rapidly. We note that even though the laser output energy increases, it does not recover completely. The maximum energy at G is only 55% of the initial energy. This is mainly attributed to inefficient removal of CO_2 (and possibly other contaminants) by the cold trap, and to NF_3 depletion in the region between E and F.

(vi) In the region between G and H, the temperature is $-150^{\circ}C$. Degradation of laser performance in that region is mainly attributed to NF_3 depletion.

(5.7) Summary

The results of the studies reported in this chapter can be summarised as follows.

(i) The gas-life of XeF lasers can be extended by circulating the laser gas mixture ($He/Xe/NF_3$) through cold traps. For the device used in this work, the optimum trap temperature lies in the region of -100 to -150°C. On a single gas fill, the longest gas-life obtained using a -150°C trap is 1500 shots/litre atmosphere. This is about 2.5 times the best gas-life obtained without the use of a cold trap.

(ii) When a cold trap is used, there is an initial rapid drop in the laser output for about 200 shots followed by a plateau. After about 2000 shots, the laser output falls off gradually due to NF_3 consumption and contaminant build-up in the laser. If the depleted NF_3 is replenished, there is only a partial recovery, and the maximum laser output is only about 75% of that obtained from fresh gas mixtures. However, this procedure extends the gas-life by more than a factor of two to 3500 shots/litre atmosphere.

(iii) Optical absorption at the laser wavelength in used gas mixtures is negligible for trap temperatures of -50°C and below. This is attributed to the removal of NO_2 (B.P. 21°C). Absorption in the region below 240nm is significantly reduced, but the absorbers are not completely removed by the trap. Since UV preionization is thought to occur below 240nm, the accumulation of contaminants which absorb in that region may lead to a deterioration of the laser gas discharge due

to inadequate preionization, and hence to a reduction of the laser extraction efficiency.

(iv) Mass spectrometric analysis of the laser gas mixture shows that when a -150°C trap is used, NO_2 is efficiently removed, which confirms the results of UV absorption spectroscopy. There are only small changes in the partial pressure of N_2O, and the partial pressures of NO and O_2 are negligible. There is strong evidence that the low levels of NO and O_2 are due to the removal of NO_2 from which they may be formed. The results also show that CO_2 accumulates in the laser.

(v) When contaminants are trapped and subsequently boiled off, the largest drop in pulse energy occurs at about -75°C, which is the sublimation point of CO_2. This is evidence of the importance of CO_2 as a major contaminant.

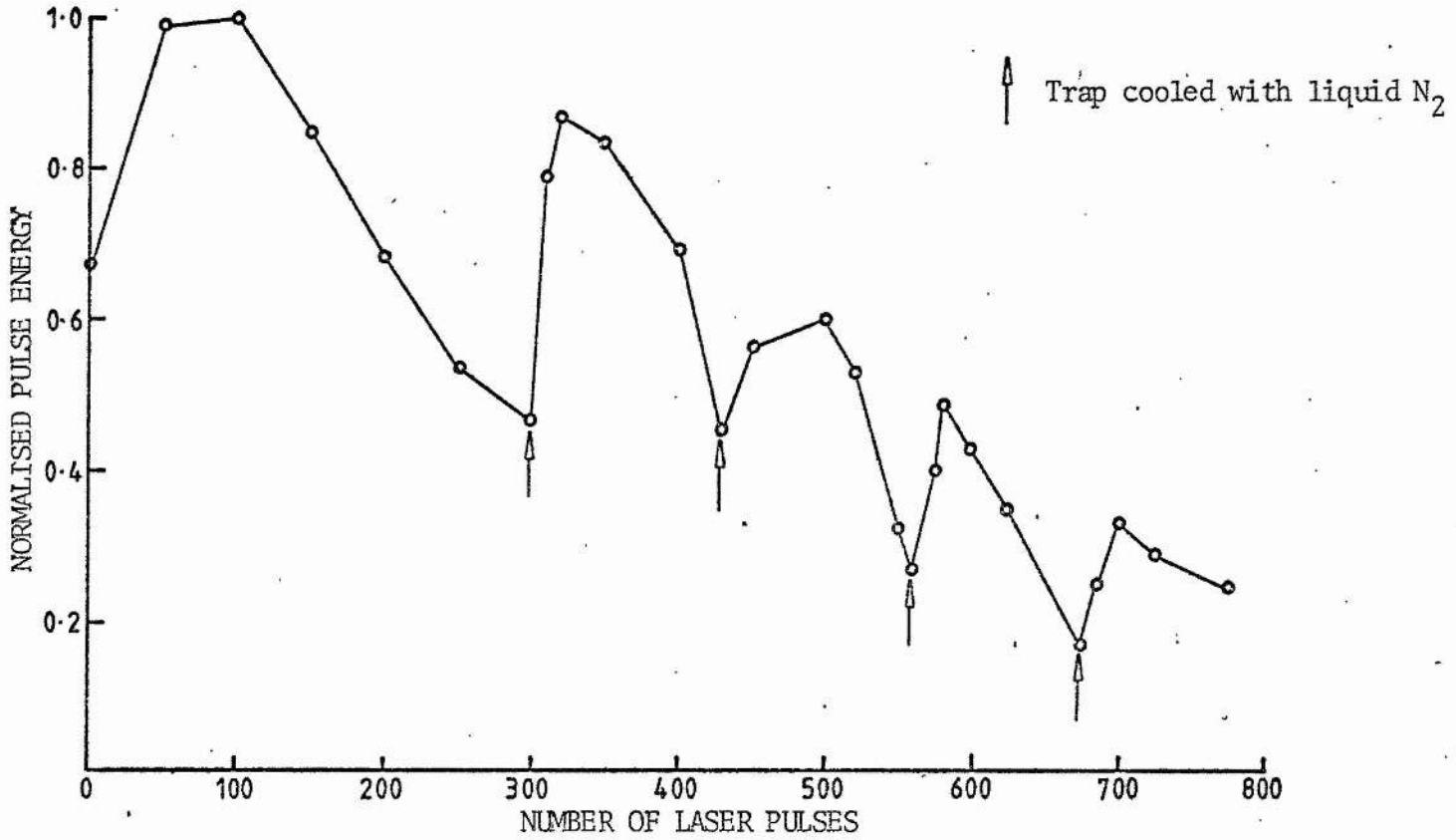

Fig.(5.1) Normalised pulse energy as a function of the number of laser pulses.

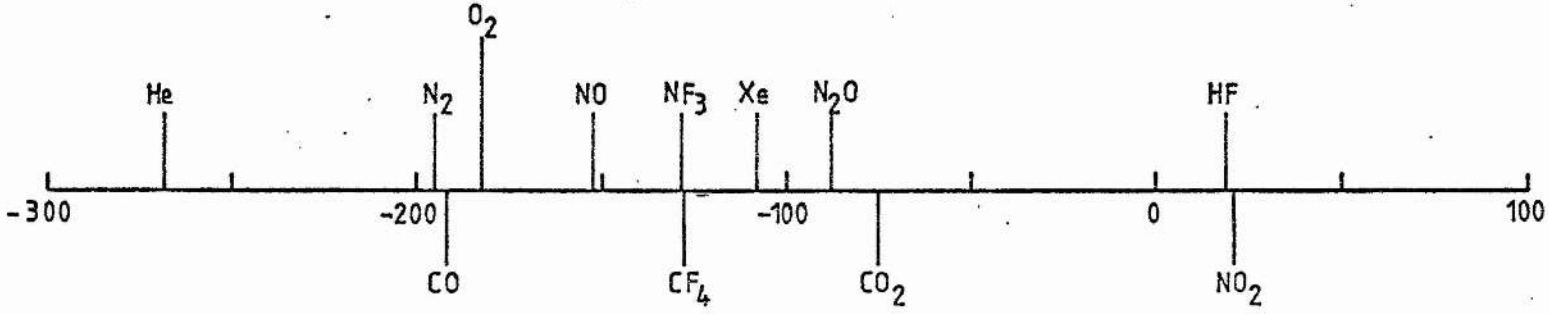

Fig.(5.2) Boiling point of He, Xe, NF_3 and contaminants which accumulate in He/Xe/NF_3 mixtures during pulsing.

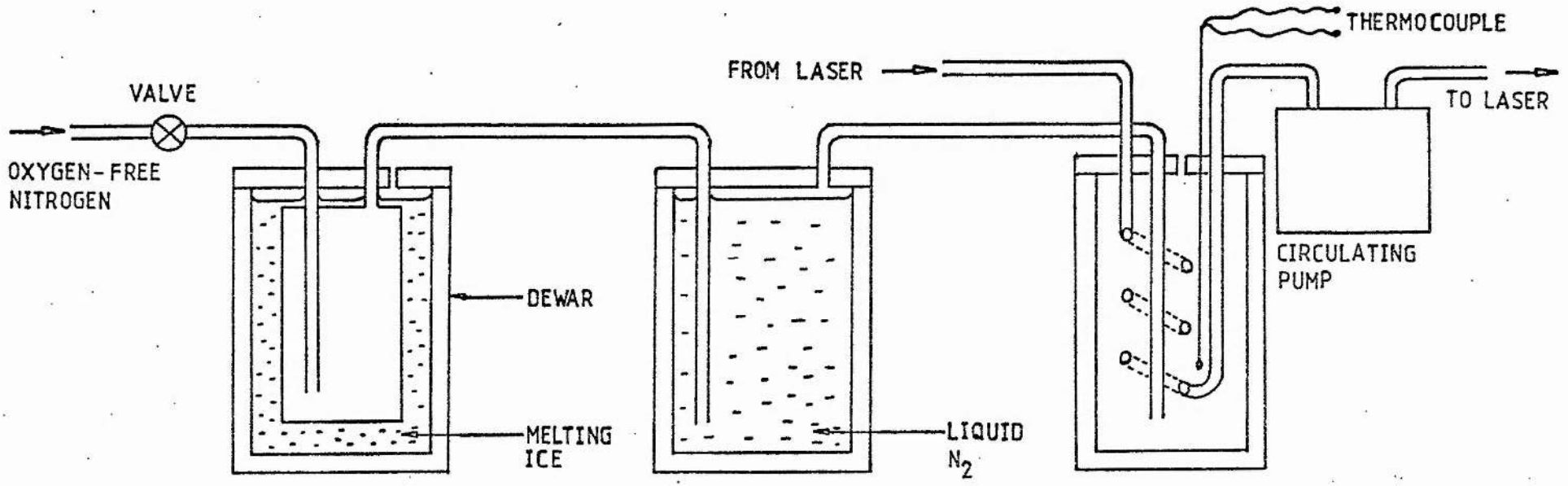

Fig.(5.3) Schematic diagram of the cold trap.

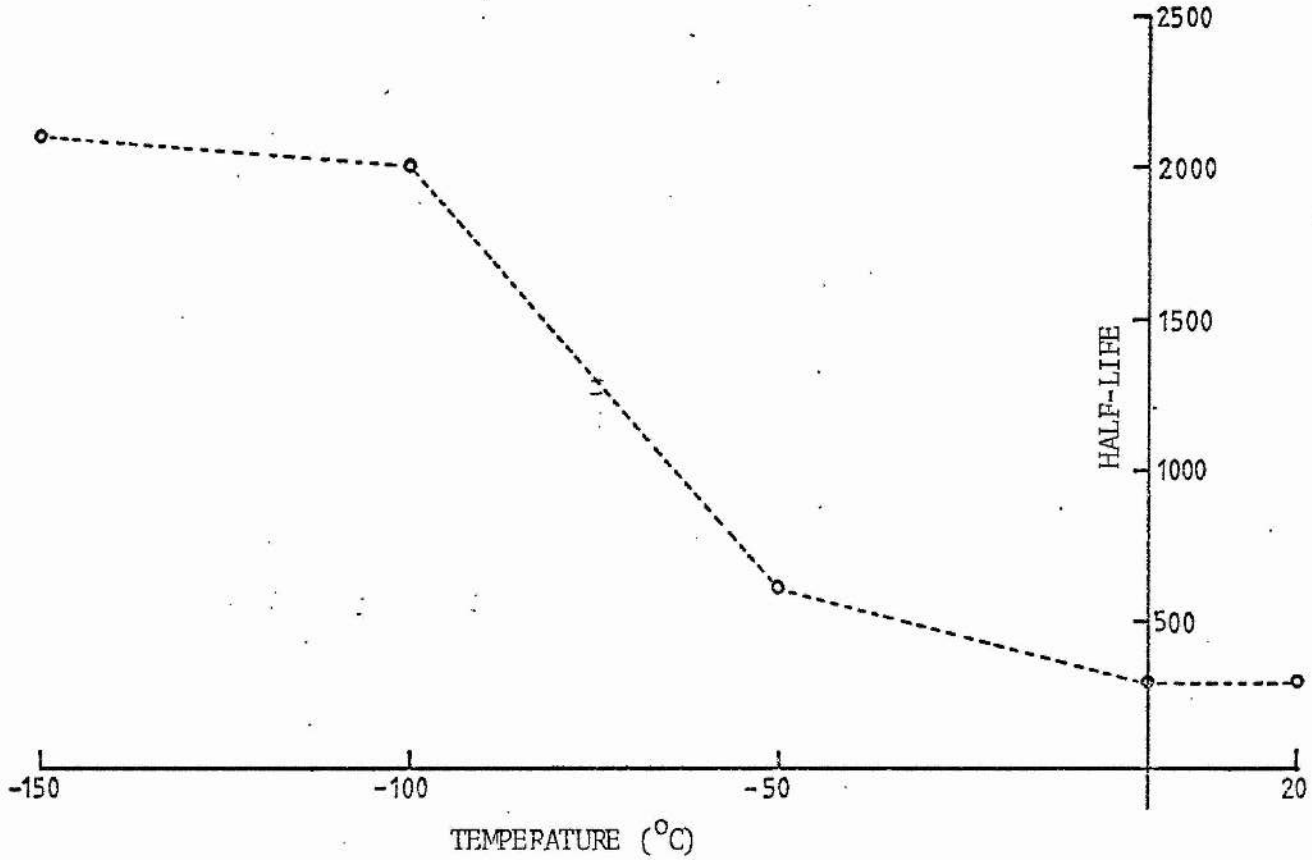

Fig.(5.4) Half-life of laser gas mixture as a function of the trap temperature.

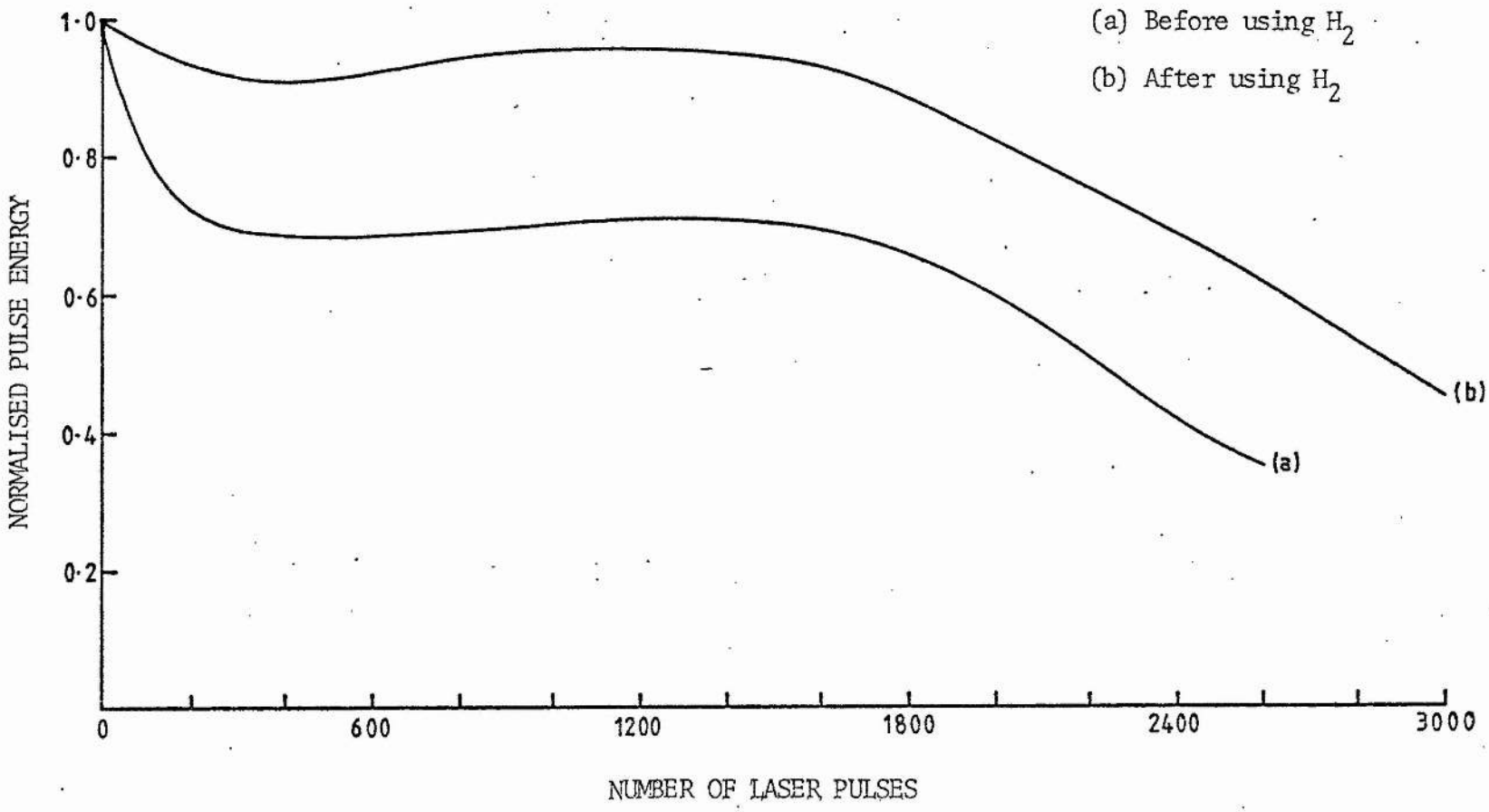

Fig.(5.5) Normalised pulse energy as a function of the number of laser pulses for a trap temperature of -150°C.

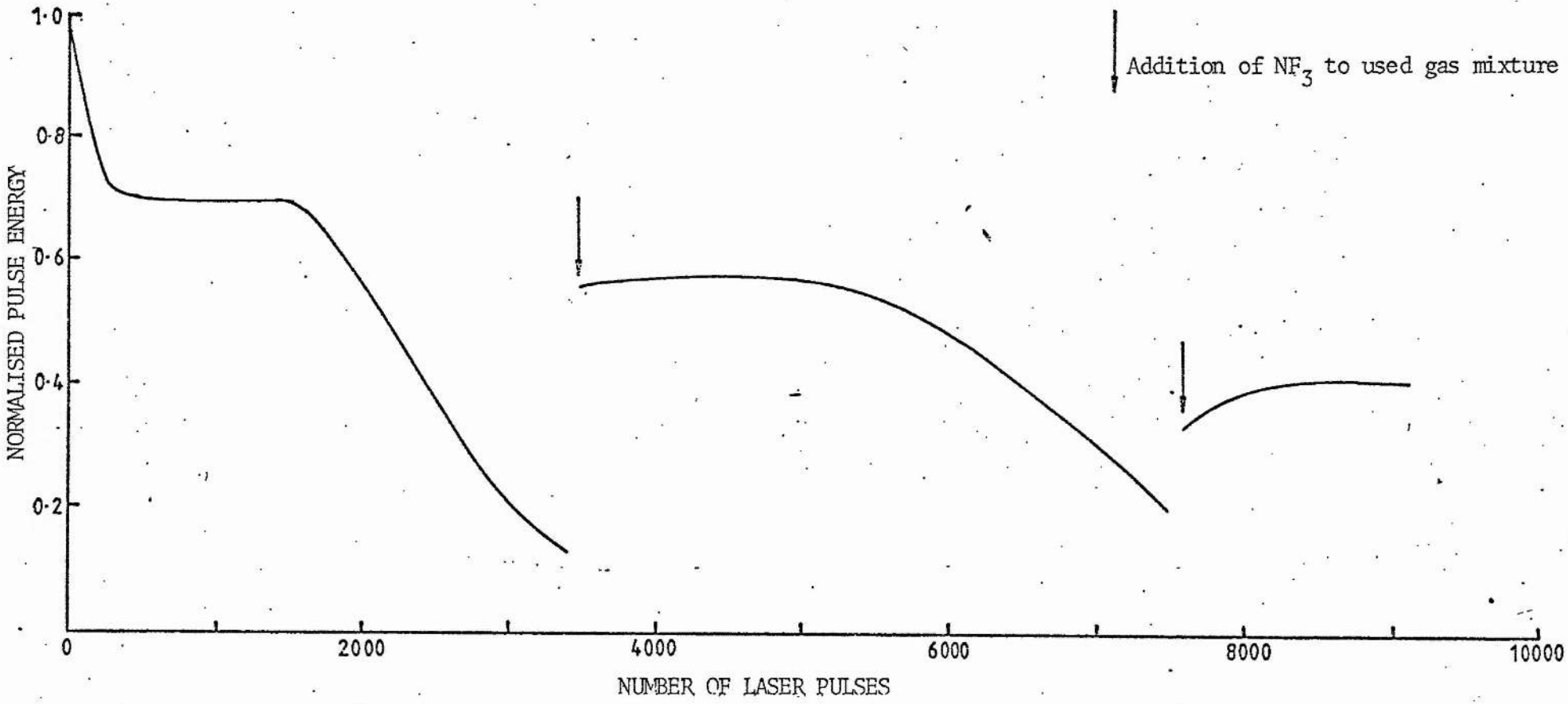

Fig. (5.6) Normalised pulse energy as a function of the number of laser pulses.

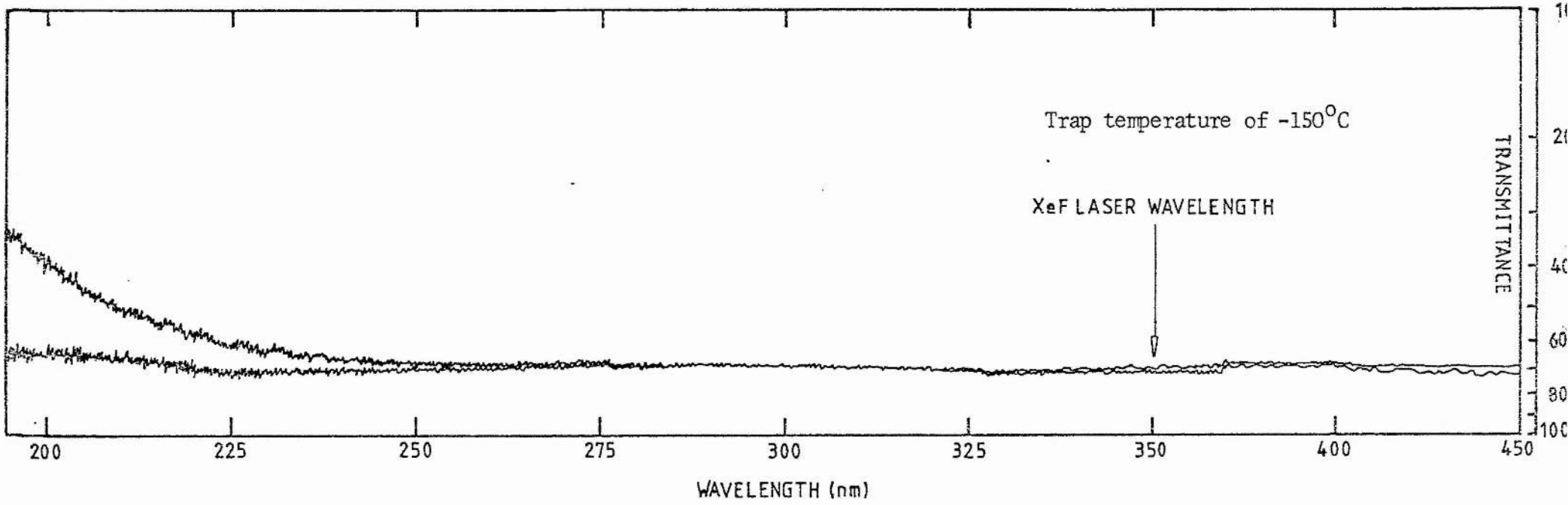

Fig.(5.7) UV absorption spectrum of (a) the evacuated absorption cell and (b) a used mixture after 1000 laser pulses.

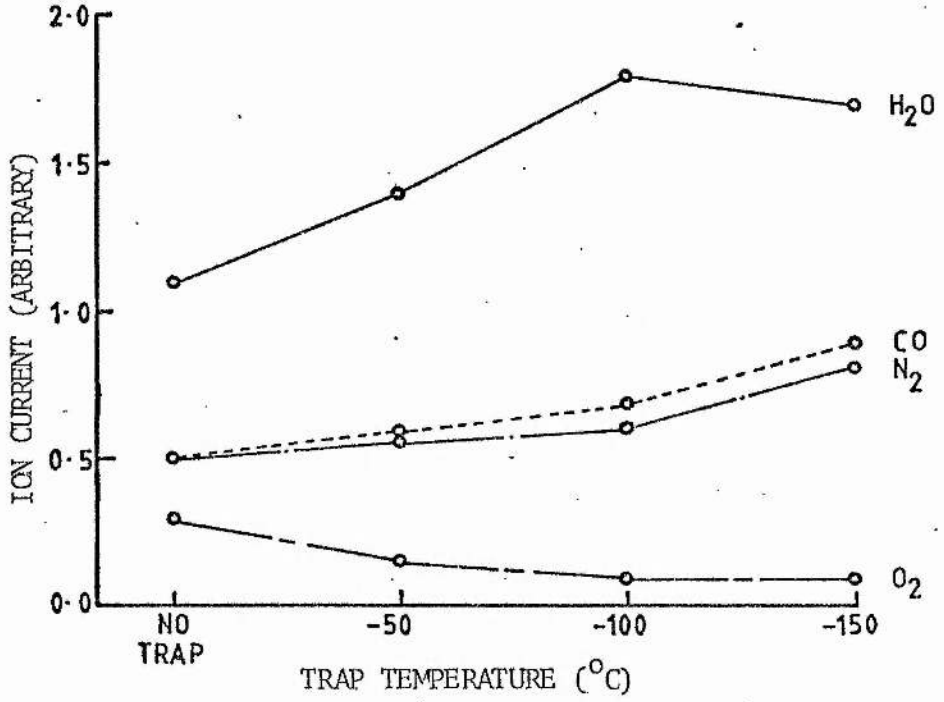

Fig.(5.8) Ion current variation for H_2O, CO, N_2 and O_2 in $He/Xe/NF_3$ mixtures as a function of the trap temperature.

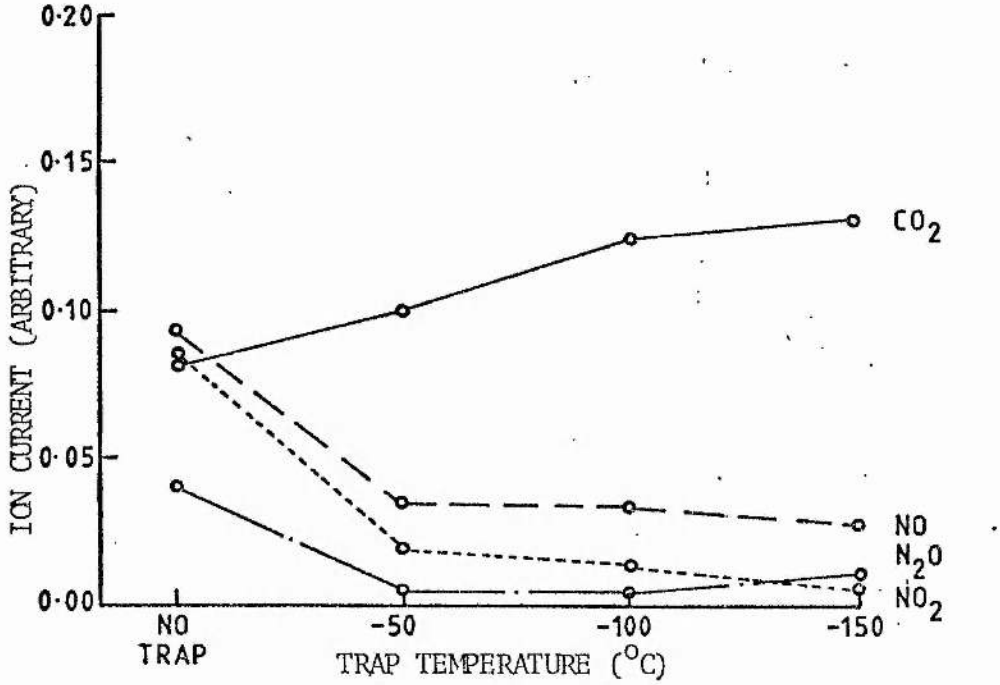

Fig.(5.9) Ion current variation for CO_2, NO, NO_2 and N_2O in $He/Xe/NF_3$ mixtures as a function of the trap temperature.

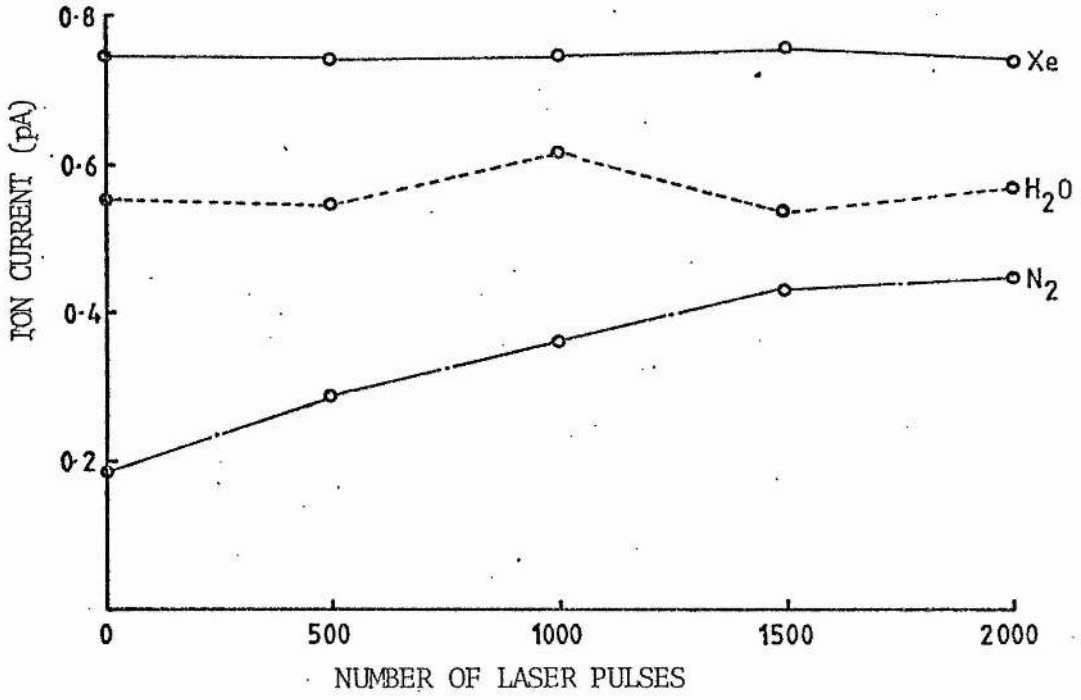

Fig.(5.10) Ion current variation for Xe, H_2O and N_2 in $He/Xe/NF_3$ mixtures as a function of the number of laser pulses and for a trap temperature of -150°C.

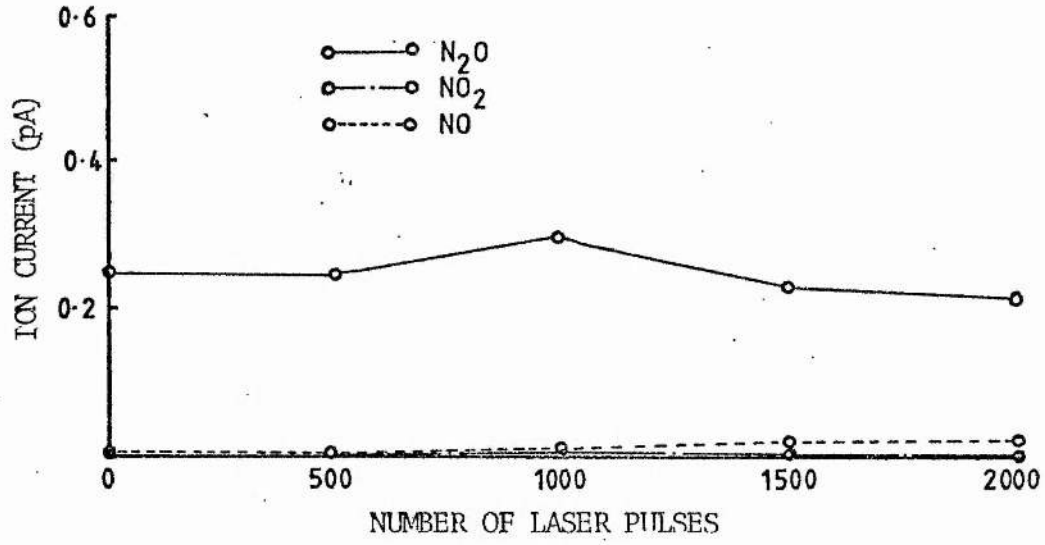

Fig.(5.11) Ion current variation for NO, NO_2 and N_2O in $He/Xe/NF_3$ mixtures as a function of the number of laser pulses and for a trap temperature of -150°C.

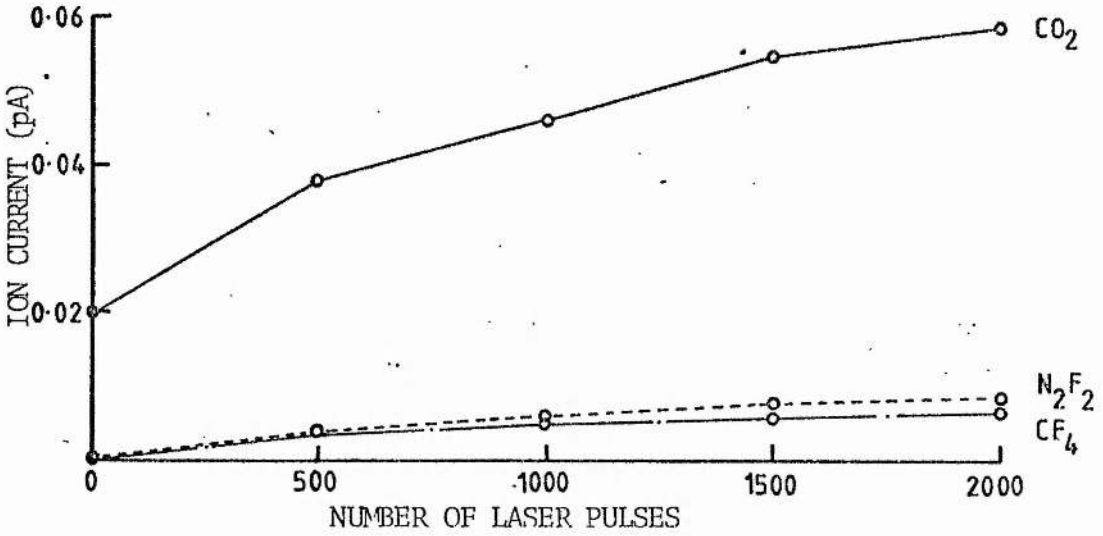

Fig.(5.12) Ion current variation for CO_2, N_2F_2 and CF_4 in $He/Xe/NF_3$ mixtures as a function of the number of laser pulses and for a trap temperature of $-150^{o}C$.

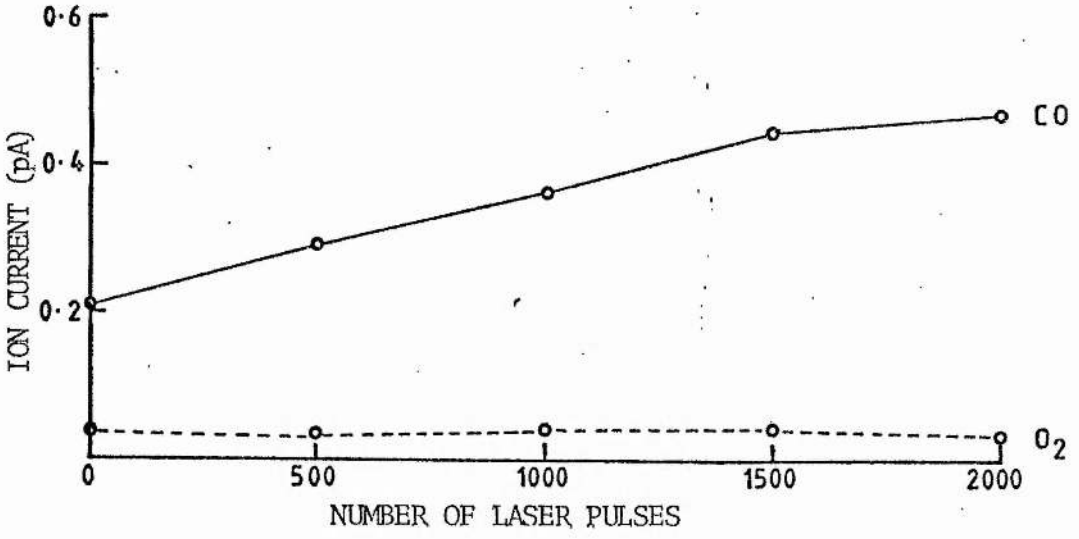

Fig.(5.13) Ion current variation for CO and O_2 in $He/Xe/NF_3$ mixtures as a function of the number of laser pulses and for a trap temperature of $-150^{o}C$.

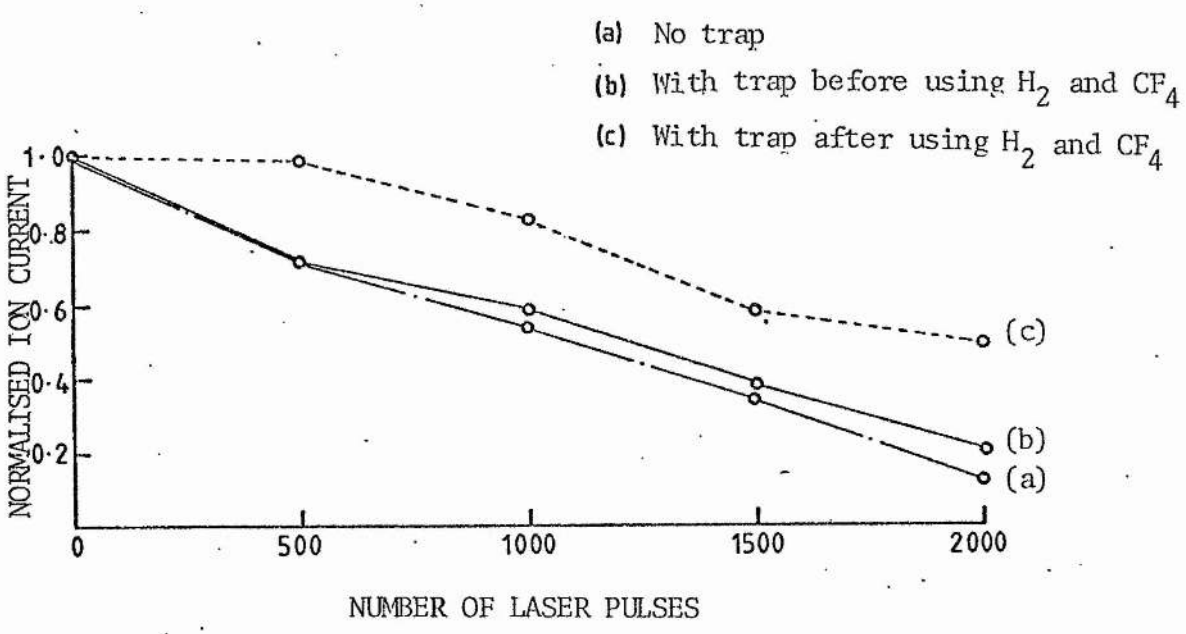

Fig.(5.14) Normalised ion current for NF_3 as a function of the number of laser pulses.

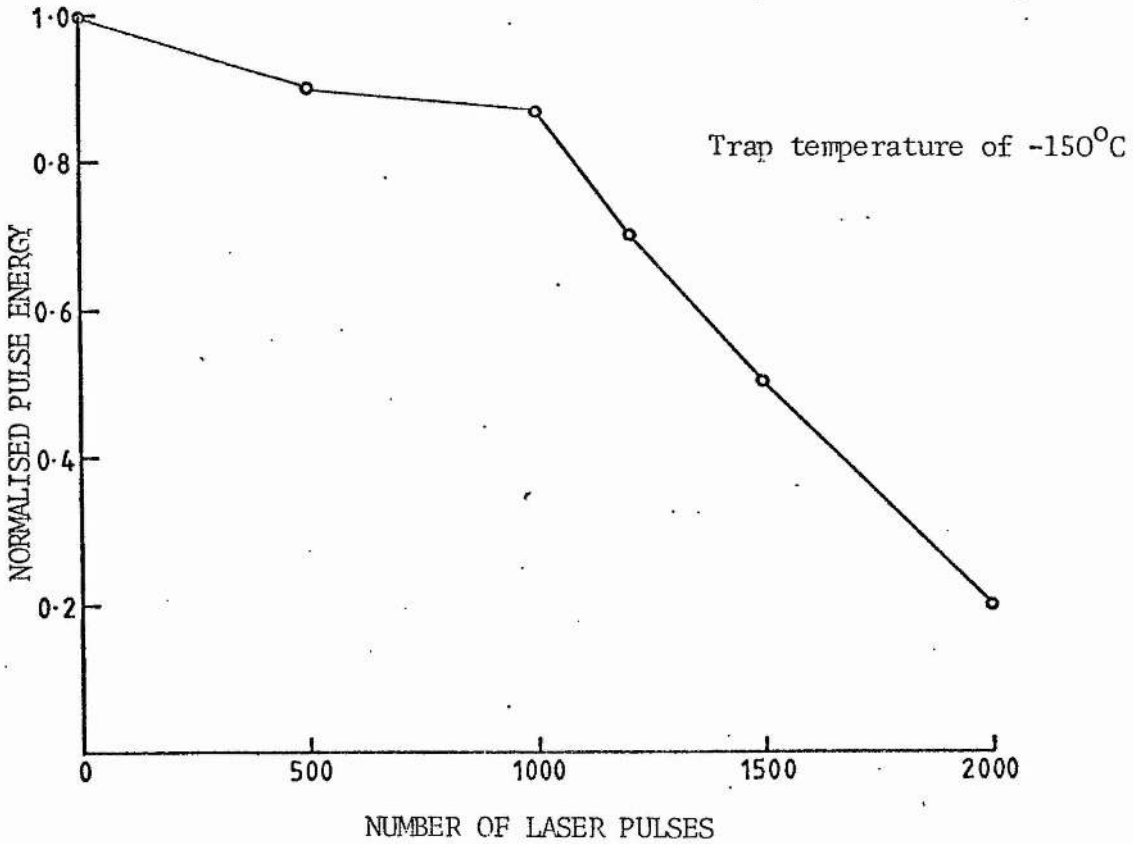

Fig.(5.15) Normalised pulse energy as a function of the number of laser pulses.

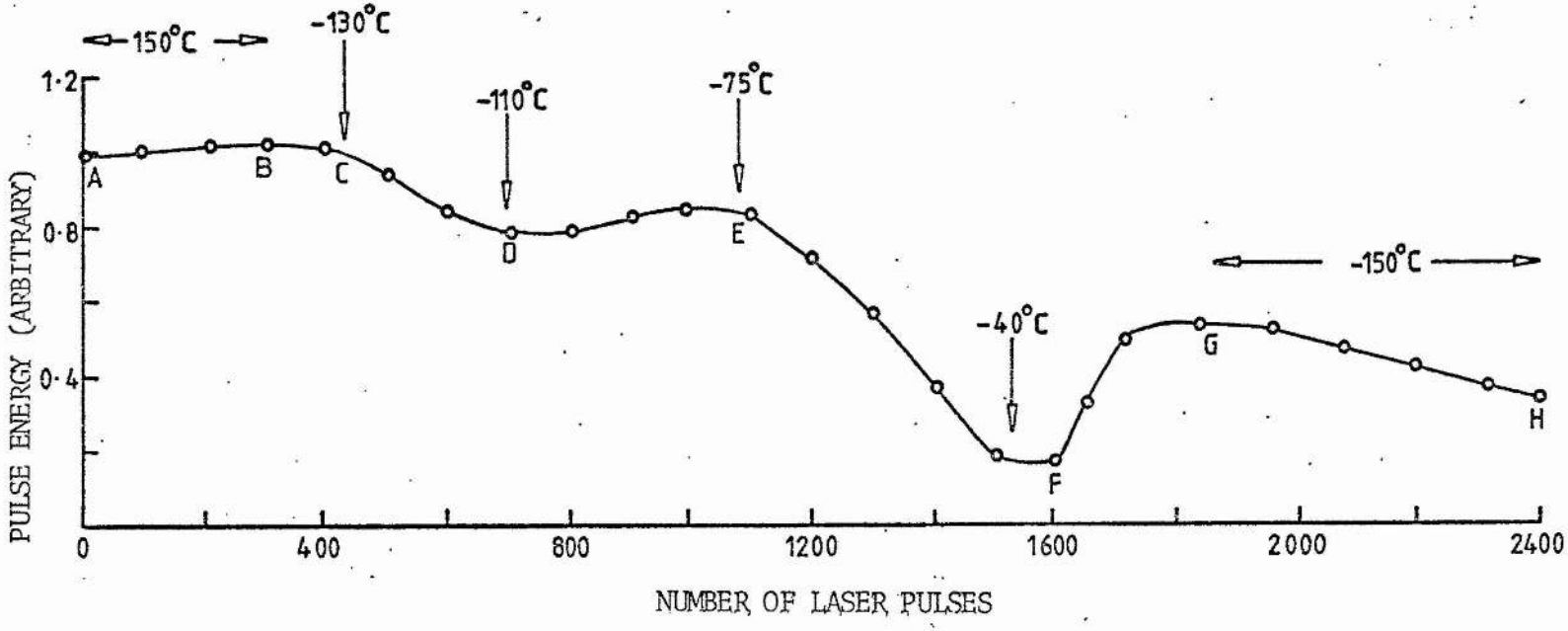

Fig.(5.16) Dependence of laser pulse energy on the cold trap temperature.

CHAPTER SIX

CONCLUSIONS

(6.1) Introduction

In this chapter, we summarise the main results and conclusions of chapters 3, 4, and 5 regarding the problem of gas contamination in discharge excited XeF lasers for $He/Xe/NF_3$ mixtures. Suggestions are made concerning the construction of these lasers, with the aim of extending the gas-life.

(6.2) NF_3 depletion and contaminant formation

In this work, it has been shown that for single gas fills of $He/Xe/NF_3$, the gas-life of discharge excited XeF lasers is limited by the depletion of NF_3, and the accumulation of contaminants in the laser. At half-energy, the laser pulse energy is approximately 50% smaller than that which would be expected if NF_3 was alone responsible for the deterioration of laser performance. This result is significant since it indicates that for single gas fills, the gas-life of XeF lasers cannot be extended by simply replenishing the NF_3 which is consumed during laser pulsing. Due to contaminant build-up, laser action will eventually terminate. The results of IR and mass spectrometric studies of the laser gas mixture show that during pulsing, N_2, O_2, CO, CO_2, NO, NO_2, CF_4, N_2F_2, NF_2 and HF accumulate in the laser. Molecules of N_2F_2 and NF_2, which are fragment products of

NF_3, accumulate during the first 300 pulses (or so), after which they are consumed. The initial rise in the partial pressure of N_2F_2 and NF_2 corresponds to the region where NF_3 is rapidly depleted. Carbon tetrafluoride (CF_4) accumulates in the laser and is not consumed. Since the rate constant for the formation of XeF^* from CF_4 is negligibly small (Velazco et al 1976), the accumulation of CF_4 constitutes a permanent loss of fluorine. Silicon tetrafluoride (SiF_4) was not detected in used gas mixtures. However, after circulating the laser gas mixture through cold traps at -150°C during pulsing, SiF_4 was detected in small amounts in the trapped contents. It is presumably formed in reactions of fluorine compounds with silicon, which is present as an impurity (0.7%) in the laser aluminium electrodes. Infrared absorption studies show the presence of HF in used gas mixtures after 2000 shots. The formation of HF may therefore account for some of the fluorine which is lost during pulsing. Other processes by which fluorine atoms may be lost include the formation of solid fluorides such as AlF_3, and the reactions of fluorine compounds with the PVDF envelope of the laser. Even though Xe is known to form xenon fluorides by direct fluorination, there is no significant change in its partial pressure, and xenon fluorides such as XeF_2, XeF_4 and XeF_6 are not formed.

The behaviour of water vapour is unpredictable, but in general its partial pressure decreases slightly during pulsing. With the exception of water vapour, the partial pressures of all contaminants which contain oxygen increase during pulsing. Water vapour may therefore be the source of oxygen for the formation of these contaminants. Oxygen atoms are presumably formed by the continued excitation and dissociation of hydroxyl radicals (OH), which may be

formed from water vapour during laser pulsing (Shahin 1971). Molecular oxygen may then be produced in very fast reactions between atomic oxygen and OH.

$$O + OH \rightarrow O_2 + H \qquad (6.1)$$

$$2OH \rightarrow H_2O + O \qquad (6.2)$$

$$OH \rightarrow O_2 + H \qquad (6.3)$$

Of the compounds which accumulate in the laser during pulsing, only NO_2 absorbs strongly at the laser wavelength. This is confirmed by the results of UV absorption spectroscopy of used gas mixtures. After 1000 laser pulses, continuous absorption at the laser wavelength is 8×10^{-2} % cm^{-1}. This is small compared to typical small signal gains of 0.1 to 1 cm^{-1} for laser devices similar to that used in this work. Consequently, NO_2 absorption is not considered to be a significant loss process.

(6.3) Effects of contaminants on laser performance

The effects of several contaminants (N_2, O_2, CO, CO_2, CF_4, H_2) on laser performance were studied by adding low concentrations of these contaminants, one at a time, to the laser gas mixture. For fresh gas mixtures, the laser pulse energy is insensitive to the addition of small amounts of N_2, H_2 and CF_4. In contrast with these results, the addition of 0.05% of CO_2, CO and O_2 reduces the laser pulse energy by 60, 40 and 20% respectively. Based on these results and on

measurements of the partial pressures of CO_2, O_2 and CO after 1000 laser pulses, the estimated change in the laser pulse energy due to the accumulation of these molecules is 20, 10 and 5% respectively.

The addition of small concentrations (< 1 torr) of N_2, CO_2, CO, O_2 and H_2 results in only small changes in the gas-life. In contrast, the addition of 2 torr of CF_4 to the laser gas mixture causes a threefold increase in the gas-life. After using $He/Xe/NF_3/CF_4$ mixtures, the number of laser pulses to half-energy obtained from the basic mixture of $He/Xe/NF_3$ increased by a factor of two. This is thought to be due to the conditioning of exposed surfaces in the laser. The even longer gas-life obtained from $He/Xe/NF_3/CF_4$ mixtures indicates that the addition of CF_4 to the basic mixture results in more favourable gas kinetics in the discharge. During the course of this work, laser emission in the infrared at about 2 μm was observed when CF_4 was substituted for NF_3 as the fluorine donor. The emission is attributed to the 5d(3/2) -> 6p(3/2) atomic line of Xe at 2.03 μm (Appendix 2). To ensure that the longer gas-life of $He/Xe/NF_3/CF_4$ mixtures was not due to laser emission in the infrared, XeF laser emission at 351nm was filtered out using an infrared transmitting filter, and the energy of the transmitted beam was measured. It was found to be less than 5% of the total energy. Similar values were obtained for $He/Xe/NF_3$ mixtures. Mass spectrometric analysis of $He/Xe/NF_3/CF_4$ mixtures during pulsing shows that the extended gas-life is mainly due to lower concentrations of NO, NO_2 and O_2.

It was mentioned earlier that the addition of small amounts of H_2 to the basic mixture does not have a significant effect on the gas-life. However, after using $He/Xe/NF_3/H_2$ gas mixtures, a fivefold improvement in the gas-life of the basic mixture was obtained. Mass

spectrometric analysis of the laser gas mixture shows that the improved gas-life is due to lower concentrations of NO_2, NO, O_2, and to a smaller rate of NF_3 depletion. The smaller rate of NF_3 depletion is attributed to the passivation of exposed surfaces in the laser when $He/Xe/NF_3/H_2$ mixtures are used. Passivation is presumably due to the reaction of these surfaces with HF formed in reactions of H_2 with NF_3 in the discharge. Even though 75% of the initial NF_3 remains after 2000 shots, the corresponding pulse energy is only 15% of that which would be expected from fresh gas mixtures containing similar concentrations of NF_3. This shows that the deterioration of laser performance is due to the accumulation of contaminants other than O_2, NO and NO_2. Mass spectrometric studies of the basic mixture ($He/Xe/NF_3$) indicate that CO, CO_2 and N_2O accumulate during pulsing and may therefore be major contaminants.

(6.4) Use of cold traps

A cold trap whose temperature was continuously variable down to $-196^{\circ}C$, was used to extend the gas-life. For trap temperatures of $-50^{\circ}C$, the gas-life increases by approximately a factor of two. The best improvement occurs at $-100^{\circ}C$, for which a sevenfold increase is obtained. At $-150^{\circ}C$, there is only a small additional improvement. For the laser device and gas mixture used in this work, the optimum trap temperature is in the region of -100 to $-150^{\circ}C$.

Of the contaminants which accumulate in the laser during pulsing, NO_2 and HF have boiling points which lie above $-50^{\circ}C$, and the boiling points of CO_2 and N_2 are above $-100^{\circ}C$. Since optical absorption at the laser wavelength by NO_2 is known to be negligibly small, the

removal of NO_2 at trap temperatures of $-50^{\circ}C$ is not considered to be directly responsible for the observed twofold increase in the gas-life. Over the wavelength range of 243.9 to 397.8nm, NO_2 is known to form NO and O_2 in the following reactions.

$$NO_2 + h\upsilon \rightarrow NO + O(^3P) \qquad (6.4)$$

$$O(^3P) + NO_2 \rightarrow NO + O_2 \qquad (6.5)$$

Reactions (6.4) and (6.5) suggest that the extended gas-life at trap temperatures of $-50^{\circ}C$ may be due to smaller concentrations of O_2 and NO, due to the removal of NO_2. This is confirmed by the results of mass spectrometric analyses of used gas mixtures, which show that for trap temperatures of $-50^{\circ}C$, the levels of NO (B.P. $-152^{\circ}C$) and O_2 (B.P. $-183^{\circ}C$) in used gas mixtures are significantly lower than in fresh mixtures. The large increase in the gas-life at trap temperatures of $-100^{\circ}C$ is mainly attributed to the removal of CO_2, and to a smaller extent N_2O.

For trap temperatures of $-150^{\circ}C$, there is a fast drop in the laser pulse energy for the first 200 shots (or so), followed by an energy plateau. After about 2000 shots, the pulse energy decreases slowly to half-energy at about 3000 shots. The deterioration of laser performance is due to the depletion of NF_3, and the accumulation of contaminants in the laser. The laser pulse energy increases to 75% of the maximum energy obtained from fresh gas mixtures, when the NF_3 consumed during pulsing is replenished. The extended gas-life is then more than five times the best result obtained without a cold trap. Mass spectrometric studies of the laser gas mixture show that during

pulsing, the partial pressures of NO, NO_2 and O_2 are small and comparable to their respective background pressures in fresh gas mixtures. There are no significant changes in the partial pressures of N_2O, Xe and H_2O, but relatively large increases in those of N_2, CO and CO_2. Since it is known that the laser pulse energy is insensitive to partial pressures of N_2 up to 1 torr, the lower pulse energy obtained after replenishing the NF_3 lost during pulsing is attributed to the accumulation of CO and CO_2 in the laser. When trapped contaminants are boiled off sequentially (in the region of the energy plateau), there is a fast drop in the laser pulse energy in the region of $-75^{\circ}C$, which is the sublimation point of CO_2. At a trap temperature of about $-40^{\circ}C$, the laser pulse energy is only 15% of that obtained from fresh gas mixtures. This is evidence that CO_2 is a major contaminant, thus confirming the results of section (6.3) in which it was shown that during laser pulsing, the accumulation of CO_2 in the laser causes the largest drop in the laser pulse energy.

(6.5) Discussion

The contaminants which accumulate in the laser can cause a reduction of laser performance through several processes, which include the following:

(i) Quenching of the XeF(B) state, and of xenon metastables (Xe^*, which are the dominant precursors of XeF^* in discharge excited XeF lasers).

(ii) Contaminant absorption at the laser wavelength, and in the

spectral region below 240nm where preionization is thought to occur.

(iii) The formation of transient species which absorb at the XeF laser wavelength.

(iv) The formation of negative ions in dissociative-attachment reactions, resulting in discharge instabilities.

The importance of collisional quenching of the XeF(B) state cannot be estimated due to a lack of quenching data. A rough estimate of contaminant quenching of Xe^* shows that for contaminant levels measured in this work, quenching of Xe^* is not significant.

The results of UV absorption spectroscopy shows that when a $-150^{\circ}C$ trap is used, there is negligible absorption at the laser wavelength. This is attributed to efficient removal of NO_2 by the trap. In the region below 240nm, optical absorption is reduced but still present. Contaminant absorption in that region may result in a deterioration of the laser discharge due to inadequate preionization. Under these conditions, the discharge is visually homogeneous, but it consists of microscopic filaments. These reduce the laser extraction efficiency as a result of inefficient excitation of XeF molecules, and the formation of refractive index gradients in the discharge region. The latter manifests itself as an apparent increase in optical absorption at the laser wavelength.

Contaminant formation in the laser may also cause a deterioration of laser performance either by enhancing the formation of transient species such as Xe_2^+, which absorb at the laser wavelength, or by forming new transient absorbing species. Transient absorption causes

a reduction of the overall laser gain, and hence a reduction of the laser output energy.

The degradation of laser performance may also be due to dissociative-attachment instabilities. These are due to an imbalance between the rate of electron production and that of electron loss by dissociative-attachment reactions. They can be significantly influenced by the presence of small concentrations of impurities. The instabilities manifest themselves in the form of striations, or in extreme cases as constrictions of the gas discharge. These cause a deterioration of the discharge homogeneity, which results in reduced laser extraction efficiencies.

The effects of UV absorption in the region where preionization takes place, and of processes (iii) and (iv) are subtle and difficult to investigate experimentally. Studies of side-light fluorescence from the laser discharge with and without cold traps, may shed some light on the significance of these processes. Both transient absorption at the laser wavelength and filamentation of the discharge are expected to cause early termination of side-light fluorescence. Consequently, gas circulation of the laser gas mixture through a $-150^{o}C$ should result in a temporal extension of side-light fluorescence. Investigations of the behaviour of the discharge current pulse may help in assessing the importance of discharge instabilities.

(6.6) Suggested design modifications for long gas-life

It has been shown that the limited gas-life of XeF lasers (for $He/Xe/NF_3$ mixtures) is due to NF_3 depletion and the accumulation of

contaminants in the laser. During pulsing, NF_3 is converted to fragment products which form solid fluorides, and stable species such as CF_4 for which the rate of formation of XeF^* in harpoon reactions with Xe^* is negligibly small. The fragmentation of NF_3 results in the deterioration of laser performance, and eventually in the termination of laser action. To achieve long gas-life, the laser and gas-handling system must be built from fluorine compatible materials, and the NF_3 consumed during pulsing must be replenished. It is worth noting here that after the first 200 shots (or so), NF_3 is depleted at an almost constant rate. It should therefore be possible to maintain its partial pressure in the gas mixture by injecting NF_3 from a reservoir at the same rate. The loss of NF_3 in reactions of fragment products with exposed materials in the laser can be minimised by a judicious choice of building materials for the laser (laser envelope, electrodes, preionizer, windows, etc.), and the gas-handling system. Plastics such as PVDF and PTFE are commonly used as building materials for the envelope of rare gas fluoride lasers. This is due to their good insulating properties, and more importantly, their compatibility with fluorine. However, in the light of the results obtained in this work, plastics are not considered to be ideal materials. They are porous, and permeable to most gases, have relatively high water contents, and cannot be baked at high temperatures. Plastics may also act as sources of carbon in the formation of molecules such as CO, CO_2 and CF_4.

The contaminant molecules which accumulate in XeF lasers ($He/Xe/NF_3$ mixtures) are composed of atoms of nitrogen, carbon, fluorine and oxygen. With the exception of N_2, CF_4, HF, N_2F_2 and NF_2, all the contaminants contain oxygen, and either nitrogen or carbon.

Consequently, the rigorous exclusion of oxygen from the discharge region should result in low levels of carbon and nitrogen oxides, and hence in significantly longer gas-lifes. In this work, the sources of oxygen in the laser have not been precisely identified. However, there is strong evidence that in the gas discharge oxygen may be formed from water vapour. If this is the case the rate of formation of oxygen, and hence of carbon and nitrogen oxides, could be significantly reduced by using a laser system which is bakable at temperatures of 100^{o}C and above.

Two materials which are considered to be suitable for building the laser envelope are stainless steel, and ceramic. The use of stainless steel presents the problem of electrical insulation. All connections to components in the laser must be made through insulating bushes. In addition, the distance between each electrode and the laser envelope must be carefully adjusted with respect to the separation of the electrodes, to prevent arcing to the metal envelope. For the same reason, "sideways preionization" cannot be used. The preionizer must be placed behind one of the main electrodes which must be perforated. However, this has the advantage of confining the discharge in the region between the main electrodes. The above problems can be avoided by using a ceramic envelope. The choice of corona preionization over the commonly used spark-array scheme may help in reducing the rate of NF_3 depletion. Nickel or monel 'corona' wires should be used in preference to stainless steel. All vacuum seals should be made with viton 'O' rings. Viton is a fluorocarbon which is compatible with fluorine, has low gas permeability and is bakable at temperatures up to 200^{o}C. Calcium fluoride flats should be used as the laser windows in preference to

quartz which is attacked by fluorine.

The implementation of these suggestions is expected to result in a substancial increase of the gas-life of XeF lasers, for $He/Xe/NF_3$ mixtures. However, it must be emphasised that N_2 will still be formed as a result of the fragmentation of NF_3. The results of section (4.3) of Chapter 4 show that for partial pressures of N_2 exceeding approximately 1 torr, there is a relatively fast drop in the laser pulse energy. Consequently, unless the nitrogen formed during pulsing is removed from the gas mixture, its accumulation in the laser will ultimately terminate laser action. Since the boiling point of N_2 is above those of Xe and NF_3, its removal by cold traps is not practicable. An alternative is the use of molecular sieves which can be chosen to selectively remove N_2.

APPENDIX ONE

COMPUTER PROGRAM 'BLUM'

THIS COMPUTER PROGRAM SOLVES A SET OF FIRST-ORDER DIFFERENTIAL EQUATIONS (EQUATIONS 2.8 TO 2.15 OF CHAPTER 2) DESCRIBING A PARELLEL-PLATE BLUMLEIN CIRCUIT, USING A VARIABLE-ORDER VARIABLE-STEP GEAR METHOD (NAG ROUTINE D02QBF, ST ANDREWS UNIVERSITY VAX COMPUTER).

INPUT PARAMETERS

LG, LL, L1, L2, C1 AND C2 ARE AS DEFINED IN CHAPTER 2.

RD0 - IMPEDANCE OF LASER DISCHARGE BEFORE GAS BREAKDOWN.

RD1 - IMPEDANCE OF LASER DISCHARGE AFTER GAS BREAKDOWN.

RG0 - IMPEDANCE OF SPARG GAP SWITCH BEFORE CLOSURE.

RG1 - IMPEDANCE OF SPARK GAP SWITCH AFTER CLOSURE.

DELD - TIME INTERVAL BETWEEN SWITCH CLOSURE AND GAS BREAKDOWN IN THE LASER.

TD - TIME INTERVAL DURING WHICH THE LASER DISCHARGE COLLAPSES FROM RD0 TO RD1.

V0 - SUPPLY VOLTAGE.

X0 - INITIAL POINT OF INTEGRATION.

NUM - NUMBER OF OUTPUT POINTS.

STEP - TIME INTERVAL BETWEEN SUCCESSIVE OUTPUT POINTS.

TOL - TOLERANCE (POSITIVE).

CONS - SCALING CONSTANT.

OUTPUT PARAMETERS

THE OUTPUT PARAMETERS ARE I1, I2, I3, I4, V1 AND VL. THESE PARAMETERS (WHICH ARE AS DEFINED IN CHAPTER 2), ARE PLOTTED AS A FUNCTION OF TIME, WITH A TIME INTERVAL DETERMINED BY 'STEP'.

PROGRAM BLUM

```
      IMPLICIT REAL*8(A-H,L,O-Z)
      DOUBLE PRECISION Y(8),CIN(7),COMM(5),COUT(16),PW(8,8),W(8,22)
      DOUBLE PRECISION CONST(5),F(8),SOL(8),XI1(50),XI2(50),XI3(50)
      DOUBLE PRECISION XI4(50),V1(50),V2(50),VL(50),Z(50),RDL(50)
      DOUBLE PRECISION X1(50),X2(50),RL(50),XL(61)
      EXTERNAL FCN,REST
      COMMON LG,LL,L1,L2,C1,C2,RD,RG,RD0,RD1,RG0,RG1,V0,CONS,DELD
      COMMON/ONE/TD,R0
      WRITE(6,50)
   50 FORMAT(1X,'LG(nH)  LL(nH)  L1(nH)  L2(nH)  C1(nF)  C2(nF)
     1  V0(KV)  X0(nS)')
      READ*,LLG,LLL,LL1,LL2,CC1,CC2,V00,X0
      WRITE(6,100)
  100 FORMAT(1X,/,'DDELD(nS)  STEP(nS)  TD(nS)  TOL  NUM'
     1 ,/)
      READ*,DELDD,STEPP,TDD,TOL,NUM
      WRITE(6,150)
  150 FORMAT(1X,/,'RRD0  RD1  RG0  RG1  CONS')
```

```
      READ*,RD0,RD1,RG0,RG1,CONS
      WRITE(6,200)LLG,LLL,LL1,LL2
200   FORMAT(1X,/,'LLG=',F5.1,'(nH)  LL=',F5.1,'(nH)  L1=',F4.1,'(nH)
     1    L2=',F4.1,'(nH)')
      WRITE(6,250)CC1,CC2,V0,X0
250   FORMAT(1X,/,'CC1=',F4.1,'(nF)  C2=',F4.1,'(nF)  V0=',F5.1,'(KV)
     1    X0=',F4.1,'(nS)')
      WRITE(6,300)DELDD,STEPP
300   FORMAT(1X,/,'TTIME DELAY BEFORE BREAKDOWN =',F5.1,'(nS)',
     1    'TIME INTERVAL =',F5.1,'(nS)')
      WRITE(6,350)TDD,NUM
350   FORMAT(1X,/,'BBREAKDOWN TIME (TD) =',F4.1,'(nS)  NUMBER OF
     1  INTERVALS =',I3)
      WRITE(6,400)RD0,RD1
400   FORMAT(1X,/,'DDISCHARGE IMPEDANCE BEFORE BREAKDOWN (RD0) =',
     1  1PD8.2,'(OHMS)')
      WRITE(6,450)RD1
450   FORMAT(1X,/,'DDISCHARGE IMPEDANCE AFTER BREAKDOWN  (RD1) =',
     1  1PD8.2,'(OHMS)')
      WRITE(6,500)RG0
500   FORMAT(1X,/,'SSPARK GAP IMPEDANCE BEFORE BREAKDOWN (RG0) =',
     1  1PD8.2,'(OHMS)')
      WRITE(6,550)RG1
550   FORMAT(1X,/,'SSPARK GAP IMPEDANCE AFTER BREAKDOWN  (RG1) =',
     1  1PD8.2,'(OHMS)')
      WRITE(6,600)CONS,TOL
600   FORMAT(1X,/,'SSCALING CONSTANT (CONS) =',1PD8.2,'   TOLERANCE
     1   (TOL)=',1PD8.2)
```

```
      N=8
      IW=8
      IW1=22
      CIN(1)=1.0
      DO 1 I=2,5
1     CIN(I)=0.0
      DO 2 I=1,3
2     COMM(I)=0.0
      MPED=0
      LG=LLG*1.0D-9
      LL=LLL*1.0D-9
      L1=LL1*1.0D-9
      L2=LL2*1.0D-9
      C1=CC1*1.0D-9/2.0
      C2=CC2*1.0D-9/2.0
      VO=VOO*1.0D+3
      X=XO*1.0D-9*CONS
      DELD=DELDD*1.0D-9*CONS
      STEP=STEPP*1.0D-9*CONS
      XEND=(NUM+1)*STEP
      TD=TDD*1.0D-9
      RDL(1)=RDO
      RO=(DLOG(RDO)-DLOG(RD1))/TD
      Y(1)=0.0
      Y(2)=VO/LG
      Y(3)=0.0
      Y(4)=0.0
      Y(5)=0.0
```

```
      Y(6)=0.0
      Y(7)=0.0
      Y(8)=0.0
      XI1(1)=0.0
      XI2(1)=0.0
      XI3(1)=0.0
      XI4(I)=0.0
      V1(1)=VO
      V2(1)=0.0
      VL(1)=0.0
      Z(1)=X
      DO 3 J=1,NUM
      COMM(4)=-1.0
      COMM(5)=STEP*J
      TTEST=COMM(5)
      IFAIL=1
      CALL D02QBF(X,XEND,N,Y,CIN,TOL,FCN,COMM,CONST,COUT,MPED,
     1  PEDERV,PW,W,IW,IW1,IFAIL)
      IF(IFAIL.GT.0)GO TO 4
      CALL D02XGF(COMM(5),X,CIN,N,W,IW,IW1,SOL,IFAIL)
      IF(IFAIL.GT.0)GO TO 4
      JJ=J+1
      RDL(JJ)=RD
      V1(JJ)=(RG*SOL(1)+LG*SOL(2))
      V2(JJ)=-L1*SOL(4)
      VL(JJ)=-(RD*SOL(5)+LL*SOL(6))-L1*SOL(4)
      XI1(JJ)=SOL(1)
      XI2(JJ)=SOL(3)
```

```
      XI3(JJ)=SOL(5)
      XI4(JJ)=SOL(7)
      Z(JJ)=COMM(5)
3     CONTINUE
      NUMM=NUM+1
      DO 5 I=1,NUMM
5     Z(I)=Z(I)*1.0D9/CONS
      WRITE(6,650)
650   FORMAT(1X,///,12X,'LINEAR PLOT',14X,'I1(*)',5X,'I2(0)',5X,'RD')
      CALL PLOT(Z,XI1,XI2,RDL,XL,NUM,CONS)
      WRITE(6,700)
700   FORMAT(1X,///,12X,'LINEAR PLOT',14X,'I3(*)',5X,'I4(0)',5X,'RD')
      CALL PLOT(Z,XI3,XI4,RDL,XL,NUM,CONS)
      WRITE(6,750)
750   FORMAT(1X,///,12X,'LINEAR PLOT',14X,'V1(*)',5X,'VL(0)',5X,'RD')
      CALL PLOT(Z,V1,VL,RDL,XL,NUM,CONS)
4     WRITE(6,800)IFAIL
800   FORMAT(1X,/,'IIFAIL=',I2)
      STOP
      END
      SUBROUTINE FCN(X,Y,F)
      IMPLICIT REAL*8(A-H,L,O-Z)
      DOUBLE PRECISION Y(4),F(4)
      COMMON LG,LL,L1,L2,C1,C2,RD,RG,RD0,RD1,RG0,RG1,V0,CONS,DELD
      COMMON/ONE/TD,R0
      CALL REST(RDD,RGG,X)
      F(1)=Y(2)/CONS
      F(2)=(((Y(3)-Y(1))/C1)-RG*Y(2)-RGG*Y(1))/(LG*CONS)
```

```
      F(3)=Y(4)/CONS
      F(4)=(((Y(5)-Y(3))/C1)-((Y(3)-Y(1))/C1))/(L1*CONS)
      F(5)=Y(6)/CONS
      F(6)=(((Y(3)-Y(5))/C1)-((Y(5)-Y(7))/C2)-RD*Y(6)-RDD*Y(5))/
     1  (LL*CONS)
      F(7)=Y(8)/CONS
      F(8)=(((Y(5)-Y(7))/C2)-(Y(7)/C2))/(L2*CONS)
      RETURN
      END
      SUBROUTINE REST(RDD,RGG,X)
      IMPLICIT REAL*8(A-H,L,O-Z)
      COMMON LG,LL,L1,L2,C1,C2,RD,RG,RD0,RD1,RG0,RG1,VO,CONS,DELD
      COMMON/ONE/TD,R0
      TDELD=DELD+0.5*1.0D-09*CONS
      IF(X.GT.TDELD)GO TO 2
1     RD=RD0
      RDD=0.0
      GO TO 3
2     RD=(RD0*DEXP(-R0*(X-DELD)/CONS))+RD1
      RDD=-R0*RD/CONS
3     RG=RG1
      RGG=0.0
      RETURN
      END
      SUBROUTINE PLOT(Z,X1,X2,RL,XL,NUM,CONS)
      IMPLICIT REAL*8(A-H,L,O-Z)
      DOUBLE PRECISION Z(50),X1(50),X2(50),RL(50),XL(61)
      DATA CIRC,STAR,DASH,PLUS,HASH/'O','*','-','+',' '/
```

```
      XMAX=0.0
      XMAX1=0.0
      XMAX2=0.0
      NUMM=NUM+1
      DO 2 I=1,NUMM
      A1=DABS(X1(I))
      A2=DABS(X2(I))
      IF(A1.GT.XMAX1)XMAX1=A1
      IF(A2.GT.XMAX2)XMAX2=A2
2     CONTINUE
      IF(XMAX1-XMAX2)3,3,4
3     XMAX=XMAX2
      GO TO 5
4     XMAX=XMAX1
5     XMAX4=-XMAX
      WRITE(6,50)XMAX4,XMAX
50    FORMAT(1X,1X,1PD8.1,5X,'0.0',5X,1PD8.1)
      STE=2.0*XMAX/20.0
      IF(STE.EQ.0.0)GO TO 7
      KO=(XMAX/STE)+1
      GO TO 10
7     KO=1
10    DO 6 I=1,NUMM
      DO 1 J=1,21
1     XL(J)=DASH
      XL(KO)=PLUS
      IF(STE.GT.0.0)GO TO 8
      K1=0
```

```
      K2=0
      GO TO 9
8     K1=X1(I)/STE
      K2=X2(I)/STE
9     IF(K1.NE.0)K1=KO+K1
      IF(K1.EQ.0)K1=KO
      IF(K2.NE.0)K2=KO+K2
      IF(K2.EQ.0)K2=KO
      XL(K1)=STAR
      XL(K2)=CIRC
      IF(K1.EQ.K2)XL(K2)=HASH
      WRITE(6,100)Z(I),(XL(J),J=1,21),Z(I),X1(I),X2(I),RL(I)
100   FORMAT(1X,F5.1,21A1,F5.1,1X,1PD9.2,1X,1PD9.2,1X,1PD8.2)
6     CONTINUE
      RETURN
      END
```

APPENDIX TWO

INFRARED LASER EMISSION

(A2.1) Introduction

During the course of this work, laser emission was observed in the infrared spectral region from discharge excited mixtures of $He/Xe/CF_4$. We report here on some of the performance characteristics of the laser, and we identify the laser transition.

(A2.2) Laser wavelength

The laser wavelength was determined to help identify the laser line. Since a calibrated IR monochromator was not available, a relatively crude set-up was used. The latter consisted of a diffraction grating (295 lines/mm) which was available at the time, and a detector which was used to locate the position of the diffracted laser beam. The laser wavelength was determined from the angle of diffraction for normal incidence of the laser beam, and the grating equation.

$$\lambda = d \sin(x)/n \qquad (2.1)$$

where λ is the wavelength, d the spacing of the grating lines, x the angle of diffraction and n the order of the diffracted beam. To start with, the laser was run on a mixture of $He/Xe/NF_3$, and the XeF laser

emission at 351nm was used to position the grating. Using the experimental set-up, a value of (351 ± 2nm) was obtained for the XeF wavelength. The wavelength of the infrared laser was measured as (2.02 ± 0.02)μm. The emission is attributed to the 5d(3/2) -> 6p(3/2) atomic line of Xe at 2.03 μm. Laser action on the same line has been previously observed from discharge excited He/Xe and Ar/Xe mixtures (Schwarz et al 1970, Targ and Sasnett 1971, Shuker et al 1975, Lisitsyn and Sorokin 1981, Olson et al 1976), and from e-beam sustained discharges in Ar/Xe and He/Xe mixtures (Newman and DeTemple 1975, Lawton et al 1979). For He/Xe mixtures, the output spectrum includes components at 2.03, 2.65, 3.43 and 3.65μm, but laser emission at 2.03μm is predominant. For Ar/Xe mixtures, the spectrum consists of lines at 1.73, 2.03, 2.65, 2.62 and 3.37μm, and laser emission at 1.73μm is predominant (Newman and DeTemple 1975). For the He/Xe/CF_4 mixtures studied here, laser emission was only observed at 2.03μm.

(A2.3) Some Performance Characteristics

The laser pulse energy was measured as a function of the partial pressure of CF_4, Xe, He and the total gas presure. For all the measurements, the laser was pulsed at a repetition rate of 1 pps, and the supply voltage was 18 KV. Th laser cavity was identical to that of the XeF laser described in Chapter 2. No attempt was made to optimise the laser pulse energy by changing either the output coupler or the 'total' reflector. Figure (A2.1)shows the laser pulse energy as a function of the partial pressure of CF_4. The partial pressure or Xe was 12 torr and the total gas pressure in the laser was 1 atmosphere. The laser pulse energy increases with the partial

pressure of CF_4 up to about 4 torr, after which the rate of change is small for partial pressures up to 10 torr. The maximum pulse energy was 0.35 mJ. This is, however, less than the true energy since the circular aperture of the energy probe is only a few millimetres in diameter, which is small compared to the laser electrode separation of 2 cm. When the back mirror (total reflector at 351 nm) is removed, the pulse energy decreases by about 27%.

In fig. (A2.2), the laser pulse energy is shown as a function of the partial pressure of Xe. The partial pressure of CF_4 was 6 torr, and the total gas pressure was one atmosphere. The laser pulse energy increases slowly with the partial pressure of Xe, and reaches a maximum at about 16 torr. For He/Xe mixtures, the laser output is also relatively insensitive to the partial pressure of Xe. However, the optimum gas mixture is normally lean in Xe, whose partial pressure is typically a few torr.

Figure (A2.3) shows the laser pulse energy as a function of the partial pressure of helium. The partial pressure of Xe and CF_4 was 12 and 6 torr respectively. The laser output appears to reach a broad maximum at about 1.5 atmospheres of helium. Higher pressures were not used for safety reasons. Figure (A2.4) shows the laser pulse energy as a function of the total gas pressure. The gas mixture consisted of $He/Xe/CF_4$ in the ratio of 180:2:1. The behaviour is similar to that shown in fig. (A2.3). The laser output increases with the total gas pressure , and appears to level off at about 1.5 atmospheres.

(A2.4) Gas-life

In fig. (A2.5), the laser output is shown as a function of the number of laser pulses. The gas-life (to half-energy) is more than 2000 shots/litre atmosphere. Mass spectrometric analysis of the laser gas mixture shows that after 4500 shots, the partial pressure of CF_4 is down by about 3%. The partial pressures of CO and CO_2 increase by 28% and 17% respectively, and those of H_2O and O_2 are down by 8% and 33% respectively. The partial pressure of N_2 does not change, and there is no evidence of the formation of oxides of nitrogen such as NO, NO_2 and N_2O. These results indicate that the short gas-life is predominantly due to the accumulation of CO_2 and CO in the laser.

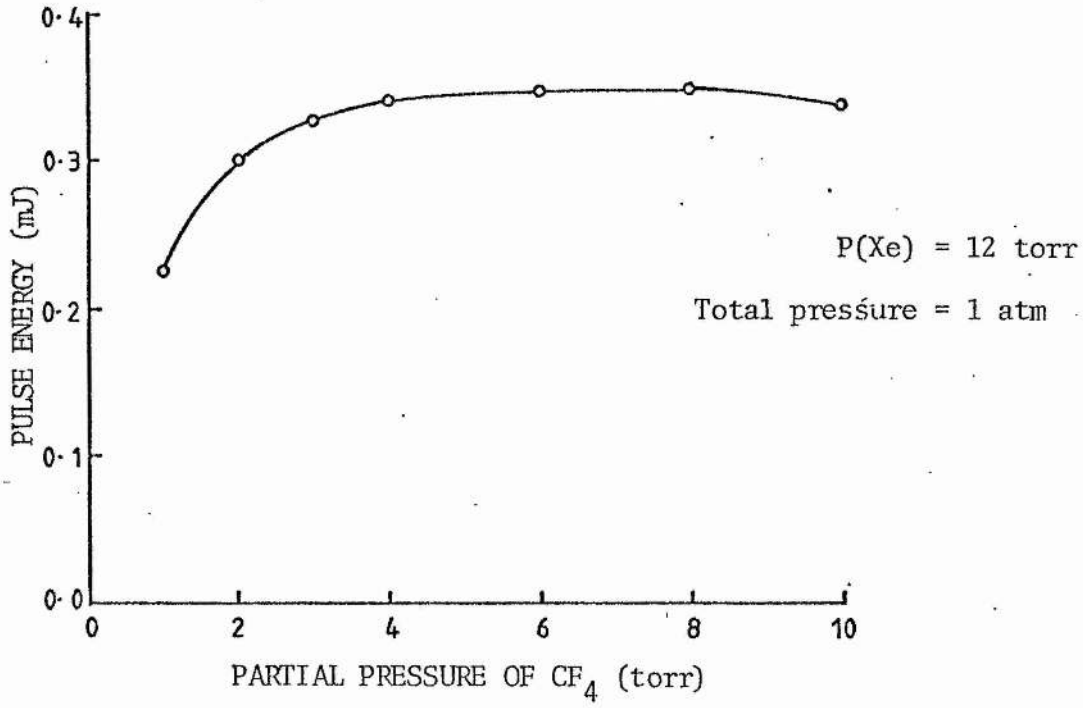

Fig.(A2.1) Laser pulse energy as a function of the partial pressure of CF_4.

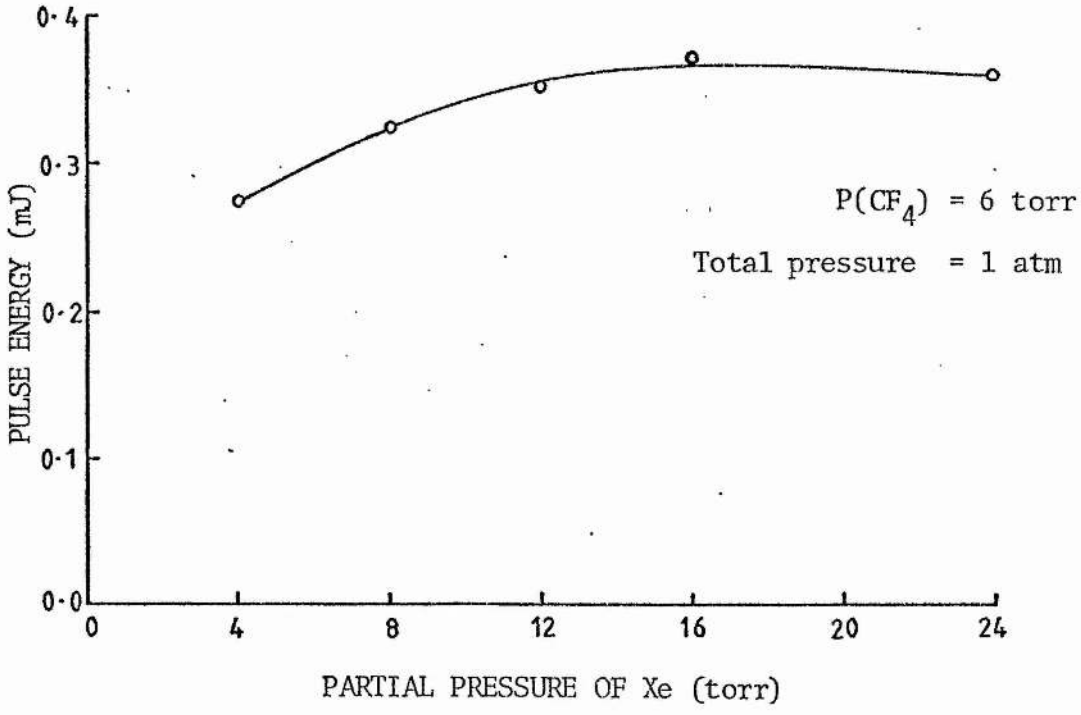

Fig.(A2.2) Laser pulse energy as a function of the partial pressure of Xe.

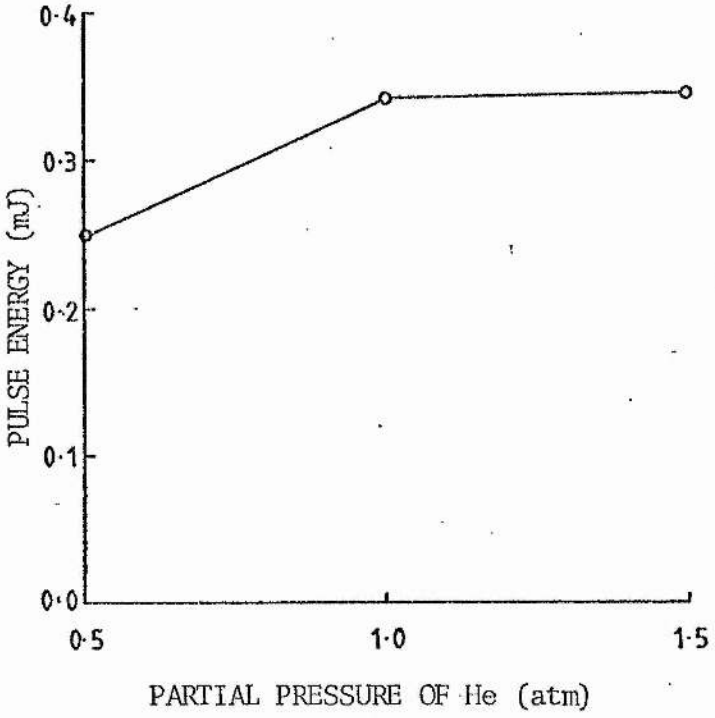

Fig.(A2.3) Laser pulse energy as a function of the partial pressure of He.

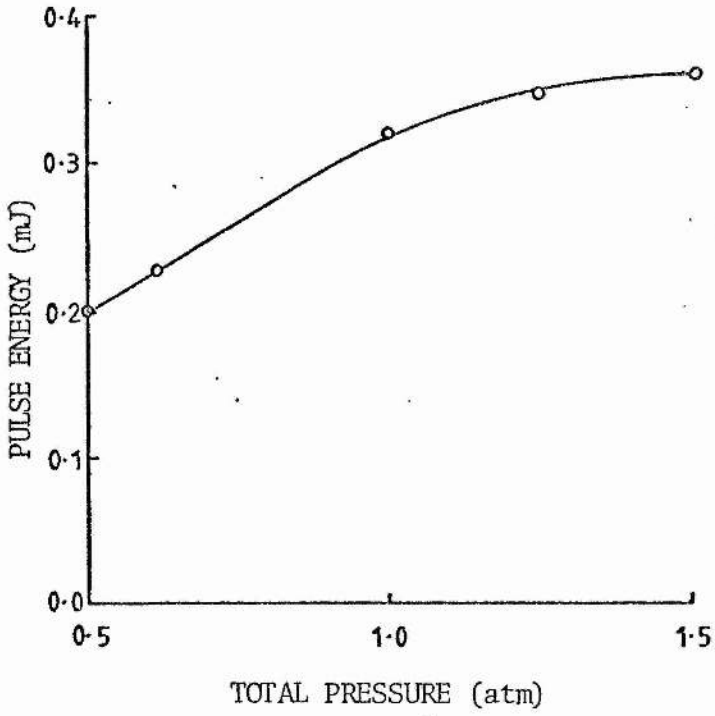

Fig.(A2.4) Laser pulse energy as a function of the total gas pressure.

REFERENCES

Andrews A.J., A.J. Kearsley, C.E. Webb, S.C. Haydon, Opt. Comm. 20, 265 (1977).

Akins R.P., G. Innis, Shao-Chi Lin, J. Appl. Phys. 49, 2262 (1978).

Ault E.R., R.S. Bradford, Jr., M.L. Bhaumik, Appl. Phys. Lett. 27, 413 (1975).

Bailey J.R., Handbook of Vacuum Physics, Vol.3, Pergamon Press (1964).

Bentley P.G., A.N. Hamer, P.B.F. Evans, The analysis of corrosive gases with a mass spectrometer, in Advances in Mass Spectrometry, ed. J.D. Waldron, Pergamon Press; London 1959.

Bhaumik M.L., R.S. Bradford Jr., E.R. Ault, Appl. Phys. Lett. 28, 23 (1976).

Bigio I.J. and R.F. Begley, Appl. Phys. Lett. 28, 263 (1976).

Bischel W.K., D.J. Eckstrom, H.C. Walker, Jr., R.A. Tilton, J. Appl. Phys. 52, 4429 (1981).

Blears J., J. Sci. Inst. 28, Suppl. 1, 36 (1951).

Brannon J.H., IEEE J. Quant. Electron. 18, 1302 (1982).

Brashears H.C. Jr., D.W. Setser, D. DesMarteau, Chem. Phys. Lett. 48, 84 (1977).

Brashears H.C. and D.W. Setser, Appl. Phys. Lett. 39, 821 (1978).

Brau C.A., Rare Gas Halogen Excimers, in Excimer Lasers, ed. C. Rhodes, Springer Verlag; Berlin 1979.

Brau C.A. and J.J. Ewing, Appl. Phys. Lett. 27, 435 (1975).

Bruce F.M., J. Inst. Electr. Eng. 94, 138 (1947).

Burlamacchi P. and R. Salimbeni, Opt. Comm. 26, 233 (1978).

Burlamacchi L., P. Burlamacchi, R. Salimbeni, Appl. Phys. Lett. 34, 33 (1979).

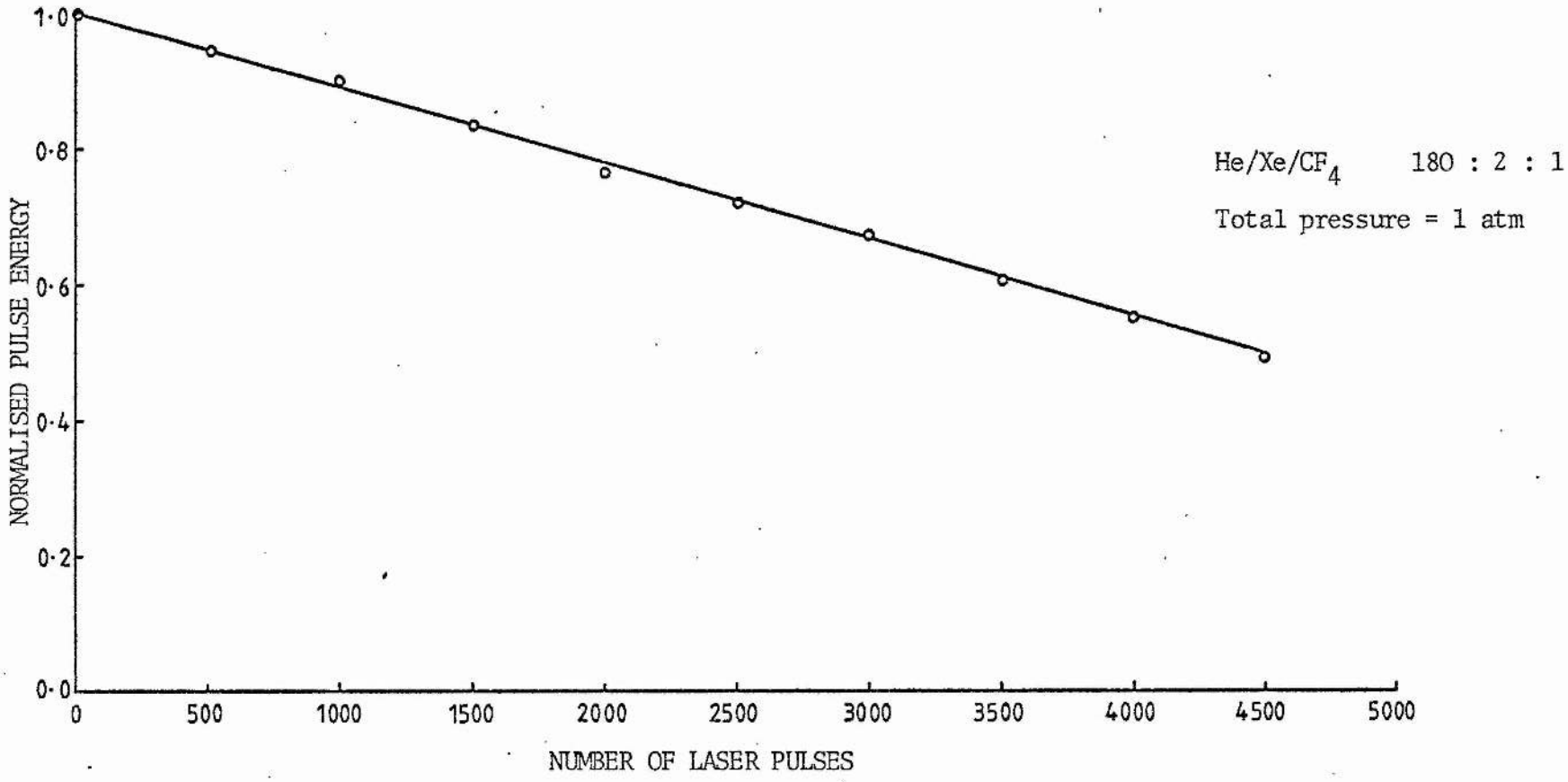

Fig.(A2.5) Normalised pulse energy as a function of the number of laser pulses.

Burnham R. and N. Djeu, Appl. Phys. Lett. 29, 707 (1976).

Burnham R., N.W. Harris, N. Djeu, Appl. Phys. Lett. 28, 86 (1976a).

Burnham R., F.X. Powell, N. Djeu, Appl. Phys. Lett. 29, 30 (1976b).

Burnham R. and S.K. Searles, J. Chem. Phys. 67, 5969 (1977).

Cary W.K. Jr., and J.A. Mazzie, IEEE Trans. Elect. Dev. ED-26, 1422 (1979).

Champagne L.F. and N.W. Harris, Appl. Phys. Lett. 31, 513 (1977).

Chang T.Y., Rev. Sci. Inst. 44, 405 (1973).

Chen Jianwen, Fu Shufen, Liu Miahong, Appl. Phys. Lett. 37, 883 (1980).

Chow W., M. Stuke, F.P. Schafer, Appl. Phys. 13, 1 (1977).

Christensen C.P., Appl. Phys. Lett. 9, 483 (1977).

Colburn C.B., Advances in Fluorine Chemistry, 3, 92 (1963); ed. M. Stacey, J.C. Tatlow, A.G. Sharpe, Butterworths; London.

Cornu A. and R. Massot, Compilation of Mass Spectral Data, Heyden and Son Ltd., London 1966.

Cotton F.A. and G. Wilkinson, Advanced Inorganic Chemistry, John Wiley and Sons; London 1972.

Cox R.A. and R.G. Derwent, J. Photochem. 6, 23 (1976).

Craig R.D. and E.H. Harden, Vacuum 16, 67 (1965).

Douglas-Hamilton D.H. and S.A. Mani, Appl. Phys. Lett. 23, 508 (1973).

Eden J.G., R.W. Waynant, S.K. Searles, R. Burnham, J. Appl. Phys. 49, 5368 (1978).

Eden J.G. and R.W. Waynant, Opt. Lett. 2, 13 (1978).

Eden J.G., J. Golden, R.A. Mahaffey, J.A. Pasour, R.W. Waynant, Appl. Phys. Lett. 35, 133 (1979).

Eight Peak Index of Mass Spectra, 1st edition, vols. 1 and 2, Mass

Spectrometry Data Centre, Atomic Weapons Research Establishment; England 1970.

Ernst W.E. and F.K. Tittel, Appl. Phys. Lett. 35, 36 (1979).

Ewing J.J. and C.A. Brau, Phys. Rev. A12, 129 (1975).

Fahlen T.S., IEEE J. Quant. Electron. QE-15, 311 (1979).

Fahlen T.S., IEEE J. Quant. Electron. 16, 1260 (1980).

Finn T.G., L.J. Palumbo, L.F. Champagne, Appl. Phys. Lett. 34, 52 (1979).

Fisher C.H., R.E. Center, G.J. Mullaney, J.P. McDaniel, Appl. Phys. Lett. 35, 26 (1979).

Foon R. and M. Kaufman, Progress in Reaction Kinetics, 8, 81 (1975).

Golde M.F. and B.A. Thrush, Chem. Phys. Lett. 29, 485 (1974).

Goodeve C.F. and J.I. Wallace, Trans. Farad. Soc. 26, 254 (1930).

Gower M.C., A.J. Kearsley, C.E. Webb, IEEE J. Quant. Electron. 16, 231 (1980).

Greene A.E. and C.A. Brau, IEEE J, Quant. Electron. 14, 951 (1978).

Hall T.C. and F.E. Blacet, J. Chem. Phys. 20, 1745 (1952).

Hasson V. and H.M. Von Bergman, Rev. Sci. Inst. 50, 1542 (1979).

Hasson V. and H.M. Von Bergman, J. Phys. E: Sci. Inst. 13, 632 (1980).

Hasson V., C.M. Lee, R. Exberger, K.W. Billman, P.D. Rowley, Appl. Phys. Lett. 31, 167 (1977).

Hawryluk A.M., J.A. Mangano, J.H. Jacob, Appl. Phys. Lett. 31, 164 (1977).

Herziger G., Wollermann-Windgasse, K.H. Banse, Appl. Phys. 24, 267 (1981).

Hipple J.A. and E.U. Condon, Phys. Rev. 68, 54 (1945).

Hoffman J.M., A.K. Hays, G.C. Tisone, Appl. Phys. Lett. 28, 538 (1976).

Hogan D.C., A.J. Kearsley, C.E. Webb, J. Phys. D: Appl. Phys. 13, L225 (1980).

Honig R. E., J. Appl. Phys. 16, 646 (1945).

Houghton J.T. and S.D. Smith, Infrared Physics, Clarendon Press; Oxford 1966.

Hsia J., Appl. Phys. Lett. 30, 101 (1977).

Hutchinson M.H.R., Appl. Phys. 21, 95 (1980).

Johnson P.M., N. Keller, R.E. Turner, Appl. Phys. Lett. 32, 291 (1978).

Johnston H.S. and G.S. Selwyn, Geophys. Res. Lett. 2, 549 (1975).

Kemmitt R.D.W. and D.W.A. Sharp, Advances in Fluorine Chemistry, 4, 142 (1965), ed. M. Stacey, J.C. Tatlow, A.G. Sharpe, Butterworths; London.

Kutschke K.O., P.A. Hackett, C. Willis, Rev. Sci. Inst. 52, 1655 (1981).

Lagowski J.J., Modern Inorganic Chemistry, Marcel Dekker Inc., New York 1973.

La Paglia S.R. and A.B.F. Duncan, J. Chem. Phys. 34, 1003 (1961).

Lawler J.E., J.W. Parker, L.W. Anderson, W.A. Fitzsimmons, IEEE J. Quant. Electron. QE-15, 609 (1979).

Lawton S.A., J.B. Richards, L.A. Newman, L. Specht, T.A. DeTemple, J. Appl. Phys. 50, 3888 (1979).

Levatter J.I. and Shao-Chi-Lin, J. Appl. Phys. 51, 210 (1980).

Levatter J.I., K.L. Robertson, Shao-Chi-Lin, Appl. Phys. Lett. 39, 297 (1981).

Liegel J., F.K. Tittel, W.L. Wilson Jr., Appl. Phys. Lett. 39, 369 (1981).

Lisitsyn V.N. and A.R. Sorokin, Sov. J. Quant. Electron. 11, 1481

(1981).

McKee T.J. and J.A. Nielson, Laser Focus, June 1982, p. 51.

McKee T.J., D.J. James, W.S. Nip, R.W. Weekes, Appl. Phys. Lett. 36, 943 (1980).

Mandl A., R. Slater, C.H. Appel, Rev. Sci. Inst. 53, 301 (1982).

Mangano J.A. and J.H. Jacob, Appl. Phys. Lett. 27, 495 (1975).

Marmo F.F., J. Opt. Soc. Am. 43, 1186 (1953).

Mendelson A.J., R. Normandin, S.E. Harris, J.F. Young, Appl. Phys. Lett. 38, 603 (1981).

Mkrtchyan M.M. and V.T. Platonenko, Sov. J. Quant. Electron. 9, 967 (1979).

Moody G.J. and J.D.R. Thomas, Noble Gases and Their Compounds, Pergamon Press; London 1964.

Murray J.R., and H.T. Powell, Appl. Phys. Lett. 29, 252 (1976).

Nakamato K., Infrared Spectra of Inorganic and Coordination Compounds, John Wiley and Sons Inc., London 1963.

Newman L.A., Appl. Phys. lett. 36, 501 (1978).

Newman L.A. and T.A. DeTemple, Appl. Phys. Lett. 27, 678 (1975).

Nighan W.L., Stability of high-power molecular laser discharges, in Principles of Laser Plasmas, ed. G. Bekefi, Wiley-Interscience; London 1976.

Nighan W.L. and W.J. Wiegand, Phys. Rev. A10, 922 (1974).

Ogawa M., J. Chem. Phys. 54, 2550 (1971).

Okabe H., Photochemistry of Small Molecules, John Wiley and Sons; Chichester 1978.

Olson R.A., D. Grosjean, B. Sarka, Jr., Rev. Sci. Inst. 47, 677 (1976).

Potts W.J., Chemical Infrared Spectroscopy, John Wiley and Sons;

London 1963.

Ramo S., J.R. Whinnery, T. Van Duzer, Fields and Waves in Communication Electronics, John Wiley and Sons Inc., London (1965).

Rogowski W., Arch. Elektrotech. 12, 1 (1923).

Rokni M., J.H. Jacob, J.A. Mangano, R. Brochu, Appl. Phys. Lett. 30, 458 (1977).

Rokni M., J.A. Mangano, J.H. Jacob, J.C. Hsia, IEEE J. Quant. Electron. 14, 464 (1978).

Rothe D.E. and R.A. Gibson, Opt. Comm. 22, 265 (1977).

Sarjeant W.J., A.J. Alcock, K.E. Leopold, Appl. Phys. Lett. 30, 635 (1977).

Schawb A.J. and F.W. Hollinger, IEEE J. Quant. Electron. QE-12, 183 (1976).

Schwartz S.E., T.A. DeTemple, R. Targ, Appl. Phys. Lett. 17, 305 (1970).

Searles S.K. and G.A. Hart, Appl. Phys. Lett. 27, 243 (1975).

Selig H., Fluoride chemistry of the noble gases, in Halogen Chemistry, vol.1, ed. V. Gutman, Academic Press; London 1967.

Shahin M.M., Chemical reactions in electrical discharges, in Reactions Under Plasma Kinetics, ed. M. Venugopalan, Wiley-Interscience; London 1971.

Sharkey A.G., C.F. Robinson, R.A. Friedel, Use of rhenium filaments and low ionizing voltages for analysing liquid products from coal hydrogenation by mass spectrometry, in Advances in Mass Spectrometry, ed. J.D. Waldron, Pergamon Press; London 1959.

Shaw M.J. and J.D.C. Jones, Appl. Phys. 14, 393 (1977).

Shields H. and A.J. Alcock, Opt. Comm. 42, 128 (1982).

Shin Sumida, Kouichi Kunimoto, Masahiro Kaburagi, Minoru Obara, Tomoo

Fujioka, Kounosuke Sato, J. Appl. Phys. 52, 2862 (1981).

Shin Sumida, Minoru Obara, Tomoo Fujioka, Appl. Phys. Lett. 33, 913 (1978).

Shuker R., A. Szoke, E. Zamir, Y. Binur, Phys. Rev. A11, 1187 (1975).

Smith D.F., J. Chem. Phys. 28, 1040 (1958).

Smith G.P. and D.L. Huestis, J. Appl. Phys. 52, 6041 (1981).

Smith A.L. and P.C. Kobrinsky, J. Mol. Spect. 69, 1 (1978).

Stappaerts A.E., Appl. Phys. Lett. 40, 1018 (1982).

Steunenberg R.K. and R.C. Vogel, J. Am. Chem. Soc. 78, 901 (1956).

Sze R.C. and T.R. Loree, IEEE J. Quant. Electron. QE-14, 944 (1978).

Sze R.C. and P.B. Scott, J. Appl. Phys. 47, 5492 (1976).

Targ R. and M.W. Sasnett, Appl. Phys. Lett. 19, 537 (1971).

Tasman A., A. Boerboom, J. Kistemaker, Mass Spectrometry, ed. A. McDowell, Mc Graw-Hill 1963.

Taylor R.S., P.B. Corkum, S. Watanabe, K.E. Leopold, A.J. Alcock, IEEE J. Quant. Electron. QE-19, 416 (1983).

Tellinghuisen J., J.M. Hoffman, G.C. Tisone, A.K. Hays, J. Chem. Phys. 64, 2484 (1976a).

Tellinghuisen J., A.K. Hays, J.M. Hoffman, G.C. Tisone, J. Chem. Phys. 65, 4473 (1976b).

Tellinghuisen J., G.C. Tisone, J.M. Hoffman, A.K. Hays, J. Chem. Phys. 64, 4796 (1976c).

Tellinghuisen J., P.C. Tellinghuisen, G.C. Tisone, J.M. Hoffman, A.K. Hays, J. Chem. Phys. 68, 5177 (1978).

Tenant R., Laser Focus, October 1981, p. 65.

Velazco J.E. and D.W. Setser, Chem. Phys. Lett. 25, 197 (1974).

Velazco J.E. and D.W. Setser, J. Chem. Phys. 62, 1990 (1975).

Velazco J.E., J.H. Kolts, D.W. Setser, J. Chem. Phys. 65, 3468 (1976).

Wang C.P. and O.L. Gibb, IEEE J. Quant. Electron. 15, 318 (1979).

Watanabe S., A.J. Alcock, K.E. Leopold, R.S.R. Taylor, Appl. Phys. Lett. 38, 3 (1981).

Waynant R.W. and J.G. Eden, IEEE J. Quant. Electron. 15, 61 (1979).